

INTER - International Network on Timber Engineering Research

2014 the International Network on Timber Engineering Research (INTER) was founded.

Scope

Presentation, discussion and documentation of research results in timber engineering and development of application rules for timber design codes or standards related to timber engineering.

Approach

Annual meetings in different countries/places hosted by meeting participants
Presentation and discussion of papers

Peer review of the abstracts before the meeting and of the papers during the meeting

Decision of the acceptance of the abstracts before the meeting by a well-defined review process

Decision of the acceptance of the papers for the proceedings during the meeting

Publication of the papers and the discussion in proceedings

Rules

All decisions including the appointment of the chairperson or the location of annual meetings are made by the participants attending a meeting.

Membership

Persons contributing to or being interested in research related to timber engineering.



MEETING FIFTY-THREE

ONLINE MEETING

AUGUST 2020

INTER

International Network on Timber Engineering Research

Proceedings

Meeting 53

17 - 19 August 2020

Online Meeting

Edited by Rainer Görlacher

Timber Scientific Publishing
KIT Holzbau und Baukonstruktionen
Karlsruhe, Germany
2020

Publisher:

Timber Scientific Publishing
KIT Holzbau und Baukonstruktionen
Reinhard-Baumeister-Platz 1
76131 Karlsruhe
Germany
2020

ISSN 2199-9740

Table of Contents

1	List of Participants	1
2	Minutes of the Meeting	7
3	INTER Papers, Online Meeting 2020	25
53 - 1 - 1	Review of the Reliability of Timber Structures in the 2020s - R Jockwer, G Fink, J Köhler	29
53 - 7 - 1	A Conceptual Model to Predict the Withdrawal Capacity of Screws Inserted Parallel to Grain in Beech, Ash and Spruce - M Westermayr, J W G van de Kuilen	47
53 - 7 - 2	FE Modelling of Timber Connections with Inclined and Cross-Wise Arranged Screws - New Findings on Testing the Shear Stiffness - B Azinović, M Frese	71
53 - 7 - 3	Embedding Strength Prediction for European Hardwood Species - T Benistand, L Bleron, J-F Bocquet	87
53 - 7 - 4	Beam-on-Foundation Modelling as an Alternative Design Method for Timber Joints with Dowel-Type Fasteners – Part 4: Joints Subjected to In-Plane Loading - R Lemaître, J-F Bocquet, M Schweigler, T K Bader	107
53 - 7 - 5	Brittle Failure Mode of Timber Connections with one Row of Fasteners Loaded Parallel-to-grain: a New Model for Splitting Failure - M Yurrita, J M Cabrero	109
53 - 7 - 6	Experimental Analysis of Brittle Failure in Timber-to-Steel Connections with Small Diameter Fasteners Loaded Parallel-to-Grain - M Yurrita, J M Cabrero, H J Blaß	125
53 - 7 - 7	Fatigue Behaviour of Notched Connections for Timber-Concrete-Composite Bridges - S Mönch, U Kuhlmann	143
53 - 11 - 1	Quality Assurance and Design of Timber Structures in Varying Climates - M Schiere, B Franke, S Franke	159
53 - 12 - 1	Shrinkage Behaviour of Reinforced Glulam Members - M Danzer, P Dietsch, S Winter	175
53 - 12 - 2	Fracture Mechanics Based Design of CLT-plates – Notches at Supports and Half-and-Half Joints - E Serrano, H Danielsson	193
53 - 12 - 3	Prediction of Torsional Stress at In-plane Shear	209

	Loading of Cross Laminated Timber - H Danielsson, M Jeleč, E Serrano	
53 - 15 - 1	Assessment of Seismic Design Factors and Proposal of Modification to Chilean Seismic Building Design Code (NCH 433) for Mid-Rise Wood Light-Frame Buildings - H Santa María, Á Salinas, J Montaña, J J Ugarte, J L Almazán, P Guindos, A Opazo, F Benedetti, V Rosales, X Estrella, F Guiñez, S Berwart, S Cárcamo, A Jara	225
53 - 16 - 1	Fire Design of I-joists in Wall Assemblies - K N Mäger, A Just, T Persson, A Wikner	243
53 - 20 - 1	Vibrations of Floors – Comparison of Measured Data and Suggested Design - P Hamm, J Marcroft, T Toratti	259
53 - 21 - 1	Revision of Testing Standards to Determine the Seismic Capacity of Timber Connections According to Eurocode 8 - C Sigrist, D Casagrande, M Piazza	277
53 - 22 - 1	Quantifying Robustness in Tall Timber Buildings - K Voulpiotis, J Köhler, R Jockwer, A Frangi	295
4	Peer Review of Papers for the INTER Proceedings	311
5	Meeting and List of CIB-W18 and INTER Papers	313

1 List of participants

AUSTRALIA

K Crews	UTS & UQ
R Shrestha	University of Technology Sydney

AUSTRIA

R Brandner	Graz University of Technology
P Dietsch	University of Innsbruck
A Fadai	Vienna University of Technology
J Füssl	Vienna University of Technology
M Gstettner	Graz University of Technology
G Hochreiner	Vienna University of Technology
M Lukacevic	Vienna University of Technology
R Maderebner	University of Innsbruck
U Mahlknecht	Graz University of Technology
B Maurer	University of Innsbruck
A Müllner	Vienna University of Technology

BELGIUM

R Celis	WOOD.BE, Brussel
D Sonck	BuildSoft, Merelbeke

CANADA

F Lam	University of British Columbia, Vancouver
T Tannert	UNBC Prince George
P Vinco da Sesso	StructureCraft, Abbotsford

CHILE

P Dechent	University of Concepcion
J Montano	Centro de Innovación en Madera

CHINA

M He	Tongji University
Z Li	Tongji University
X Zheng	Tongji Univerisity

CROATIA

M Jelec	University of Osijek
---------	----------------------

ESTONIA

A Just Tallinn University of Technology
K N Mäger Tallinn University of Technology
E Tuhkanen Tallinn University of Technology

FINLAND

G Fink Aalto University
J Jaaranen Aalto University

FRANCE

C Allemand CSTB, Champs-sur-Marne
J-F Bocquet LERMAB, Epinal

GERMANY

S Aicher MPA University Stuttgart
S Aurand Karlsruhe Institute of Technology (KIT)
H J Blaß Karlsruhe Institute of Technology (KIT)
T Claus University of Kassel
G D Arenzo University of Kassel
M Danzer Technical University of Munich
S Egnér Karlsruhe Institute of Technology (KIT)
M Frese Karlsruhe Institute of Technology (KIT)
J Frohnmüller University of Kassel
J Gauß University of Stuttgart
S Glattacker Karlsruhe Institute of Technology (KIT)
R Görlacher Karlsruhe Institute of Technology (KIT)
P Hamm Biberach University of Applied Sciences
E Kuck Karlsruhe Institute of Technology (KIT)
U Kuhlmann University of Stuttgart
S Mönch University of Stuttgart
C Sandhaas Karlsruhe Institute of Technology (KIT)
M Schenk Technical University of Munich
M Steilner Karlsruhe Institute of Technology (KIT)
C Tapia Camu MPA University of Stuttgart
J Töpler University of Stuttgart
M Vedovelli Karlsruhe Institute of Technology (KIT)
M Westermayr Technical University of Munich
L Windeck Karlsruhe Institute of Technology (KIT)
S Winter Technical University of Munich

ITALY

D Casagrande National Research Council of Italy
L Marchi University of Padova
R Scotta University of Padova
D Trutalli Montebelluna

JAPAN

K Kobayashi Shizuoka University
T Nagashima Sumitomo Forestry CO.,LTD., Tsukuba
S Nakashima Building Research Institute, Tsukuba
T Tsuchimoto Building Research Institute, Tsukuba

NEW ZEALAND

J Brown University of Canterbury
W Dong University of Canterbury
B Moerman University of Canterbury
P Quenneville The University of Auckland
T Wright University of Canterbury

NORWAY

R Tomasi Norwegian University of Life Science

REPUBLIC OF KOREA

J K Oh Seoul National University

SLOVENIA

B Azinovic Slovenian National Building and Civil Engineering Institute

SPAIN

J M Cabrero Universidad de Navarra, Pamplona
M Yurrita Universidad de Navarra, Pamplona

SWEDEN

T Bader Linnaeus University, Vaxjö
H Danielsson Lund University
R Jockwer Chalmers Technical University
R Lemaitre Linnaeus University, Vaxjö
M Schweigler Linnaeus University, Vaxjö
E Serrano Lund University

SWITZERLAND

T Ehrhart	ETH Zurich
A Frangi	ETH Zurich
S Franke	University of applied sciences BFH, Biel
P Grönquist	ETH Zurich
C Leyder	ETH Zurich
P Palma	EMPA, Duebendorf
M J Schiere	University of applied sciences BFH, Biel
C Sigrist	University of applied sciences BFH, Biel
R Steiger	EMPA, Duebendorf
K Voulpiotis	ETH Zurich

THE NETHERLANDS

G Ravenshorst	Delft University of Technology
---------------	--------------------------------

TURKEY

A Ceccotti	Bogazici University, Istanbul
------------	-------------------------------

UNITED KINGDOM

I Abeysekera	Arup, London
A Lawrence	Arup, London
E Toumpanaki	University of Bristol

USA

S Breneman	WoodWorks - Wood Products Council
J Dolan	Washington State University
E McDonnell	Holmes Structures, Portland
G Montgomery	Swinerton Builders, Greenville
B Yeh	APA - The Engineered Wood Association, Tacoma

2 Minutes of the Meeting

by F Lam, Canada

CHAIRMAN'S INTRODUCTION

P Dietsch welcomed the delegates to the 7th International Network of Timber Engineering Research (INTER) which was held as an on-line meeting because of the Covid 19 pandemic. The INTER Core group had coordinated with the original Chilean host to change the meeting format and postpone hosting the INTER meeting in Chile potentially in 2021. He thanked the participants of this meeting for participating despite the time zone challenges. In total 97 participants from 24 countries registered for the 7th INTER meeting with 26 participants from outside Europe. He also thanked Karlsruhe Institute of Technology KIT for hosting of this meeting on relatively short notice.

This is the 53rd meeting of the group including the series of former CIB-W18 meetings. By moving to an Online-meeting, INTER could continue its tradition of yearly meetings to discuss research results related to timber structures with the aim of transferring them into practical applications.

The chair introduced all the participants.

Twenty-five papers were accepted for this meeting with 40 submitted abstracts. 17 of the accepted papers will be presented here as 8 authors with accepted abstracts deferred their presentations to the 2021 meeting of INTER. The papers were selected based on a review process for the abstracts with 4 acceptance criteria (state of the art, originality, assumed content, and relation to standards or codes). 19 members acted as reviewers and each abstract was reviewed by at least 7 reviewers. Full papers were requested to be submitted one month before the meeting to facilitate distribution to the participants prior to the meeting.

Papers brought directly to the meeting were not accepted for presentation, discussions, or publication. Same rule applied to papers where none of the authors was present or papers which were not defended by one of the authors. The presentations were limited to 20 minutes each, allowing time for meaningful discussions after each presentation. The Chair asked the presenters to conclude the presentation with a general proposal or statements concerning impact of the research results on existing or future potential applications and development in codes and standards.

The topics covered in this meeting were: Robustness (1) Test methods (1) Serviceability (1) Fire (1) Structural Stability (1) Laminated Members (3), Environmental Conditions (1) Timber Joints and Fasteners (7) and Limit States Design

(1). Numbers in parentheses are the number of papers presented in each topic based on initial allocation.

Notes were not be presented in this meeting due to the time limitation of 4 hours meeting time each day, which was necessary to best accommodate for the time zone differences..

The Chair encouraged the tradition of active questions and discussion processes for our meeting and reviewed the rules and guidelines for web-based participation, for presentations and the question/discussion process.

He invited all authors to amend their papers according to the comments and recommendations received before submit the final paper for the proceedings. Finalized papers must be sent to Rainer Görlacher at the latest end of September this year.

GENERAL TOPICS

CEN/TC 250/SC 5 Design of timber structures: P Dietsch provided a short update of the activities. S Winter will provide more details on Eurocode activities next year.

LIMIT STATE DESIGN

53 - 1 - 1 Review of the Reliability of Timber Structures in the 2020s - R Jockwer, G Fink, J Köhler

Presented by R Jockwer

P Dietsch commented that the COV of different timber products are now over 20 years old and suggested that plans are needed to check these values and update these values for new timber products. R Jockwer agreed.

F Lam commented that structural reliability theory and tools are available but comprehensive database that can correctly characterize both the variability and the underlying distribution form are generally not available for reliability analysis of products commonly used nowadays. This is especially important for connections, components, systems and structures where multiple modes of failure are important and development of verified models would be needed. In cases when extreme loading are encountered better understanding of the loads are needed to correctly characterize the performance as the variability of load could dominate the analysis. R Jockwer agreed.

U Kuhlmann worked on the development of reliability background of Eurocode and supported F Lam's point that the load side and understanding the assumptions behind the load side being important as γ_m influence can be masked by γ_f . Current

proposed modification of γ_f for wind loads under discussion is disadvantageous for both steel and timber structures. We have to be careful as we only know the value for simple structures and try to extrapolate to more practical buildings. R Jockwer agreed in general and development of further knowledge is needed for structures that can be dominated by the load side variability and perhaps how more dead load at the material level can deal with the challenge. U Kuhlmann said that load factors being fixed by others with high influence is a problem. P Dietsch commented that background book for Eurocode EC0 should still be the base and good justification would be needed to make significant changes. He also agreed with F Lam's point of needing data for wind and seismic cases.

S Aicher agreed with U Kuhlmann's points and recommended to look in depth at γ_m for more gains. For example τ consideration with COV of 15% in glulam may be unrealistic and γ_m for LVL and other engineered wood products with low COV should be reconsidered.

A Ceccotti agreed with the concerns; however, k_{mod} of 1.1 for timber for wind is good. R Jockwer said this is a different topic.

TIMBER JOINTS AND FASTENERS

53 - 7 - 1 A Conceptual Model to Predict the Withdrawal Capacity of Screws Inserted Parallel to Grain in Beech, Ash and Spruce - M Westermayr, J W G van de Kuilen

Presented by M Westermayr

R Brandner commented on the difference in measured strength for moisture variation consideration of 9 to 18 %. M Westermayr said this is the source of material. Other test procedures were used for considering moisture content effects where Push-Push tests were used hence lower strengths were measured. In the other tests push-pull tests were used which yielded higher values. R Brandner said that they did not find any test set up influence.

R Brandner asked about shear tests where the shear area is different from the screw case and asked if the difference in shear strengths can be explained by size effects.

M Westermayr said that the failure zone of screw withdrawal would be predetermined hence statistical size effect should not apply. Nevertheless the height of the shear specimen was lower than that specified by EN408 to account for different shear areas.

R Brandner commented that the compression zone in the EN 408 tests should be low and would not influence the shear strength. Also commented that other load directions are much more reliable compared to the parallel to grain direction. P

Dietsch said influence of shear and compression perpendicular to grain should be dependent on level of shear strain reached.

S Winter commented on the minimum penetration distance of screws for end grain application and pondered how should we deal with density variation issues. M Westermayr responded that there are past data regarding minimum penetration distance requirements; however, there are associated practical issues involved. He was surprised by the variation of density even within one laminate. This issue needed further consideration and may be lower effective number of elements should be taken as a conservative approach and that more work is needed.

G Hochreiner stated that stiffness information would be useful with consideration of the geometry of the screws. M Westermayr said the shear strength and withdrawal strength relationship might indicate information for shear modulus which could be considered for stiffness consideration. G Hochreiner commented that the ductility for earthquake application by using large diameter screws might be appropriate. Also if displacement data was available from testing it should be used for stiffness consideration.

S Aicher said influence on screw diameter should be further investigated. Also comparison of this conceptual approach with what has been approved in Switzerland would be important. M Westermayr agreed with the need for comparison and said both screw diameter and insertion length will be investigated further.

A Frangi said that low conservative values were used in Switzerland for this application. Long term behaviour and influence of moisture changes are important. Also in Switzerland a minimum penetration length of 100 mm is required. Finally issues of ductility considerations are interesting.

R Brandner commented that the push-pull test set up used might create unwanted moment which could influence the test results. Also ductility with these screw joints should deal with overstrength design of the screws and put the ductile element somewhere else. M Westermayr agreed.

53 - 7 - 2 FE Modelling of Timber Connections with Inclined and Cross-Wise Arranged Screws - New Findings on Testing the Shear Stiffness - B Azinović, M Frese

Presented by B Azinović

P Dietsch asked what would be the effect of screws not perfectly aligned at the set angle. B Azinovic agreed that this could influence the K_s values.

M Cabrero asked how was the size of the cohesive zone determined. B Azinovic commented that the stiffness of the soft material was assumed to be 5 times lower

than the orthotropic material. Also fracture energy calibration was considered by checking the prediction of initiation of failure against test data.

F Lam questioned whether friction should be relied upon in practice where drying out could create gaps and influence friction. B Azinovic agreed in general but friction could be considered if there was no gaps.

G Hochreiner asked whether the ductility shown in the experimental load slip curve was due to the timber or steel. B Azinovic said timber.

G Hochreiner commented that the gaps in shear plane in practice might result in different stiffness values. He suggested a two stage approach where for serviceability limit state friction could be considered and for ultimate limit state friction should be omitted.

R Brandner commented that fracture zone might be different for different screw insertion angles. He was not sure how the model could deal with this. B Azinovic agreed as the work only dealt with two angles.

J Brown asked if shear tension load arrangements were considered. B Azinovic said it could be done but it was not considered so far.

53 - 7 - 3 Embedding Strength Prediction for European Hardwood Species - T Benistand, L Bleron, J-F Bocquet

Presented by J-F Bocquet

B Azinovic received confirmation that complete data on embedment stiffness is available from their database including different screws types, grain angle and screw diameter.

G Hochreiner asked whether the 5 mm deformation limitation in the standard makes sense for hardwood. J-F Bocquet responded that they are staying with the standard limitation for now. Limitation of the embedment might be related to joint area.

R Brandner asked why assumed normal distribution for density and embedment strength as normal distribution could extend to negative values. He suggested that Lognormal distribution might be better. J-F Bocquet responded that the choice is based on literature and Lognormal distribution fitting was not done.

53 - 7 - 4 Beam-on-Foundation Modelling as an Alternative Design Method for Timber Joints with Dowel-Type Fasteners – Part 4: Joints Subjected to In-Plane Loading - R Lemaître, J-F Bocquet, M Schweigler, T K Bader

Presented by R Lemaître

P Quenneville asked why the evaluation of Kser started from origin and not started from the post cyclic zone. R Lemaître said that there was no initial gaps/clearance in the connection between the steel plate and timber.

P Gronquist asked if the BoF approach was compared with other models and compared the difference between timber and steel. R Lemaître said no this was not done.

E Serrano asked about consideration of coupled and uncoupled springs to model connector behaviour. R Lemaître responded that uncoupled springs were used because comparisons with test results showed good agreement for the embedment behaviour. However the path of the dowel movements between simulations and test results were different. Perhaps coupled springs should be considered.

C Sigrist asked about the power function in the proposal and whether it was possible to determine the power from the model. R Lemaître responded that it was possible by regression approach of the test data one could fit the BoF approach to get the power parameter.

C Sigrist commented that models that can consider axially loaded connectors and K_u would also be needed. R Lemaître responded that past work on 2-D BoF presented in INTER could deal with axially loaded connections. K_u could be estimated from the current approach.

G Hochreiner asked whether out-of-plane bending behaviour could be predicted. R Lemaître responded that this BoF model could work in principle but more work would be needed as the coefficients of the stiffness matrix would need more consideration and input.

53 - 7 - 5 Brittle Failure Mode of Timber Connections with one Row of Fasteners Loaded Parallel-to-grain: a New Model for Splitting Failure - M Yurrita, J M Cabrero

Presented by M Yurrita

R Brandner commented that tension perpendicular to grain strengths needed size effects consideration. M Yurrita responded that size effect was not considered. Based on comparisons with test data the model seemed to be validated. R Brandner commented that data from literature was used and questioned whether the same data set should be used for both model calibration and validation. M Yurrita said yes because of limited availability of data. B Brandner said using the same data set for both calibration and validation explained why good agreements were obtained.

P Dietsch commented that high tension perpendicular to grain strength values were adopted in the model and current design values accepted by standard bodies are low

and will not be changed. M Yurrita responded that long term effects were considered in current conservatively set design values for tension perpendicular to grain and may be other factors can be adjusted in the model to account for the need for the high tensile strength perpendicular to grain values for input.

G Ravenshorst questioned how to arrive at the tension perpendicular to grain stress from loading in the parallel to grain direction. M Yurrita explained that this was a local effect and a factor of 2.1 was obtained in the study for the transformation.

R Jockwer commented that careful consideration of failure modes with combined tension perpendicular to grain and shear stresses is necessary. He also stated that as the tension stress perpendicular to grain stresses were localized, product standard values would not apply. P Dietsch discussed the test volume of specimens for standard tension perpendicular to grain tests relative to connection size.

H Danielsson and M Yurrita discussed application of model based on fracture mechanics which are also species dependent.

A Frangi commented that we wanted to avoid brittle failure so rules are needed on the safe side to ensure brittle failure capacity would be high enough. P Dietsch commented that the current European model are on the safe side, hence implicitly could account for other factors such as shrinkage effects etc.

53 - 7 - 6 Experimental Analysis of Brittle Failure in Timber-to-Steel Connections with Small Diameter Fasteners Loaded Parallel-to-Grain - M Yurrita, J M Cabrero, H J Blaß

Presented by M Yurrita

P Dietsch suggested that work should focus on improving existing models.

F Lam received confirmation that the COV of the data was low and commented that higher COV is expected for brittle wood failure modes. M Yurrita said that the specimens were chosen carefully to avoid major defects in the connections.

P Quenville commented about the assessment of test configuration on the results as the use of short specimens might create a dominant single shear plane that would influence the bottom shear plane.

M Yurrita responded that other tests also showed one shear plane. P Quenville was not sure all models had been developed with consideration of this test configuration. Using test configuration that differed from other research might influence the results. M Yurrita agreed and will examine this issue.

C Sigrist commented on the last slide which showed a big difference between brittle and mixed failure and asked whether this is because of penetration length and

location of shear plane. M Yurrita responded this was not the case in general and showed that the overall data did not have this issue. The last slide showed the difference between two tested materials.

G Fink asked about the conversion of the material properties for Beech LVL from characteristic properties for model input. M Yurrita will look into this further.

A Ceccotti requested that the ductility definite be consistent between static and seismic considerations.

R Brandner stated that Beech LVL properties need many size effect adjustments and asked if this was considered. M Yurrita said this was not done in this study. R Brandner commented further that the depth of LVL and secondary layer effect in LVL would also need to be considered.

53 - 7 - 7 Fatigue Behaviour of Notched Connections for Timber-Concrete-Composite Bridges - S Mönch, U Kuhlmann

Presented by S Mönch

G Montgomery received clarification that the rebar in the test set up had slack and did not influence the test. It was used as a safety measure in case the specimen tipped over. G Montgomery commented that during his testing with CLT/glulam with inclined screws eccentricity was encountered under high load had created tensile stress orthogonal to the loaded direction and split the glulam specimen.

S Aicher commented about the S/N curve comparison between the test results and Eurocode and asked how was the 5th percentile curve obtained from the mean curve based on mean values. S Mönch responded that he used all the data values and performed statistical evaluation to obtain the 5th percentile S/N curve. S Aicher commented the slope of the 5th percentile S/N might be higher for better fit.

G Ravenshorst received confirmation of the load path of the test specimen and the possible failure modes and only compression loads were applied.

P Dietsch commented that the paper should end with clear proposals for implications to standards.

ENVIRONMENTAL CONDITIONS

53 - 11 - 1 Quality Assurance and Design of Timber Structures in Varying Climates - M Schiere, B Franke, S Franke

Presented by M Schiere

P Dietsch asked if the model climate was compared with real climate conditions. M Schiere replied that this was done in the past where Fourier analysis was used that showed 1st amplitude was governing.

S Aicher commented that the simulation of sinusoidal climate disregarded contribution of singular events. Based on his experience singular climate events contribute significantly to damage and should be considered as climatic variation. M Schiere agreed that singular climate events as well as location of timber elements within a building should be considered. S Aicher added that time dependent damage model would be appropriate.

P Dietsch asked about the influence of the laying of screed for floors. M Schiere responded that data showed that it could cause change in relative humidity and temperature experienced by the floor and be treated as a singular climate event.

LAMINATED MEMBERS

53 - 12 - 1 Shrinkage Behaviour of Reinforced Glulam Members - M Danzer, P Dietsch, S Winter

Presented by M Danzer

E Serrano asked about the reverse finding for inclined reinforcement cases of A and B. M Danzer responded that the differential moisture content was not as high for A compared to B and large scatter was found in the results.

R Jockwer commented that use of external reinforcement per Eurocode 5 can slow down moisture diffusion. He asked would you recommend using external reinforcement. M Danzer said that the results would be the same if the time for test were longer. So it would only be a question of time. Moisture transfer speed may be higher in direction of the grain which may be the case if the ends were not sealed. In the end it would be a question of the stiffness of the reinforcement. P Dietsch added the tests were conducted in a slow drying process. In practice more rapid drying condition might exist where external reinforcement might be valuable. S Winter agreed with P Dietsch and stated if we were able to quantify damping effect (relaxation) then external reinforcement would be beneficial.

T Ehrhart stated why would we take it for granted that we have large differential moisture content. Timber should be dried to proper moisture content appropriate to its end use. M Danzer agreed in general if the end use condition was known. P Dietsch agreed that this point is covered in the standard and cost of drying may be a hindering issue. Drying the timber to within 3% moisture content of the expected end use conditions would avoid the problem. S Winter stated that the standard is an

idealized situation. The industry practice during construction, scheduled maintenance of say swimming pools and conditions of long term use of structure would need to be considered as well.

S Aicher stated that the influence of the use of LVL as external reinforcement might be over interpreted. He asked whether the LVL used had any cross bands. Without cross bands the LVL might have been too stiff and could affect the results. P Dietsch confirmed that the LVL had cross bands. S Aicher stated he would refrain from penalizing the external reinforcement technique as based on his experience damping of the drying procedure and relaxation appearing with external reinforcement would be a better way to avoid formation of cracks.

T Ehrhart added that the industry would not know the end use condition of the beams as it should be the responsibility of the engineer to specify the right moisture condition for the beam end use condition.

R Brandner questioned the sampling procedure as only two producers were considered. M Danzer responded that the number of specimen was a question of available space and testing resources, the observed scatter in the data of the specimen was already high and agreed that a larger number of specimens would be better.

53 - 12 -2 Fracture Mechanics Based Design of CLT-plates – Notches at Supports and Half-and-Half Joints - E Serrano, H Danielsson

Presented by E Serrano

P Dietsch and E Serrano discussed scaling of the test specimens in relation to the dimensions of the specimen that one can handle in the lab.

S Aicher stated that the material tested had unusual aspect ratio of the thickness to width of the laminae which could have suppressed rolling shear failures. Typical material would see more rolling shear failure. E Serrano stated that the material was obtained from Swedish industries. He stated that the Rolling shear failure load occurred at a level 3 times of that for the 90 degree orientation; hence, rolling shear failure should not happen in the typical cases. S Aicher said he agreed with the statement for the material tested.

G Hochreiner asked about the combined effect of tension perpendicular to grain and shear strains. E Serrano responded that in the past nonlinear fracture mechanics approach with combined mode were considered. This could handle the combined stress case.

G Hochreiner stated that there might be different effects at the mean and 5th percentile level. E Serrano said that this is an issue of variability as well as codification of the results which have not been investigated here.

P Dietsch quoted S Winter in that a proposal for Eurocode 5 consideration should be submitted by April 2021.

53 - 12 - 3 Prediction of Torsional Stress at In-plane Shear Loading of Cross Laminated Timber - H Danielsson, M Jeleč, E Serrano

Presented by H Danielsson

P Dietsch commented that this work could contribute towards working group 1 for Eurocode 5 on CLT design.

R Tomasi questioned whether model D, which is based on equilibrium, considered different torsional moments through the thickness of the panel. H Danielsson stated that yes and the layup and thickness of the laminae would make a difference. R Tomasi discussed past test results with 3 and 5 layers CLT where internal layer thickness had an effect. H Danielsson said this would agree with the model prediction.

STRUCTURAL STABILITY

53 - 15 - 1 Assessment of Seismic Design Factors and Proposal of Modification to Chilean Seismic Building Design Code (NCH 433) for Mid-Rise Wood Frame Buildings - H Santa María, Á Salinas, J Montaña, J J Ugarte, J L Almazán, P Guindos, A Opazo, F Benedetti, V Rosales, X Estrella, F Guiñez, S Berwart, S Cárcamo, A Jara

Presented by J Montano

D Dolan asked did you only deal with platform frame as he was involved in the design of two balloon frame systems in Chile where lack of proper guidance from code on ductility drove the design towards using of base isolators.

J Montano said that the study did not consider balloon frame construction. D Dolan said that most construction in Chile seemed to be more interested in balloon frame construction. J Montano said survey data showed that platform framing is more popular in Chile.

A Ceccotti asked whether there is a timber design code in Chile dealing with this area. J Montano said there are two codes in Chile related to this. For statics there is a NCH for timber design but it does not cover shear walls. A general design code for seismic design would cover all material including timber. A Ceccotti commented that R factor depends on country structural code and if the code body is very conservative R factor for timber might be very different and more penalizing. D Dolan said R factor of 3 was used for the two buildings that he was involved in. A Ceccotto said R factors should be set for ones' own country.

R Dietsch commented that R factor of 6.5 in the conclusion should be tied to the type of construction and suggested an editorial check for the language of the manuscript.

FIRE

53 - 16 - 1 Fire Design of I-joists in Wall Assemblies - K N Mäger, A Just, T Persson, A Wikner

Presented by K N Mäger

A Frangi asked whether we have the consolidation phase (Phase 4). K N Mäger responded yes. For small rectangular sections we did not have this but for I joist this is possible to be a bit more accurate by adopting a reduced slope. A Frangi commented that Phase 3 is very short. K N Mäger agreed but this is useful for I-Joist considerations. A Frangi asked if the model could be trusted to predict with accuracy one to two minutes differences in view of the complex behaviour. K N Mäger responded that there are difficulties in fire test to take good pictures but the model predicted failure mode is close to reality. Also she is confident with time to failure predictions based on test results comparisons.

BJ Yeh asked why the testing with I joist as wall elements as this application is uncommon in N. America. K N Mäger said in Sweden eight storey buildings have been built with I-joist as wall elements because of thermal efficiency requirements. B J Yeh commented that in the picture showing the loaded confirmation tests wall sheathing should be placed on the fire side (hot side). K N Mäger responded that the configuration came from industry practice.

S Aicher commented that the effective cross section of the I Joist flange might have been too small. This assumption might contribute to the calculated results being too conservative. K N Mäger agreed but decided not to challenge Eurocode values.

F Lam asked about the variability of the full size wall tests with no replicates. K N Mäger agreed but cost of full scale fire tests are high and small specimen fire tests with replications work well.

SERVICEABILITY

53 - 20 - 1 Vibrations of Floors – Comparison of Measured Data and Suggested Design - P Hamm, J Marcroft, T Toratti

Presented by P Hamm

P Dietsch commented that this is an interesting case where standardization work of the working group has concluded while essential related research is still on-going.

S Breneman asked about the open office system with beams spanning 12 m with CLT and whether there would be a difference between beam supported floors or wall supported floors. P Hamm responded that beam supported floors have lower frequencies and more deflection under the 1 kN load. Also that their findings and observations are applicable to both cases.

I Abeysekera asked if the UK Vrms signal was taken over one time step or over the entire signal. P Hamm said over one time step but would need to confirm. I Abeysekera asked about the position of the walker and sensor. P Hamm said sensor was always positioned at centre while walker was positioned at the center for resonance measurements and walker walked around for transient vibration measurements. I Abeysekera questioned whether the test matched calculated mode shape when the walker walked around and discussed the influence of the walker's walking position relative to the geometry of the floor.

P Dietsch asked I Abeysekera as the main investigator of the formulas covered in this paper, if he compared his proposed model with test results and whether Arup has test data. I Abeysekera said that the model was based on mechanistic approach. They have some test results of long floors with CLT on glulam but not for shorter floors.

A Frangi questioned whether so many performance classes needed to be proposed especially when so many of them are deemed unacceptable. He commented that fewer classes maybe less economical but would simplify design and he asked who made the decisions on these classes. P Hamm said that the performance classes should be set by individual countries and based on the information from floors in Germany and UK, a large range of floor performance levels were needed.

TEST METHODS

53 - 21 - 1 Revision of Testing Standards to Determine the Seismic Capacity of Timber Connections According to Eurocode 8 - C Sigrist, D Casagrande, M Piazza

Presented by C Sigrist and D Casagrande

J Dolan commented that he is involved in a test program considering collapse. The results indicated the short period buildings showing higher level of collapse compared to general observed behaviour in real earthquakes. Modeling large displacement greater than $0.8 F_{max}$ as a post peak response would be needed for collapse considerations. He suggested that obtaining information for $0.4 F_{max}$ as a post peak response would be appropriate. C Sigrist responded that there is much information on monotonic tests and the approach to conduct fewer cyclic tests with push out may be appropriate as test methods not only for connections but for components and structures would also be needed. J Dolan added that system behaviour would take over after post peak behaviour and it would be important to model this for collapse.

G Hochreiner stated that inclusion of damping information would be important. C Sigrist responded that this is included via the cyclic tests.

U Kuhlmann said that the thesis of F Bruehl was just finalized dealing with ductility under static loading. Even though this is different from cyclic loading the information may be useful for consideration here and absolute deformation limits would be important. D Casagrande agreed that deformation limitation would need to be considered.

A Ceccotti discussed why reduction of resistance was needed in the standard for consideration.

G Hochreiner agreed that maximum deformation limit would be needed. He also stated that minimum spacing distance for development of plastic behaviour of connections would be needed also. C Sigrist responded that rules for connection spacing requirements are available in standards.

F Lam commented that test protocol should reflect correct failure modes of structures under earthquake excitations. Under the CUREe project cyclic test protocols were developed by considering computer simulations of the behaviour of single degree of freedom systems under different earthquakes. Would this approach be considered here later. D Casagrande said that they are aware of the CUREe protocols and will consider them later. J Dolan commented that the CUREe protocol will be updated to consider large displacements.

P Quenneville asked will this protocol consider supplementary energy dissipative devices. C Sigrist stated that this area should be considered in different work and not here. P Quenneville commented that it is strange that different protocols would be needed for supplementary energy dissipative devices as these should be considered as part of the system. C Sigrist disagreed and D Casagrande said that new Eurocode 8 has plans for a new standard to address this area.

ROBUSTNESS

53 - 22 - 1 Robustness in Tall Timber Buildings - An Improved Framework -
K Voulpiotis, J Köhler, R Jockwer, A Frangi

Presented by K Voulpiotis

P Dietsch asked if the model can differentiate between single cause failures versus systematic failures. K Voulpiotis responded yes this can be done by reduction of strengths in a series of members.

P Dietsch stated that the CLT elements were assumed to act as 2-D plates. In practice mostly 1-D action is available in CLT. K Voulpiotis responded that the 1-D action is not too interesting for the robustness studies. This can be considered easily by changing the a few lines in the computer code. Floor to beam connections are very important.

E Serrano asked when you talked about robustness at different scale there seemed to be no coupling between these scales. If you change one scale how would it impact the analysis? K Voulpiotis responded that it is the combination of scale that make this work more interesting. This is not done yet but can be studied easily with more computer runs.

G Fink stated that in reality member and connection sizes are designed to be slightly over the target. How would you consider this in terms of robustness. K Voulpiotis stated that ultimate limit states were considered to consider the geometry. R Jockwer added that the study aimed to get nominalized rating for robustness and one could assume for over design of member ahead in the model and also consider the precise case for comparison.

U Kuhlmann asked about the direct and indirect consequence definition. K Voulpiotis explained as an example the direct consequence as the area supported by the failure of a column.

ANY OTHER BUSINESS

None

VENUE AND PROGRAMME FOR NEXT MEETING

Due to the uncertainties from the Covid 19 pandemic, the venue for next INTER meeting cannot be definitely settled now. It will either be Chile or Online, coordination with the organizers of WCTE in Chile is needed.

Possible Venue

2021 Chile or Online

2022 Munich

2023 Biel, Switzerland

2024 Shanghai, China

2025 Padua, Italy

2026 Turkey

CLOSE

The Chair thanked the group for their support, participation and attendance of this web-based INTER meeting. He thanked the presenters and participants for their contributions. C Sandhaas, R Görlacher, H Blaß and their team are thanked for hosting the event and creating a functioning Online environment. He thanked R Görlacher for work for INTER throughout the year. He also thanked F Lam for accepting the challenge of taking the minutes and notes for the questions and discussions in this format.

3 INTER Papers, Online Meeting 2020

- 53 - 1 - 1 Review of the Reliability of Timber Structures in the 2020s - R Jockwer, G Fink, J Köhler
- 53 - 7 - 1 A Conceptual Model to Predict the Withdrawal Capacity of Screws Inserted Parallel to Grain in Beech, Ash and Spruce - M Westermayr, J W G van de Kuilen
- 53 - 7 - 2 FE Modelling of Timber Connections with Inclined and Cross-Wise Arranged Screws - New Findings on Testing the Shear Stiffness - B Azinović, M Frese
- 53 - 7 - 3 Embedding Strength Prediction for European Hardwood Species - T Benistand, L Bleron, J-F Bocquet
- 53 - 7 - 4 Beam-on-Foundation Modelling as an Alternative Design Method for Timber Joints with Dowel-Type Fasteners – Part 4: Joints Subjected to In-Plane Loading - R Lemaître, J-F Bocquet, M Schweigler, T K Bader
- 53 - 7 - 5 Brittle Failure Mode of Timber Connections with one Row of Fasteners Loaded Parallel-to-grain: a New Model for Splitting Failure - M Yurrita, J M Cabrero
- 53 - 7 - 6 Experimental Analysis of Brittle Failure in Timber-to-Steel Connections with Small Diameter Fasteners Loaded Parallel-to-Grain - M Yurrita, J M Cabrero, H J Blaß
- 53 - 7 - 7 Fatigue Behaviour of Notched Connections for Timber-Concrete-Composite Bridges - S Mönch, U Kuhlmann
- 53 - 11 - 1 Quality Assurance and Design of Timber Structures in Varying Climates - M Schiere, B Franke, S Franke
- 53 - 12 - 1 Shrinkage Behaviour of Reinforced Glulam Members - M Danzer, P Dietsch, S Winter
- 53 - 12 - 2 Fracture Mechanics Based Design of CLT-plates – Notches at Supports and Half-and-Half Joints - E Serrano, H Danielsson
- 53 - 12 - 3 Prediction of Torsional Stress at In-plane Shear Loading of Cross Laminated Timber - H Danielsson, M Jeleč, E Serrano
- 53 - 15 - 1 Assessment of Seismic Design Factors and Proposal of Modification to Chilean Seismic Building Design Code (NCH 433) for Mid-Rise Wood Frame Buildings - H Santa María, Á Salinas, J Montaña, J J Ugarte, J L Almazán, P Guindos, A Opazo, F Benedetti, V Rosales, X Estrella, F Guiñez, S Berwart, S Cárcamo, A Jara

- 53 - 16 - 1 Fire Design of I-joists in Wall Assemblies - K N Mäger, A Just, T Persson, A Wikner
- 53 - 20 - 1 Vibrations of Floors – Comparison of Measured Data and Suggested Design - P Hamm, J Marcroft, T Toratti
- 53 - 21 - 1 Revision of Testing Standards to Determine the Seismic Capacity of Timber Connections According to Eurocode 8 - C Sigrist, D Casagrande, M Piazza
- 53 - 22 - 1 j kobustness in Tall Timber Buildings
- K Voulpiotis, J Köhler, R Jockwer, A Frangi

Review of the reliability of timber structures in the 2020s

Robert Jockwer, Chalmers University of Technology, Gothenburg, Sweden

Gerhard Fink, Aalto University, Espoo, Finland

Jochen Köhler, NTNU – Norwegian University of Science and Technology, Trondheim, Norway

Keywords: Eurocode 5, Structural reliability, Ductility, Safety, Connections

1 Introduction

1.1 Motivation

In the recent decades there was a strong development in timber engineering leading to the design and construction of more advanced timber structures and buildings. Timber buildings of unprecedented height have been completed all over the world and further technological developments in the fields of material, connections, processing and construction are ongoing. This developments in design, construction and technology needs to be accompanied by a corresponding development of codes and standards in order to maintain the desired reliability of the structures.

In the course of the revision of Eurocodes an Ad-hoc group has been formed as part of CEN/TC 250/SC 10 in order to review and evaluate the theoretical background of the presently implemented safety concept (*CEN/TC250/SC10*, 2018). The group consists of experts of all sub-committees, i.e. all construction materials are represented. For timber structures experts from CEN TC250/SC5 report the experience and future needs for the safety concept of future Eurocode generations based on its implementation in Eurocode 5 (EN 1995:2004 (*CEN*, 2004)).

1.2 Background of design of timber structures

The design rules for timber structures are based on a mixture of experience and reliability theory, whereas the former is dominating.

Based on the design experience from successful structures as well as structural failures, building traditions have been developed. Some of the current design rules, procedures and practice are, to a certain extend, still based on them. Examples are certain details

for simple structures that are prescriptive rather than designed (e.g. the notch depth of step joints) or the common spacing between studs in the framing of wall panels.

A more detailed (and ideally more efficient) design is possible if more detailed knowledge about the load bearing behaviour exists. Material testing is used to evaluate the strength of materials and mechanical models are developed to apply these strength values for the estimation of the load bearing behaviour and capacity of a structural detail or an entire structure. The more refined the mechanical models are and the better the strength of the material is known, the better the load bearing behaviour of a structure can be estimated. Nevertheless, the uncertainties associated to these mechanical and material models have to be understood and considered. Beside the resistances of the structure also the individual loads acting on the structure as well as their joint appearance are subject to specific uncertainties. It might be necessary to treat loads resulting from different sources (e.g. permanent load, imposed load, wind load, snow load) differently.

Good understanding and quantification of the uncertainties associated to the estimation of actions and resistance is essential to estimate the reliability of the structure. This allows to optimise structures with regards to different parameters such as costs or safety and in order to calibrate design codes (e.g. (Köhler *et al.*, 2019)).

1.3 Application of the reliability based safety concept in EN 1995-1-1:2004

A brief introduction into the concept of reliability based code calibration for load and resistance factored design can be found in Köhler, Steiger, *et al.*, 2012.

EN 1995:2004 specifies the design rules for the use of timber and wood based products in structural design. Timber and most of the derivated wood based building products are complex inhomogeneous materials and it cannot be referred to material properties without reference to the corresponding test conditions in terms of loading mode, size, time, surrounding climate, etc. The standard test configurations for structural timber and the relevant engineered wood products are given in EN 408 (CEN, 2010) and reflects to a certain degree the potential application of timber elements of full size dimensions as beams or columns in structures. As discussed in (Fink *et al.*, 2018), material properties are thus defined on an element level, i.e. material properties are defined as the load bearing capacity of timber material specimens of defined size and conditioning and assessed in accordance with an agreed testing procedure (EN 408 (CEN, 2010)). E.g. the tensile strength of timber is not an ultimate stress property of the timber material; it is rather the tensile capacity of the test specimen, divided by the cross section. In contrast to EN 408, ASTM D143 (ASTM, 2014) reflects test methods on small clear specimens and, consequently, the derived properties are not representative for structural applications. This is of particular relevance for structural timber, where the failure usually occurs in areas with significant growth irregularities such as

knots. Despite this dependency on the test method, in EN 1995:2004 the term “material property” is used for simplicity (as in the entire timber engineering profession) as a proxy for the more correct term “properties of standardized test specimen examined under standardized test conditions”. The inaccuracy of this definition of “material property” becomes relevant when deviating in design from the standardized configurations and conditions used in the material testing.

1.3.1 General definition of the design material property of timber

The design value of a material property X_d as defined in Eurocode 0

$$X_d = \eta \frac{X_k}{\gamma_m} \quad (1)$$

is applied in EN 1995:2004 as follows:

$$X_d = k_{mod} \frac{X_k}{\gamma_M} \quad (2)$$

where:

X_k characteristic value of strength property;

γ_M, γ_m partial factor for a material property;

k_{mod} modification factor taking into account the effect of the duration of load and moisture content.

η mean value of the conversion factor taking into account volume and scale effects, effects of moisture and temperature, and any other relevant parameters.

In EN 1995:2004 the factor k_{mod} is used a conversion factor from standardized test load duration and moisture conditions to the anticipated conditions in the structure. Depending on the material property, different additional modification factors should be considered for the determination of the design value of material strength; e.g.:

- Size factors k_h, k_l : As discussed above, the characteristic value of strength is associated to the dimension and configuration of the specimen in the standardized test. If deviating in design from this dimension, the design value of the strength property may be adopted: for members of small heights in bending or tension made of glulam or solid timber the strength may be increased by a factor k_h , whereas for members of any differing height made of LVL the strength should increased or decreased. In addition, for members in tension a length factor k_l should be considered for LVL.
- System factor k_{sys} : The modification and partial factors in Eq. (2) is calibrated for a single component. For structural systems composed of a number of components, where local failure does not directly lead to failure of the entire structure,

the system factor k_{sys} maybe be applied. Examples are floor beams as analysed by Rosowsky and Yu, 2004. However, the system factor does not apply for non-redundant systems where local failure may lead to progressive failure.

- Volume and distribution factors k_{vol} , k_{dis} : The tensile strength perpendicular to the grain of a member is strongly dependent on the stressed volume and the stress distribution (e.g. *Ehlbeck and Kürth*, 1991). For tapered, curved, or cambered beams the factors k_{vol} and k_{dis} consider these effects.

The partial factor for the material property $\gamma_M = \gamma_{Rd} \times \gamma_m$ in Eq. (2) is used for the calculation of the design material property (for which γ_m is specified in Eq. (1)) but covers, e.g. for the case of bending strength of a beam, also the modelling uncertainty of the underlying mechanical model for the derivation of bending strength (γ_{Rd} is foreseen in EN 1990:2002). As long as the underlying mechanical model for the determination of strength and stresses is simple (e.g. for tension parallel to grain and for bending), such a simplification might be acceptable. In cases involving more complex models, such as for instability of members, end-notched beams, or holes in beams, a clear separation in the consideration of the associated uncertainties would be advisable.

1.3.2 General definition of the design resistance

For the design of e.g. connections, not the design value of the material property but the design value of the resistance is used. The design value of the resistance or load-carrying capacity R_d is defined as:

$$R_d = k_{mod} \frac{R_k}{\gamma_M} \quad (3)$$

where:

R_k characteristic value of load-carrying capacity.

The characteristic value of the load-carrying capacity e.g. of a connection according to the European Yield Model (EYM) according to EN 1995:2004 is determined using the respective characteristic values of the strength. In the design equation an additional factor is considered when yielding of the fastener governs the failure, in order to account for the associated lower variability of steel compared to timber (*Blaß and Ehlbeck*, 1998). A clear separation of the sources of uncertainties is clearly necessary, i.e. the partial factor should distinguish between material (through γ_m) and model (through γ_{Rd}) uncertainties. In the final draft "Basis of design and materials" by Project team SC5.T3, 2020, for the revised version of EN 1995 the partial factor for the determination of the design value of resistance in Eq. (3) is denoted γ_R , which follows this strategy.

Table 1. Recommended partial factors γ_M for material properties and resistances

Fundamental combinations	γ_M
Solid timber	1.3
Glued laminated timber LVL, plywood, OSB	1.25 1.2
Connections	1.3
Punched metal plate fasteners	1.25
Accidental combinations	1.0

1.4 Challenges

The universal use of the partial material factor γ_M is illustrated in Tab. 1 from EN 1995:2004, where different partial factors are suggested for both, material properties and resistances.

In timber engineering the resistance is sometimes estimated based on simple mechanical models, as for tension parallel to grain strength, or on extensive mechanical models that include several material properties, as for the estimation of the characteristic load-carrying resistance of dowel-type fastener connections. The simplified definition of the partial factor γ_M in dependency of the material (or connection) type does not account e.g. for potential differences in the resistance models.

EN 1995 is implementing the design concept prescribed by EN 1990 only to a limited extend. For the design of timber structures several factors, that have a considerable impact on the probability of failure, the associated consequences and thus the level of safety, are not consistently considered. Examples are:

- Model uncertainties: for the mechanical model to estimate the material properties as well as the resistance of connections, the model uncertainties are not considered explicitly for individual failure scenarios.
- Failure modes: no differentiation is made with regard to the different failure modes of timber structural elements and the associated different failure behaviour and distribution characteristics.
- Ductility and brittleness: it is not explicitly distinguished between the ductility and brittleness of different failure modes, especially for connections (e.g. splitting of the timber, embedment failure of timber, yielding of the fastener).
- Stiffness and non-linearity: the stiffness of members and a possible non-linear load-deformation behaviour has a considerable impact on the resulting action effects in a structure. Nevertheless, the impact of the variability of the stiffness or non-linearity of the load-deformation behaviour of members and connections is not considered.
- Strength degradation (DOL, fatigue, cyclic load): the empirical evidence on the degradation of the material strength due to the duration of load (DOL), fatigue, or

cyclic loading exists only for basic failure modes (bending, tension) of basic material.

- design assisted by testing: tests may be used to gain further information about the material properties of special products or the resistance models of special elements.
- Influences from moisture content variations: so far only the impact of the mean moisture content on the strength level is considered in EN 1995:2004, however, not the possibility of moisture induced stresses arising from moisture content variations.
- Execution and quality control: the sensitivity of the reliability of a timber structure with regard to precision and quality in execution is not specifically considered though different configurations and details (such as slender elements or bonded connections) are highly dependent on it.
- Expertise and information: It is not distinguished between conventional and specialised structures (e.g. buildings vs. silos, towers & masts); data rich and data scarce situations; existing and new structures.

A selection of the above mentioned aspects are discussed in this paper in more detail. For some of them a more detailed description can be found in (*Köhler and Fink, 2015*).

2 Aspects related to the partial factor for a material property

2.1 Ratio of permanent and variable loads in modern timber structures

A simple design equation according to the load and resistance factor design can be expressed as shown in Eq. (4).

$$z \frac{R_k}{\gamma_M} - \gamma_G G_k - \gamma_Q Q_k \geq 0 \quad (4)$$

The design variable z is to be chosen by the designer to satisfy the condition. The partial factor γ_M , γ_G , and γ_Q for the characteristic value of the resistance (R_k), and the permanent (G_k) and variable loads (Q_k), respectively, can be calibrated for the desired target reliability. Since a variety of different loading scenarios is relevant for design, the limit state equation developed from Eq. (4) may be formulated for the purpose code calibration as follows in a normalized form (denoted by $\hat{\cdot}$) using the random variables of \mathbf{R} , \mathbf{G} , and \mathbf{Q} and an additional model uncertainty \mathbf{X} .

$$g = z \cdot \mathbf{X} \cdot \hat{\mathbf{R}} - (1 - \alpha) \hat{\mathbf{G}} - \alpha \hat{\mathbf{Q}} \quad (5)$$

Where the load ratio $\alpha \in [0.1]$ is a parameter that represents different fractions of permanent and variable loads.

Since the partial factors for the loads are set in EN 1990:2002 for all materials, only γ_M can be calibrated accounting for the specific characteristics of timber structures.

The impact of the coefficient of variation (CoV) of a lognormal distributed resistance \mathbf{R} on a calibrated partial factor γ_M^* is shown in Fig. 1 for a target reliability index $\beta = 4.2$. (Note that the reliability target recommended in EN 1990:2002 is $\beta = 4.7$). In the example the coefficient of variation of the model uncertainty \mathbf{X} was assumed to be 10%. The distribution characteristics of the loads are summarized in Tab. 2.

Table 2. Assumed distribution characteristics of loads.

Prop.	Distribution function	Mean value	CoV	Characteristic value	γ
G	Normal	1	10%	50%	$\gamma_G = 1.35$
Q	Gumbel	1	40%	98%	$\gamma_Q = 1.5$
R	Lognormal	1	variable	5%	-
X	Lognormal	1	10%	-	-

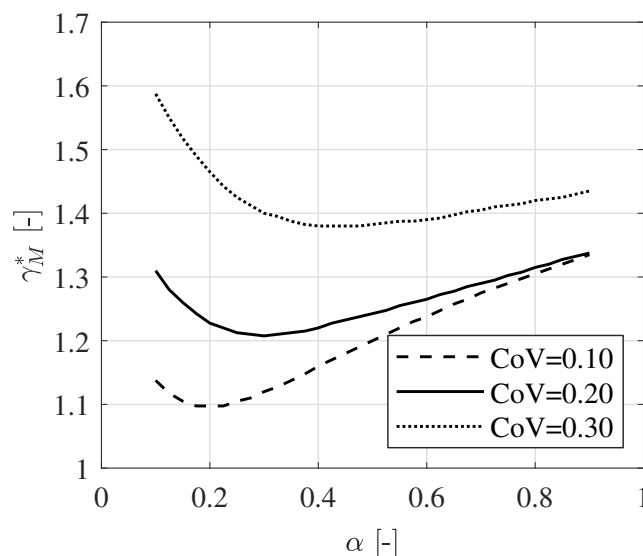


Figure 1. Fitted partial material factors γ_M^* in dependency of load ratio α and variability of the resistance for a target reliability index $\beta = 4.2$.

It can be seen that the calibrated partial factor γ_M^* as shown in Fig. 1 is quite different for different load ratio α and CoV of the resistance. This makes careful generalisation necessary.

Examples of coefficients of variation for different properties of wood based products are summarized in Tab. 3. For bending, and for tension and compression parallel to the grain, the CoV decreases with increasing homogenisation of the material. The CoV of tension and compression perpendicular to the grain is less affected by the homogenisation.

The load ratio α depends mainly on the type of structure whereas the CoV of the resistance is associated to the material, the quality control scheme (grading) and the failure

Table 3. Examples of CoV of the strength properties of structural timber, glulam and the resistance of connections.

Property	Solid Timber ¹⁾	Glulam ¹⁾	Connections
Bending	25%	15%	
Tension parallel to grain	30%	18%	
Compression parallel to grain	20%	12%	
Shear	25%	15%	
Tension perp. to grain	25%	25%	
Compression perp. to grain	10%	10%	
Brittle			≈ 17% ²⁾
Ductile			≈ 5% ²⁾

1) JCSS, 2001

2) Jorissen, 1998

mode. In Köhler, Steiger, et al., 2012 different load ratios for roof trusses, rafters and ceiling beams structures are discussed. For light rafters and ceiling beams common load ratios are $\alpha \gtrsim 0.5$. For these construction types the use of solid timber elements is common.

In contrast to these (traditional) construction types the situations of modern timber structures of tall timber buildings and timber concrete composite floors may be studied. For these construction types wood based products such as glulam or LVL are often used, also engineered wood products made partly or entirely from hardwoods become popular.

For structural elements with a low CoV in resistance, the application in situations with dominating permanent load (i.e. low load ratios α) is most beneficial. Examples can be columns in tall timber buildings made of LVL or ductile connections in heavy roof trusses. In contrast, for structural elements with a high CoV only small changes in the calibrated partial factors occur. A distinction of different structural elements and applications would allow for the following partial factors in Tab. 4.

Table 4. Average calibrated partial factors γ_M^* for different material property characteristics and building types

Dominant load	Example	Expected α	COV = 0.25	COV = 0.15
Variable loads	Traditional floor beam	0.5-0.9	1.32	1.26
Mixed loads	TCC, heavy roofs	0.4-0.7	1.31	1.22
Permanent loads	Columns in tall timber buildings	0.2-0.5	1.29	1.15

2.2 Representative loading cases

The simple loading case of a beam in bending can be chosen as a reference to evaluate the reliability of timber elements. However, due to the anisotropy of the material different structural elements, such as tension members, columns in compression parallel to the grain, or supports in compression perpendicular to grain, will result in different partial factors when aiming at a similar reliability (Köhler, Steiger, et al., 2012). In addition, it has to be considered that different loading situations and the resulting failure

of the structural elements are associated with different consequences of the failure of a structure. Currently, a range of design situation in the reference structure representing 30% bending, 30% shear, 10% axial force, and 30% buckling failure is suggested for the calibration of partial factors (CEN/TC250/SC10/AHG, 2020). In order to allow for a more representative calibration of different modern timber structures this share of design situation should be reviewed and potential other failure modes should be considered, such as ductile or brittle connection failures. In addition, the related model uncertainties have to be reviewed.

In Tab. 5 an overview of different design situations of typical components of structures are summarized. The design criteria are arranged according to the governing source of failure, i.e. the type of fracture or dominating material property. Depending on the geometry and configuration of the different components, either of the design criteria becomes relevant. Even for simple components, a variety of different design situations can be relevant. The source of failure can be parallel or perpendicular to grain fracture, stiffness related failure, or a more ductile failure leading to excessive deformations.

Table 5. Overview of typical design situations of different components

Source of failure	Beam	Column	Connection
Fracture parallel to grain	Bending	Compression par.	Net tension failure
Fracture perp. to grain & shear	Shear		Shearing and splitting (n_{ef})
Stiffness related failure	Lateral Torsion Stability	Stability	
Other	Compression perp.		EYM

2.3 Impact of failure mode on partial factor

In EN 1995:2004 the partial material factor γ_M is defined for the different wood based materials and products as discussed in Section 1.3.1. A distinction between different failure modes in different products and materials is not made. Nevertheless, it is well known and discussed in literature (Köhler, Steiger, et al., 2012), that the different failure modes in materials, such as bending, shear or compression perpendicular to grain, may require different partial material factors in order to achieve a consistent reliability indices due to the differences in distribution characteristics for these failure modes. This issue will be more relevant even for modern wood based materials such as LVL, where certain material characteristics, such as the orthotropy, might be much more pronounced. E.g. calibrating the partial material factors for Beech LVL for the case of bending and applying this parameter in rolling shear or tension perpendicular to grain, might be highly imprecise.

The same is true when analysing the different failure modes in connections, where a variety of different failure modes might occur. Currently a uniform partial material factor γ_M is applied for connections in general, however, additional calibration factors are included in the resistances model of the European yield model for failure modes with plastic hinges in the fasteners. When implementing design rules for brittle fail-

ure modes for connections in EN 1995, which describe fracture in the timber and are based on e.g. shear strength and tension perpendicular to grain material properties, the distinction between partial factors for the different association material properties and resistance models becomes more crucial. Especially failure modes associated to tension perpendicular to grain failure require special consideration compared to the failure modes of the European Yield Model.

3 Aspects related to timber connections

Connections are often the key elements in timber structures and are a frequent cause for failures and damages observed in practice. The interaction of different materials, the variety of different failure mechanisms, and non-linear load-deformation behaviour with different deformation capacity influence the resistance, its variability and the resulting consequences of failure. As discussed in Chapter 1.3, the design of timber members is based on the comparison of design values of stress vs. material strength. In connections in timber structures, the design resistance is used, which is determined using a resistance model and different material strength values. Both these strength values and the resistance model may be source of uncertainties. In addition, there different strength values and resistance models describe failure modes with different load-deformation and failure behaviour. The aspect of failure behaviour is not properly considered for the current version of EN 1995:2004 and will be discussed in the following. For that reason different groups of connections are distinguished.

3.1 Connections with laterally loaded fasteners of small diameter

A first group of connection types, that shall be defined at this point, are those connections made with laterally loaded fasteners of small diameter. Examples are connections with staples or nails. These types of connections were studied e.g. by (*Granholm, 1949*), (*Meyer, 1957*), or (*Mack, 1966*) when describing the resistance and non-linear load-deformation behavior of such connections. The resistance of connections with multiple fasteners n is determined by multiplying the resistance of the single fastener with the effective number of fasteners $n_{ef} \leq n$, which takes into account for the unequal load-distribution between the fasteners and the possibility of brittle failure modes (*Jorissen, 1998*). If the fasteners have sufficient spacing and edge & end distances the risk of brittle failure modes in the timber such as splitting can be reduced.

The resistance of the fasteners in the connection is influenced by the embedding strength of the timber and the yield moment of the fasteners and shows ideally a ductile failure behaviour, that allows for the redistribution of loads between multiple fasteners.

In case the ductile failure behaviour can be achieved, the fasteners can be modelled as resistance elements in a parallel system. The probability of failure $P_{f,sys,parallel}$ of a system of m resistance elements can be estimated according to Eq. (6) where F_j is the

failure of the j 's element (*Faber, 2003*). The resulting probability of failure $P_{f,sys,parallel}$ of this parallel system will be lower than the smallest probability of failure of all individual elements $P(F_j)$.

$$P_{f,sys,parallel} = P\left[\bigcap_{j=1}^m (F_j)\right] \quad (6)$$

Various research has been done to evaluate the influence of the of the different material properties and the corresponding partial material factors (e.g. *Blaß and Ehlbeck, 1998*) or the influence of friction and rope effect (e.g. *Svensson and Munch-Andersen, 2014*). For fasteners with ductile failure in wall diaphragms the resistance according to the EYM may be increased by 20% according to Method A in EN 1995:2004. This increase may be justified by parallel system of resistance elements and the expected resistance increase of friction and rope effect.

3.2 Engineered connections

Another group of connections, that is distinguished at this point, is more divers with regard to fastener types and failure behaviour. Examples are dowelled or bolted connections, connections with bonded-in rods or axially loaded self-tapping screws. Typically, in these connections the resistance of the fasteners is on a similar load level compared to the resistance of the surrounding timber. That means, that the failure mode of the connections depends on the specific configuration and the failure behaviour can be either brittle or ductile. Examples of brittle failure mechanisms in dowelled connections are evaluated e.g. in (*Cabrero and Yurrita, 2018*). If a brittle failure mechanisms occurs or if the ductility is insufficient, the load between different fasteners (or resistance elements) cannot be sufficiently redistributed when approaching the load-carrying capacity.

In case a brittle failure behaviour may be expected, the different resistances of fasteners and timber should be modelled as resistance elements in a serial system. The probability of failure of a serial system can be estimated as follows:

$$P_{f,sys,serial} = P\left[\bigcup_{j=1}^m (F_j)\right] \quad (7)$$

The resulting probability of failure $P_{f,sys,serial}$ of this serial system will be larger than the largest probability of failure of the individual elements $P(F_j)$.

Aiming for a ductile failure mode and designing for sufficient over-strength of the brittle failure mode in such connections enables the load-redistribution between fasteners in a connection as discussed in (*Jockwer et al., 2018*) and allows to account for the lower probability of failure according Eq. (6). Simply designing the characteristic or design

value of the ductile failure mode to be smaller than the brittle failure mode might not be sufficient, due to the associated different variability of the failure modes. A common proposal is to design the 95%-fractile of the resistance of the ductile failure mode to be smaller than the 5%-fractile of the resistance of the brittle failure mode. Probabilities of an occurrence of brittle failure modes $P[R_{brittle} < R_{ductile}]$ in dependency of different over-strength ratios is shown in Tab. 6. The resistances are modelled lognormal distributed with $CoV = 10\%$ and $CoV = 30\%$ for the ductile and brittle resistance, respectively. Such variation may be expected for connections with a ductile failure mode due to yielding of steel and a brittle failure mode due to block shear failure (c.f. Tab. 3).

Table 6. Probabilities of an occurrence of brittle failure modes in dependency of different over-strength ratios for the examples of lognormal distributed ductile ($R_{ductile}$, $CoV = 10\%$) and brittle resistance ($R_{brittle}$, $CoV = 30\%$).

Over-strength ratio	$P[R_{brittle} < R_{ductile}]$
Based on characteristic values	
$R_{brittle,05} = 1.0R_{ductile,05}$	$1.52 \cdot 10^{-1}$
$R_{brittle,05} = 1.5R_{ductile,05}$	$9.74 \cdot 10^{-3}$
$R_{brittle,05} = 2.0R_{ductile,05}$	$5.52 \cdot 10^{-4}$
Based on design values *)	
$R_{brittle,d} = 1.0R_{ductile,d}$	$1.11 \cdot 10^{-2}$
$R_{brittle,d} = 1.5R_{ductile,d}$	$1.64 \cdot 10^{-4}$
Based on fractile values	
$R_{brittle,05} = R_{ductile,50}$	$5.97 \cdot 10^{-2}$
$R_{brittle,05} = R_{ductile,95}$	$1.85 \cdot 10^{-2}$
*) with $\gamma_{ductile} = 1.1$, $\gamma_{brittle} = 1.3$, $k_{mod} = 0.8$	

The probabilities of an occurrence of a brittle failure modes $P[R_{brittle} < R_{ductile}]$ is not directly related to the probability of failure of the connection, but implies that if failure occurs, such failure would be brittle. Hence, it can be discussed which probability of occurrence would be acceptable, a value in the percentage range be a reference.

4 Other aspects

4.1 Mixed failure modes and interaction of stresses

In EN 1995:2004 different interaction criteria for combined bending with tension or compression parallel to the grain are included. These interaction criteria refer mainly to instability issues in case of compression as it occurs in columns prone to buckling or beams prone to lateral torsional instability. However, no complete interaction criterion for different stresses is included in EN 1995:2004 as proposed by e.g. (Van der Put, 1982) or as discussed by (Steiger and Gehri, 2011) for the limited case of the interaction of shear with perpendicular to the grain stresses.

If complex structures and elements, that deviate from the simple straight beam shape, are analysed by means of FEM, such interaction criteria have to be used in order to ac-

count for the potential detrimental effect of interaction of stresses. At the same time, it has to be accounted for the potential change in failure behaviour and distribution characteristics. For example the combination of shear and compresses perpendicular to the grain stresses is dominated by the shear fracture where the compression leads to an effective strength increase whereas in the case of shear and tension perpendicular to the grain it is dominated by the fracture in tension perpendicular to grain with a strong reduction in effective strength.

4.2 Size and configuration dependency of shear strength

The shear strength of a material property can determined according to EN 408 using a compression specimen loading with an inclination of 14° to the grain and characteristic strength value in shear are specified in the corresponding product standards for solid timber (CEN, 2016) or glulam (CEN, 2013). The strength values specified in these product standards are used e.g. for the design of beams in bending, with an interaction of shear and compression perpendicular to grain, but also for the design of notches at beam supports, with an interaction of shear and tension perpendicular to grain. The failure of timber in shear shows a highly brittle behaviour and is dependent on the size of the stressed volume. In loading situations deviating from that in the test of EN 408 the strength values might not be adequate. Such loading situation can occur e.g. in connection, where block shear failure mechanisms can be observed.

4.3 Moisture induced stresses

In (JCSS, 2001) three different types of actions are distinguished:

1. Actions from concentrated or distributed forces acting on the structure are denoted by "load".
2. Actions from imposed displacements or thermal effects in the structure are denoted by "indirect action".
3. Actions from environmental influences which may cause changes with time in the material properties or in the dimensions of a structure.

With regard to the environmental influences acting on timber elements, the moisture content resulting from the relative humidity is amongst the most dominant. The absolute level of moisture content has an impact on the strength of the material whereas changes in moisture content induce dimensional changes of the elements (i.e. swelling and shrinkage). The impact of moisture content on the strength is considered to a certain extend by the modification factor k_{mod} , however, the impact from dimensional changes of the elements is so far not considered. Since timber shows only a minor sensitivity to dimensional changes from thermal effects but rather due to changes in

moisture content, this effect should be considered as an indirect action more specifically.

The swelling and shrinkage of wood has been studied in various research (e.g. Fortino et al., 2009, Angst-Nicollier, 2012). However, so far hardly any adequate models exist for the consideration of swelling and shrinkage in the design of structures. Examples of "best practice" (such as proposed by Dietsch, 2012) can give a hint to the development of more advanced models for design.

5 Conclusions

EN 1995:2004 has implemented the load and resistance factor design concept with partial factors. The partial material factors γ_M for timber can be related to the bending strength of a light structure. In other cases, e.g. when the distribution characteristics of strength or resistance deviate, or where the load characteristics are different, the design solutions obtained with the recommended partial material factors in EN 1995:2004 do not satisfy the target reliability.

In order to achieve efficient structures, that satisfy the target reliability, the source of the uncertainties involved in the design and verification process should be identified and considered, which, so far, is not adequately done in EN 1995:2004 and may lead partly to unnecessary inefficiency, partly to non-conservatism.

Hence, in more advanced structures, the application of the recommended partial material factors from EN 1995:2004 should be treated with care, when considering amongst others the following aspects:

- distribution characteristics of strength and resistance;
- failure mode, failure behaviour and interaction of failure modes;
- model uncertainties in the resistance model;
- environmental impacts and duration of load effects;
- system effects.

Further relevant topics of importance for the evaluation of the reliability of timber structures are e.g.

- the importance of the serviceability limit case in the design of structures;
- the consideration of new wood-based materials (e.g. Beech LVL);
- the integration of (semi)-empirical design equations;
- consideration of hidden safety in the current design regulations.

6 References

- Angst-Nicollier, V. (2012). “Moisture induced stresses in glulam”. PhD thesis. Norwegian University of Science and Technology.
- ASTM (2014). *D143 - 14, Standard Test Methods for Small Clear Specimens of Timber*. ASTM International.
- Blaß, H.J. and J. Ehlbeck (1998). “Simplified design of connections with dowel-type fasteners”. In: *Proc. of CIB-W18 Meeting 31*. Paper No. CIB-W18/31-7-8.
- Cabrero, J. M. and M. Yurrita (2018). “Performance assessment of existing models to predict brittle failure modes of steel-to-timber connections loaded parallel-to-grain with dowel-type fasteners”. In: *Engineering Structures* 171, pp. 895–910. DOI: 10.1016/j.engstruct.2018.03.037.
- CEN (2004). *EN 1995-1-1: Eurocode 5: Design of timber structures - Part 1-1: General - Common rules and rules for buildings*. Bruxelles, Belgium: European Committee for Standardization CEN.
- (2010). *EN 408: Timber structures - Structural timber and glued laminated timber - Determination of some physical and mechanical properties*. Bruxelles, Belgium: European Committee for Standardization CEN.
 - (2013). *EN 14080: Timber structures - Glued laminated timber and glued solid timber - Requirements*. Bruxelles, Belgium: European Committee for Standardization CEN.
 - (2016). *EN 338: Structural timber - Strength classes*. Bruxelles, Belgium: European Committee for Standardization CEN.
- CEN/TC250/SC10 (2018). *N003 SC 10 Decision 13 Ad-Hoc Group on ‘Reliability Background in the Eurocodes’*. Tech. rep. Bruxelles, Belgium: CEN.
- CEN/TC250/SC10/AHG (2020). *‘Reliability Background in the Eurocodes’ (2020): Working draft of Technical Report for the reliability background of Eurocodes*. Tech. rep. Bruxelles, Belgium: CEN.
- Dietsch, P. (2012). “Einsatz und Berechnung von Schubverstärkungen für Brettschicht-holzbauteile”. PhD thesis. Technische Universität München.
- Ehlbeck, J. and J. Kürth (1991). “Influence of Perpendicular-to-Grain Stressed Volume on the Load-Carrying Capacity of Curved and Tapered Glulam Beams”. In: *Proc. of CIB-W18 Meeting 24*. Paper No. CIB-W18/24-12-2.
- Faber, M. H. (2003). *Risk and safety in Civil Engineering. Lecture Notes*. Institute of Structural Engineering, Swiss Federal Institute of Technology, Zurich.
- Fink, G., D. Honfi, J. Köhler, and P. Dietsch (2018). *Basis of design principles for timber structures*. A state-of-the-art report by COST Action FP1402/WG1, Shaker, Germany.
- Fortino, S., F. Mirianon, and T. Toratti (2009). “A 3D moisture-stress FEM analysis for time dependent problems in timber structures”. In: *Mechanics of Time-Dependent Materials* 13, pp. 333–356.
- Granholm, H (1949). *Om sammansatta balkar och pelare med särskild hänsyn till spikade träkonstruktionr.* 88. Gothenburg, Sweden: Chalmers Tekniska Högskola.

- JCSS (2001). *Probabilistic model code*. URL: <http://www.jcss.byg.dtu.dk/>. Joint Committee on Structural Safety.
- Jockwer, R., G. Fink, and J. Köhler (2018). “Assessment of the failure behaviour and reliability of timber connections with multiple dowel-type fasteners”. In: *Engineering Structures* 172, pp. 76–84.
- Jorissen, A. (1998). “Double shear timber connections with dowel type fasteners”. PhD thesis. Delft, The Netherlands: Technische Universiteit Delft.
- Köhler, J. and G. Fink (2015). “Aspects of code based design of timber structures”. In: *Proc. of the 12th International Conference on Applications of Statistics and Probability in Civil Engineering (ICASP12)*. Vancouver, BC.
- Köhler, J., J. D. Sørensen, and M. Baravalle (2019). “Calibration of existing semi-probabilistic design codes”. In: *Proc. of the 13th International Conference on Applications of Statistics and Probability in Civil Engineering (ICASP13)*. Seoul, South Korea.
- Köhler, J., R. Steiger, G. Fink, and R. Jockwer (2012). “Assessment of selected Eurocode based design equations in regard to structural reliability”. In: *Proc. of CIB-W18 Meeting 45*. Paper No. CIB-W18/45-102-1. Växjö, Sweden.
- Mack, J. J. (1966). *The strength and stiffness of nailed joints under short-duration loading*. Div. of forest products technological paper no. 40. Melbourne, Australia: CSIRO.
- Meyer, A. (1957). “Die Tragfähigkeit von Nagelverbindungen bei statischer Belastung”. In: *Holz als Roh-und Werkstoff* 15.2, pp. 96–109.
- Project team SC5.T3 (2020). “N 1244: Basis of design and materials, Sub-task 8, Final draft”. In: *CEN/TC 250/SC 5*.
- Rosowsky, D.V. and G. Yu (2004). “Partial factor approach to repetitive-member system factors”. In: *Journal of Structural Engineering* 130.11, pp. 1829–1841. DOI: 10.1061/(ASCE)0733-9445(2004)130:11(1829).
- Steiger, R. and E. Gehri (2011). “Interaction of shear stresses and stresses perpendicular to the grain”. In: *Proc. of CIB-W18 Meeting 44*. Paper No. CIB-W18/44-6-2.
- Svensson, S. and J. Munch-Andersen (2014). “Study of the Rope-effect on the Load-carrying Capacity of Nailed Connections”. In: *Proc. of INTER Meeting 47*. Paper No. INTER/47-7-4.
- Van der Put, T.A.C.M. (1982). “A general failure criterion for wood”. In: *IUFRO Timber engineering group meeting*, pp. 323–342.

Discussion

The paper was presented by R Jockwer

P Dietsch commented that the COV of different timber products are now over 20 years old and suggested that plans are needed to check these values and update these values for new timber products. R Jockwer agreed.

F Lam commented that structural reliability theory and tools are available but comprehensive database that can correctly characterize both the variability and the underlying distribution form are generally not available for reliability analysis of products commonly used nowadays. This is especially important for connections, components, systems and structures where multiple modes of failure are important and development of verified models would be needed. In cases when extreme loading are encountered better understanding of the loads are needed to correctly characterize the performance as the variability of load could dominate the analysis. R Jockwer agreed.

U Kuhlmann worked on the development of reliability background of Eurocode and supported F Lam's point that the load side and understanding the assumptions behind the load side being important as γ_m influence can be masked by γ_f . Current proposed modification of γ_f for wind loads under discussion is disadvantageous for both steel and timber structures. We have to be careful as we only know the value for simple structures and try to extrapolate to more practical buildings. R Jockwer agreed in general and development of further knowledge is needed for structures that can be dominated by the load side variability and perhaps how more dead load at the material level can deal with the challenge. U Kuhlmann said that load factors being fixed by others with high influence is a problem. P Dietsch commented that background book for Eurocode EC0 should still be the base and good justification would be needed to make significant changes. He also agreed with F Lam's point of needing data for wind and seismic cases.

S Aicher agreed with U Kuhlmann's points and recommended to look in depth at γ_m for more gains. For example τ consideration with COV of 15% in glulam may be unrealistic and γ_m for LVL and other engineered wood products with low COV should be reconsidered.

A Ceccotti agreed with the concerns; however, k_{mod} of 1.1 for timber for wind is good. R Jockwer said this is a different topic.

A Conceptual Model to Predict the Withdrawal Capacity of Screws Inserted Parallel to Grain in Beech, Ash and Spruce

Maximilian Westermayr, Technical University of Munich, Professorship of Wood Technology, Munich, Germany

Jan Willem van de Kuilen, Technical University of Munich, Professorship of Wood Technology, Munich, Germany; Delft University of Technology, Biobased Structures and Materials, Delft, The Netherlands

Keywords: screw withdrawal, shear strength, angle between screw axis and grain direction, moisture content, screw type, density variation

1 Introduction

In addition to the wooden components, like cross laminated timber or glued laminated timber, connections are key requirements for the design of safe and efficient timber structures. A big variety of fasteners, such as bolts, nails or glued-in rods are available to join the components in timber structures. Further well-known and frequently used fasteners in timber construction are screws, which allow simple installation and often provide economic solutions.

The load-bearing mechanism of a screw is governed by the angle between the screw axis and the applied load as well as the screw axis and the angle with the wood fibre. If a screw is loaded along its axis, either screw withdrawal or steel tensile failure are the possible failure modes. Focusing on withdrawal failure, the pull-out property of a screw depends, amongst others, on the angle between screw axis and grain direction of the penetrated timber component. The European standard for the design of timber structures EN 1995-1-1:2010 (in the following “EC5”) as well as many technical approvals of screws only allow the design of screws for angles $\geq 30^\circ$ between screw axis and grain direction. An explanation for the given limitation may be that research mainly focused on the performance of screws inserted with angles $\geq 30^\circ$ between screw axis and grain direction. With the investigations of Blaß et al. (2006), Hübner (2013), Ringhofer (2017), Brandner et al. (2019a) and Jockwer (2019), just some of the studies are mentioned which dealt with the withdrawal behaviour of screws. However, the mechanisms behind the load carrying capacity of screws applied with small angles between screw axis and grain direction appears to be complex and not entirely understood.

For screws applied in grain direction, the influence of density variations appears to be much higher than for screws applied with an angle between screw axis and grain direction, as it will be shown in this study. A possible density variation parallel to the grain may lead to a higher inaccuracy of density related models predicting the withdrawal capacity, as these models are generally calibrated on the local density measured in the vicinity of the screw, but the design models are based on the characteristic density of the entire structural component. This aspect introduces the content of this study. In a first step, drill cores were extracted from spruce and beech board segments in and perpendicular to grain direction to determine the density variations in the two prime orthotropic directions, longitudinal and perpendicular. As the density variation in longitudinal direction can be considerable and the failure of parallel to grain loaded screws shows a very local shear failure around the outer screw thread, withdrawal and shear tests were performed on the same material and checked for their relation. Further, possible influences on the withdrawal strength resulting from the timber component as well as possible influences resulting from the screw were examined. Finally, conceptual approaches are presented to predict the withdrawal capacity of screws loaded with low angles between screw axis and grain direction.

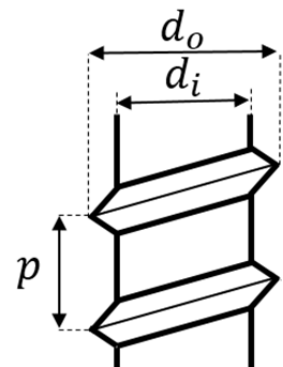
2 Materials and Methods

2.1 Materials

This study includes the three species beech (*Fagus s.*), ash (*Fraxinus e.*) and spruce (*Picea a.*). Origin of the beech and ash timber was Central Germany and origin of the spruce timber was Czech Republic. Some of the spruce boards had an increased proportion of compression wood and pitch pockets. All specimens were produced using a PVAc adhesive with increased moisture resistance according to the manufacturers' specifications. Except for the investigation regarding different screw types (*Types 1-5*), the same screw (*Type 6*) was used for all other parts of this study. The screw *Type 6* is a self-drilling structural screw, representing a common screw applied in timber construction. The six screws are from four different manufacturers and were chosen according to their differences in thread geometry and shape of the tip. Table 1 summarizes the thread properties of the applied screws.

Table 1. Thread properties of the screws applied in this study.

	Type1	Type2	Type3	Type4	Type5	Type6
d_o [mm]	10.0	10.0	10.0	10.0	10.0	11.0
d_i [mm]	6.4	6.2	6.3	6.0	6.5	6.6
d_i/d_o [-]	0.64	0.62	0.63	0.60	0.65	0.60
p [mm]	5.5	4.6	6.6	5.1	4.8	5.8
p/d_o [-]	0.55	0.46	0.66	0.51	0.48	0.53



The thread properties are mean values gained from five measuring points of 10 randomly selected screws of each screw type.

2.2 Methods

2.2.1 Density variation

Drill cores with a diameter of 10 mm and a length of 50 mm were removed from 40 beech and 40 spruce sections ("section" is defined in chapter 2.2.2/Figure 2) to determine the local density variation depending on the wood anatomical direction. The size of the drill cores represent the screw diameters and screw insertion lengths applied in the withdrawal tests of this study. Three drill cores were removed in grain and three drill cores were removed perpendicular to grain direction from each section as illustrated in Figure 1. The sawing pattern of the sections was typical for the application in glued laminated timber and thus mainly led to 90°-drill cores with tangential or mixed tangential-radial direction.

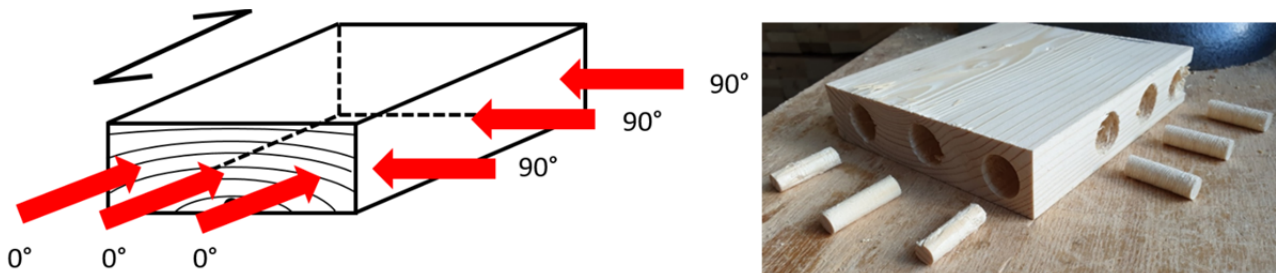


Figure 1. Illustration of the drill core removal for density determination.

The distance between the drill cores was 40 mm. The wood moisture content of the drill cores was determined by oven dry method according to EN 13183-1:2002 and density was determined by performing buoyancy method and adjustment to a reference moisture content of 12% according to EN 384:2019.

2.2.2 Shear and withdrawal specimen production

The study can be divided into four major test groups, which will be explained in detail later in this chapter. For all of these four groups, the same basic logic of specimen production in form of matched samples was applied, as visualized in Figure 2.

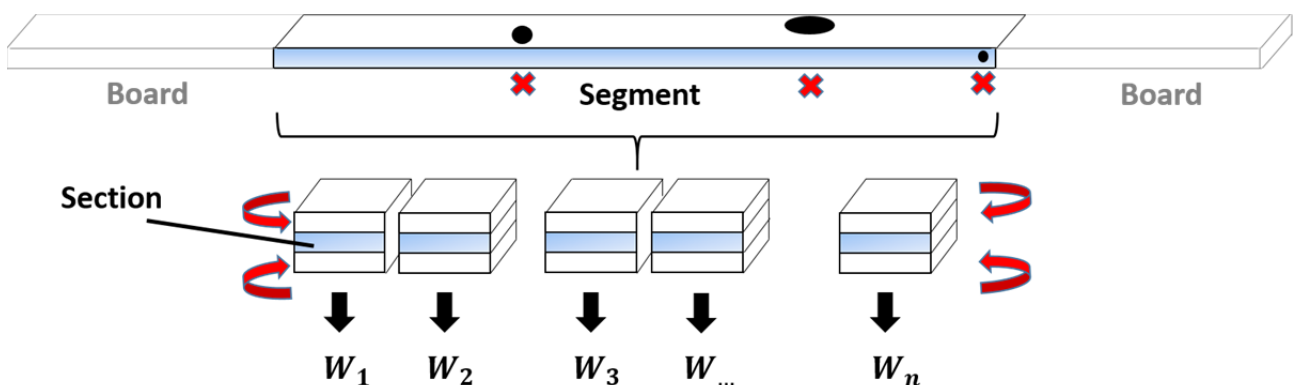


Figure 2. Withdrawal specimen production process (matched samples). W =Withdrawal specimen

At first, a segment with a low amount of wood defects was chosen and cut from the raw material in form of boards. Always just one segment was cut from each board. The remaining obvious wood defects in each segment like knots or pitch pockets

were cut out as well and the segments were divided in further small sections. The sections were glued with additional timber boards on both sides to obtain a bigger cross section for avoiding splitting during test procedure and to exclude effects from a too narrow spacing. After curing of the adhesive, all specimens were cut to their final length and predrilled with the core diameter of the applied screw. The length of the predrilled channel was measured immediately before screw insertion with a digital calliper. The tips of all screws were protruding.

Directly after withdrawal testing, a small sample was extracted from each specimen next to the screw channel to determine the wood moisture content by oven dry method according to EN 13183-1:2002 and density with buoyancy method. Densities were adjusted to a reference moisture content of 12% according to EN 384:2019.

Specific variations of this basic specimen production process with regard to the four major test groups are explained in the following.

2.2.2.1 Relation of strength values gained by shear and withdrawal tests

Referring to Figure 2, one withdrawal specimen W_1 as well as two shear specimens S_1 and S_2 were produced from one segment. For this, the segments were cut in longitudinal direction, as shown in Figure 3.



Figure 3. Shear (S) tests and withdrawal (W) tests performed on the same raw material.

Two different types of shear specimens were produced. On the one hand standard shear specimens according to EN 408:2012 (in the following “EN 408”), on the other hand modified EN 408-specimens with a groove to reduce the shear plane (in the following “EN 408mod”) as it is shown in Figure 3 on the very left. The EN 408mod specimens had a width of 10 mm and a height of 15 mm in the reduced, grooved plane, leading to a shear area of $\sim 3000 \text{ mm}^2$. As thicker steel plates are required for shear testing of hardwood species, all specimens but also including spruce were produced using 20 mm thick steel plates. The shear specimens were glued onto the steel plates with an epoxy resin according to the manufacturers’ specifications. The corresponding withdrawal specimens had a screw insertion length l_{eff} of $\sim 75 \text{ mm}$, leading to a shear area of $\sim 2592 \text{ mm}^2$ by using a screw with $d_o = 11 \text{ mm}$. As a result, the shear areas of the EN 408mod and withdrawal specimens were on a comparable level. The withdrawal tests were performed with a push-pull test setup.

2.2.2.2 Influence of moisture content (MC) on the withdrawal strength of beech

Referring to Figure 2, four withdrawal specimens $W_1 - W_4$ were produced from each segment. First of all, the sections for the later specimens $W_1 - W_4$ were stored in four different relative air humidity conditions of 40, 65, 75 and 85 %rh and a constant temperature of 20 °C. When constant mass was reached according to EN 318:2002, the sections were immediately joined with the two timber pieces, were cut to length and predrilled. The screw was inserted and the tip was cut off, which was necessary for the push-push testing. The screws were inserted on a length of $l_{eff} \sim 60$ mm.

2.2.2.3 Influence of the screw axis-to-grain angle on the withdrawal strength

Beech and spruce segments were chosen, which appeared visually straight grained. The global grain angle of each beech segment was then determined using a 10 mm grid in longitudinal direction with help of the method described in Ehrhart et al. (2018), using the orientation of the wood rays. This process is shown in Figure 4.

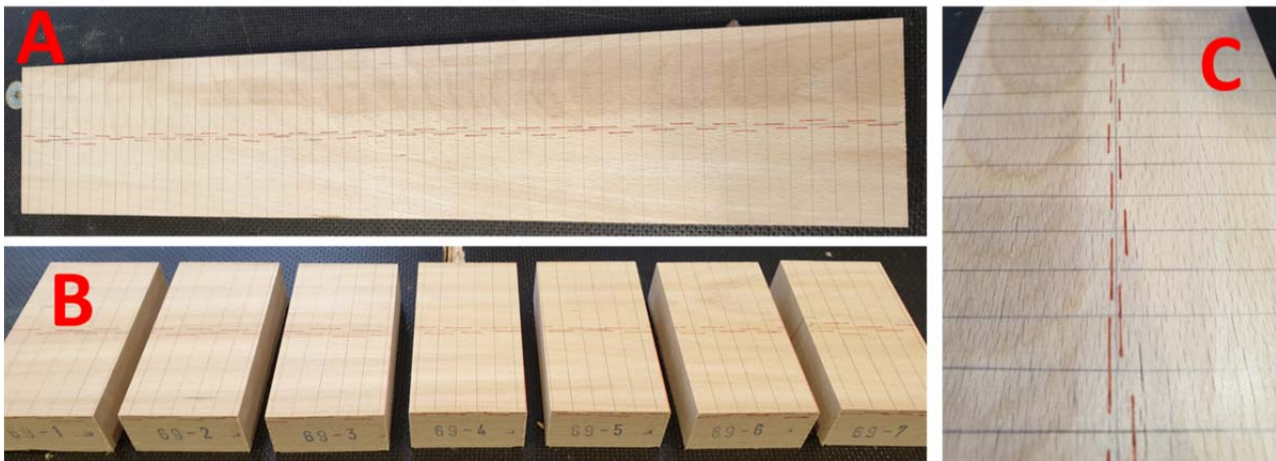


Figure 4. Measurement of global fiber angle on segment (A) and section (B). Zoom of the grid (C), the wood ray orientation is marked by the red lines.

The grain direction of spruce was assessed according to DIN 4074-1:2012. The segments were subsequently cut to sections and the sections were processed to raw specimens. The raw specimens were then cut according to their grain angle to nine specimens $W_1 - W_9$ with a mitre saw to the intended grain angles of 0°, 5°, 10°, 15°, 20°, 25°, 30°, 45° and 90°. The tests were executed using the push-pull test method.

2.2.2.4 Influence of different tip geometries on the withdrawal strength

The influence of tip geometries of five different screws were examined using beech and spruce timber. Consequently, five specimens $W_1 - W_5$ were produced from each segment. In a first step, the screw with tip was inserted into the specimen and a push-pull test was performed. Directly afterwards, the screw with tip was removed and a screw with cut-off tip was inserted into the same specimen and the push-pull test was repeated. The idea behind this approach was to investigate the influence of different tip shapes developing different degrees of pre-damage during screw insertion process. To enable insertion of screws without tip, a screw with tip was used to

cut the first 2-3 thread turns. The screw with tip was then removed and the screw without tip was installed. The distance between the two screw channels of the screw with and without tip was $3d_o$, the distance to the edge of the specimen at least $2.5d_o$. The screws were inserted over a length of $l_{eff} \sim 50\text{mm}$. For testing screws with and without tip, pilot holes with d_c were used.

2.2.3 Test execution

In total, three different test methods were applied for the determination of mechanical properties, one shear test method and two withdrawal test methods.

The shear tests were performed according to EN 408:2012 using a universal testing machine with constant traverse speed. The shear strength was calculated as follows:

$$f_v = \frac{F_{max} \cos 14^\circ}{lb}$$

The push-pull withdrawal tests were performed following EN 1382:2016. The push-push withdrawal tests were performed force controlled with a constant increase of the load. The design of the test stand followed the push-push configuration described in Blaß et al. (2006). The withdrawal strength was calculated according to the following expression.

$$f_{ax} = \frac{F_{max}}{d_o \pi l_{eff}}$$

After testing, each specimen was checked for wood defects around the screw channel as well as the failure pattern. Outlier values in the later data analysis were only excluded if they were obviously caused by visually detectable wood defects like knots or failure in the glue line concerning the shear specimens. Characteristic values of mechanical properties were calculated according to EN 14358:2016.

3 Results and Discussion

3.1 Density variation

This chapter gives an impression about the density variation in spruce and beech timber depending on the wood anatomical direction. Figure 5 shows the cumulative frequency distributions of the density variations of the drill cores of the 40 examined beech and spruce sections.

Figure 5 on the left shows on the x-axis the mean COV of the three drill core sample densities within one section for the beech and spruce and the 0° and 90° samples separately, representing the density variation within one section. Figure 5 on the right shows the maximum density variation in kg/m^3 resulting from the difference of the drill cores with the highest and the lowest density of the three drill cores within each section for each species and anatomical direction.

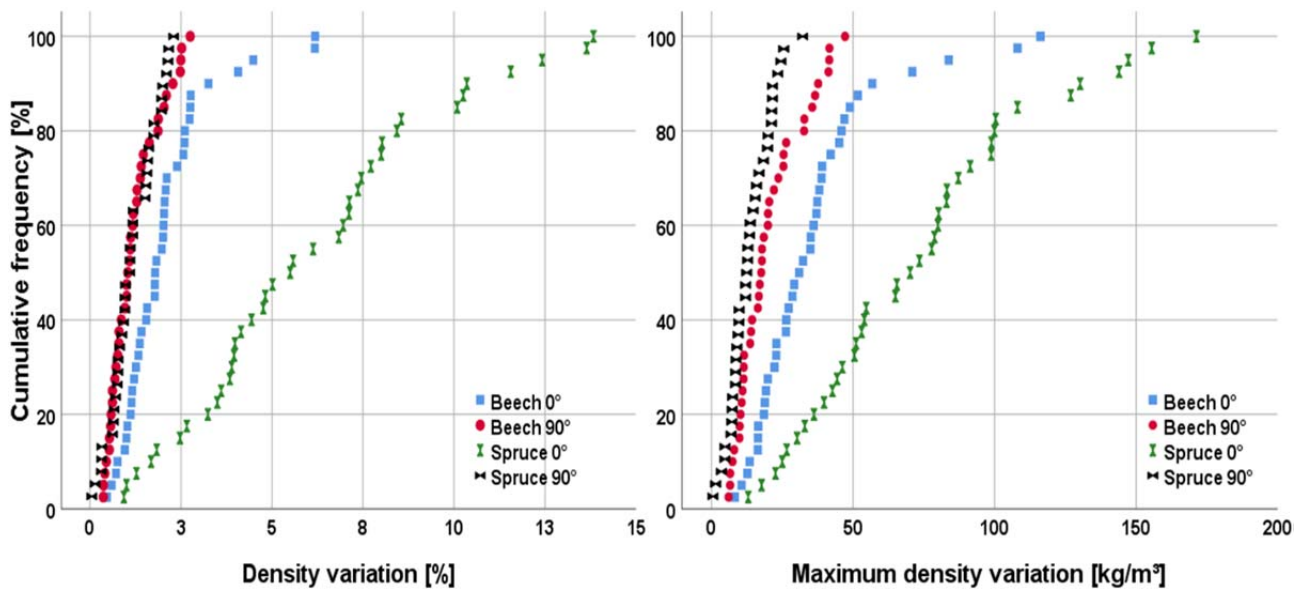


Figure 5. Density variations depending on the species and anatomical direction.

The density variation is higher in grain direction compared to the density variation perpendicular to grain direction for both species. Concentrating on Figure 5 on the left, the mean COV of the drill cores of the perpendicular to grain samples is relatively low with 1.2% for beech and 1.2% for spruce as well. In contrast, the mean COVs of the parallel to grain samples are 2.1 % for beech and 6.1 % for spruce.

The mentioned trend becomes even clearer when focusing on the absolute maximum density variation in kg/m^3 shown in Figure 5 on the right. The maximum density variation parallel to grain is significantly higher than perpendicular to grain direction. The mean maximum density variations perpendicular to the grain are 13.4 kg/m^3 for spruce and 20.3 kg/m^3 for beech. The maximum density variations parallel to the grain are 36.4 kg/m^3 for beech and 73.8 kg/m^3 for spruce. The maximum difference in density between two drill cores from the same section regarding perpendicular direction and spruce is 171 kg/m^3 .

Density calibrated prediction models may consequently be less reliable for the calculation of the withdrawal capacity of parallel to grain inserted screws, than for screws applied with an angle between screw axis and grain direction. For example a glued laminated timber beam of a high strength class would lead to a relatively high withdrawal capacity, although local variation in density is high in longitudinal direction and would thus probably lead to a high scatter in actual withdrawal capacities. This may also affect the load carrying capacity of screw groups by unequal load distribution between the single screws.

Screws applied with an angle between screw axis and grain direction always penetrate a number of growth rings, which thus leads to a compensation of zones with low density, resulting in a more or less homogeneous density level. The density may get more homogeneous, the more growth rings are penetrated, which is especially the case in radial direction. In contrast to that, parallel to grain inserted screws are

oriented along the growth rings which may be growth rings with either very high local density (e.g. narrow growth rings in softwood, compression wood) or very low local density (e.g. large growth rings, juvenile wood). The smaller the d_o of the parallel to grain applied screw, the bigger may be the expected scatter in load carrying capacity as a result of density variations.

With the background of a high scatter in densities parallel to the grain, a density related approach to calculate the withdrawal capacity with a positive correlation of strength (class) and density should be discussed. The application of a conservative, constant density or shear strength level for the calculation of the withdrawal design capacity of parallel to grain inserted screws independent of the strength class of the component may be on the safe side.

3.2 Relation of strength values gained by shear and withdrawal tests

As shown in the previous chapter, the density may show a considerably high variation in grain direction. Additionally, a very local shear failure was observed around d_o for screws loaded in grain direction. This leads to the assumption, that the withdrawal capacity may be calculated with the shear strength of the timber. In consequence, withdrawal and shear specimens were produced using the same sections of the species beech, spruce and ash. The obtained strength values for the different test methods and species are shown in Figure 6.

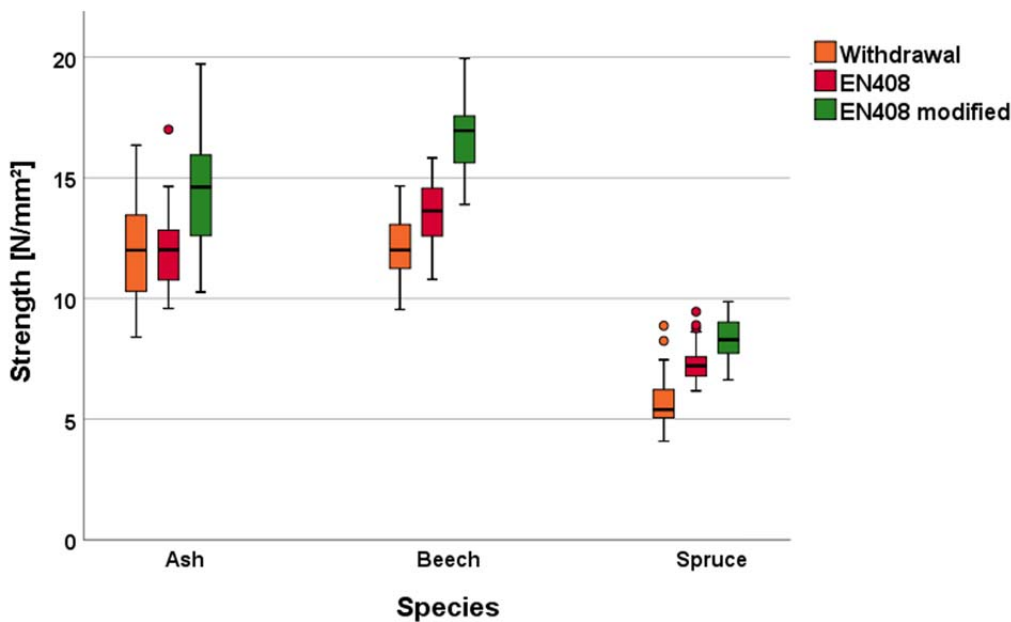


Figure 6. Strength values obtained from withdrawal and shear tests for ash, beech and spruce.

The mean shear strength values obtained by the withdrawal test method and the EN 408 test method are on comparable level with the EN 408 strength values on a slightly higher level. Although the shear areas in the withdrawal and in the EN 408mod specimens were similar, the EN 408mod specimens reached a significantly higher mean shear strength. Table 2 summarizes some statistical properties.

Table 2. Statistical properties for each species and each test method.

		Ash			Beech			Spruce		
		Withdrawal	EN408	EN408 Mod	Withdrawal	EN408	EN408 Mod	Withdrawal	EN408	EN408 mod
n		31	29	31	30	28	30	30	30	30
Strength [N/mm ²]	mean	12.0	11.9	14.5	12.1	13.6	16.7	5.7	7.3	8.3
	COV	17	13	17	10	9	8	18	11	10
	5% fv	8.3	9.0	9.9	9.9	11.4	14.3	3.8	5.9	6.7
Density [kg/m ³]	mean	610			708			489		
	COV	12			5			9		
MC [%]	mean	8.2			8.2			9.1		

The groove in the EN 408mod specimens leads to a higher shear strength compared to the standard EN 408 specimens, which might be attributed to higher perpendicular to grain stresses in the reduced specimen area as well as size effects. Consequently, the identified size effect of spruce is compared with a literature analysis given in Brandner et al. (2012) examining the role of different geometrical characteristics on the shear strength of spruce solid and glued laminated timber. The best match between measured data of this study and the calculated size effect according to Brandner et al. (2012) was derived considering the shear area A_s of the right censored spruce solid timber dataset (p.5). On a reference moisture content level of 12 %, the mean calculated shear strength of 8.1 N/mm² and 9.3 N/mm² are somewhat higher than the measured mean shear strength of 6.7 N/mm² and 7.6 N/mm² for the EN 408 and the EN 408mod specimens respectively. However, the delta in shear strength caused by the two different shear areas of the EN 408 and the EN 408mod specimens seems reasonable according to the above-mentioned study. On characteristic level, the following quotients of withdrawal to EN408 shear strength $\frac{f_{k,Withdrawal}}{f_{k,408}}$ were calculated from the data given in Table 2:

Ash: 0.92; Beech: 0.87; Spruce: 0.65

These ratios may allow the calculation of the withdrawal capacity based on the used reference screw geometry ($d_o=11\text{mm}$; $l_{eff}=75\text{ mm}$) from EN 408 shear strength.

3.3 Influence of the moisture content on the withdrawal strength of beech

The withdrawal strength of screws in beech timber was examined for different air humidity levels, as corresponding data exist already for spruce and ash. The beech specimens were stored at 20 °C and 40, 65, 75 and 85% rh until constant mass was reached, resulting in mean wood moisture contents of 9.0, 11.8, 14.1 and 18.2% respectively. The relation between the wood moisture contents and the withdrawal strength values is shown in Figure 7. A reason for the generally lower withdrawal strength values in this chapter compared to the strength values given for example in chapter 3.2 is presumed in the applied test method. The push-push test method applied in this chapter may lead to a slightly different stress distribution along the screw

within the wooden component initiating an earlier failure compared to the push-pull test method applied in the other parts of this study.

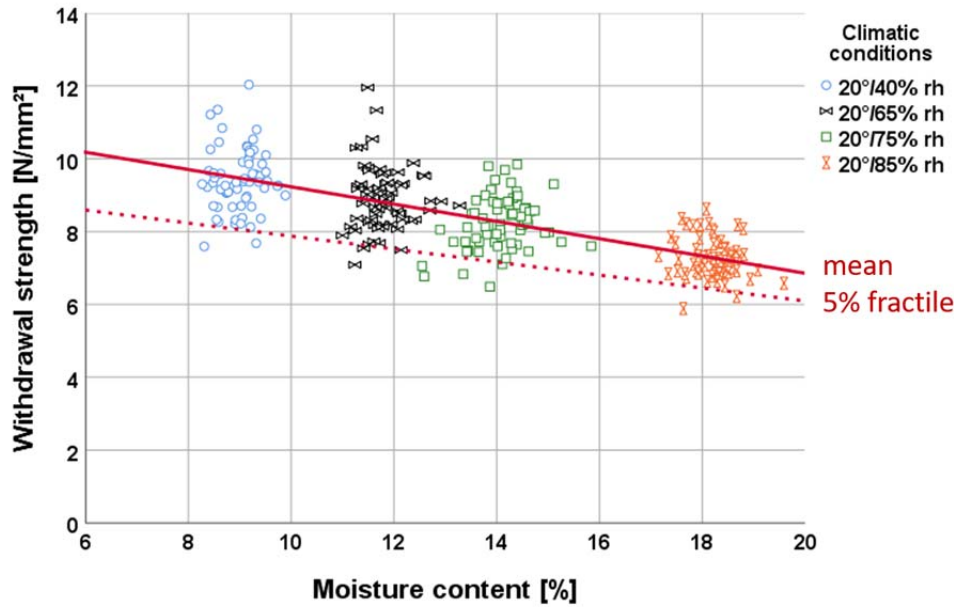


Figure 7. Relation of wood moisture content and withdrawal strength for beech timber.

The red solid line in Figure 7 shows the relation of the mean moisture content of the four groups and the corresponding mean withdrawal strength values using linear fit. The dashed red line correlates the mean moisture contents of the four groups with the characteristic withdrawal strength values. Regression analysis led to R^2 -values of 1.00 on mean and 0.95 on characteristic level for linear model calculation. The main statistical data are compiled in Table 3.

Table 3. Strength, wood moisture and density properties depending on the climatic conditions.

		20°/40%	20°/65%	20°/75%	20°/85%
n		66	66	67	67
Strength [N/mm ²]	mean	9.4	8.9	8.2	7.3
	COV	9	10	9	7
	5% fv	8.2	7.6	6.9	6.5
MC [%]	mean	9.0	11.8	14.1	18.2
	COV	4	4	4	2
Density [kg/m ³]	mean	717	714	713	710
	COV	5	5	5	5

The linear relation yields a decrease in withdrawal strength of 2.5 % on mean and a decrease in withdrawal strength of 2.2 % on characteristic level for 1 % increase of wood moisture content. This strength reducing effect can be expressed by the following moisture content modification factor k_{mc} .

$$k_{mc,mean} = 1.00 - 0.025 * (u - 12) \text{ for } 9\% \leq u \leq 18\%$$

$$k_{mc,k} = 1.00 - 0.022 * (u - 12) \text{ for } 9\% \leq u \leq 18\%$$

A similar decrease of the withdrawal strength of 2.7% for 1% increase in moisture content was found by Hübner (2013) for ash. For spruce, Ringhofer et al. (2014) reported a plateau level with no change in withdrawal strength between 8% and 12% moisture content and a decrease in withdrawal strength of 3.6% per 1% increase in moisture content between 12% and 20% wood moisture content.

3.4 Influence of the screw axis-to-grain angle on the withdrawal strength

Withdrawal tests were performed on beech and spruce specimens with angles between screw axis and grain direction between 0° and 90°. The following Figure 8 shows the relation of the angle between screw axis and grain direction and the corresponding withdrawal strength values for the species beech.

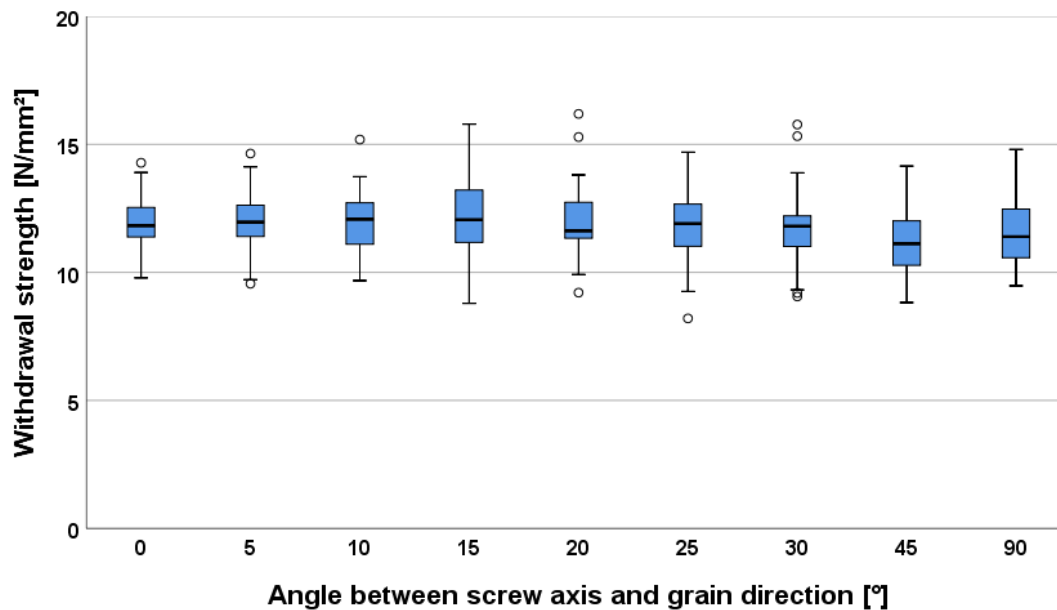


Figure 8. Relation between screw axis-to-grain angle and withdrawal strength for beech.

The species beech shows homogeneous strength values independent of the screw axis-to-grain angle. Further, the variation in strength properties are quite similar for the investigated angles which is also confirmed by the statistical data given in Table 4. In contrast, the study of Schilling (2017) shows minimum withdrawal strength values for 0° loaded screws in beech compared to higher angles, although specimen numbers were quite inhomogeneous for the different screw axis-to grain angle groups.

Table 4. Mechanical properties in dependence of the screw axis-to-grain angle for the species beech.

		0°	5°	10°	15°	20°	25°	30°	45°	90°
n		40	40	40	40	40	40	40	40	40
Strength [N/mm ²]	mean	12.0	12.0	12.0	12.2	12.0	11.7	11.8	11.2	11.5
	COV	9	10	9	12	11	12	12	11	10
	5% fv	10.1	9.7	10.2	9.5	9.9	9.3	9.2	9.1	9.9
Density [kg/m ³]	mean	714	715	716	716	713	714	715	716	706
	COV	5	6	5	5	5	6	6	6	6
MC [%]	mean	8.8	8.8	8.9	8.8	8.8	8.5	8.6	8.6	9

Figure 9 shows the mean and characteristic withdrawal strength values for each screw axis-to-grain angle group of the species beech. The red and blue graphs illustrate the linear function fitting mean and characteristic values. The red and blue dashed graphs mark the overall mean and characteristic strength.

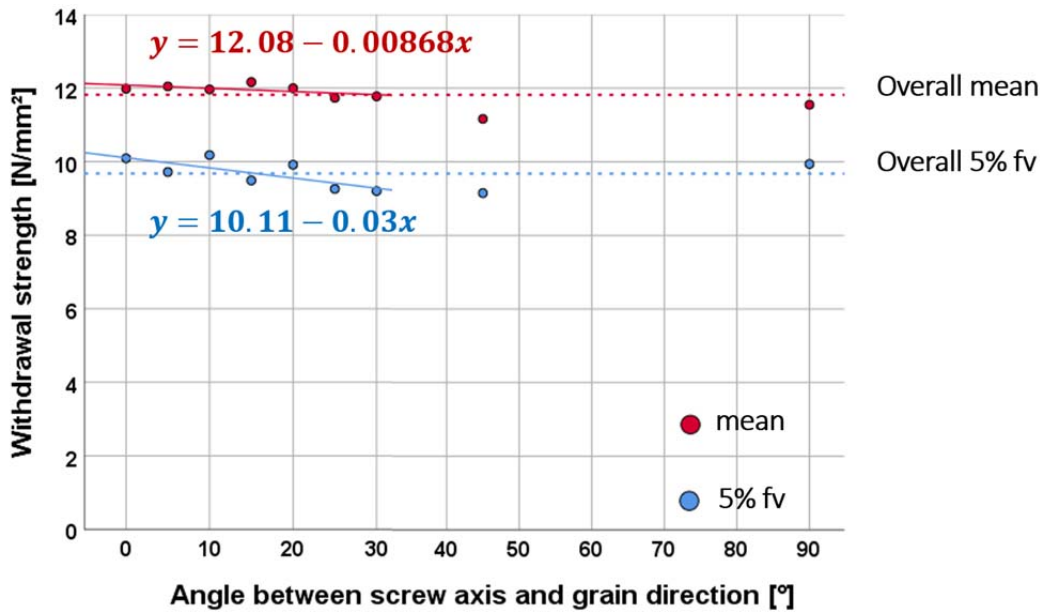


Figure 9. Linear fit for screw axis-to-grain angles $\leq 30^\circ$ on mean and characteristic level for beech.

The linear regression for the mean and characteristic strength values of screw axis-to-grain angles $\leq 30^\circ$ led to R^2 -values of 0.39 and 0.58 respectively. As the differences in withdrawal strength between the different screw axis-to-grain angle groups between 0° and 90° are low and no real trend is noticeable, the adjustment of the withdrawal strength may be negligible for the different screw axis to grain angle groups. This finding for the species beech should be verified by other studies. In contrast to the species beech, different results were observed for the species spruce. The relation between screw axis-to-grain angle and withdrawal strength is illustrated in Figure 10.

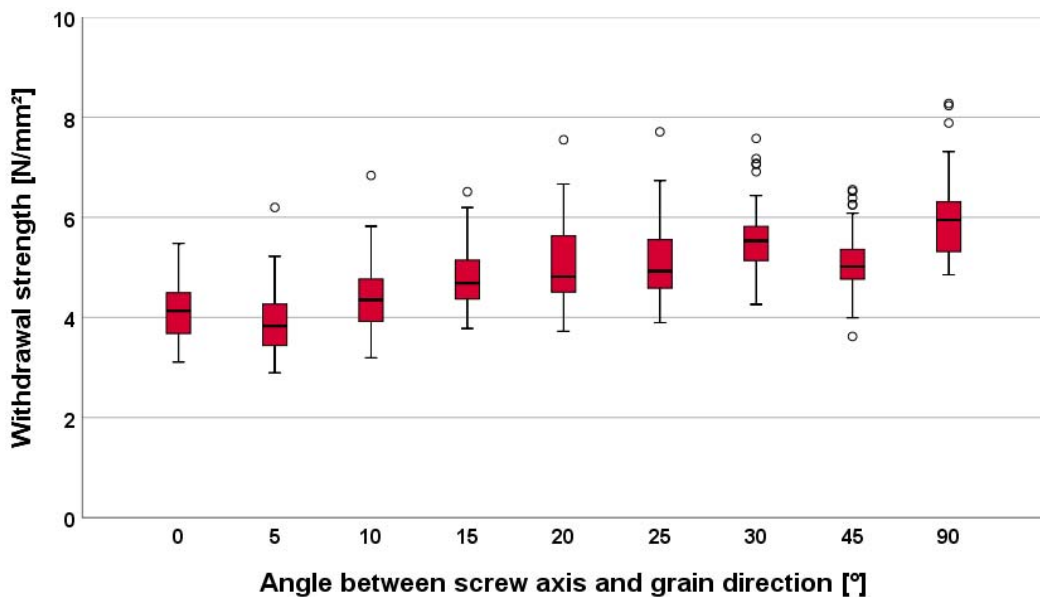


Figure 10. Relation of screw axis-to-grain angle and withdrawal strength for spruce.

It can be recognized, that the lowest withdrawal strength values were determined for screws applied parallel or with small angles to the grain and the highest strength values were found for perpendicular to grain inserted screws. Table 5 summarizes the statistical results of the data analysis.

Table 5. Mechanical properties depending on the screw axis-to-grain angle for the species spruce.

		0°	5°	10°	15°	20°	25°	30°	45°	90°
n		42	42	42	41	42	42	42	42	41
Strength [N/mm ²]	mean	4.2	3.9	4.4	4.8	5.1	5.1	5.6	5.2	6.0
	COV	13	17	16	15	16	15	14	13	14
	5% fv	3.4	2.9	3.4	3.8	3.9	4.1	4.5	4.0	5.0
Density [kg/m ³]	mean	530	523	521	504	513	506	508	488	507
	COV	10	11	9	11	10	11	11	11	10
MC [%]	mean	9.7	9.7	9.5	9.4	9.2	9.2	9.1	9.7	9.6

Mean as well as characteristic withdrawal strength values tend to decrease with decreasing screw axis-to-grain angles. A possible explanation for the lower characteristic value of the 45° group may be the comparably lower densities of the 45°-specimens. The linear regression analysis on mean and characteristic withdrawal strength level for spruce and screw axis-to-grain angles ≤30° is shown in Figure 11.

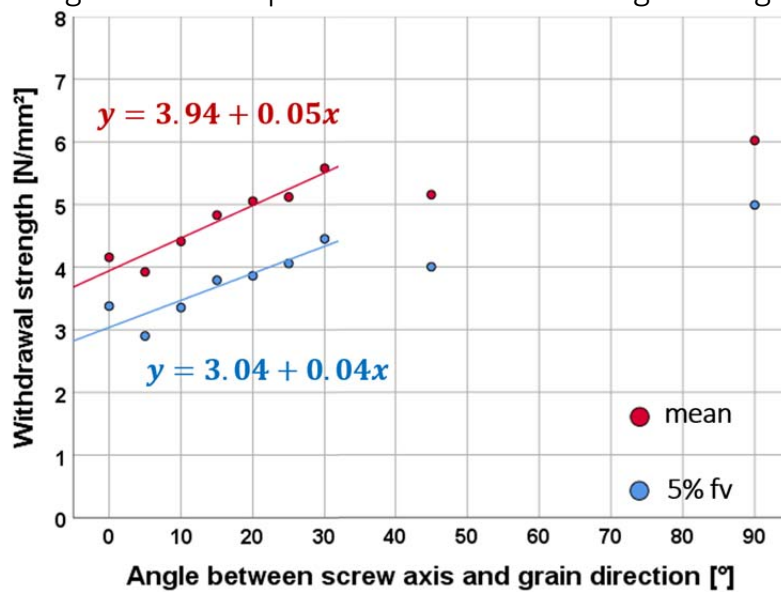


Figure 11. Linear fit for screw axis-to-grain angles ≤30° on mean and characteristic level.

On mean level, linear regression yields a R² value of 0.92, on characteristic level a R² value of 0.82. Similar to the moisture content modification factor k_{mc} , a screw axis-to-grain angle modification factor k_{α} is introduced for spruce.

$$k_{\alpha,mean} = 1.00 - 0.0076 * (30 - \alpha) \text{ for } 0^{\circ} \leq \alpha \leq 30^{\circ}$$

$$k_{\alpha,k} = 1.00 - 0.0072 * (30 - \alpha) \text{ for } 0^{\circ} \leq \alpha \leq 30^{\circ}$$

3.5 Influence of different tip geometries on the withdrawal strength

As shown in Westermayr and Van de Kuilen (2019), different screw types led to varying withdrawal strength values in beech, whereby no relation between thread geometry and withdrawal strength was found. Therefore, it was assumed, that the different tip shapes led to pre-damaging of the timber component during screw insertion. The tips of the different screw types used in this investigation are shown in Figure 12.



Figure 12. Tip shapes of the five different screw types applied in this part of the study.

For this reason, always 40 screws with and 40 screws without tip of each screw type were inserted and tested in withdrawal. All screws had the same outer diameter of 10 mm. The corresponding results are shown in Figure 13 for spruce and beech.

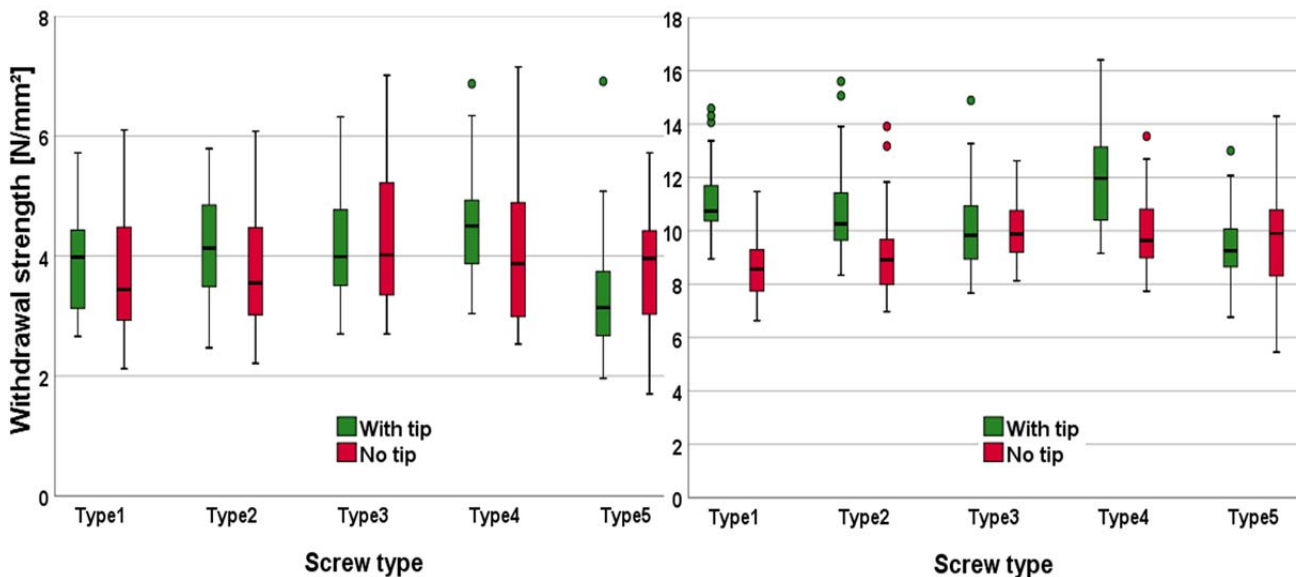


Figure 13. Withdrawal strength of screw types with/without tip in spruce (left) and beech (right).

The data show that the tip shapes of the different screw types lead to different withdrawal strength values. While screw type 3 shows no difference in mean withdrawal strength if inserted with or without tip, the mean withdrawal strength of the screw types 1, 2 and 4 is higher if installed with tip. In contrast, screw type 5 shows a lower mean withdrawal strength when the screw was inserted with tip. These observations are valid for both species. Table 6 summarizes the ratio in withdrawal strength of the five screw types applied without tip compared to the same screws installed with tip

$\frac{f_{ax,without\ tip}}{f_{ax,with\ tip}}$ on mean and characteristic strength level.

Table 6. Ratio of withdrawal strength if screw was applied without tip and density properties.

			Type1	Type2	Type3	Type4	Type 5
Beech	Strength [%]	mean	77	86	99	81	103
		5% fv	73	85	99	83	92
	Density [kg/m ³]	mean	728	721	728	729	726
		COV	5	5	6	6	5
	MC [%]	mean	8.3	8.3	8.2	8.2	8.3
Spruce	Strength [%]	mean	95	88	105	90	113
		5% fv	82	94	94	86	98
	Density [kg/m ³]	mean	504	499	509	502	494
		COV	11	11	11	10	12
	MC [%]	mean	9.7	9.8	9.7	9.7	9.5

After data analysis it can be summarized, that not the thread geometries but especially the shapes of the tips lead to different withdrawal strength values as a result of pre-damaging during screw installation. But also the sharpness and the concentricity of the thread may have an influence on the withdrawal strength. At this point it is mentioned, that the applied screws are not optimized for parallel to grain application and the tips are primarily shaped for easy installation without predrilling in softwood. Especially screws with optimized geometries for hardwood applications may lead to different results for instance in beech. An optimized tip geometry for application parallel to grain seems reasonable.

3.6 Conceptual models for the prediction of the withdrawal capacity of parallel to grain inserted screws

As shown in the beginning of this study, the wood density variation for screws inserted in grain direction can be substantial for the withdrawal capacity. For this reason, the application of a constant, conservative withdrawal strength independent of the strength class of the structural component may appear to be on the safe side for the design of parallel to grain inserted screws. For the calculation of the withdrawal strength, three possibilities are conceivable.

- Experimental determination of the withdrawal strength itself
- Calculation of the withdrawal strength from EN 408 shear strength values
- Calculation of the withdrawal strength using the density

The required minimum l_{eff} of a screw loaded along its axis is $6d$ according to EC5. As the screw applied in this study has an outer diameter of 11 mm, the minimum l_{eff} according to EC5 is 66 mm. This corresponds approximately with the l_{eff} of 75 mm applied in chapter 3.2 of this study, which compares shear and withdrawal strength. In consequence, the following model is calibrated on the measured withdrawal strength of screws inserted with $l_{eff}=75$ mm and the shear strength determined ac-

According to EN 408:2012. The withdrawal capacity can thus be calculated by the following equation.

$$R_{ax,k} = n_{eff} \cdot f_{ax,k} \cdot (d \cdot \pi \cdot l_{eff}) \cdot k_{mc} \cdot k_{\alpha}$$

The withdrawal strength for beech, ash and spruce can be taken as follows.

$$f_{ax,k,beech} = 9.9 \text{ N/mm}^2 ; f_{ax,k,ash} = 8.3 \text{ N/mm}^2 ; f_{ax,k,spruce} = 3.8 \text{ N/mm}^2$$

The withdrawal strength can further be calculated using the characteristic EN 408 shear values and factors of chapter 3.2:

$$f_{ax,k,beech} = f_{v,408,k,beech} \cdot 0.87 = 11.4 \text{ N/mm}^2 \cdot 0.87$$

$$f_{ax,k,ash} = f_{v,408,k,ash} \cdot 0.92 = 9 \text{ N/mm}^2 \cdot 0.92$$

$$f_{ax,k,spruce} = f_{v,408,k,spruce} \cdot 0.65 = 5.9 \text{ N/mm}^2 \cdot 0.65$$

Finally, the withdrawal strength can be calculated using the characteristic density of the specimens of chapter 3.2:

$$f_{ax,k,beech} = \rho_{k,beech} \cdot 0.0153 = 645 \text{ kg/m}^3 \cdot 0.0153$$

$$f_{ax,k,ash} = \rho_{k,ash} \cdot 0.0166 = 501 \text{ kg/m}^3 \cdot 0.0166$$

$$f_{ax,k,spruce} = \rho_{k,spruce} \cdot 0.0092 = 410 \text{ kg/m}^3 \cdot 0.0092$$

The calculation of the preceding paragraph is just based on the specimens of chapter 3.2. For a more reliable model, the data of chapter 3.2 are combined with further EN 408 test data published by Van de Kuilen et al. (2017) and additional withdrawal strength values obtained on the same material as used in this study. The following table 7 gives the mechanical properties of the combined dataset.

Table 7. EN 408 shear and withdrawal properties of the combined dataset.

		Ash		Beech		Spruce	
		Withdrawal	EN408	Withdrawal	EN408	Withdrawal	EN408
n		31	98	124	110	40	57
Strength [N/mm ²]	mean	12.0	11.9	11.4	12.8	5.6	6.4
	COV	17	14	11	11	18	20
	5% fv	8.3	9.6	9.4	10.4	4.4	4.1
Density [kg/m ³]	mean	659		719		445	
	COV	12		5		15	

Regarding the combined dataset, the withdrawal strength can be taken as:

$$f_{ax,k,beech} = 9.4 \text{ N/mm}^2 ; f_{ax,k,ash} = 8.3 \text{ N/mm}^2 ; f_{ax,k,spruce} = 4.4 \text{ N/mm}^2$$

Considering new factors describing the relation of the characteristic values obtained from EN 408 tests and withdrawal tests, the withdrawal strength can be calculated by the following expressions:

$$f_{ax,k,beech} = f_{v,408,k,beech} \cdot 0.90 = 10.4 \text{ N/mm}^2 \cdot 0.90$$

$$f_{ax,k,ash} = f_{v,408,k,ash} \cdot 0.86 = 9.6 \text{ N/mm}^2 \cdot 0.86$$

$$f_{ax,k,spruce} = f_{v,408,k,spruce} \cdot 1.07 = 4.1 \text{ N/mm}^2 \cdot 1.08$$

Applying the characteristic density of the combined dataset to calculate the withdrawal strength leads to the expressions as follows:

$$f_{ax,k,beech} = \rho_{k,beech} \cdot 0.0142 = 661 \text{ kg/m}^3 \cdot 0.0142$$

$$f_{ax,k,ash} = \rho_{k,ash} \cdot 0.0158 = 526 \text{ kg/m}^3 \cdot 0.0158$$

$$f_{ax,k,spruce} = \rho_{k,spruce} \cdot 0.0131 = 337 \text{ kg/m}^3 \cdot 0.0131$$

The modification factors $k_{mc,k}$ and $k_{\alpha,k}$ can be described as:

$$k_{mc,k} = 1.00 - x \cdot (u - 12)$$

$$x_{beech} = 0.022 ; x_{ash} = 0.027 \text{ for } 9\% \leq u \leq 18\%$$

$$x_{spruce} = 0 \text{ for } 8\% \leq u \leq 12\% ; x_{spruce} = 0.036 \text{ for } 12\% < u \leq 20\%$$

$$k_{\alpha,k} = 1.00 - x \cdot (30 - \alpha) \text{ for } 0^\circ \leq \alpha \leq 30^\circ$$

$$x_{beech} = 0 ; x_{spruce} = 0.0072$$

The $k_{mc,k}$ -factors for ash and spruce are data from Hübner (2013) and Ringhofer et al. (2014). Figure 14 finally compares withdrawal capacities for screw axis-to-grain angles between 0° and 30° calculated with different models for beech and spruce.

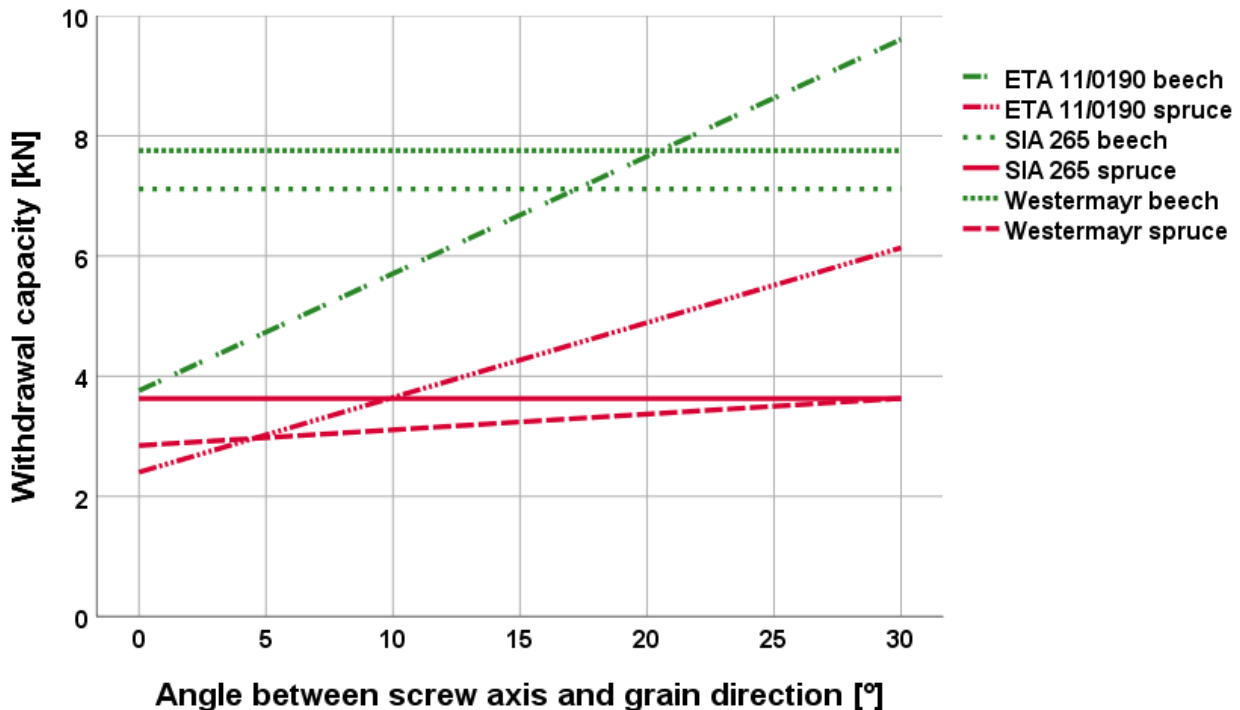


Figure 14. Withdrawal capacities of beech and spruce calculated by the model presented in this study compared to ETA 11/0190:2018 and SIA 265:2012.

For the calculations, the input parameters $d_c=11\text{mm}$, $l_{eff}=75\text{mm}$ as well as the characteristic densities of the combined dataset were used. The results of SIA

265:2012 show similar withdrawal capacities as the model presented in this study for both species. The functions of ETA 11/0190:2018 show higher gradients with lower withdrawal capacities for 0° and higher withdrawal capacities for angles above 10-20°.

At this point, it is explicitly stated that the models of this study would have to be written as design equations yet that can be used in a Eurocode 5 design format. This relates to various strategies one can take when relating strength values to 'declared' strength or density values in strength class tables. Furthermore, effects resulting from screw diameter and screw insertion length are not taken into account in the model approach presented. Further, only a limited number of specimens was tested resulting in an uncertainty especially in the calculated characteristic values and the resulting factors. As described in the materials-chapter, some of the spruce material used for this study had a relatively high amount of compression wood. Nevertheless, the model gives an approach to calculate the withdrawal strength of parallel to grain inserted screws based on shear strength values, with the background of a considerable local density scatter of timber in grain direction.

4 Conclusions and Outlook

This paper gives an overview of the withdrawal behaviour of screws applied parallel to the grain in beech, ash and spruce. The local density variation is higher in grain direction than perpendicular to grain direction. As a result, this may cause higher scatter in the design of parallel to grain inserted screws.

As an alternative, shear strength determined according to EN 408:2012 seems to be in reasonable compliance with the withdrawal strength and may be suitable for predicting the withdrawal capacity of parallel to grain applied screws. A linear decrease of around 2.5% for each 1% increase in moisture content is found for the withdrawal strength in beech.

The screw axis-to-grain angle seems not to affect the withdrawal strength in beech too much, although the withdrawal strength of screws in the species spruce shows a linear decrease for decreasing angles between screw axis and grain direction.

It was observed, that the tip shapes of different screw types lead to significantly different withdrawal strengths. Finally, conceptual models are presented for calculating the capacity of parallel to grain inserted screws based on either a constant withdrawal strength, EN 408 shear strength or the wood density.

In further next steps, the effects resulting from varying screw diameters, effective screw insertion lengths and tensile capacity of the screws will be integrated in the models to cover the possible failure modes.

5 Acknowledgements

We want to sincerely thank Marco Pommer, who did a great job during his Master Thesis' at Wood Research Munich, collecting a lot of data used in this study.

6 References

- Blaß, H. J.; Bejtka, I.; Uibel, T. (2006): Tragfähigkeit von Verbindungen mit selbstbohrenden Holzschrauben mit Vollgewinde. In German. Karlsruher Berichte, Band 4. Universitätsverlag Karlsruhe, ISBN 3-86644-034-0.
- Brandner, R.; Gatternig, W.; Schickhofer, G. (2012): Determination of shear strength of structural and glued laminated timber. Conference paper, International Council for Research and Innovation in Building and Construction, Working Commission W18 - Timber Structures, Växjö, Sweden.
- Brandner, R.; Ringhofer, A.; Reichinger, T. (2019a): Performance of axially loaded self-tapping screws in hardwood: Properties and design. *Engineering Structures* 188, p.677-699.
- Brandner, R.; Ringhofer, A.; Sieder, R. (2019b): Duration of Load Effect on Axially-Loaded Self-Tapping Screws Inserted Parallel to Grain in Soft- and Hardwood. Conference paper, INTER-Meeting 6, Tacoma, USA.
- Ehrhart, T.; Steiger, R.; Frangi, A. (2018): A non-contact method for the determination of fibre direction of European beech wood (*Fagus sylvatica* L.). *European Journal of Wood and Wood Products*, vol. 76: no. 3, pp. 925-935.
- Hübner, U. (2013): Mechanische Kenngrößen von Buchen-, Eschen- und Robinienholz für lastabtragende Bauteile. Monographic series TU Graz, Timber Engineering & Technology, Volume 3, ISBN: 978-3-85125-314-6.
- Jockwer, R. (2019): Tragverhalten von Schrauben in Buchenholz. Conference Paper, 25. Internat. Holzbau-Forum 2019, Innsbruck, Austria.
- Ringhofer, A. (2017): Axially loaded self-tapping screws in solid timber and laminated timber products. Monographic series TU Graz, Timber Engineering & Technology, Volume 5, DOI 10.3217/978-3-85125-555-3.
- Ringhofer, A.; Grabner, M.; Silva, C.; Branco, J.; Schickhofer, A. (2014): The influence of moisture content variation on the withdrawal capacity of self-tapping screws. *Holztechnologie* 55 3 p.33-40.
- Schilling, S. (2017): Anschlüsse in Buchen-Brettschichtholz –Leistungsfähige Verbindungen für einen hochwertigen Baustoff –Zugverbindungen. Masters Thesis, ETH Zürich, Switzerland.
- Van de Kuilen, J.W.G., Gard, W.F., Ravenshorst, G.J.P., Antonelli, V., Kovryga, A., (2017): Shear strength values for soft- and hardwoods, INTER-Meeting 4, Paper 50-6-1, Kyoto, Japan.

- Westermayr and Van de Kuilen (2019): Withdrawal strength of screws and screw groups in European beech (*Fagus s.*) parallel to the grain. Conference paper, INTER-Meeting 6, Tacoma, USA.
- DIN 4074-1:2012: Strength grading of wood – Part 1: Coniferous sawn timber. DIN.
- EN 318:2002: Wood-based panels - Determination of dimensional changes associated with changes in relative humidity. CEN.
- EN 384:2019: Structural timber – Determination of characteristic values of mechanical properties and density. CEN.
- EN 408:2012: Timber structures – Structural timber and glued laminated timber– Determination of some physical and mechanical properties. CEN.
- EN 1382:2016: Timber structures – Test methods – Withdrawal capacity of timber fasteners. CEN.
- EN 1995-1-1:2010: Design of timber structures - Part 1-1: General and rules for buildings. CEN.
- EN 13183-1:2002 Moisture content of a piece of sawn timber - Part 1: Determination by oven dry method. CEN.
- EN 14358:2016: Timber structures – Calculation and verification of characteristic values. CEN.
- SIA 265:2012: Timber structures. SIA.
- ETA 11/0190:2018: Würth self-tapping screws. European Organisation for Technical Assessment.

Discussion

The paper was presented by M Westermayr

R Brandner commented on the difference in measured strength for moisture variation consideration of 9 to 18 %. M Westermayr said this is the source of material. Other test procedures were used for considering moisture content effects where Push-Push tests were used hence lower strengths were measured. In the other tests push-pull tests were used which yielded higher values. R Brandner said that they did not find any test set up influence.

R Brandner asked about shear tests where the shear area is different from the screw case and asked if the difference in shear strengths can be explained by size effects.

M Westermayr said that the failure zone of screw withdrawal would be predetermined hence statistical size effect should not apply. Nevertheless the height of the shear specimen was lower than that specified by EN408 to account for different shear areas.

R Brandner commented that the compression zone in the EN 408 tests should be low and would not influence the shear strength. Also commented that other load directions are much more reliable compared to the parallel to grain direction. P Dietsch said influence of shear and compression perpendicular to grain should be dependent on level of shear strain reached.

S Winter commented on the minimum penetration distance of screws for end grain application and pondered how should we deal with density variation issues. M Westermayr responded that there are past data regarding minimum penetration distance requirements; however, there are associated practical issues involved. He was surprised by the variation of density even within one laminate. This issue needed further consideration and may be lower effective number of elements should be taken as a conservative approach and that more work is needed.

G Hochreiner stated that stiffness information would be useful with consideration of the geometry of the screws. M Westermayr said the shear strength and withdrawal strength relationship might indicate information for shear modulus which could be considered for stiffness consideration. G Hochreiner commented that the ductility for earthquake application by using large diameter screws might be appropriate. Also if displacement data was available from testing it should be used for stiffness consideration.

S Aicher said influence on screw diameter should be further investigated. Also comparison of this conceptual approach with what has been approved in Switzerland would be important. M Westermayr agreed with the need for comparison and said both screw diameter and insertion length will be investigated further.

A Frangi said that low conservative values were used in Switzerland for this application. Long term behaviour and influence of moisture changes are important. Also in Switzerland a minimum penetration length of 100 mm is required. Finally issues of ductility considerations are interesting.

R Brandner commented that the push-pull test set up used might create unwanted moment which could influence the test results. Also ductility with these screw joints should deal with overstrength design of the screws and put the ductile element somewhere else. M Westermayr agreed.

FE modelling of timber connections with inclined and cross-wise arranged screws - new findings on testing the shear stiffness

Boris Azinovič

Slovenian National Building and Civil Engineering Institute (ZAG Ljubljana)

Matthias Frese

Karlsruhe Institute of Technology, Timber Structures and Building Construction

Keywords: screw connections, inclined, cross-wise, shear stiffness, compression-shear test method, FE modelling, friction

1 Introduction

1.1 Technical background and impetus for the work

Connections with inclined and cross-wise arranged screws are widely used in timber constructions as e.g. trusses, mechanically jointed beams, and moment resisting frame corners. Their shear stiffness (k_s) is relevant for both serviceability and ultimate limit state design. However, currently available testing methods and calculation models can yield significantly different values of stiffness compared to those effective in real structures (e.g. Blass and Steige 2018).

The shear stiffness of connections with inclined arranged screws to be determined by the test procedure in Fig. 1a depends, amongst others, on following parameters:

1. axial stiffness or slip modulus in screw axis (k_{ax}) where k_{ax} in turn depends on screw diameter (d), penetration length (l_{ef}), density (ρ_1 and ρ_2), and angle between screw axis and grain direction (α);
2. compressive stress (by H due to specimen inclination β and by the component Z_H of the screw tension force Z) and friction ($H \cdot \mu$ and $Z_H \cdot \mu$) in the common interface of the connected members; and
3. embedment stiffness (k_{lat}) of the proportionally lateral loading where k_{lat} in turn includes the bending stiffness of the screw.

The load-carrying behaviour of connections with screws inclined under $\alpha = +/- 45^\circ$ can be determined accurately with truss models (Fig. 1b). So far, a truss model states a simplifying alternative to capture the continuously distributed compressive (σ_c) and

friction stress (Fig. 1c). The relevant scientific work on this is e.g. Blass and Bejtka 2002, Kevarinmäki 2002, Tomasi et al. 2010, and Jockwer et al. 2014.

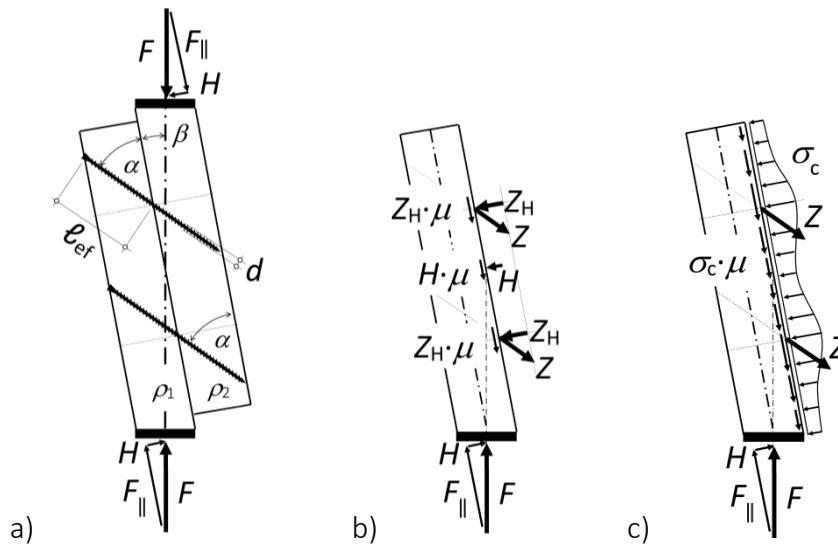


Fig. 1: Compression shear test with inclined screws (a); equilibrium using truss model (b), and continuously distributed compressive stress and friction (c).

Viewed intuitively, the shear stiffness of connections with more or less optimally inclined and therefore mainly axially loaded screws mostly depends on the axial stiffness k_{ax} . In case of cross-wise arranged screws the load transfer by tension and compression screws becomes much more complicated compared with inclined ones stressed merely in tension (Fig. 2 a and b), since multiple transfer mechanisms, effective in crossed screw couples, contribute to the shear stiffness.

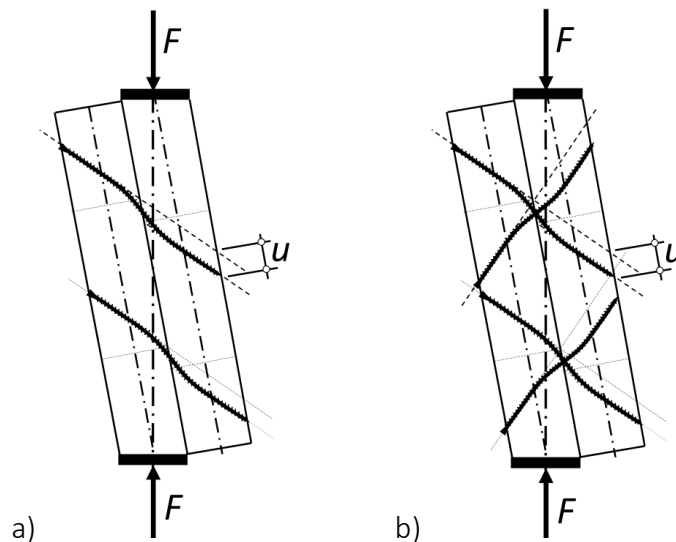


Fig. 2: Deformation models of shear tests with inclined (a) and cross-wise arranged screws (b).

The EAD (2016) contained up to now a general description to determine k_{ax} taking into account the governing parameters. Though, a specified and explicitly described testing method was missing. For that and other reasons, a compression shear test using two cross-wise arranged screw couples was developed by Blass and Steige (2018), where k_{ax} is back-calculated by test values of k_s , see Eq. (1). Based on their findings and recommendations, this testing method was recently included in the new draft of

this EAD (2020). That will close an important gap in terms of axial stiffness since neither EN 14592 nor EN 1382 provide any method for k_{ax} .

$$k_{ax} = \frac{k_s}{2 \cdot \cos^2 \alpha} \quad (1)$$

Blass and Steige (2018 P. 82) have stated that an alternative compression shear test using merely two inclined tension screws yields significantly lower k_{ax} values than in the case of cross-wise arranged ones, although one should expect both values to be similar. Those k_{ax} values are back-calculated with Eq. (2).

$$k_{ax} = \frac{k_s \cdot (1 - \mu \cdot \tan \beta)}{\cos^2 \alpha \cdot (1 + \mu \cdot \tan \alpha)} \quad (2)$$

The reason for the difference between both k_{ax} values could not be explained yet. However, there may be a connection with the fact that the effect of friction is once assumed to have no influence (Eq. 1) and once is mechanically considered (Eq. 2). In the present paper the research to discover such differences in detail is, therefore, based on the current state-of-the art and follows these working hypotheses:

- In case of cross-wise arranged screws, friction likewise contributes to the shear stiffness, since the component H of the loading F on the specimen is effective in the interface at least to some extent.
- In case of merely inclined screws, the compressive stress in the common interface does not only effect friction but also compression perpendicular to the grain. Hence, compression perpendicular to the grain may state a further compliance that must not contribute to the k_{ax} value.
- Due to the two preceding aspects, back-calculated k_{ax} values using Eq. (1) must turn out higher than those back-calculated with Eq. (2).

The authors of this paper suppose limits in the application of the 2D truss model particularly in case of cross-wise arranged screws. Hence, complex deformations of screws and timber (Fig. 2b) can be described only up to a certain level with truss models. Figure 3 establishes elementary considerations on the deformation mechanism in connections with merely inclined (a) and cross-wise arranged screws (b). Assuming the same displacement (u) between the respective members and small shear deformation ($\tan \gamma < 0.01$) the interface is once closed and afterwards elastically compressed and once neutral, because the compression screws tend to pry open the common interface and the tension screws effect exactly the contrary. In both drawings hinges (displayed by circles) are assumed, where bending would arise in connecting screws. The comparison between the two mechanisms in Fig. 3a and b, respectively, makes clear that compression deformation, illustrated by the shortened length (<1) in direction perpendicular to the grain, may contribute to additional shear displacement in case of connections with inclined screws. It is to assume that the different mutual movements of the two members and the change in the screw angles

given by the respective α values somehow has an impact on the global system answer in terms of stiffness. Note that for larger shear displacements ($\tan\gamma \gg 0.01$) the actual strain in the tensile screw becomes higher than in the compression screws.

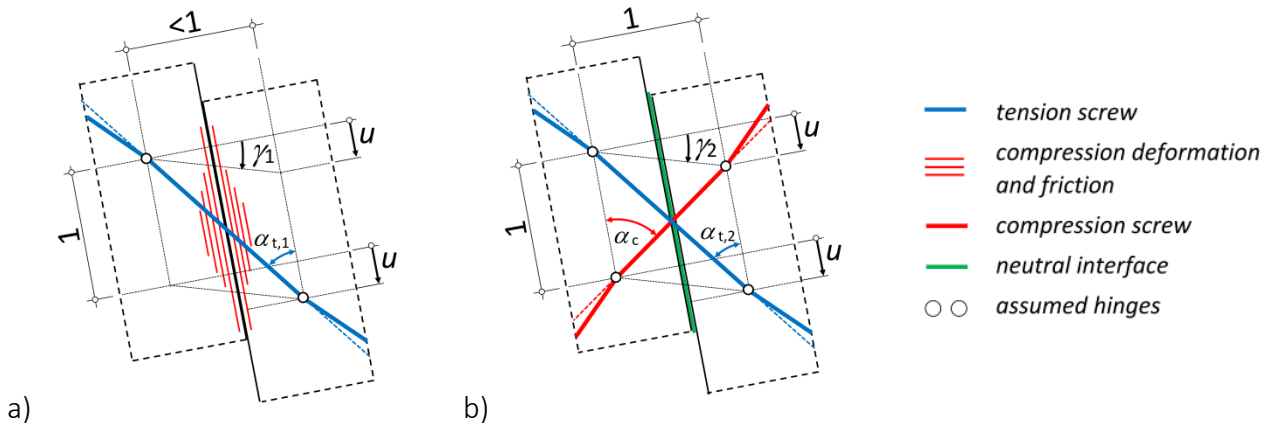


Fig. 3: Simplified deformation mechanism in the local vicinity of an inclined screw (a) and cross-wise arranged screws (b).

Previous research (e.g. Blass and Bejtka 2002, Kevarinmäki 2002, Tomasi et al. 2010) focused on local equilibriums based on truss models in a narrow space taking into account axial and lateral screw forces, embedment reactions, bending capacity, and friction. Though, the possible effect of different mutual movements, elastic compression perpendicular to the grain, and 3D effects on the global system answer was not investigated so far. The authors see, therefore, room for improvement in describing and analysing the problem and reasons to further investigate the load slip behaviour of compression shear tests.

1.2 Objective of the study

The paper aims at looking into some crucial interacting parameters in the determination of k_s . In order to quantify the influences of the contributing parameters and of the screw arrangement and in order to make clear their mutual interference, FE analyses are seen as suitable means for this task. The findings should contribute to a better understanding of the suggested testing method and may facilitate the interpretation of corresponding test results. The single aims of the paper are:

- calibration of a numerical model with cohesive zone surfaces using screw withdrawal experiments
- validation of the numerical models for connections with inclined and cross-wise arranged screws using already available compression shear experiments
- analysis of axial forces in cross-wise arranged screws
- analysis of the share of friction in the shear force for both connection types
- description of the distribution of compressive stresses in the interface for both connection types
- effect of a variable friction coefficient and of the screw inclination and penetration length on the load-carrying behaviour of connections with inclined screws

2 Modelling of inclined and cross-wise arranged screws and simulations

2.1 FE model and calibration

Fig. 4 illustrates the main features of the three-dimensional FE model. In contrast to the proposed test setup using specimens inclined at the angle β , both compression shear tests with inclined (a) and cross-wise arranged screws (b) are vertically oriented. Hence, they are equipped with lateral supports to take up the horizontal reaction H (cf. Fig. 1a). The timber part on the left side was supported at the bottom in both vertical and horizontal direction and the other one on the right side was held by a sliding support as shown in Fig. 4a and b. Linear elastic orthotropic elements were used for timber. The wood screw interface and the "damaged wood" due to the self-tapping thread were modelled by cohesive surfaces and orthotropic elements with reduced stiffness (Fig. 4c). Such modelling approach was already used for inclined screwed connections with a large gap between the elements (Avez et al. 2016).

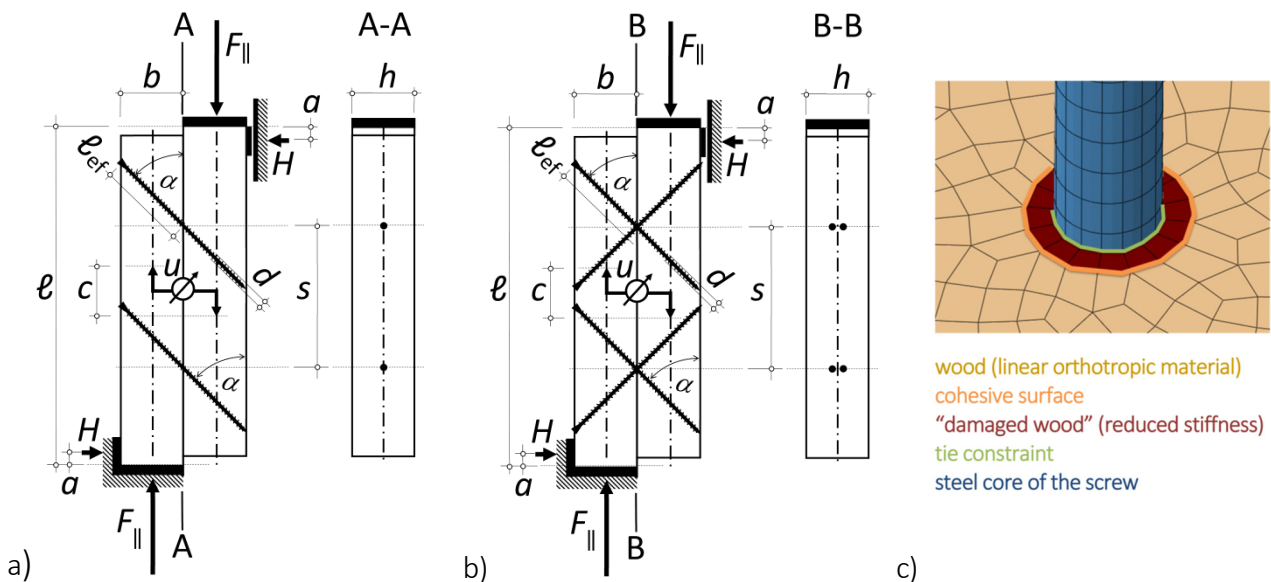


Fig. 4: Geometry of the FE model with inclined (a) and cross-wise arranged screws (b) (adopted from Blass and Steige 2018); transfer from wood to steel (c).

The necessary parameters for the cohesive surfaces and for the "damaged wood" material were calibrated using small-scale withdrawal tests (see Blass and Steige 2018). This calibration was performed first for behaviour in the linear part, where stiffness characteristics for orthotropic material in damaged wood were reduced compared to surrounding wood. Then, it was performed for initiation and evolution of damage of cohesive surface, where four parameters for the cohesive zone model were defined to fit the curve from screw withdrawal experiments (Table 1). The same input parameters were finally used for the simulations with inclined and cross-wise arranged screws presented in this paper. The effect of cohesive surfaces is comparable to that of the local bond-slip model proposed by Pranjić (2020). The steel core of the screw was modelled as isotropic

material and with ideal plasticity. The contact between the timber parts was modelled as penalty friction, where the friction coefficient μ equalled 0.50.

Table 1: Material parameters of the FE model.

Orthotropic material									
	E_1	E_2	E_3	ν_{12}	ν_{13}	ν_{23}	G_{12}	G_{13}	G_{23}
	[MPa]	[MPa]	[MPa]	[-]	[-]	[-]	[MPa]	[MPa]	[MPa]
wood	11000	370	370	0.45	0.30	0.35	690	690	40
damaged wood	2000	70	70	0.45	0.30	0.35	100	100	10
Isotropic material									
	E [MPa]		ν [-]	σ_y [MPa]					
steel core of the screw	210000		0.30	800					
Cohesive surface									
	σ_u	τ_1 & τ_2	$K_{nn}, K_{tt,1}$ & $K_{tt,2}$				G_f	η [-]	
	[MPa]	[MPa]					[N/mm]		
interface between wood and damaged wood	5.0	7.0	default contact enforcement value				3.75	0.001	

Note: wood: E_1, E_2, E_3 ... elastic moduli in the longitudinal, radial and tangential directions, $\nu_{12}, \nu_{13}, \nu_{23}$... Poisson's ratios, where the first index refers to the direction of the applied stress and the second index to the direction of lateral deformation; G_1, G_2, G_3 ... moduli of rigidity in the 12, 13 and 23 planes respectively; steel: E ... elastic modulus, ν ... Poisson's coefficient, σ_y ... yield stress; cohesive surface: σ_u ... strength in the normal direction, limited by the perpendicular to the grain tensile strength of spruce, τ_1, τ_2 ... shear strengths (calibrated value); $K_{nn}, K_{tt,1}, K_{tt,2}$... stiffness in the normal and shear directions G_f ... fracture energy, mode independent (calibrated value), η ... viscosity coefficient (a sufficiently small value to have a negligible effect on the final result).

2.2 Numerical test programme

In the first step, two different angles α were examined each for the two connection types with inclined and cross-wise arranged screws. The configurations are specified in Table 2. Therewith it was intended to validate the respective numerical results with experimental ones determined by Blass and Steige (2018) for the same test set-up.

Table 2: Geometry of the test specimens and therewith designed FE models.

configuration	connection type	b [mm]	h [mm]	ℓ [mm]	a [mm]	ℓ_{ef} [mm]	α [°]	d [mm]	d_k [mm]	s [mm]
1	inclined	80	110	480	20	113	45	8	5.1	200
2	inclined	65	110	615	20	130	30	8	5.1	270
3	cross-wise	80	110	480	20	113	45	8	5.1	200
4	cross-wise	65	110	615	20	130	30	8	5.1	270

Note: d ... diameter of the screw d_k ... diameter of the steel core

In the second step, the initially designed models were used for parameter variations to examine their respective effects on the given system responses. The corresponding numerical test programme is composed in Table 3.

Table 3: Numerical test programme.

Variation	Effect on
relative displacement u	axial forces in cross-wise arranged screws
screw arrangement (inclined or cross-wise) and relative displacement u	share of friction in total shear force and compliance due to compression
screw arrangement (inclined or cross-wise)	distribution of compressive stresses at a constant shear displacement
friction coefficient and screw inclination	shear stiffness and load-carrying capacity

3 Results

3.1 Validation of the numerical model

Fig. 5 shows the comparison between the load displacement curves obtained by the numerical simulations and experimental tests. The upper diagrams represent the two configurations with inclined screws and the two lower ones the configurations with cross-wise arranged screws. On the whole, the comparisons show that the simulated load slip behaviour agrees with actual one. The four simulated curves lie within the limits established by the respective experimental ones. Due to the initial slip observed in experiments with merely inclined screws and caused by unavoidable gaps between two members, the simulated curves turn out steeper for small displacements than the experimental ones. In the simulation though, the shear stiffness is available from the starting point on, without any initial shift. However, beyond a displacement u of 0.2 mm the slope of the simulated and experimental curves corresponds relatively good to each other. In all four cases, the nonlinear course is captured by the simulations.

In order to compare the numerical and experimental results also by numbers, the following two output variables were defined:

- Maximum shear force ($F_{\parallel, \max}$) occurring during the loading

- Global shear stiffness (k_s) determined as the ratio $\frac{F_{40} - F_{10}}{u_{40} - u_{10}}$

where F_{40} and F_{10} are 40% and 10% of $F_{\parallel, \max}$, respectively, and u_{40} and u_{10} are the corresponding relative displacements measured between two fixed points at the distance c of approx. 110 mm (see Fig. 4a and b).

The maximum shear force and the global shear stiffness values were evaluated for the experiments ($F_{\parallel, \max, e}$ and $k_{s, e}$) and for the numerical simulations ($F_{\parallel, \max, n}$ and $k_{s, n}$). The experimental results in Table 4 are given as mean values. The last two columns contain the respective relative error between the numerical and experimental values. They show that the numerical estimation of the maximum shear load is partly very accurate. The differences lie between 2 and 6%. In case of global shear stiffness though, the numerical estimation turns out less accurate. The numerical stiffness is

16 and 21% higher than the experimental one for inclined screws, 3 % higher for configuration 3 and 24% lower for configuration 4 of cross-wise arranged screws. The relative errors are seen as a consequence of: (i) initial shift in case of inclined screws or stiffer model, (ii) unintended variations of the screw-to-grain angle in the experiments, (iii) relatively low number of specimens in the experiments ($n = 5$), and (iv) modelling simplifications (in terms of embedment behaviour of the screws, interface model without the screw thread etc.).

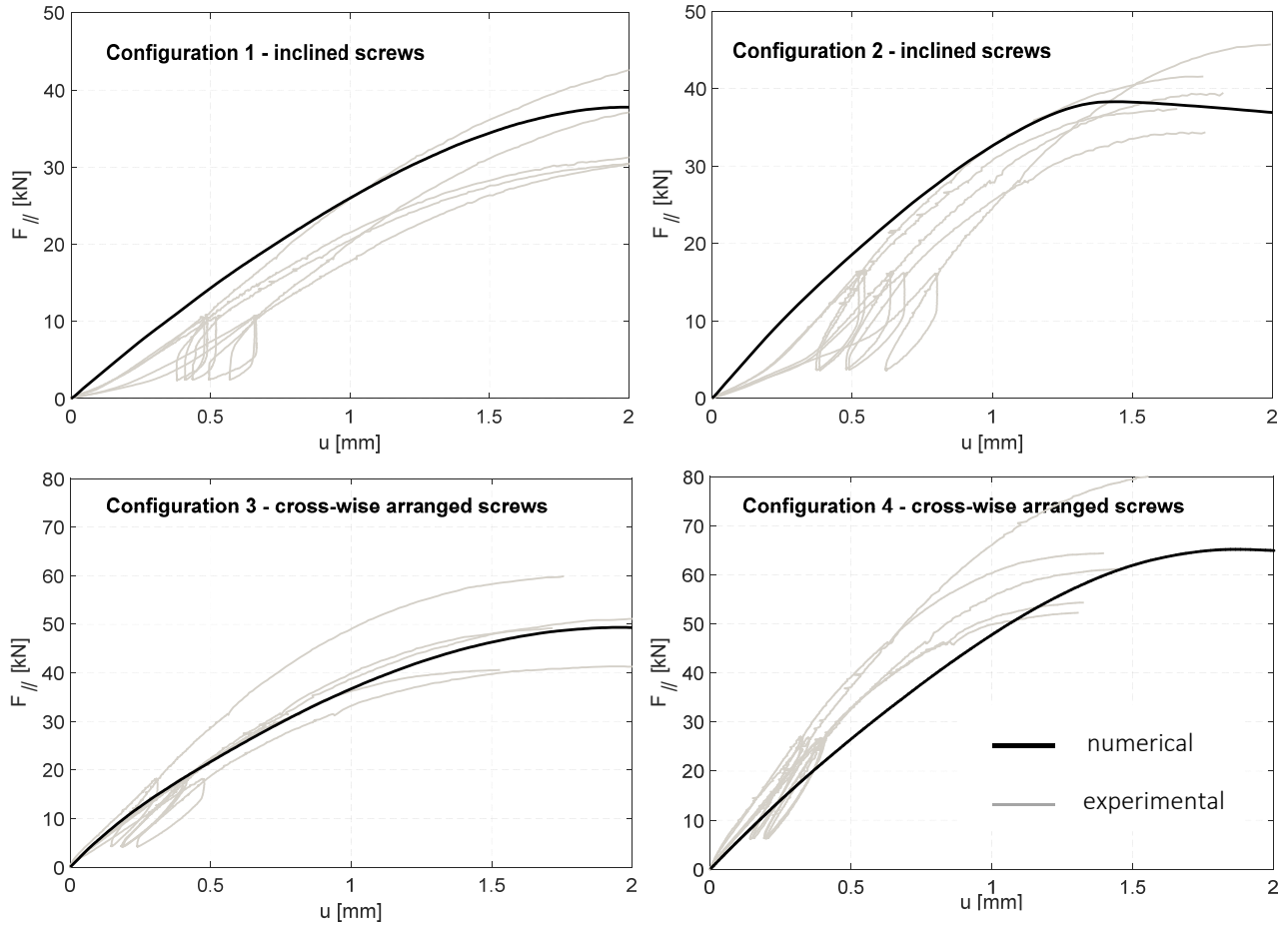


Fig. 5: Comparison of numerical and experimental results for four connection types differing in the screw-to-grain angle and test configuration (inclined and cross-wise arranged screw connection).

Table 4: Mean results of experimental investigation and numerical model prediction.

configuration	connection type	Experimental		Numerical		Relative error	
		$F_{ ,max,e}$ [kN]	$k_{s,e}$ [kN/mm]	$F_{ ,max,n}$ [kN]	$k_{s,n}$ [kN/mm]	$\frac{F_{ ,max,n}}{F_{ ,max,e}}$	$\frac{k_{s,n}}{k_{s,e}}$
1	inclined	35.9	24.2	35.2	29.4	0.98	1.21
2	inclined	39.7	33.0	38.5	38.3	0.97	1.16
3	cross-wise	48.5	44.6	49.3	46.4	1.02	1.03
4	cross-wise	62.5	70.0	66.3	53.2	1.06	0.76

Note: index e ... experimental, index n ... numerical

3.2 Analysis of axial forces in cross-wise arranged screws

The FE model enables to analyse the axial forces in the screws and their distribution along the penetration length. Fig. 6 shows the absolute values of the axial forces (Z) in each screw of the cross-wise arranged screw connection. The forces depend on the relative displacement u between the two timber parts. They are evaluated for the cross-section at the transition from one timber part to the other. Configuration 3 is shown. The results indicate that the absolute value of the tension forces is higher than that of the compression forces if the displacement u or the shear deformation γ increases. According to the drawing in Fig. 3b, the strains in a tension screw become larger than those in compression screws in case of $\tan(\gamma) \gg 0.01$. In this regard, the response of the FE model agrees with the theory in Fig. 3b.

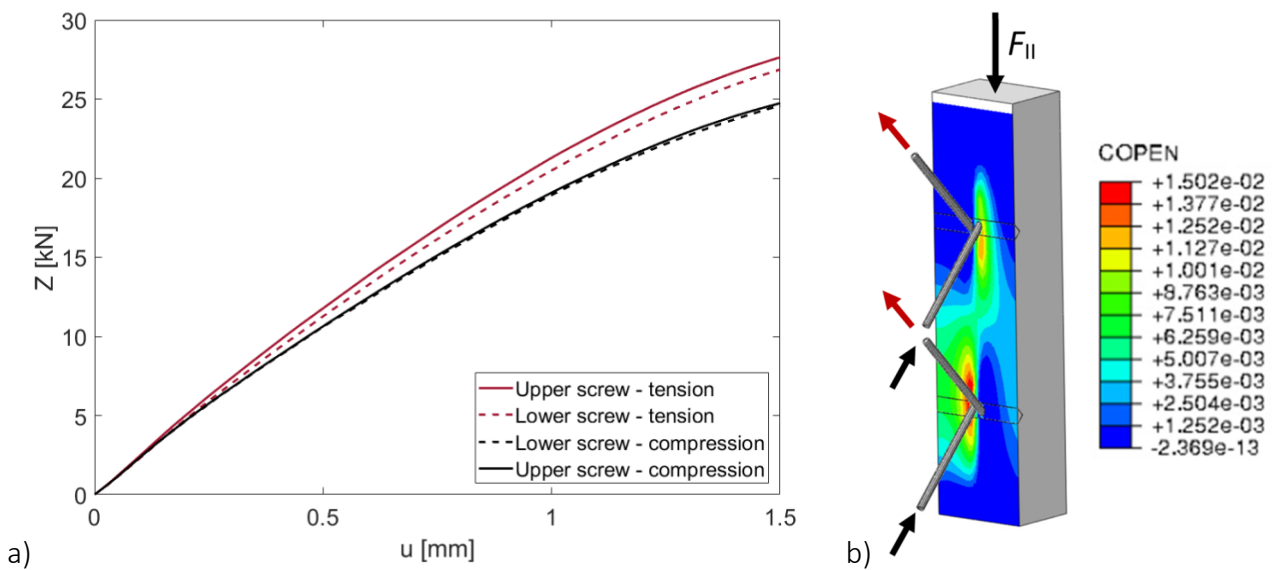


Fig. 6: Internal forces in screws (a) and gap opening size (b) for the cross-wise arranged screw connection (configuration 3) at $u = 1.0$ mm.

Additionally, Fig. 6b illustrates the size of the gap which arises between two timber parts due to the increasing shear displacement. The image proves the assumption from Fig. 3b that the interface between the timber parts is neutral, since only the top and bottom of the surface are slightly compressed. In the area between the crossed screws, however, the two timber parts are mostly separated, except locally at the position of the compression screws. This is an indication, that compression perpendicular to the grain (and friction) will not have a significant influence on the shear stiffness for the cross-wise screw connections.

3.3 Analysis of share of friction in the shear force

The shear force F_{II} in the connection is transferred from one timber part to another primarily by screws and friction in the surface between the timber parts. To analyse the relation between the share of friction in total shear force, the coefficient η is defined according to Eq. (3)

$$\eta = F_c \cdot \mu / F_{II} \quad (3)$$

F_c is the resulting force perpendicular to the interface integrated from the compressive stresses by Eq. (4)

$$F_c = \int_A \sigma_c dA \quad (4)$$

where A is the area of one wood surface between the connected members.

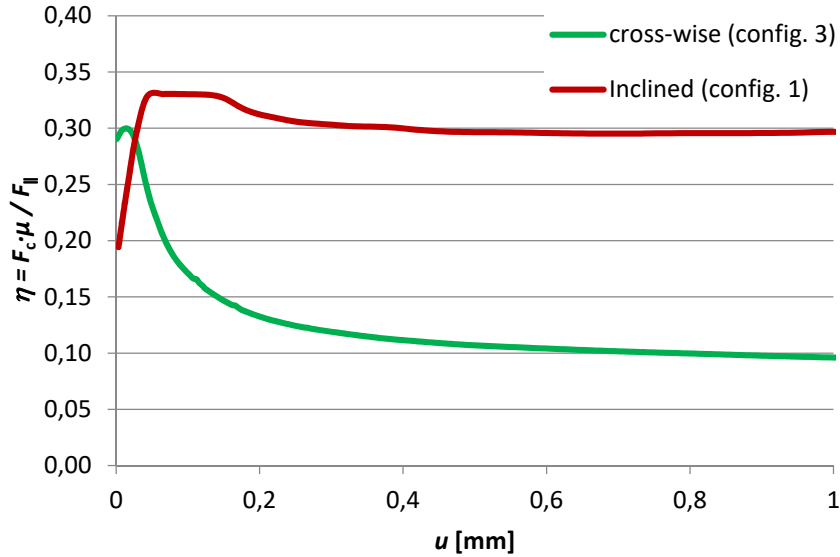


Fig. 7: Share of friction in total shear force (η) depending on relative displacement.

Fig. 7 shows the relationship between the coefficient η and the displacement u for inclined and cross-wise arranged screws. The diagram makes clear that the course of η is each initially nonlinear and reduces for higher relative displacements on a constant level. Beyond a displacement of 0.3 mm and 0.6 mm friction effects about 30% of the shear force F_{II} in case of inclined screws and 10% in case of cross-wise arranged ones, respectively. Hence, in terms of friction there is a significant difference between the two connection types. In case of cross-wise arranged screws, the results indicate, that a higher friction coefficient than 0.5 would not result in a significant increase of $F_{II,max}$. The share of friction in the total shear stiffness k_s cannot be described by a constant ratio throughout the entire range of the displacement u , since the coefficient η obviously reduces for larger relative displacements. This means that for minor displacements u (e.g. u_{10}) the share of friction in shear force is higher than that for major ones (e.g. u_{40}). To show the influence of friction on the shear stiffness in the range between 10% and 40% of $F_{II,max}$, a fictitious value of $k_{s,sc}$ is defined by equation (5) which represents merely the share of the screws in shear stiffness in this range:

$$k_{s,sc} = \frac{3 - 4 \cdot \eta_{40} + \eta_{10}}{3} \cdot k_s$$

where η_{40} and η_{10} are the share of friction in total shear capacity at the corresponding displacements u_{40} and u_{10} , respectively. For the analysed examples, $k_{s,sc}$ is approx. 71% of total k_s (config. 1: inclined) and approx. 91% (config. 3: cross-wise). In the given dis-

placement range, the influence of friction on k_s for configuration 3 is therewith somewhat lower than 10% which applies for larger displacements beyond 0.6 mm. Using these η values in the evaluation below turns out that the share of the screws in the shear stiffness in configuration 1 and 3 (Table 4) differs by almost 2. This is obviously due to the number of screws: two inclined ones in configuration 1 and four in cross-wise arrangement in configuration 3. The little difference between 2.02 and 2 though may give evidence that compression perpendicular to the grain actually states a further compliance in connections with inclined screws. Hence, the shear stiffness in configuration 3 is somewhat higher than twice the stiffness in configuration 1.

$$\text{Configuration 1: } k_{s,n} = 29.4 \rightarrow k_{s,sc} = 0.71 \cdot 29.4 = 21.00 \text{ kN/mm}^2$$

$$\text{Configuration 3: } k_{s,n} = 46.4 \rightarrow k_{s,sc} = 0.91 \cdot 46.4 = 42.33 \text{ kN/mm}^2$$

$$42.33/21.00 = 2.02 > 2$$

3.4 Description of compressive stresses in the interface

Fig. 8 illustrates the distribution of compressive stresses acting on one surface of the interface. Part a) shows the distribution for modelled specimens with inclined screws and b) the one for those with cross-wise arranged screws. In case of inclined screws, the compressive stress is approximately constant along a vertical corridor running through the two screws. Near both screws though, there is a slight increase in stress. However, in case of cross-wise arranged screws, the compressive stresses between the timber parts are concentrated at the top and bottom of the surface. Since the tensile and compression forces in cross-wise arranged screws more or less mutually neutralise, the compressive stresses in the interface result primarily from the normal force H . Both illustrations give evidence that such stress distributions cannot be captured by truss models.

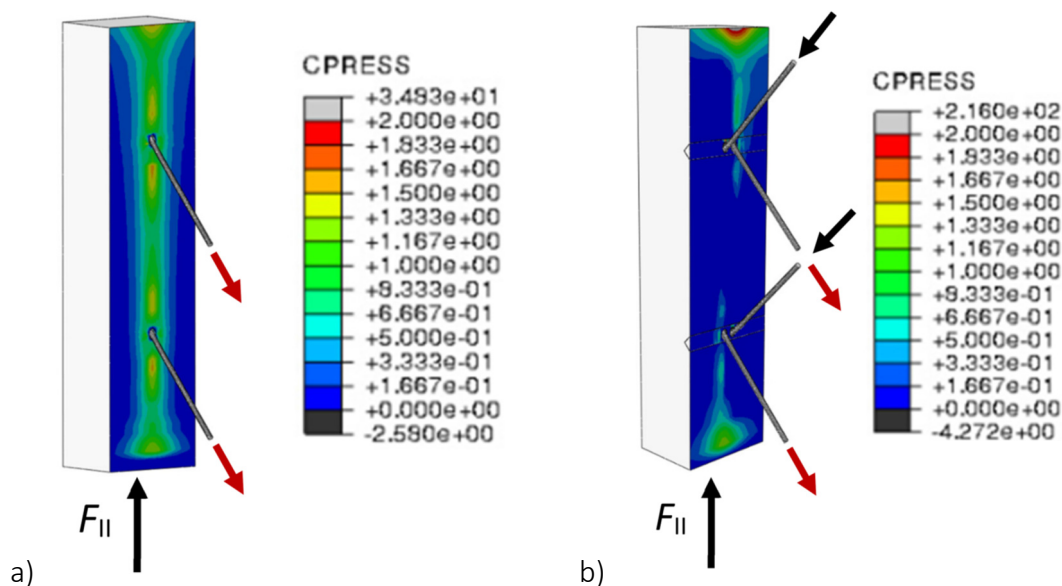


Fig. 8: Compressive stress in the interface for modelled specimens with inclined (a) and cross-wise arranged screws (b) each at $u = 1.5$ mm.

In case of modelled specimens with cross-wise arranged screws, the compressive stresses and consequently friction, therefore, highly depend on the geometry of the

timber parts. If slender timber parts ($b \ll \ell$) are used, the influence of friction would be negligible on the shear force F_{II} . However, if b equals ℓ , the effects of friction due to major horizontal forces H on the shear force cannot be neglected.

3.5 Effect of variable friction on the load-carrying behaviour

The preceding FE results have confirmed that the influence of friction is far higher in case of inclined screw models than in case of cross-wise screw models. While friction plays a subordinate role in connections with cross-wise arranged screws, friction states a crucial factor in connections with inclined screws. For this reason, a sensitivity analysis was performed with the inclined screw model only. The main purpose was to establish how a variable friction coefficient at the interface between the timber parts influences the global response of the connection. The secondary purpose was to evaluate and show this influence for the screw inclinations $\alpha = 30^\circ$ and 45° (config. 1 and 2). Note that a change of α likewise effects a change in the penetration length; ℓ_{ef} is 113 mm in the case of configuration 1 and 130 mm in case of configuration 2. The results are illustrated in Fig. 9. They show that μ and α significantly influence the stiffness (Fig. 9a) as well as the load-carrying capacity (Fig. 9b).

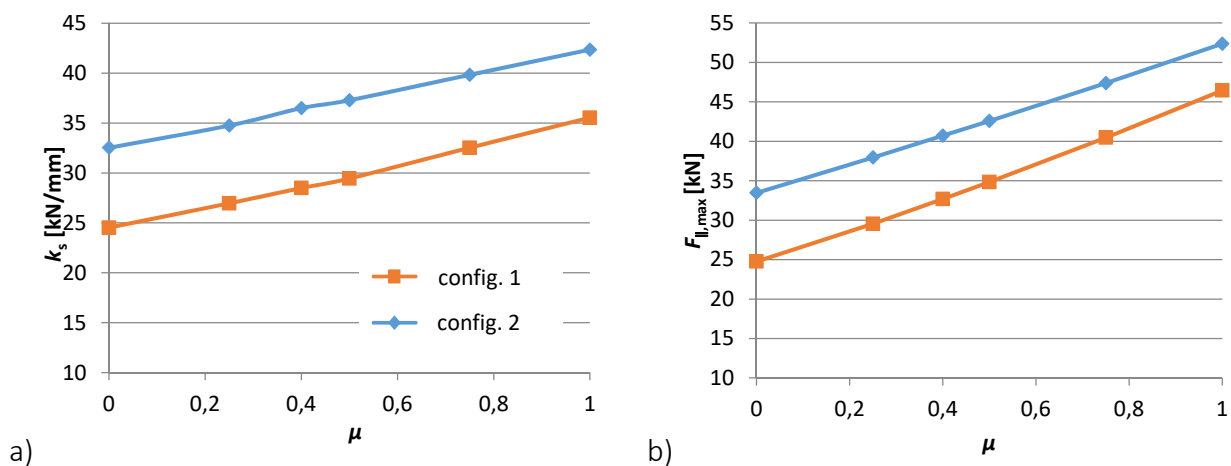


Fig. 9: Influence of μ and test configuration on shear stiffness (a) and ultimate shear load (b).

The friction coefficient between two real timber members can vary somewhere between 0.25 and 0.50. Its actual level depends on many factors, such as: surface treatment, type of wood, grain orientation, moisture content etc. The hypothetical friction coefficient value of 0 could in reality represent a situation in which the surface of timber members would be smoother (e.g. application of surface coatings, foil etc.). A high value of friction coefficient (e.g. $\mu = 1.0$) could be achieved with an insertion of a roughened surface (e.g. perforated metal, compressed wood etc.). Corresponding research results were recently published e.g. by Aurand and Blass (2020).

Generally, the diagrams of the sensitivity analysis show that an increase of friction coefficient from 0.25 to 1.0 can cause a rise in k_s of approx. 20% for models with $\alpha = 30^\circ$ and approx. 30% for those with $\alpha = 45^\circ$. The same increase of the coefficient would cause an even higher rise in total shear capacity: approx. 35% for $\alpha = 30^\circ$ and approx. 55% for $\alpha = 45^\circ$.

4 Conclusions and consequences

The following conclusions can be drawn from the study:

- 3D FE analysis turn out as a suitable method to investigate the complexity of the load-displacement behaviour of compression shear tests with inclined or cross-wise arranged screws. Almost all contributing components could be adequately modelled. The model can, therefore, reflect the boundary conditions and the response of actual screwed connections.
- Comparisons with experimental tests show that the accuracy of the numerically determined stiffness is sufficient. Hence, the modelled compression shear test is a reliable method for the determination of k_s . Model improvements may concern the full evolution of damage between the transfer from wood to screw and embedment behaviour of the screws.
- Axial forces in cross-wise arranged screws mutually neutralise so that merely the force H , which results from the geometry or eccentricity of the test set-up in compression shear tests, effects friction. In case of larger relative displacements, the absolute value of the axial force in the tension screw becomes higher than that in the crossing compression screw.
- The FE analyses clearly reflected the fact that the share of friction in total shear stiffness is higher for inclined than for cross-wise arranged screws. The analyses revealed that the influence of friction is largest for small shear displacements and it reduces until a relatively constant influence is reached beyond a relative displacement of approx. 0.5 mm. Such a difference could be accounted to the fact that often the friction coefficient at the initiation of slipping from a sticking condition is different from the friction coefficient during established sliding. The reason is supposed in penalty friction formulation used in the numerical model.
- In case of compression shear specimens with inclined screws, compressive stresses in the interface are more or less wave-like distributed along the interface. However, specimens with cross-wise arranged screws exhibit compressive stresses which are locally concentrated each at the top and at the bottom of the interface.
- Apart from the arrangement inclined or cross-wise, main drivers for the shear stiffness are the axial stiffness k_{ax} of the screw, where k_{ax} in turn depends on the inclination α and penetration length, and the friction coefficient μ .
- There are signs that compression perpendicular to the grain slightly influences the shear stiffness in case of inclined screws.
- The load-displacement behaviour of connections with inclined screws could be improved with the increase of friction coefficient. It was determined, however, that the rise in k_s is limited and that further studies are necessary to answer whether an increase of friction coefficient is actually a reasonable solution to improve the load-displacement behaviour. An additional increase of k_s could also be achieved by

increasing the stiffness perpendicular to the grain – e.g. by insertion of a layer with higher stiffness between the timber parts.

Based on the study, the following consequences can be established:

- In evaluations of compression shear tests with cross-wise arranged screws one should consider that back-calculated axial stiffness values k_{ax} are influenced by friction to some extent.
- The geometry of the test specimens has an impact on the share of friction in the total shear force. With slender specimen ($b \ll \ell$) the influence of friction on the stiffness and load-carrying capacity of the cross-wise arranged screw connections could be neglected.
- Future studies are foreseen to validate the results of experimentally determined k_s values. That concerns e. g. FE models for different structural applications using connections with inclined and cross-wise arranged screws.
- Future work is necessary in this field to find an optimal combination of material with high stiffness and friction, with the aim to achieve high performance timber connections with inclined screws.

Acknowledgment

The research was financially supported by the project InnoCrossLam, which is funded under the umbrella of ERA-NET Cofund ForestValue by MIZŠ and by DAAD for funding the Research stay of Boris Azinović at KIT. The Research stay was a pleasant experience due to warm hospitality of all personnel at KIT.

5 References

- Blass HJ, Steige Y: Steifigkeit axial beanspruchter Vollgewindeschrauben. Karlsruher Berichte zum Ingenieurholzbau (Bd. 34). KIT. 2018
- Bejtka I, Blass HJ: Joints with inclined screws. Proceedings from CIB meeting - W18. Kyoto, Japan. 2002
- Avez C, Descamps T, Serrano E, Leoskool L: Finite element modelling of inclined screwed timber to timber connections with a large gap between the elements. EurJWoodProd 74: 467–471. 2016
- Kevarinmäki A: Joints with inclined screws. Proceedings from CIB meeting - W18. Kyoto, Japan. 2002
- Tomasi R, Crosatti A, Piazza M: Theoretical and Experimental Analysis of Timber-to-Timber Joints Connected with Inclined Screws. ConBuildMat 24(9):1560–71. 2010
- Jockwer R, Steiger R, Frangi A: Fully Threaded Self-tapping Screws Subjected to Combined Axial and Lateral Loading with Different Load to Grain Angles. Materials and Joints in Timber Structures. RILEM. 2014
- Pranjic A: Extended three-phase bond behaviour model between glulam wood matrix and axially loaded self-tapping screws. Doktorandenkolloquium Holzbau Forschung + Praxis. Stuttgart, Germany. 2020
- Aurand S, Blass HJ: Verbinder aus Kunstharzpressholz mit veränderter Oberfläche zur Erhöhung der Reibung in der Scherfuge. Bautechnik 97 (Sonderheft Holzbau):44-54. 2020
- EAD 130118-00-0603. Screws for use in timber constructions. 2016
- EAD 130118-00-0603. Screws for use in timber constructions. draft 2020
- EN 1382:2016 Timber structures - Test methods - Withdrawal capacity of timber fasteners
- EN 14592:2017 Timber structures - Dowel-type fasteners – Requirements

Discussion

The paper was presented by B Azinović

P Dietsch asked what would be the effect of screws not perfectly aligned at the set angle. B Azinovic agreed that this could influence the Ks values.

M Cabrero asked how was the size of the cohesive zone determined. B Azinovic commented that the stiffness of the soft material was assumed to be 5 times lower than the orthotropic material. Also fracture energy calibration was considered by checking the prediction of initiation of failure against test data.

F Lam questioned whether friction should be relied upon in practice where drying out could create gaps and influence friction. B Azinovic agreed in general but friction could be considered if there was no gaps.

G Hochreiner asked whether the ductility shown in the experimental load slip curve was due to the timber or steel. B Azinovic said timber.

G Hochreiner commented that the gaps in shear plane in practice might result in different stiffness values. He suggested a two stage approach where for serviceability limit state friction could be considered and for ultimate limit state friction should be omitted.

R Brandner commented that fracture zone might be different for different screw insertion angles. He was not sure how the model could deal with this. B Azinovic agreed as the work only dealt with two angles.

J Brown asked if shear tension load arrangements were considered. B Azinovic said it could be done but it was not considered so far.

Embedding strength prediction for European Hardwood species

Thibault Benistand, ENSTIB/LERMAB, University of Lorraine, France

Laurent Bleron, ENSTIB/LERMAB, University of Lorraine, France

Jean-François Bocquet, ENSTIB/LERMAB, University of Lorraine, France

Keywords: embedment tests, hardwood, Eurocode

1 Introduction

In Europe, the number of buildings made with timber is increasing. Builders mainly use solid timber, glulam, CLT and LVL from softwoods. In order to ease the tensions over softwood resources (such as drought and insects) and to keep maintaining sustainable exploitation of forests, designers will have to reintroduce hardwoods into buildings. In Europe, the species with the highest potential for this usage are beech, ash, oak, birch and poplar. While some studies have made it possible to validate or modify the estimation of mechanical properties for these species (e.g., Kovriga et al., 2019), a great deal of research remains to be carried out on the justification of the joints. Regarding the difficulties of using nails in hardwood, this study will be focused only on fasteners such as bolts and dowels.

2 Embedding strength in hardwood

In Eurocode 5 (EN 1995-1-1), the estimation of dowel-type fastener strength capacity is still based on the limit analysis theory proposed by Johansen (1949). The calculation is based on the geometric parameters of the connection (thickness and dowel diameter), the yield moment of the fastener $M_{y,Rk}$ and the timber properties: the embedding strength $f_{h,\alpha,k}$.

Equation (1) of Eurocode 5 is based on several studies (Whale and Smith, 1986; Ehlbeck and Werner, 1992) and allows the estimation of the characteristic embedding strength. Ehlbeck and Werner carried out embedment tests in different hardwood and tropical wood species. They showed that the embedding strength for these species was 10% higher than the strength measured for softwoods. Despite these conclusions, only the equation determined for softwoods was retained in the writing of the European calculation standard (1).

$$f_{h,0,k} = 0.082 (1 - 0.01 \times d) \rho_k \quad (1)$$

Larsen (1973) showed that the embedding strength of fasteners with a diameter greater than 8mm depended on the angle between the force and the grain direction. This variation can be described using the Hankinson approach (2). This formula introduces the corrective coefficient k_{90} which corresponds to the ratio between the embedding strength parallel and perpendicular to the grain. In EN 1995-1-1, a corrective factor specific to hardwoods is proposed. This equation was established from the tests of Ehlbeck and Werner (1992) by dividing the embedment equation at 0° proposed in the Eurocode by the characteristic experimental embedding strength obtained for beech and azobe.

$$f_{h,\alpha,k} = \frac{f_{h,0,k}}{k_{90} \cos^2 \alpha + \sin^2 \alpha} \quad (2)$$

with $k_{90} = 1.3 + 0.01d$ for softwood and $k_{90} = 0.9 + 0.01d$ for hardwood

Since Ehlbeck and Werner's 1992 study, further studies have been proposed to characterise the embedding strength of hardwoods. These include :

- Sandhaas and al. (2013), who proposed to simplify the calculation code using a formula without integrating the diameter effect.
- Kobel and Frangi (2014), who proposed specific embedment values for beech LVL.

In 2008, Hubner et al. (2008) planned to predict embedding strength with a mathematical form in power law, in accordance with a proposal from Blass and Uibel (2007). This equation was proposed in the draft of EN 1995-1-1 (2019-09-21).

$$f_{h,0,k} = 0.015 \rho^{1.19} d^{-0.179} \quad (3)$$

Franke and Magniere (2014) studied the embedding strength for softwood and hardwood depending on the angle between the load and the grain direction. For each angle direction between the load and the grain (0° , 25° , 55° and 90°) and for each diameter (6, 12, 20 and 30 mm) they conducted 10 tests on beech and spruce. They confirmed the validity of the Hankinson equation for softwoods, and proposed a new equation (4) for hardwoods with a variation on the trigonometric coefficients. This relationship was based on mean values and needed to be studied with characteristic values in order to be used in design standards.

Schweigler et al. (2018) summarised the different behaviour laws that existing for softwood embedding strength variations in function of the angle between force and grain.

$$f_{h,\alpha,mean} = \frac{f_{h,0}}{k_{90} \cdot \sin^{1.2} \alpha + \cos^{1.5} \alpha} \quad (4)$$

Numerous studies point out the impact of the roughness of fasteners on the value of the embedding strength parallel to the grain. For softwood, Rodd (1973) and Bleron (2000) found a 47% increase in embedding strength due to the use of knurl fasteners compared to smooth fasteners. Hohenwarter (2014) present tests conducted by Spork in 2007 in spruce with a diameter of 20mm. He confirmed the influence of the roughness on the embedding strength. His results indicated an increase of 16% of embedding strength between knurl fasteners and electrogalvanised fasteners. They also showed a diminution of 6% between smooth and electrogalvanised dowels. As such, the impact of the roughness of rods is of such importance that this parameter cannot be chosen randomly. In order to obtain precise embedding strength equations and a better competitiveness of hardwood species in timber buildings, it appears essential to perform tests with a roughness similar to dowels used in timber construction.

As is the case with all mechanical properties of wood, embedment strength is impacted by variations in moisture content. Hubner et al. (2008) studied the impact of moisture content on the embedding strength of ash and proposed a factor of correction of 3% per percent of moisture content for embedding strength parallel to the grain, and 4% per percent of moisture content for embedding strength perpendicular to the grain. Sandhass et al. (2013) used the same correction for embedding strength as that described in EN 384 for the compression parallel to the grain (3% per percent of moisture content).

A review of the literature regarding embedment strength shows that it is necessary to improve the reliability of prediction of this property. It also shows that the domain of prediction must be extended to the species most likely to be used. As a result, this study will focus on two main hardwood species that are widespread in Europe (beech and oak) and two fast-growing species (poplar and birch). In order to use test results in the BOF (Beam On Foundation) modelling approach, embedding strength displacement evolution will be analysed according the method proposed by Schweigler et al. (2019).

3 Materials and method

3.1 Test setup

When it was possible, the embedment strength tests were carried out according to the directives of EN 383 (2007).

The tests were carried out on a universal testing machine with a capacity of 250 kN. Figure 1 shows the principle of the test setup used for executing the embedding strength tests in the two main directions (0° and 90°). The test setup included two lateral steel jaws which embedded the rod to limit its deformations under bending.

A stack of grinded metal plates and linear needle bearings allowed for free horizontal movement of the sample. This was essential to correctly measure the vertical load applied on the sample when there was an angle between the direction of loading and the grain.

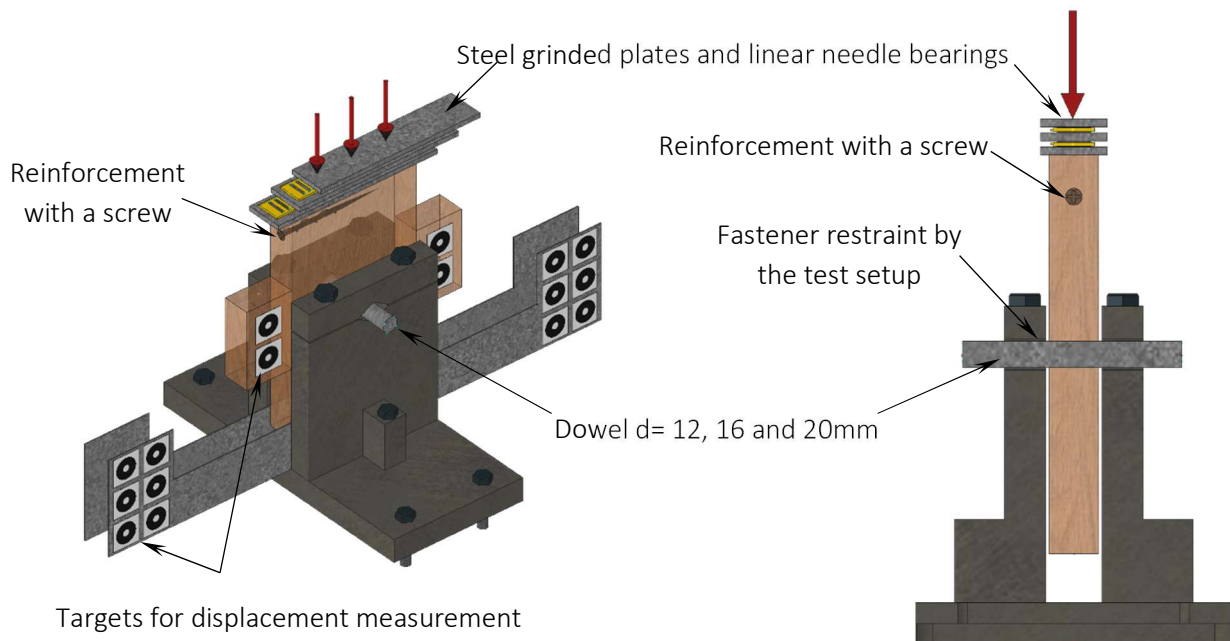


Figure 1: Test setup for embedding strength test (angle of 0° and 90° between force and grain).

In order to provide embedment properties for finite element models (such as beam on foundation), the densification phase after the plastic threshold needed to be as long as possible. To limit the opening of cracks due to transversal tension in the sample at 0° and 30° , it was reinforced with a screw.

In order to be as close as possible to real-world application, the rods used for the tests were similar to those often installed in timber buildings. The use of galvanised steel provided realistic roughness between the dowel and the timber. Considering the high embedding strength that can be achieved with hard wood, and to maintain a thickness sufficiently large for the sample, a high-quality steel was chosen (steel class 8.8).

For loading angles other than 0° and 90° , the recommendations concerning the dimensions and the protocol for loading the samples found in EN 383 (2007) had to be adapted as shown in Figure 2. The same loading setup was used, but the sample dimensions were enlarged by gluing with a polyurethane adhesive (KLEIBERIT 510 polyurethane). To conduct the analysis after testing, only the density where the rod was inserted was retained. It was measured before bonding.

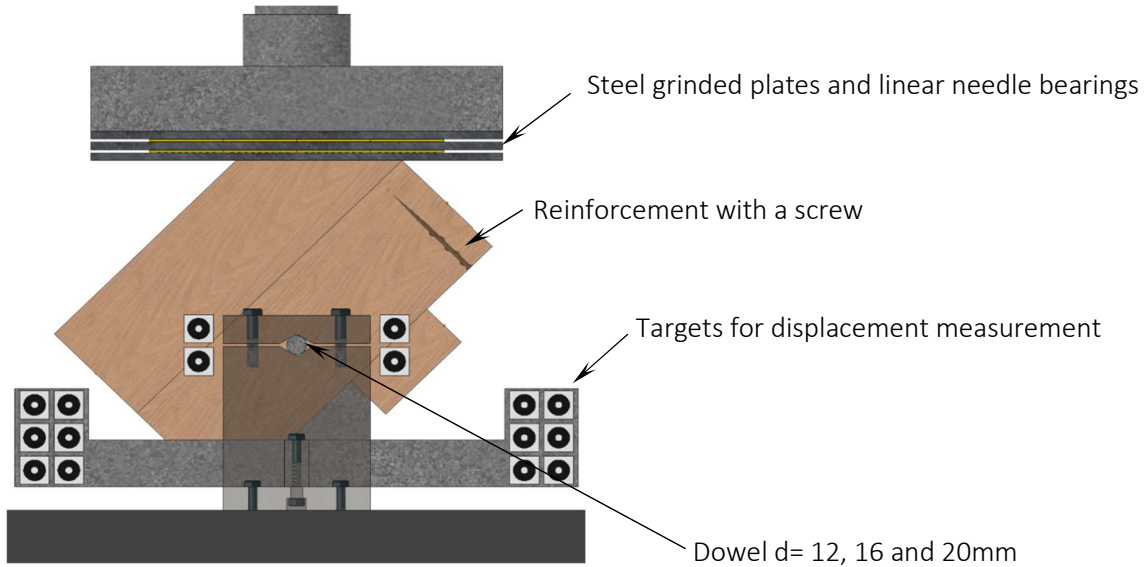


Figure 2: Experimental setup for tests with an angle between the direction of loading and the grain.

3.2 Samples

The dimensions of the sample were fixed according to EN 383 (2007), as shown in Figure 3. The minimum dimensions l_1 and a_1 are shown in Table 1. At a 45° angle, the distances were determined by linear interpolation. According to the norm, the thickness of the test samples should be between $1.5d$ and $4d$. To conform to this criterion, a thickness of 30 mm was used for a rod with a diameter of 12 mm. A thickness of 35 mm was used for rods with a diameter between 16 mm and 20 mm.

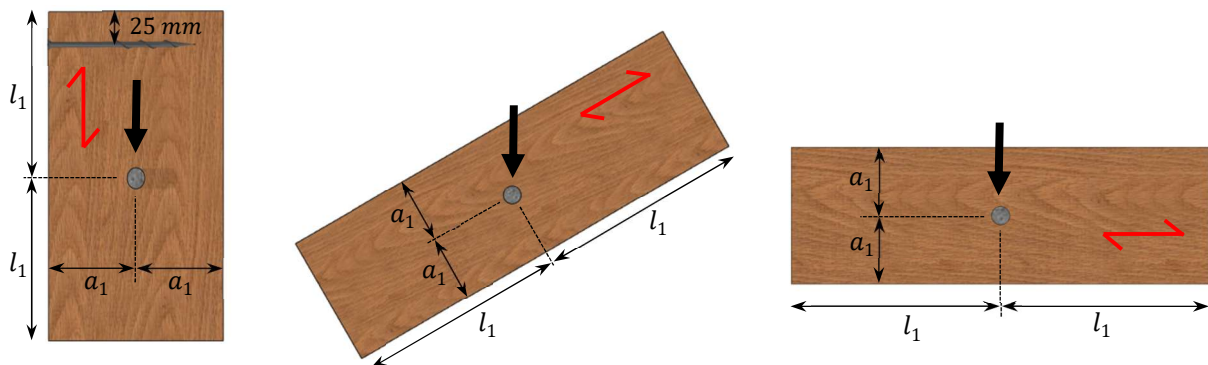


Figure 3: Sizes of specimen according EN 383 (2007). (Note: schema with angle does not exist in EN 383).

Table 1: Size of specimen according to Table 1 in EN 383 (2007).

Angles [°]	0	30	60	90
l_1	7.d	11.5 d	15.7 d	20.d
a_1	3.d	3.7 d	4.5 d	5.d

Before machining the samples, the boards were conditioned for three weeks at a temperature of 20°C and a relative humidity of 65% to tend towards a humidity of the woods around 12%. After the test, the moisture content was measured using a drying method according to NF EN 13183-1 (2002).

3.3 Data analysis

The test curves f_h (embedment displacement) were analysed according to the method developed by Schweigler et al. (2019) to extract the different stiffnesses and the embedment strength. All these results are available on DIVA (<http://urn.kb.se/resolve?urn=urn:nbn:se:lnu:diva-87945>).

In accordance with EN 384 (2018), the density for all interpretations was corrected to indicate a reference moisture content of 12%, as follows:

$$\rho = \rho(u)[1 - 0,005(u - u_{ref})] \text{ for } 8\% < u < 18\% \text{ with } u_{ref} = 12\% \quad (5)$$

Despite an undeniable impact of moisture content on embedding strength, the regulation does not impose to correct the values obtained by taking care of it. However, following the example of Sandhaas et al. (2013), the values obtained were corrected using the formula proposed for axial compression as presented in EN 384, namely:

$$F_{c,0} = F_{c,0}(u)[1 - 0,03(u - u_{ref})] \text{ for } 8\% < u < 18\% \text{ with } u_{ref} = 12\% \quad (6)$$

The tests conducted by Hubner et al. (2008) showed that the embedding strength perpendicular to the grain decreased by 3% per percent of moisture content. For this reason, a global criterion of correction for the embedment according to any angle between the effort and the grain of the wood was considered, as follows:

$$f_{h,\alpha} = f_{h,\alpha}(u)[1 - 0,03(u - u_{ref})] \text{ for } 8\% < u < 18\% \text{ with } u_{ref} = 12\% \quad (7)$$

The characteristic values at the fifth percentile and the characteristic mean values were expressed by following the prescriptions given by EN 384 (2018) (§5.5.1) which requires the use of the calculation methods defined in EN 14358 (2016). These values must be expressed in accordance with the requirements of EN 1990 with a confidence level of $\alpha = 75\%$.

The average densities and the average local embedding strength are expressed in Table 6 as characteristic averages. The other mean values in the table are arithmetic means.

In order to propose equations for structural design, the embedment strength mean equation as a function of diameter and density was estimated for each angle and each species. These mean equations were then transformed into a characteristic equation according to the method used by Ehlbeck and Werner (1992) and Hubner et al. (2008). The factor γ was calculated according to equation (8) to adjust the curve of the linear regression as a function of the coefficient of variation of the density and the embedding strength. The characteristic equation is obtained by multiplying the mean equation by the correction coefficient γ , as follows:

$$\gamma = \frac{x(P = 0.05|N(\mu; COV_{f_h}))}{x(P = 0.05|N(\mu; COV_{\rho}))} \quad (8)$$

4 Test results

The tests results presented in Table 6 (see appendix) were consistent with the results presented in the literature review. Density COV varied from 4% to 9% and embedment strength COV varied between 8% and 14%. Despite similar densities between beech and oak, tests show significant differences on the embedding strength capacity depending on the species; the beech was, on average, 16% stronger than oak.

5 Discussion

5.1 Embedding strength parallel to the grain

For dowels with a diameter of 12 mm and 16 mm, the data analysis shows a correlation coefficient of between 0.28 and 0.73 for the embedment strength parallel to the grain and the density (Table 3). For dowels with a diameter of 20 mm, this correlation coefficient remains high for beech ($R^2 = 0.59$), but decreases for birch ($R^2 = 0.33$), oak ($R^2 = 0.23$) and poplar ($R^2 = 0.13$). The data also show that the embedment strength can be plotted as a function of density for each rod size. Therefore, it is possible to define a relationship of the type $f_h / \rho = f(d)$ (Figure 4).

Table 2. R^2 coefficient for relation between embedment strength and density for each species and each diameter

	Poplar	Birch	Beech	Oak
D12	0.28	0.38	0.70	0.70
D16	0.64	0.55	0.73	0.57
D20	0.13	0.34	0.60	0.24

The average equation of embedding strength for each species is shown on Figure 5 in comparison with the equations presented in CIB 25-7-2, which was used as a basis for EN 1995-1-1 (2004). With the exception of poplar and birch, the average equations obtained by the tests are higher. This suggests that the code and its equation (1) tend to underestimate the embedding strength of hardwoods.

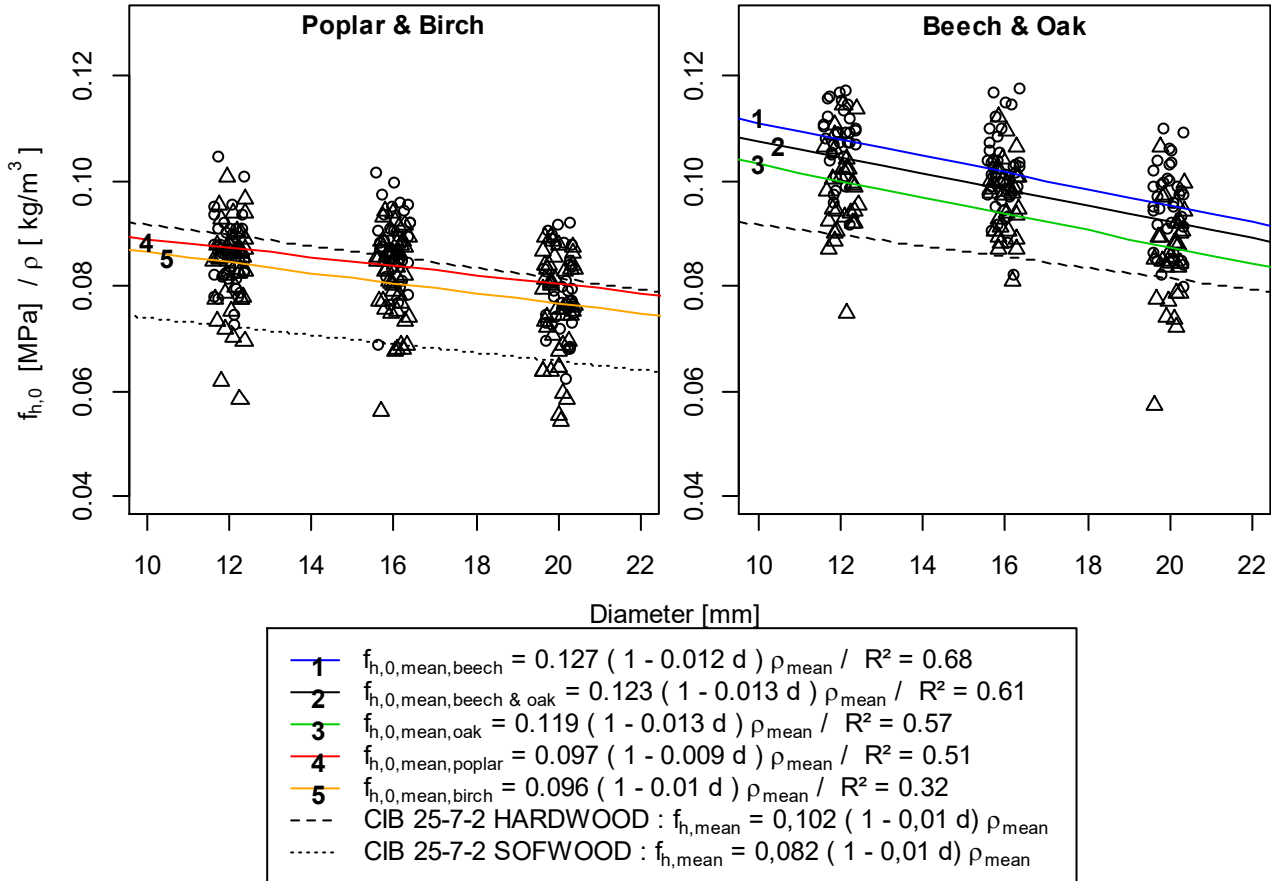


Figure 4: Embedding strength parallel to the grain as a function of diameter and density. The variation of the diameter is due to an artificial jitter to make the curve easier to read.

The difference between Ehlbeck and Werner's (1992) proposal (CIB 25-7-2) and the beech test results is between 18% and 20%. This gap could be explained in part by the natural variability linked to the growth of the trees, but the main reason for this disparity comes from the difference in roughness between the smooth rod used in the 1992 study and the galvanised rods used in the current study.

Table 3 shows the conversion of the average equations into a characteristic equation using the method explained in the previous section. The equations proposed for poplar and birch are quite close to each other and are clearly lower than the equations obtained for beech and oak. The hypothesis, made in France, that poplar behaves like a coniferous species is thus verified. Birch can also be considered as a softwood when estimating its embedding strength.

Table 3: Characteristic relationships of the embedding strength parallel to the grain.

Species	$f_{h,0,mean} =$	γ	$f_{h,0,k} =$
Poplar	$0.097(1 - 0.009 d) \rho_{mean}$	0.930	$0.091(1 - 0.009 d) \rho_k$
Birch	$0.096(1 - 0.010 d) \rho_{mean}$	0.849	$0.082(1 - 0.010 d) \rho_k$
Beech	$0.127(1 - 0.012 d) \rho_{mean}$	0.869	$0.111(1 - 0.012 d) \rho_k$
Oak	$0.119(1 - 0.013 d) \rho_{mean}$	0.857	$0.103(1 - 0.013 d) \rho_k$

Extracting a characteristic equation from the cumulative average results of all species would make no sense because the density differences between poplar and other hardwood species are significant. The coefficients of variation of 17% on the density and 27% on the embedment would lead to the expression a characteristic equation equivalent to the current equation of the Eurocode (1). This solution does not give an optimal report on the performances of hardwood species.

For oak and beech, a new embedment strength equation (9) should be proposed. This equation is obtained by setting a COV of 15% for embedment (14.2% in reality) and a COV of 6.5% for density, as follows:

$$f_{h,0,k} = 0.104 (1 - 0.013 d) \rho_k \quad (9)$$

Compared to the current equation of the Eurocode (1), this new mathematical relationship allows an average gain of 22% of embedding strength for organs with a diameter of between 12 mm and 20 mm. This new equation overestimates the embedding strength for oak to a maximum of 3.6% and underestimates the strength for beech by an average of 9.7%. By using the same COV for the density as that proposed in EN 384 (COV = 10%) and the COV generally used for strength (20%), it is possible to estimate equation (10), which never underestimates the embedding strength compared to all the results of the study:

$$f_{h,0,k} = 0.099 (1 - 0.013 d) \rho_k \quad (10)$$

Following the work of Hubner et al. (2008), it is possible to express a general average and characteristic equation to estimate the embedment strength as a function of density and diameter for all species. The transformation between mean and characteristic equations is made by considering a COV of 10% for the density and 20% for the embedment strength, as follows:

$$f_{h,mean} = 0,00504 \cdot \rho_{mean}^{1,529} \cdot d^{-0,195} \quad (11)$$

$$f_{h,k} = 0,00459 \cdot \rho_k^{1,529} \cdot d^{-0,195} \quad (12)$$

As shown in Figure 5, this new equation underestimates the characteristic embedment strength for birch by 10% for the diameter 20mm, but gives safe results for the other three species. The equation proposed by Hubner et al. (2008) corrects this problem but significantly underestimates the strength for beech and oak.

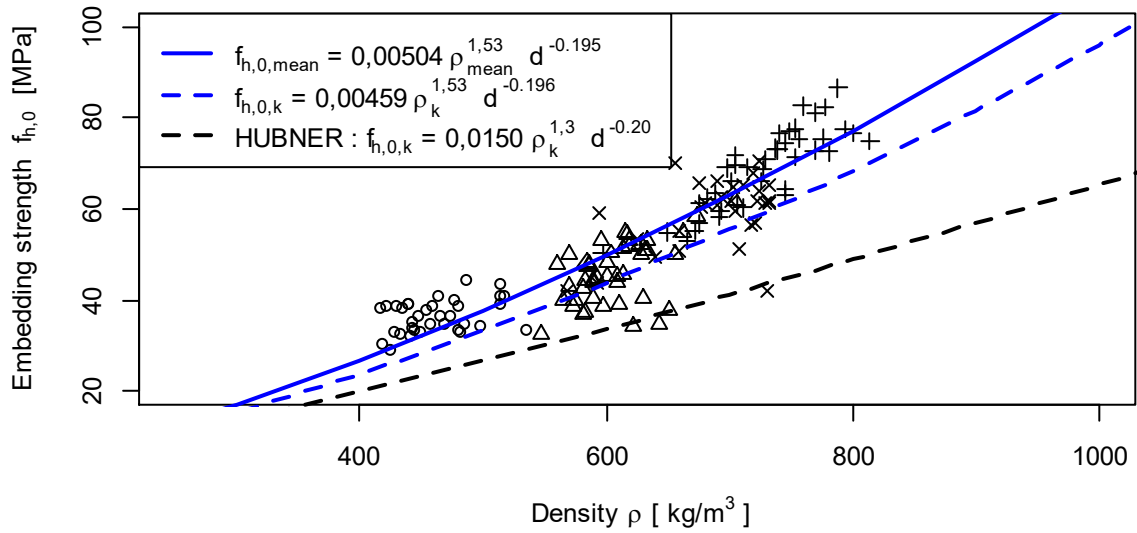


Figure 5: Embedding strength parallel to the grain as a function of density for a diameter of 20 mm.

5.2 Embedding strength perpendicular to the grain

Figure 8 shows that the embedment strength perpendicular to the grain is largely dependent on the timber species. The tests allowing the writing of Eurocodes (CIB 25-7-2) were carried out with beech timber. The results of this proposal to forecast embedment strength are comparable to those obtained in this experimental study. As indicated in the literature review, the roughness of the dowel has no effect on the embedment strength perpendicular to the grain. The small difference observed can be explained by natural variability linked to wood growth.

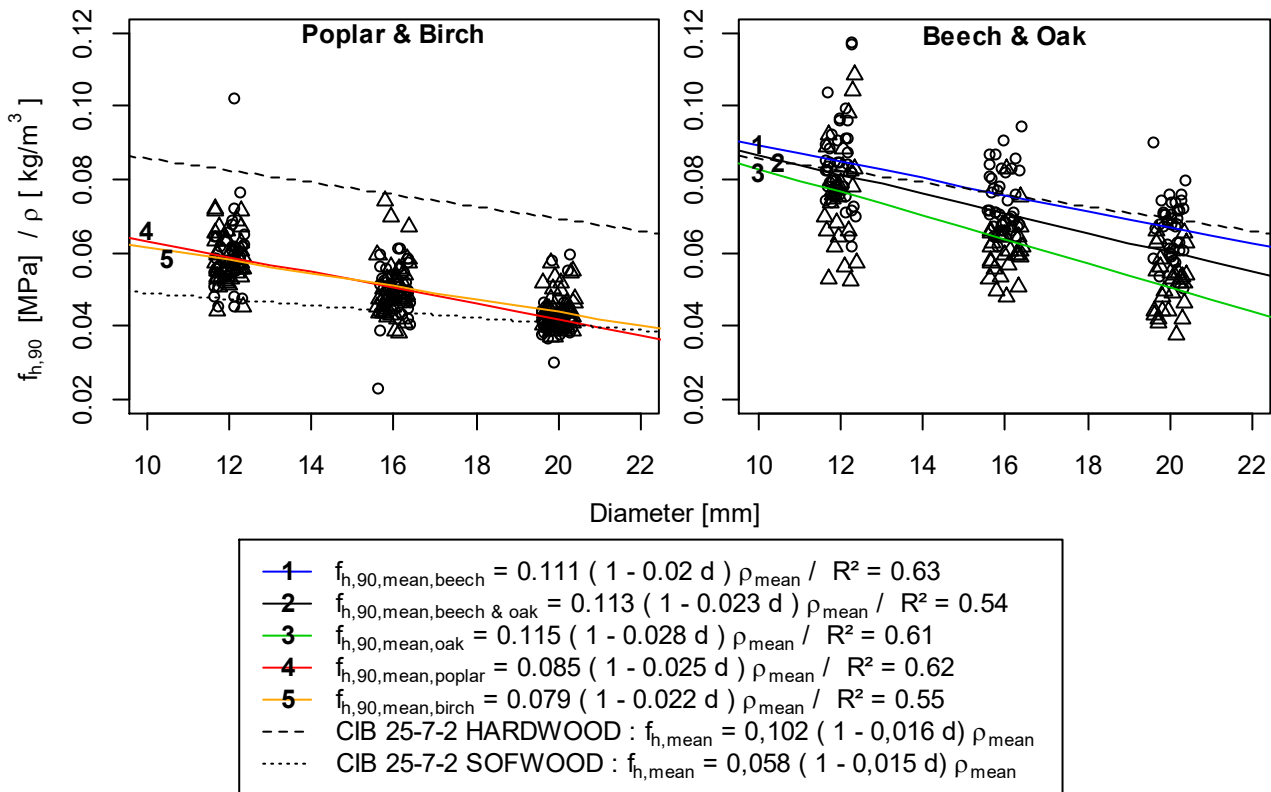


Figure 6: Embedding strength perpendicular to the grain as a function of diameter and density. The variation of the diameter is due to an artificial jitter to make the curve easier to read.

The average equations regarding embedment strength parallel to the grain are converted into characteristic equations in Table 4. In Eurocode 5, the determination of the embedment perpendicular to the grain is based on the Hankinson formula, in which a coefficient k_{90} is introduced as $k_{90} = f_{h,0,k}/f_{h,90,k}$. The equation of k_{90} is defined for rods with diameters ranging from 12 mm to 20 mm.

Table 4: Characteristic relationships of the embedding strength perpendicular to the grain and k_{90} coefficient according the definition of EN 1995-1-1.

Species	$f_{h,90,mean} =$	γ	$f_{h,90,k} =$	$k_{90} =$
Poplar	$0.085 (1 - 0.025 d) \rho_{mean}$	0,724	$0.061 (1 - 0.025 d) \rho_k$	$1.017 + 0.072 d$
Birch	$0.079 (1 - 0.022 d) \rho_{mean}$	0,752	$0.060 (1 - 0.022 d) \rho_k$	$1.141 + 0.042 d$
Beech	$0.111(1 - 0.020 d) \rho_{mean}$	0,740	$0.083(1 - 0.020 d) \rho_k$	$1.238 + 0.022 d$
Oak	$0.115(1 - 0.028 d) \rho_{mean}$	0,657	$0.076 (1 - 0.028 d) \rho_k$	$0.86 + 0.071 d$
Beech & Oak	$0.113(1 - 0.023 d) \rho_{mean}$	0,677	$0.077 (1 - 0.023 d) \rho_k$	$1.147 + 0.039 d$

Using the characteristic equation to predict embedment strength parallel to the grain found for each species, the experimentally defined reduction factor k_{90} is shown not to be as low as that proposed by Eurocode 5 (2).

For birch and poplar, the prediction made using the equations of Eurocode 5 (1) to predict embedment strength and the factor k_{90} for softwood underestimates embedment strength by nearly 2% compared to the experimental results (the maximum deviation is 10% for poplar with a diameter of 16 mm). Without modifying EN 384 density classes, this difference is largely compensated by the systematic under-evaluation of density (C24 at 350 kg/m³ when experimental results show an average characteristic density of 400 kg/m³ for poplar).

Using the Eurocode 5 equations (1) and (2) with the experimental results of beech timber, the difference between the prediction and the results is a maximum of 1.5%. However, for oak timber, the calculation code tends to overestimate the embedment strength by nearly 17% on average compared to the experimental results, which is not acceptable. Consequently, two correction approaches may be proposed:

- keep equation (1) to estimate embedment strength parallel to the grain and define a new k_{90} (15), or
- use the proposed equation (9) and define the k_{90} equation associated (14).

For these two approaches, the characteristic embedment strength perpendicular to the grain is define in (13) with a COV of 25% and 6.5% for the density (measured values). With this correction, the equation underestimates the perpendicular embedment of oak by an average of 9% and of beech by an average of 30%.

$$f_{h,90,k} = 0.0746 (1 - 0.0234 d) \rho_k \quad (13)$$

$$k_{90} = 1.15 + 0.04 d \quad (14)$$

$$k_{90} = 0.88 + 0.039 d \quad (15)$$

The same methodology can be applied to define a coefficient k_{90} associated with the proposed equation (12). It is noticeable that the expression proposed by Hubner et al. (2008) gives a similar prediction to that of equation (16), even if the set of coefficients are different. Consequently, the difference between the two studies in terms of embedding strength parallel to the grain is probably linked to the roughness of the dowel used for the tests. The modification of the average equation into a characteristic equation and its comparison with equation (12) makes it possible to propose a general factor k_{90} for hardwoods and softwoods (17). While these new equations give results close to experimental values, they overestimate the embedment strength for birch by 13% and for oak by 3%. For specific study, if the overestimation for birch timber is not acceptable, the k_{90} factor describe by equation (18) should be used.

$$f_{h,90,mean} = 1,88 \cdot 10^{-4} \cdot \rho_{mean}^{2,133} \cdot d^{-0,564} \tag{16}$$

$$k_{90} = 1.065 + 0.041 d \tag{17}$$

$$k_{90} = 1.32 + 0.040 d \tag{18}$$

5.3 Embedding strength with an angle to the grain

According to Figure 7, the variation of the embedding strength at an angle of 30° between the load direction and the grain is quite similar for beech and oak. For embedment at an angle of 60°, the tests highlight three phenomena:

- When the diameter of the rods increases, the diminution of embedment strength for beech timber is more important than it is for oak timber.
- The embedding strength of 20 mm diameter rods is higher than that of 16 mm diameter rods.
- For beech and oak timber, the embedding strength at an angle of 60° is lower than the embedding perpendicular to the grain, as show by Franke and Magniere.

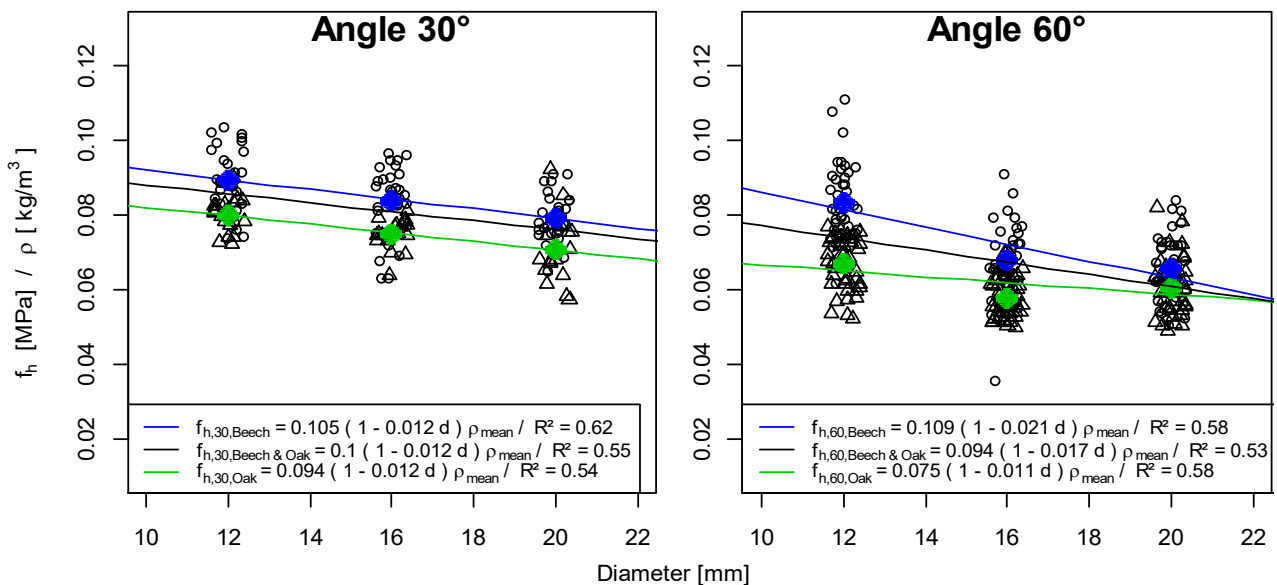


Figure 7: Embedding strength $f_{h,5mm}$ with an angle of 30° and 60° between the load direction and the grain as a function of the diameter and density for beech and oak timber.

Among all the relationships proposed by Schweigler et al. (2018) to describe the evolution of the embedding strength as a function of the angle, only the Hankinson formula (2) with a trigonometric coefficient lower than two makes it possible to predict a 60° embedding strength lower to the embedding strength perpendicular to the grain.

$$f_{h,\alpha} = \frac{f_{h,0} \cdot f_{h,90}}{f_{h,0} \cdot \sin^{b_1} \alpha + f_{h,90} \cdot \cos^{b_2} \alpha} \quad (19)$$

The four possible variations of the trigonometric parameters are:

- b_1 and b_2 equal: $b_1 = b_2$;
- b_1 and b_2 equal and definite as a function of the diameter: $b_1 = b_2 = f(d)$;
- b_1 and b_2 different; and
- b_1 and b_2 different and definite as a function of the diameter: $b_1 = f(d)$ and $b_2 = f(d)$.

To define these coefficients, two thirds of the data are randomly extracted and used for the non-linear regression, while the last third is used to validate the model. The different parameters for the Hankinson formula are summarised in Table 5.

For the equation using the same coefficient b_1 and b_2 , the difference between the prediction and the last third of data varies from 9.6% to 11.5%. If the diameter variation is considered in the parameters b_1 and b_2 , the prediction is only improved by 1%. As a result, the equation based on constant coefficients b_1 and b_2 is sufficiently accurate to describe the variation of the embedment strength as a function of the grain angle.

Table 5: Coefficients b_1 and b_2 for the Hankinson formula (19) for each variation tested.

Species	$b_1=b_2$	$b_1=b_2=f(d)$	b_1	b_2	$b_1=f(d)$	$b_2=f(d)$
Beech	1.650	$0.015 d^2 - 0.47 d + 5.2$	1.76	1.51	$-0.01 d^2 + 0.35 d - 1.22$	$0.035 d^2 - 1.17 d + 10.8$
Oak	1,698	$0.008 d^2 - 0.164 d + 2.252$	1.782	1.416	$-0.032 d^2 + 0.977 d - 5.543$	$0.106 d^2 - 3.001 d + 21.811$
Beech & Oak	1.624	$0.011 d^2 - 0.310 d + 3.716$	1.80	1.43	$-0.018 d^2 + 0.044 d - 2.88$	$0.044 d^2 - 1.33 d + 11.1$

In practice, only characteristic values of embedding strength are considered to design connection. Because the coefficients of variation depend on the grain angle and the rod size (between 8% and 23%), it is impossible to convert the mean equation into a characteristic equation using a global coefficient of variation. Therefore, the new equation is established with characteristic embedment strength values determined at each angle. The embedding strength parallel and perpendicular to the grain are determined using equations (9) and (14). The characteristic values for embedment at an angle of 30° and 60° are extracted from tests results.

The mean and characteristic embedding strength equations are plotted in Figure 8. If a trigonometric coefficient of 1.598 is needed to fit the results for a mean law, the value of two can be kept for the characteristic law. Even if the difference between the predictions made by the standard and the embedding strength parallel and perpendicular tests results appears important, the deviation is less significant when the force is applied with an angle to the grain. The current prediction of the embedding strength made by the standard equation underestimates the embedding strength at an angle of 30° (7.6%) and overestimates it at an angle of 60° (12.4%). The previous relative gap with the trigonometric parameters set at two is 4.6% and 8.8%, respectively.

When the embedding strength is estimated with a power function, the same analysis gives a trigonometric best factor equal to 2.033.

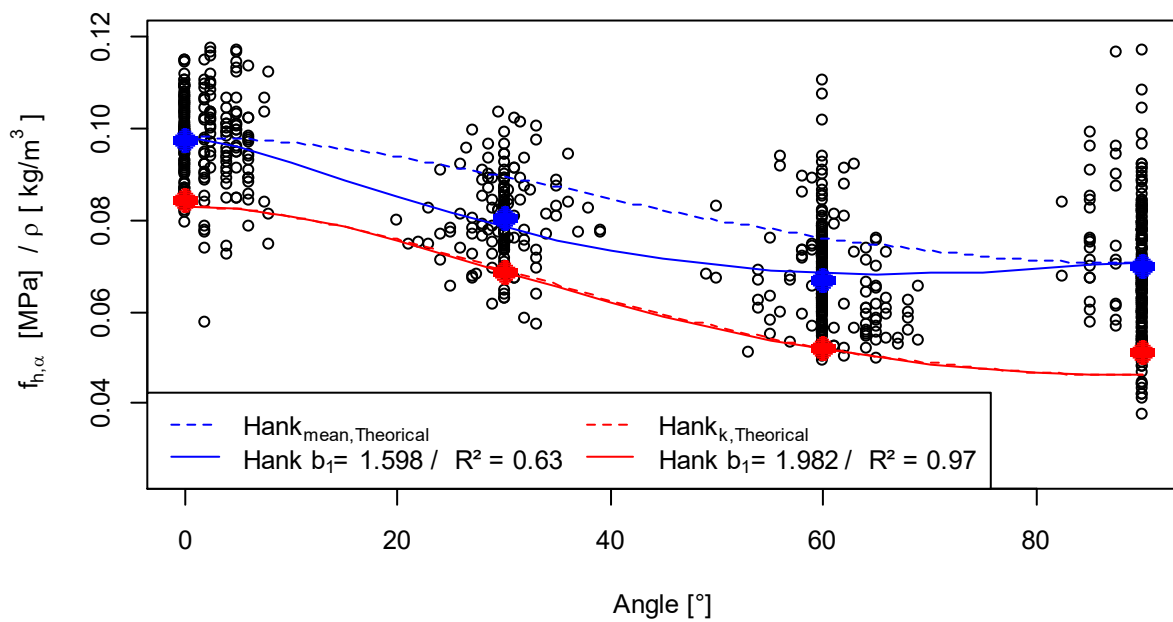


Figure 8: Variation of embedding strength as a function of the diameter, density and angle between the load direction and the grain for beech and oak.

6 Conclusions

This study highlights that the embedding strength of poplar and birch can be accurately estimated by using the current Eurocode 5 equations recommended for softwoods. However, important differences can be found in other hardwood species (oak and beech). With the current equations (1) and (2), the embedment parallel to the grain is largely undervalued. For oak timber, embedment strength perpendicular to the grain is overestimated.

Therefore, for a better prediction of the embedment strength of hardwood, a new equation for the strength parallel to the grain must be used (10). A modification of this relationship implies necessarily to define a new ratio k_{90} (14). If the Hankinson formula must be adapted to correctly fit the mean laws, a parametric coefficient of two is sufficient for a characteristic estimation.

For hardwood (beech and oak), the current study proposes the following equation for embedding strength:

$$f_{h,\alpha,k} = \frac{0.100 (1-0.013 d) \rho_k}{(1.15+0.04 d) \cos^2 \alpha + \sin^2 \alpha} \quad (20)$$

Tests revealed significant differences between the densities of the tested woods and the densities estimated by mechanical grading. For example, with visual grading (NF B 52-001 in France), the majority of hardwoods are attributed to the D24 class. This underestimation of the density leads to a difference of 30% on the prediction of the embedment strength. Before any modification is made to the embedment strength equations in the Eurocode 5, a reassessment of the density proposed in EN 338 must be implemented in order to enable an increase the use of hardwoods in timber construction.

7 Outlook

To improve this proposal, further tests should be conducted on other hardwood species such as birch, ash and chestnut... An further study based on a largest range of densities and constituted of hardwood and softwood will allow validation of the equation with an exponent on the density parameter.

As the embedding strength parallel to the grain is largely impacted by the roughness of the fasteners, two different approaches could be plan to a revision of standard. The first approach would involve the use of smooth fasteners which minimise strength and allow defining safety behaviour. The second approach would precisely quantify this phenomenon and integrate a new factor in the definition of the embedding strength to take this into consideration.

8 Acknowledgements

A part of this study has been realised as part of the EFEUR5 project (2015-2020), financed by the Agence Nationale de la Recherche (convention ANR-15-CE08-0027).

This study has been carried out within the project hardwood_joint, which is supported under the umbrella of ERA-NET Cofund ForestValue by BMLFUW (AT), ADEME (FR), FNR (DE), Vinnova, Swedish Energy Agency and Formas (SE). ForestValue has received funding from the European Union's Horizon 2020 research and innovation programme under grant agreement N_ 773324.

9 References

- Blass, H. J., Uibel, T. (2007) Tragfähigkeit von stiftförmigen Verbindungsmitteln in Brettsper Holz – KIT Scientific Publishing – ISBN 978-3-86644-139-3
- Bleron, L. (2000) Contribution à l'optimisation des performances d'assemblages bois en structure. Analyse de la portance dans les assemblages de type tige, Thesis (only available in French), University of Lorraine.
- Ehlbeck, J., Werner, H. (1992) Softwood and Hardwood Embedding strength for dowel-type fasteners, CIB-W18/25-07-2, Åhus, Sweden.
- EN 383:2007. Timber structures. Test methods. Determination of embedment strength and foundation values for dowel type fasteners. CEN.
- EN 384 (2018) Structural timber – Determination of characteristic values of mechanical properties and density. CEN.
- EN 1990 (2003) Eurocode Basis of structural design. CEN. (Eurocode 0)
- EN 1995-1-1 (2004): Design of timber structures – Part 1-1: General and rules for buildings. CEN. (Eurocode 5).
- EN 13183-1 (2002) Moisture content of a piece of sawn timber – Part 1: Determination by oven dry method. CEN.
- EN 14358 (2016) Timber structures – Calculation and verification of characteristic values. CEN.
- Franke, S., Magniere, N. (2014) Discussion of Testing and evaluation methods for the embedment behaviour of connections, INTER/47-7-1, Bath, United Kingdom.
- Hohenwarter, J. (2014) Vergleich der Lochleibungsfestigkeit in Folge von Zug- und 367 Druckbelastung. GRAZ University of Technology.
- Hübner, U., Bogensperger, T., Schickhofer, G. (2008) Embedding strength of European hardwoods, CIB-W18/41-7-5, Andrews, Canada.
- Johansen, K.W. (1949) Theory of Timber Connections, International Association for Bridge and Structural Engineering (ABSE) Pub. 9, p. 249–262.
- Kobel, P., Frangi, A., Steiger, R. (2014) dowel-type connections in LVL made of beech wood, INTER/47-7-2, Switzerland
- Kovriga, A., Stapel, P., Van De Kuilen J. W. G. (2019) Mechanical properties and their interrelationships for medium-density European hardwoods, focusing on ash and beech, Wood Material Science and Engineering
- Larsen, H. J. (1973) The yield load of bolted and nailed joints, International Union of Forestry Research Organisation Division V (IUFRO V), Rapport NR. R 52 1974, p. 16–31.
- Rodd, P. D. (1973) The analysis of timber joints made with circular dowel connectors, Thesis, University of Sussex.

- Sandhaas, C., Ravenshorst, G. J. P., Blass, H. J., Van De Kuilen, J. W. G. (2013) Embedment tests parallel-to-grain and ductility aspects using various wood species, *European Journal of Wood and Wood Products*, Vol 71, num 5, p. 599–608.
- Schweigler, M., Bader, T. K., Vessby, J., Eberhardsteiner, J. (2017). “Constrained displacement boundary conditions in embedment testing of dowel-type fasteners in LVL”. In: *Strain* 53(6). DOI: 10.1111/str.12238.
- Schweigler, M., Bader, T. K., Hochreiner, G., Lemaître, R. (2018). “Parameterization equations for the nonlinear connection slip applied to the anisotropic embedment behaviour of wood”. In: *Composites Part B: Engineering* 142, pp. 142–158.
- Schweigler, M., Bader, T. K., Bocquet, J.-F., Lemaître, R., Sandhaas, C. (2019) Embedment test analysis and data in the context of phenomenological modelling for dowelled timber joint design, INTER-52-7-8.
- Whale, L. R. J., Smith, I. (1986) Behaviour of nailed and bolted joints under short-term lateral load – Conclusions from some recent research, CIB-W18/19-7-1, Florence, Italy.

Table 6: Density and embedding strength for each test configuration

Species	α [°]	d [mm]	N	H [%]	$\rho_{m,12\%}$ [kg/m ³]	$\rho_{k,12\%}$ [kg/m ³]	COV ρ	$f_{h,5mm,mean}$ [MPa]	$f_{h,5mm,k}$ [MPa]	COV $f_{h,5mm}$
Poplar	0°	12	40	9.70%	501	436	7%	43.03	37.04	8%
		16	38	10.37%	456	389	8%	39.70	31.76	12%
		20	35	9.93%	459	404	7%	35.90	30.05	10%
	90°	12	39	9.80%	483	412	8%	28.42	21.04	17%
		16	39	11.21%	450	401	6%	22.15	15.53	16%
		20	40	11.10%	466	397	9%	19.49	14.92	14%
Birch	0°	12	45	10.09%	603	553	5%	50.14	39.92	12%
		16	45	9.52%	609	554	5%	49.40	40.00	12%
		20	45	9.85%	604	549	5%	45.46	34.74	15%
	90°	12	45	10.18%	613	561	5%	35.48	28.11	13%
		16	45	10.19%	611	552	6%	30.09	22.49	18%
		20	45	9.99%	609	554	5%	26.75	21.15	14%
Beech	0°	12	35	11.55%	745	697	4%	79.69	68.10	8%
		16	40	11.26%	721	647	6%	73.04	59.57	11%
		20	40	11.49%	723	643	6%	67.99	53.61	13%
	30°	12	29	11.53%	720	668	4%	63.61	50.39	13%
		16	32	11.43%	674	567	9%	55.80	39.52	17%
		20	30	11.94%	702	648	4%	55.07	44.96	11%
	60°	12	42	11.45%	737	670	5%	60.44	45.96	15%
		16	43	11.89%	700	599	8%	46.85	31.34	20%
		20	39	13.10%	701	646	5%	45.70	36.46	12%
	90°	12	40	11.95%	721	636	7%	60.12	41.92	20%
		16	40	12.00%	704	624	7%	52.01	38.70	17%
		20	40	12.04%	710	631	6%	47.23	34.80	16%
Oak	0°	12	30	12.50%	702	619	7%	68.45	53.67	14%
		16	30	12.90%	715	625	7%	68.75	58.28	9%
		20	30	11.70%	682	603	7%	58.14	45.16	13%
	30°	12	20	11.35%	684	612	6%	54.48	46.89	8%
		16	19	11.22%	672	555	10%	50.47	41.89	10%
		20	17	11.73%	682	604	6%	47.39	35.70	15%
	60°	12	40	11.76%	688	578	9%	45.43	32.41	18%
		16	46	11.73%	641	563	7%	36.58	29.29	13%
		20	39	13.49%	707	647	5%	42.70	32.82	15%
	90°	12	30	13.20%	696	610	7%	52.59	33.53	23%
		16	29	12.68%	700	608	7%	42.50	32.32	15%
		20	29	11.04%	702	632	6%	35.95	27.11	16%

N: Number of samples

d: Diameter of dowel

H: Mean moisture content

$\rho_{m,12\%}$: Mean density at 12% of MC

$\rho_{k,12\%}$: Characteristic density at 12% of MC

$f_{h,5mm,mean}$: Mean embedding strength

$f_{h,5mm,k}$: Characteristic embedding strength

$f_{h,inter,mean}$: Mean embedding strength

Discussion

The paper was presented by J-F Bocquet

B Azinovic received confirmation that complete data on embedment stiffness is available from their database including different screws types, grain angle and screw diameter.

G Hochreiner asked whether the 5 mm deformation limitation in the standard makes sense for hardwood. J-F Bocquet responded that they are staying with the standard limitation for now. Limitation of the embedment might be related to joint area.

R Brandner asked why assumed normal distribution for density and embedment strength as normal distribution could extend to negative values. He suggested that Lognormal distribution might be better. J-F Bocquet responded that the choice is based on literature and Lognormal distribution fitting was not done.

Beam-on-Foundation Modelling as an Alternative Design Method for Timber Joints with Dowel-Type Fasteners – Part 4: Joints Subjected to In-Plane Loading

Romain Lemaître, Department of Building Technology, Linnaeus University, Växjö, Sweden

Jean-François Bocquet, ENSTIB/LERMaB, University of Lorraine, Épinal, France

Michael Schweigler, Department of Building Technology, Linnaeus University, Växjö, Sweden

Thomas K. Bader, Department of Building Technology, Linnaeus University, Växjö, Sweden

By request of the authors this paper will be published in the INTER proceedings 2021

Brittle failure mode of timber connections with one row of fasteners loaded parallel-to-grain: a new model for splitting failure

Miguel Yurrita. Wood Chair. Department of Building Construction, Services and Structures. University of Navarra. 31009 Pamplona, Spain. myurrital@alumni.unav.es

José Manuel Cabrero. Wood Chair. Department of Building Construction, Services and Structures. University of Navarra. 31009 Pamplona, Spain. jcabrero@unav.es

Keywords: Timber connection , Brittle failure , Splitting , Parallel-to-grain , Large diameter fastener , Eurocode 5

1 Introduction

Timber connections with steel dowel-type fasteners may fail in a ductile or a brittle way. In the case of Europe, the design of timber connections has traditionally focused on the ductile failure by means of the European Yield Model. Lately, several standards and authors have also dealt with brittle failure modes in connections. *Cabrero and Yurrita* (2018) analysed and compared the existing models. A new brittle model for timber connections with large diameter dowel-type fasteners loaded parallel-to-grain with improved performance was proposed by *Yurrita and Cabrero* (2020).

However, the latter model focused on connections with two or more rows of fasteners and their corresponding failure modes: row shear, block shear and net tension. It was deemed necessary to develop a similar approach for connections with a single row of fasteners, in which splitting may lead to the failure of the connection.

Fig. 1 depicts a typical configuration of a timber-to-steel connection with two shear planes and a single row of fasteners. The timber elements are defined by their main dimensions, width b and thickness h_w ; and the steel plate by its thickness t_p . The connection has a total of 5 fasteners ($n_c = 5$) with a diameter d , which fit in pre-drilled holes of diameter d_0 . The parallel-to-grain spacing between fasteners is defined as a_1 , a_3 is the distance from the last fastener to the loaded edge and a_4 is the distance from the row of fasteners to the lateral edge of the timber member. Finally, the length of the connection is $L_c = a_1 (n_c - 1) + a_3$.

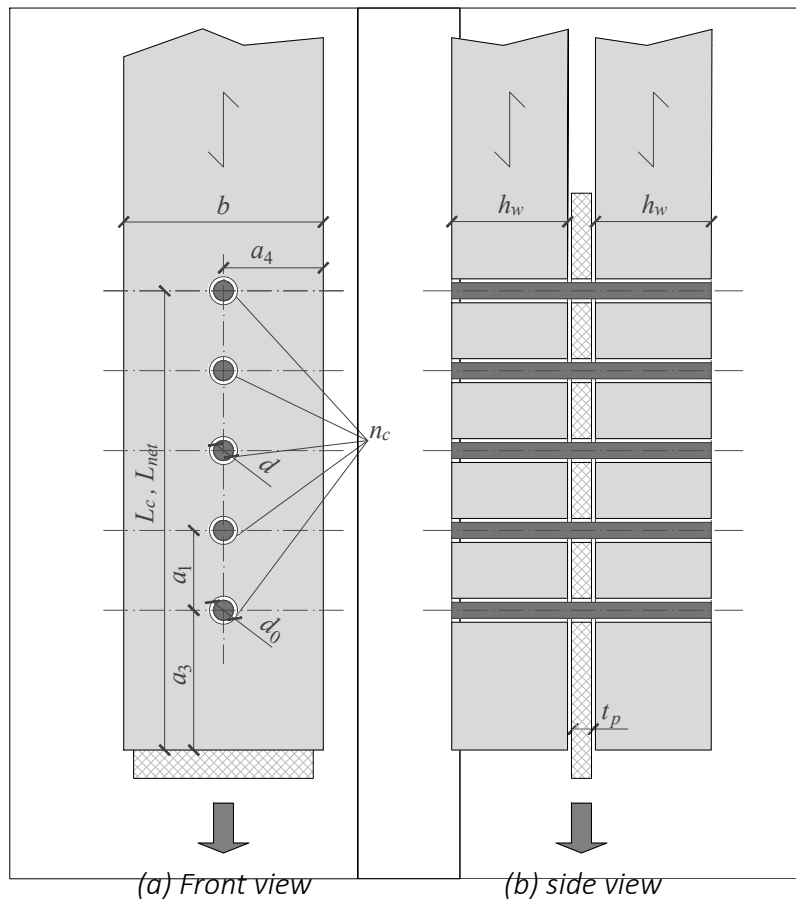


Figure 1. Basic geometry of a generic timber-to-steel connection with two shear planes and a single row of large diameter dowel-type fasteners.

The possible failure modes of a timber connection with a single row of large diameter dowel-type fasteners loaded parallel-to-grain (depicted in Fig. 2) are: embedment - Fig. 2a-, which is the only ductile mode; splitting - Fig. 2b-; row shear - Fig. 2c- and net tension - Fig. 2d-.

Splitting was not considered by *Yurrita and Cabrero* (2020), as this brittle failure mode is not expected to lead to the failure of a connection with a group of fasteners (where row shear and block shear are the typical brittle failure modes, as reported by *Yurrita, Cabrero, and Quenneville* (2019)). This work aims at completing the model proposed by *Yurrita and Cabrero* (2020) by considering splitting failure mode in connections with a single row of fasteners.

2 Existing approaches

Several authors have already dealt with failure of timber connections with a single row of fasteners. Some of them are based on the principles of fracture mechanics, as *Jorissen* (1998), who developed a formula dealing with splitting; and *Jensen and Quenneville* (2011), who considered only row shear.

Other approaches, such as the one by *Jockwer et al.* (2018) and *Hanhijärvi and Kevarinmäki* (2007) provide splitting formulae based on the tensile perpendicular-to grain

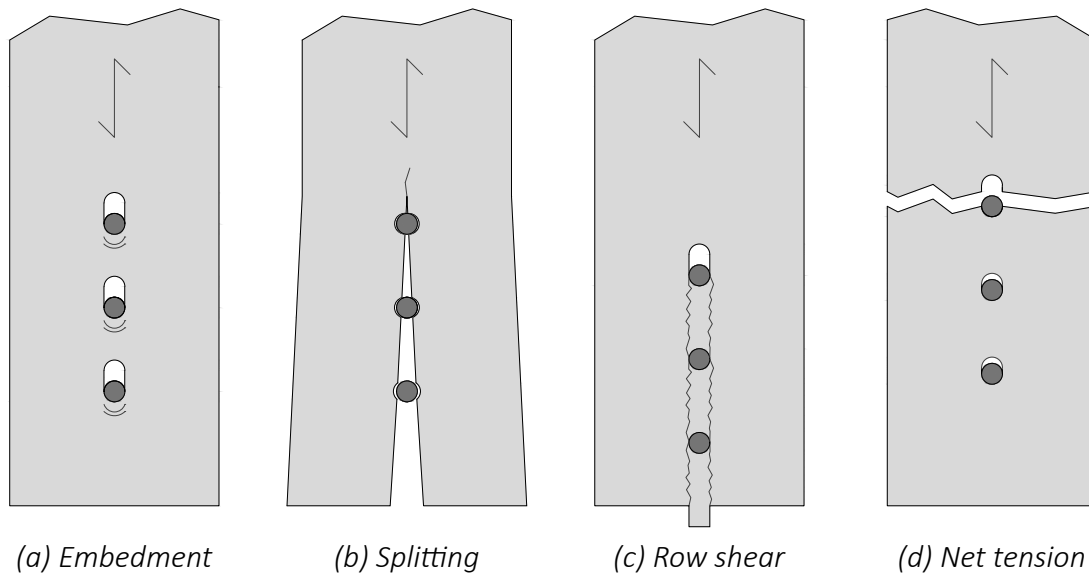


Figure 2. Possible failure modes of a timber connection with a single row of large diameter fasteners: embedment is the only ductile failure mode, the rest are brittle.

strength. The main differences between both correspond to the definition of the failure area: in the case of *Jockwer et al.* (2018), it was derived for connections with only one fastener (their main aim was to study the material variability, not splitting). *Hanhijärvi and Kevarinmäki* (2007) considered two splitting cases (the crack starting either at the end of the loaded timber edge or at the fastener hole closest to the loaded timber edge). They considered row shear failure in the case of single-row connections as well.

Finally, the *Eurocode 5* (2004) does not directly deal with splitting or row shear, but they are implicitly considered when the ductile approach (the European Yield Model EYM) is combined with the effective number of fasteners n_{ef} , a reduction factor that aims at preventing such brittle failure modes.

3 New design model for splitting

The new approach completes the brittle model proposed by *Yurrita and Cabrero* (2020) for connections with two or more rows of fasteners, where the possible brittle failure modes leading to the failure of the connection are block shear, row shear, and net tension. In the herein analysed case of connections with a single row of fasteners, block shear is no longer feasible due to the absence of a head tensile plane. However, now splitting may occur.

The proposal takes the existing approaches for row shear F_{row} and net tension F_{tens} from *Yurrita and Cabrero* (2020), and proposes a new one for splitting F_{spl} (which will be explained in Sect. 3.1). The minimum of them is the brittle load capacity of the connection:

$$F_{brittle} = n_w \min \begin{cases} F_{spl} \\ F_{row} \\ F_{tens} \end{cases} \quad (1)$$

where n_w is the number of timber elements of the connection (as an example, there are two timber elements in the connection depicted in Fig. 1).

3.1 Splitting

The splitting capacity of a single timber member F_{spl} is proposed to be calculated as:

$$F_{spl} = 2.1(L_{net} + 2d)t_{ef}f_{t,90}. \quad (2)$$

The approach considers splitting as a consequence of perpendicular-to-grain tensile stresses. Therefore, the formula (2) defines the area which supports the perpendicular tensile stress, and verifies it against the corresponding timber strength, $f_{t,90}$. This area is defined by the effective thickness t_{ef} of the timber element (defined in Section 3.4 and previously presented by *Yurrita and Cabrero (2019)*) and its length, taken as the net length of the connection ($L_{net} = (n_c - 1)a_1 + a_3 - (n_c - 0.5)d_0$) plus an extra distance of $2d$, which considers an additional propagation of the crack. The numerical factor of 2.1 is derived from a calibration process which corrects the slope of the fitting line passing through the origin to the results from the database of tests described in Section 4.

3.2 Row shear

The row shear capacity F_{row} was already defined by *Yurrita and Cabrero (2020)*. For a connection with a single row of fasteners,

$$F_{row} = k_v 2L_c t_{ef} f_v \quad (3)$$

where $k_v = 0.4 + 1.4 \sqrt{\frac{G}{E_0}}$; f_v is the shear strength and the area is defined by the effective thickness t_{ef} of the timber element (see Section 3.4) and the connection length $L_c = (n_c - 1)a_1 + a_3$.

3.3 Net tension

Net tension F_{tens} , again as defined by *Yurrita and Cabrero (2020)*, considers the net cross sectional area of the timber element. The load capacity for a connection with one row of fasteners would be:

$$F_{tens} = (2a_4 - d_0)t_{t,0} = (b - d_0)t_{t,0}. \quad (4)$$

3.4 Effective thickness of the timber element

The effective thickness used for both splitting and row shear models is the proposal by *Yurrita and Cabrero* (2019), which is based on a beam on elastic foundation model. Expressions for thin and thick plates, as defined in current *Eurocode 5* (2004), in which the clamping boundary conditions of the fastener are assumed to be different, are derived:

- Thin plates ($t_p \leq 0.5d$):

$$\text{Outer members: } t_{ef} = \begin{cases} 0.66t & \text{if } \frac{t}{d} \leq 3 \\ \max(0.76 - \frac{t}{30d}; 0.2) t & \text{if } \frac{t}{d} > 3 \end{cases} \quad (5)$$

$$\text{Inner members: } t_{ef} = \begin{cases} t & \text{if } \frac{t}{d} \leq 7 \\ \max(1.7 - \frac{t}{10d}; 0.5) t & \text{if } \frac{t}{d} > 7 \end{cases} \quad (6)$$

- Thick plates ($t_p \geq 1.0d$):

$$\text{Outer members: } t_{ef} = \begin{cases} t & \text{if } \frac{t}{d} \leq 3 \\ \max(1.17 - \frac{t}{18d}; 0.35) t & \text{if } \frac{t}{d} > 3 \end{cases} \quad (7)$$

$$\text{Inner members: } t_{ef} = \begin{cases} t & \text{if } \frac{t}{d} \leq 11.5 \\ \max(1.95 - \frac{t}{12d}; 0.65) t & \text{if } \frac{t}{d} > 11.5 \end{cases} \quad (8)$$

The previous formulae were proposed for the case of timber-to-steel connections. However, as it will be shown in the validation process in Section 4, several tests of timber-to-timber connections are also considered. Therefore, an additional formula for the effective thickness of outer members in timber-to-timber connections is derived:

$$\text{Outer members: } t_{ef} = \begin{cases} 0.66t & \text{if } \frac{t}{d} \leq 2 \\ \max(0.8 - \frac{t}{13d}; 0.2) t & \text{if } \frac{t}{d} > 2 \end{cases} \quad (9)$$

4 Validation of the new design model

A total of 9 experimental campaigns have been considered in this work to evaluate the prediction accuracy of the five existing models and the proposal. The gathered database comprises 1 149 single tests distributed in 172 configurations of connections with a single row of large diameter dowel-type fasteners. Further information about the joint configuration, the timber product, the used type of fastener and the number of fasteners is given in Table 1.

Table 1. Summary of the tests used for the validation of brittle failure.

Author	Number of		Joint scheme			Fastener Type		Timber product			Failure mode				
	Config.	Tests	sws	ws ^a	wsw	www	Bolt	Dowel	Glulam	LVL	Solid	1	2+	Ductile	Brittle
Jorissen (1998)	49	768	-	-	-	49	49	-	-	-	49	5	44	18	31
Massé et al. (1998) ^b	8	40	8	-	-	-	-	8	4	-	4	2	6	2	6
Quenneville and Mohammad (2000) ^b	5	50	-	-	5	-	5	5	-	-	-	5	-	3	2
Mohammad and Quenneville (2001) ^b	17	170	-	8	9	-	-	17	17	-	9	9	8	-	17
Blass and Schmid (2002)	23	83	-	-	23	-	-	23	6	-	-	-	23	-	23
Jensen and Quenneville (2011)	16	104	16	-	-	-	-	16	-	16	-	8	8	2	14
Sandhaas (2012)	35	165	-	-	-	35	-	35	-	-	35	12	23	13	22
Misconel et al. (2016) ^b	6	30	-	-	6	-	-	6	-	6	0	2	4	-	6
Iraola (2016)	13	39	-	-	13	-	-	13	-	-	13	3	10	-	13
Total	172	1449	24	8	56	84	54	118	32	22	110	46	126	38	134
Number	-	-	14.0%	4.7%	32.6%	48.8%	31.4%	68.6%	18.6%	12.8%	64.0%	26.7%	73.3%	22.1%	77.9%
%	-	-	14.0%	4.7%	32.6%	48.8%	31.4%	68.6%	18.6%	12.8%	64.0%	26.7%	73.3%	22.1%	77.9%

^aThe ws configurations have been considered together with the wsw ones for the validation in Section ??
^b Only the test with one row of fasteners were considered.

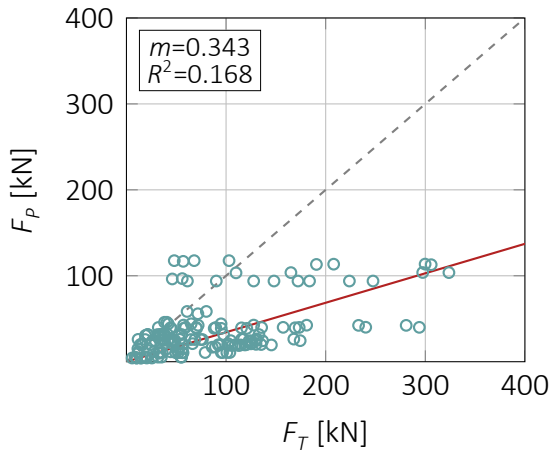
The comparison of the prediction ability of the different models has been performed at a mean level, which is considered to be more adequate than the characteristic one due to the reduced number of replicates tested per configuration. The mean material properties have been obtained from the characteristic ones by means of the model explained by *Jockwer et al. (2018)* and *Cabrero, Honfi, et al. (2019)*, which is based on the probabilistic model for timber proposed by the *Joint Committee on Structural Safety (2006)*. The obtained values were used to calculate the theoretical brittle load capacity of each test configuration according to the six analysed models: *Jorissen (1998)*, *Jensen and Quenneville (2011)*, *Jockwer et al. (2018)*, *Hanhijärvi, A. and Kevarinmäki, A. (2008)*, *Eurocode 5 (2004)* and the proposal.

In the case of the tensile strength perpendicular-to-grain $f_{t,90}$, the characteristic values provided by the design standards have been agreed as a fixed low boundary for the different timber products and strength classes (as an example, the value of the characteristic tensile strength perpendicular-to-grain $f_{t,90}$ is defined in *EN338 (2016)* for all solid softwood and hardwood strength classes as 0.4 and 0.6 N/mm², respectively). These restrictions aim at considering the reduced timber capacity due to long term effects and shrinkage cracks. In order to make an appropriate evaluation of the models, more realistic values were obtained from *Green et al. (1999)*, based on results by the American Forest Products Laboratory, have been considered. Values ranging from 2.0 to 5.0 N/mm² are used depending on the wood species reported in the tests (spruce, pine, douglas fir, radiata pine, southern pine, red cedar, larch, hemlock, beech, azobe). This values were applied for all the models except for the one from *Hanhijärvi and Kevarinmäki (2007)*, since this particular one was calibrated to the values in the European standards and, therefore, considering higher values of $f_{t,90}$ would lead to overpredicted load-carrying capacities. For this case, the mean strength obtained from the characteristic values of $f_{t,90}$ is used.

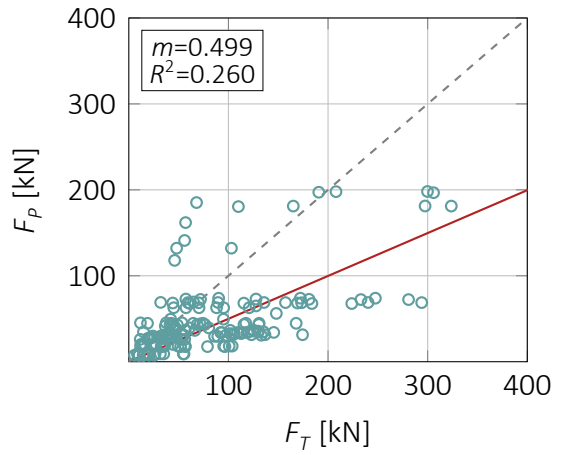
The predicted results from the studied models and the proposal are plotted in Fig. 3. Here, the test results (F_T , abscissas axis) are compared to the theoretical predictions (F_p , ordinates axis). A linear fitting passing through the origin of coordinates and its corresponding slope m and coefficient of correlation R^2 are provided. Finally, the ideal correlation 1:1, depicted as a dashed line, is given for reference.

The models from *Jorissen (1998)* (Fig. 3a) and *Jensen and Quenneville (2011)* (Fig. 3b), both based on fracture mechanics, obtain the most conservative results. Also the *Eurocode 5 (2004)* (Fig. 3e) is too conservative. Just the opposite trend is observed in the cases of *Jockwer et al. (2018)* (Fig. 3c) and *Hanhijärvi and Kevarinmäki (2007)* (Fig. 3d), which tend to overestimate the splitting capacity. Finally, the proposal (Fig. 3f) provides the most accurate results, obtaining the closest slope to the ideal one ($m = 0.994$), and the least scattered graphic ($R^2 = 0.902$).

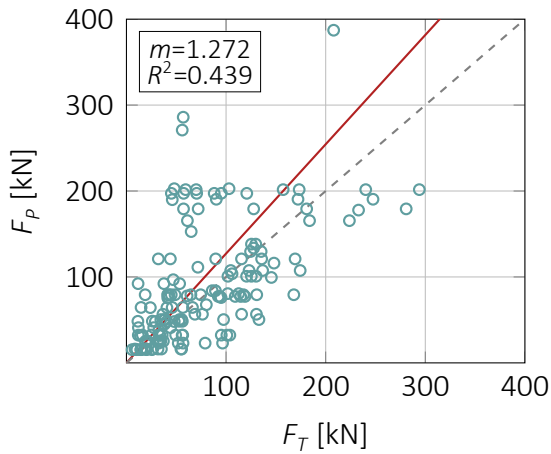
Similar conclusions may be obtained from the boxplot graphic shown in Fig. 4 where the ratio between the predicted load F_p and the test load capacity F_T is used as the main



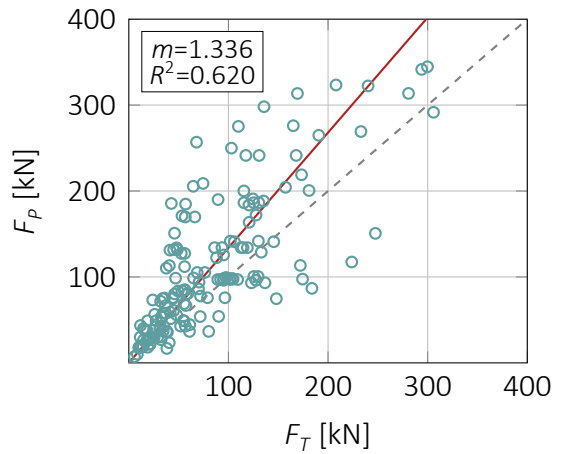
(a) Jorissen (1998)



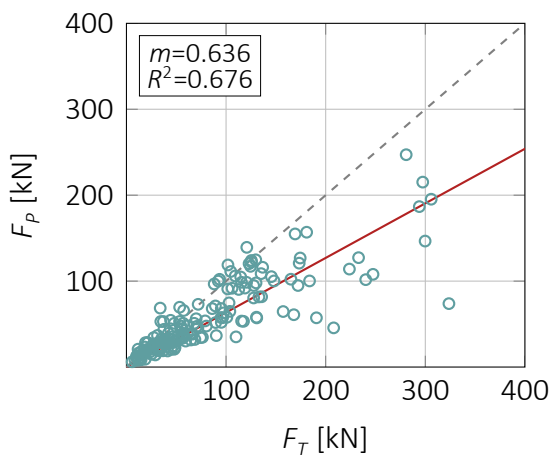
(b) Jensen and Quenneville (2011)



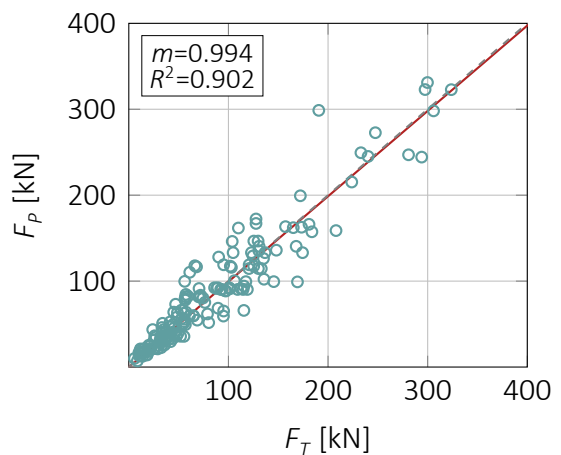
(c) Jockwer et al. (2018)



(d) Hanhijärvi and Kevarinmäki (2007)



(e) Eurocode 5 (2004)



(f) Proposal

Figure 3. Comparison between the load capacity values obtained from the tests F_T and the corresponding theoretical values F_p predicted by the existing models and the proposal.

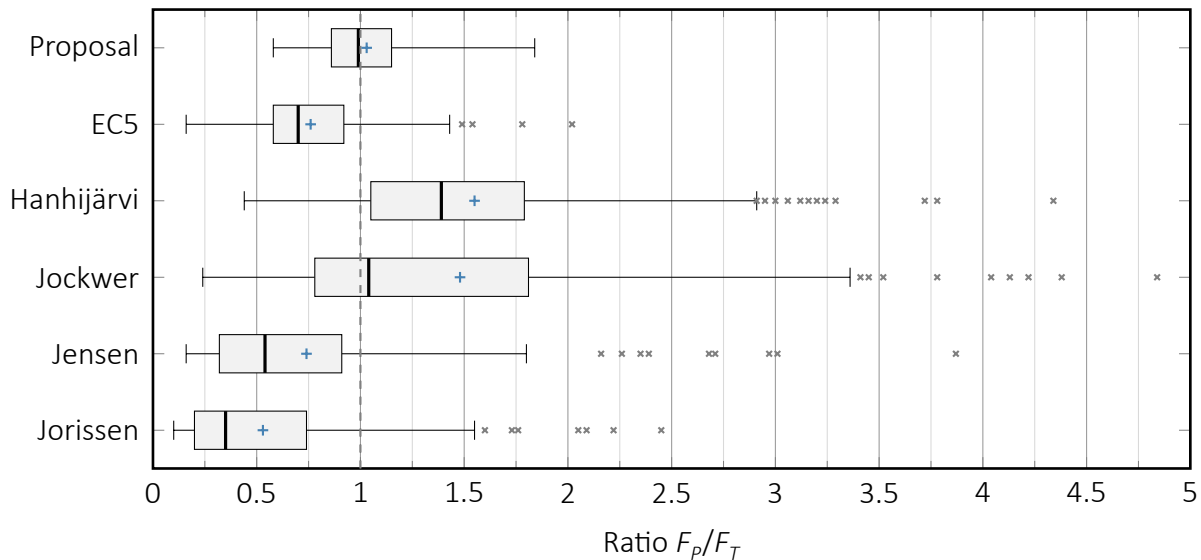


Figure 4. Boxplot considering the accuracy of the predicted ratio between the predicted failure load F_p and the tested failure load F_T . Mean value depicted with a cross.

Table 2. Evaluation of the accuracy obtained by the four studied models and the proposal. The used metrics are the coefficient of determination Q^2 , the mean root error (MRE) and its standard deviation (SD), the slope of the fitting line m , the correlation coefficient c and the concordance correlation coefficient CCC, as described in Cabrero and Yurrita (2018).

Model	Q^2	MRE (SD)	m	c	CCC
Jorissen (1998)	-0.018	0.704 (1.129)	0.214	0.567	0.218
Jensen and Quenneville (2011)	0.0243	0.601 (0.977)	0.342	0.688	0.405
Jockwer et al. (2018)	0.569	0.493 (0.711)	1.068	0.746	0.820
Hanhijärvi and Kevarinmäki (2007)	0.415	0.530 (0.857)	1.429	0.844	0.830
Eurocode 5 (2004)	0.448	0.429 (0.881)	0.453	0.908	0.573
Proposal	0.962	0.154 (0.207)	1.015	0.961	0.982

parameter. The proposal reaches clearly the best behaviour: no outliers, and being both its average (signalled by the cross inside the box) and median (central line within the box) values the closest to the ideal ratio $F_p/F_T = 1$, and moreover, featuring the shortest (least scattered) box and whiskers. As previously explained, the existing models can be easily divided in two groups: the conservative –namely Jensen and Quenneville (2011), Jorissen (1998) and the Eurocode 5 (2004)– and the unconservative group –Jockwer et al. (2018) and Hanhijärvi and Kevarinmäki (2007)–.

A statistical analysis considering the results altogether is given in Table 2. Here, several metrics are used to evaluate the four models: the coefficient of determination Q^2 (best values are those closest to 1), the mean root square error MRE and its corresponding standard deviation SD (lower values are the best ones), the fitting slope m , the correlation coefficient c (values closer to 1 are the best) and, finally, the concordance correlation coefficient CCC (values close to 1 are the best ones, with a recommended threshold value of 0.85). The reader is referred to Cabrero and Yurrita (2018) for a detailed description of these metrics.

Jorissen (1998) and Jensen and Quenneville (2011) obtain the worst metrics. The re-

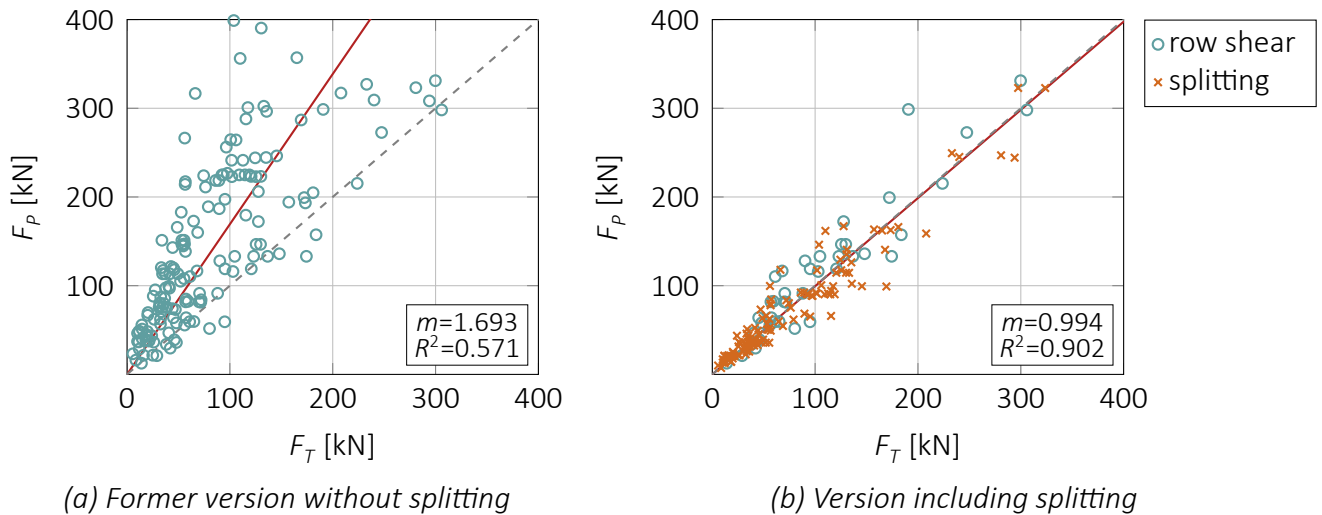


Figure 5. Comparison of the accuracy of the proposal by Yurrita and Cabrero (2020) before and after considering splitting.

maining three existing models rank differently depending on the considered metrics: the *Eurocode 5* (2004) is the best of them according to the c and MRE parameters; *Jockwer et al.* (2018) gets higher ratings considering Q^2 and m ; and finally *Hanhijärvi and Kevarinmäki* (2007) obtains the best CCC parameter (0.83) –almost even with *Jockwer et al.* (2018), (0.82)–. According to this metric, CCC , which is considered as the most comprehensive one, these two models (*Hanhijärvi and Kevarinmäki* (2007) and *Jockwer et al.* (2018)) reach the best performance among the already existing models, even though they fall below the recommended threshold value of 0.85. Finally, the proposal clearly surpasses the existing approaches, and it consistently gets the first position in all the metrics.

Since the new splitting approach is intended to be included in the model from *Yurrita and Cabrero* (2020), a comparison of the prediction accuracy of the two cases (the model before including splitting, and the updated version considering it) is given in Fig. 5. Although the linear fitting takes all the test predictions into account, the predicted failure modes are given. Consequently, when the former version of the model is applied (Fig. 5a), all the tests were expected to fail under row shear. However, when splitting is additionally considered (Fig. 5b) most of the tests are considered to split. Considering splitting implies an improvement of both of the slope (from $m = 1.693$ to $m = 0.994$) and the coefficient of correlation (from $R^2 = 0.571$ to $R^2 = 0.902$).

4.1 Discussion about tensile strength perpendicular-to-grain

As already stated, the mean experimental values of the tensile strength perpendicular-to-grain $f_{t,90}$ given by *Green et al.* (1999) are used in this work, since the values from standards are a safe low boundary.

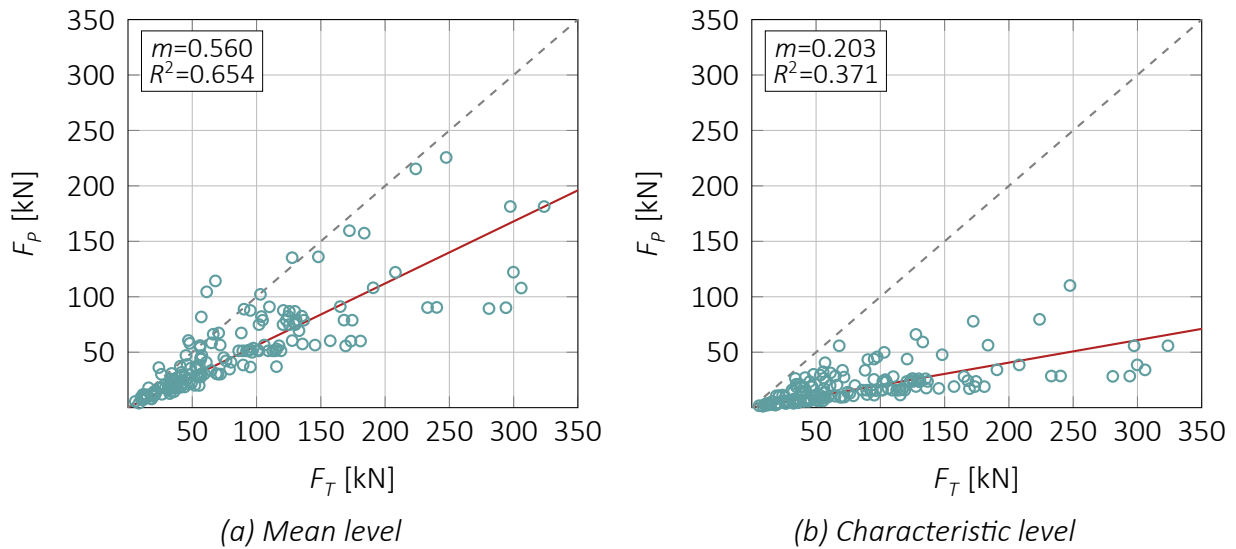


Figure 6. Accuracy of the model when the values of the tensile strength perpendicular-to-grain given in European standards, $f_{t,90}$, are applied instead of those from Green et al. (1999) (and shown in Fig. 3f). Results are shown at both mean and characteristic levels.

The used realistic values within this study allowed to distinguish between different timber products and, therefore, to obtain more accurate and realistic predicted load carrying capacities. Fig. 6 plots the prediction accuracy obtained by the proposal when the standard values are used, considering both mean (Fig. 6a) and characteristic (Fig. 6b) levels. The resulting splitting load capacities are quite conservative, as proved by the slope of the fitted line, which is reduced from $m = 0.994$ (Fig. 3f) to $m = 0.560$ at the mean level, and even to $m = 0.203$ at the characteristic one. Moreover, the scattering of results increases ($R^2 = 0.902$ decreases to $R^2 = 0.654$ and $R^2 = 0.371$ at mean and characteristic levels, respectively).

To overcome these conservative results, different possibilities arise: they could be either assumed or somehow corrected by a coefficient (a factor of 3.75 replacing the factor of 2.1 from (2) would modify the slope $m = 0.560$ from Fig. 6a to $m = 1.00$).

5 Conclusions

The model from Yurrita and Cabrero (2020) for brittle failure in timber connections with large diameter dowel-type fasteners loaded parallel-to-grain has been completed to consider splitting failure for those cases of connections with one row of fasteners. The new splitting model is based on the determination of the area (defined by the net length of the connection $L_{net} + 2d$ and effective thickness t_{ef} of the timber element) subjected to the tensile perpendicular-to-grain stress (and, therefore, the corresponding strength $f_{t,90}$ is considered).

The existing models and the proposal have been bench-marked considering an extensive database of experimental results. For this evaluation, more realistic values of tension perpendicular-to-grain strength $f_{t,90}$ than the ones given in the European standards

were used. The validation demonstrates a clear improvement of the prediction accuracy when applying the new approach.

A discussion should be established about the influence of the conservative values of the standard tensile strength values in the splitting capacity, in order to determine whether the derived conservative prediction is assumed or whether it should be corrected by increasing the numerical factor.

6 Acknowledgements

The research has been performed thanks to the network formed within the European COST Action FP1402. The first author is supported by a PhD fellowship from the Programa de Becas FPU del Ministerio de Educación y Ciencia (Spain) under the grant number FPU15/03413. He would also like to thank the Asociación de Amigos of the University of Navarra for their help with a fellowship in early stages of this research.

7 References

- Blass, H. J. and Schmid, M. (2002). *Spaltgefahr von Nadelhölzern*. Tech. rep. Karlsruhe, Germany: TH Karlsruhe.
- Cabrero, J. M. and Yurrita, M. (2018). “Performance assessment of existing models to predict brittle failure modes of steel-to-timber connections loaded parallel-to-grain with dowel-type fasteners.” In: *Engineering Structures* 171. doi:10.1016/j.engstruct.2018.03.037, 895-910 (INTER version 51–7–12).
- Cabrero, J. M., Honfi, D., Jockwer, R., and Yurrita, M. (2019). “A probabilistic study of brittle failure in dowel-type timber connections with steel plates loaded parallel to the grain”. In: *Wood Material Science & Engineering* 14.5. doi:10.1080/17480272.2019.1645206, pp. 298–311.
- EN338 (2016). *Structural timber - Strength classes*. CTN 56.
- Eurocode 5 (2004). *CEN:EN 1995-1-1:2004 - Eurocode 5: Design of timber structures - Part 1-1: General - Common rules and rules for buildings*. Comité Européen de Normalisation (CTN).
- Green, D. W., Winandy, J. E., and Kretschmann, D. E. (1999). “Wood handbook : wood as an engineering material”. In: General technical report FPL ; GTR-113. Madison, WI :USDA Forest Service, Forest Products Laboratory. Chap. 4: Mechanical properties of wood, pp. 4.1–4.45.
- Hanhijärvi, A. and Kevarinmäki, A. (2008). “Timber Failure Mechanisms in High-Capacity Dowelled Connections of Timber to Steel”. In: *VTT PUBLICATIONS 677*. Espoo, Finland. ISBN: 9789513870904.
- Hanhijärvi, A. and Kevarinmäki, A. (2007). “Design method against timber failure mechanisms of dowelled steel-to-timber connections”. In: *CIB-W18 Timber Structures*. Bled, Slovenia, Paper 40-7–3.

- Iraola, B. (2016). “Simulación del Comportamiento Mecánico de la Madera en Uniones Estructurales y su Aplicación mediante Modelos Tridimensionales de Elementos Finitos”. PhD thesis. Universidad de Navarra. ISBN: 9788578110796.
- Jensen, J. L. and Quenneville, P. (2011). “Experimental investigations on row shear and splitting in bolted connections”. In: *Construction and Building Materials* 25.5. doi:10.1016/j.conbuildmat.2010.11.050, pp. 2420–2425. ISSN: 09500618.
- Jockwer, R., Fink, G., and Köhler, J. (2018). “Assessment of the failure behaviour and reliability of timber connections with multiple dowel-type fasteners”. In: *Engineering Structures* 172. doi:10.1016/j.engstruct.2018.05.081, pp. 76–84.
- Joint Committee on Structural Safety, ed. (2006). *Probabilistic Model Code*. JCSS. Chap. 3.5. Properties of Timber.
- Jorissen, A. J. (1998). “Double shear timber connections with dowel type fasteners”. PhD thesis. TU Delft.
- Massé, D., Salinas, J., and Turnbull, J. (1998). *Lateral strength and stiffness of single and multiple bolts in glue laminated timber loaded parallel to grain*. Tech. rep. Ottawa, Canada: Engineering and Statistical Research Centre, Research Branch, Agriculture.
- Misconel, M., Ballerini, M., and Kuilen J W G, V. de (2016). “Steel-to-timber joints of beech-lvl with very high strength steel dowels”. In: *Proceedings of the World Conference on Timber Engineering, WCTE*. Vienna, pp. 269–276. ISBN: 978-3-903024-35-9.
- Mohammad, M. and Quenneville, P. (2001). “Bolted wood-steel and wood-steel-wood connections: verification of a new design approach”. In: *Canadian Journal of Civil Engineering* 28.2. doi:10.1139/l00-105, pp. 254–263. ISSN: 0315-1468.
- Quenneville, P. and Mohammad, M. (2000). “On the Failure Modes and Strength of Steel-Wood-Steel Bolted Timber Connections Loaded Parallel to Grain”. In: *Canadian Journal of Civil Engineering* 27.4, pp. 761–773.
- Sandhaas, C. (2012). “Mechanical Behaviour of Timber Joints With Slotted-in Steel Plates”. PhD thesis. TU Delft. ISBN: 9789085708377.
- Yurrita, M. and Cabrero, J. M. (2020). “New design model for brittle failure in the parallel-to-grain direction of timber connections with large diameter fasteners”. In: *Engineering Structures* 217. doi:10.1016/j.conbuildmat.2019.04.100, (INTER version 52–7–7).
- Yurrita, M. and Cabrero, J. M. (2019). “Effective thickness of dowel-type fasteners at the elastic range for steel-to-timber connections under brittle failure mode in the parallel-to-grain direction: a new method based on a beam on elastic foundation”. In: *Engineering Structures* 209. doi:10.1016/j.engstruct.2019.109959, (INTER version 52-7-5).
- Yurrita, M., Cabrero, J. M., and Quenneville, P. (May 2019). “Brittle failure in the parallel-to-grain direction of multiple shear softwood timber connections with slotted-in steel plates and dowel-type fasteners”. In: *Construction and Building Materials* 216. doi:10.1016/j.conbuildmat.2019.04.100, pp. 296-313 (INTER version 51–7–10).

Discussion

The paper was presented by M Yurrita

R Brandner commented that tension perpendicular to grain strengths needed size effects consideration. M Yurrita responded that size effect was not considered. Based on comparisons with test data the model seemed to be validated. R Brandner commented that data from literature was used and questioned whether the same data set should be used for both model calibration and validation. M Yurrita said yes because of limited availability of data. B Brandner said using the same data set for both calibration and validation explained why good agreements were obtained.

P Dietsch commented that high tension perpendicular to grain strength values were adopted in the model and current design values accepted by standard bodies are low and will not be changed. M Yurrita responded that long term effects were considered in current conservatively set design values for tension perpendicular to grain and may be other factors can be adjusted in the model to account for the need for the high tensile strength perpendicular to grain values for input.

G Ravenshorst questioned how to arrive at the tension perpendicular to grain stress from loading in the parallel to grain direction. M Yurrita explained that this was a local effect and a factor of 2.1 was obtained in the study for the transformation.

R Jockwer commented that careful consideration of failure modes with combined tension perpendicular to grain and shear stresses is necessary. He also stated that as the tension stress perpendicular to grain stresses were localized, product standard values would not apply. P Dietsch discussed the test volume of specimens for standard tension perpendicular to grain tests relative to connection size.

H Danielsson and M Yurrita discussed application of model based on fracture mechanics which are also species dependent.

A Frangi commented that we wanted to avoid brittle failure so rules are needed on the safe side to ensure brittle failure capacity would be high enough. P Dietsch commented that the current European model are on the safe side, hence implicitly could account for other factors such as shrinkage effects etc.

Experimental analysis of brittle failure in timber-to-steel connections with small diameter fasteners loaded parallel-to-grain

Miguel Yurrita. Wood Chair. Department of Building Construction, Services and Structures. University of Navarra. 31009 Pamplona, Spain. myurrital@alumni.unav.es

José Manuel Cabrero. Wood Chair. Department of Building Construction, Services and Structures. University of Navarra. 31009 Pamplona, Spain. jcabrero@unav.es

Hans Joachim Blaß. Timber Structures and Building Construction.

Karlsruhe Institute of Technology. 76131 Karlsruhe, Germany. hans.blass@kit.edu

Keywords: Timber connection, Brittle failure, Experimental tests, Parallel-to-grain, Small diameter fastener, Plug shear

1 Introduction

Timber joints with steel fasteners are among the most used in timber construction. When the load-carrying capacity of the connection is reached, either a ductile (yielding of the fastener and embedment in the timber) or a brittle (crack of the wood) failure mode may occur. The reached failure mode depends on the materials of the connection and its geometry. Fig. 1 depicts the geometry of a typical timber-to-steel connection with 15 (3 rows and 5 columns) small diameter fasteners (defined as those not protruding the whole timber thickness, such as nails, screws or rivets). The main geometrical parameters and the used nomenclature within this paper are included in Fig. 1.

An accurate prediction of both ductile and brittle load-carrying capacities is of utmost importance to properly design timber connections. Traditionally, ductile failure mode has been considered by applying the European Yield Model (EYM), which in the *Eurocode 5* (2004), is combined with the reduction factor given by the effective number of fasteners n_{ef} , which includes some brittle failure modes such as splitting or row shear in the same calculation process. However, models dealing directly with brittle failure modes are included in the informative Annex A (for block shear and plug shear) in the *Eurocode 5* (2004).

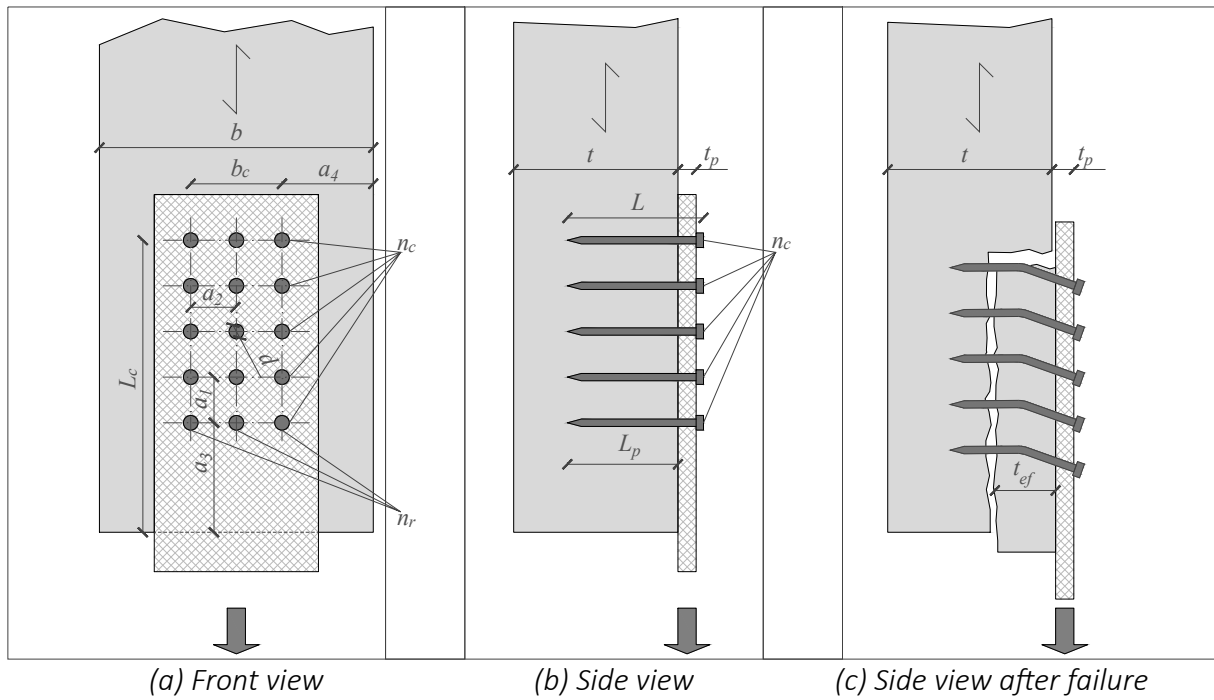


Figure 1. Basic geometry of a generic timber-to-steel connection with small diameter fasteners.

In previous studies *Cabrero and Yurrita (2018)* analysed the existing models for brittle failure of connections. As a consequence, a model dealing with brittle failure mode of connections with large diameter fasteners loaded parallel-to-grain was proposed (*Yurrita and Cabrero (2019)* and *Yurrita and Cabrero (2020)*).

However, in the case of connections with small diameter fasteners, most of the available experimental results were based on rivet connections (*Foschi and Longworth (1975)*, *Zarnani (2013)*, *Zarnani and Quenneville (2014)*, *Choquette (2016)*). It was required to improve the existing database of experimental test results with more tests in which nails and screws were used as fasteners. Therefore, as a preliminary step (similar to the work performed by *Yurrita, Cabrero, and Quenneville (2019)* for connections with large diameter fasteners), an experimental test campaign has been conducted in order to deeply analyse brittle failure in this kind of connections.

2 State of the art

Fig. 2 depicts the main brittle failure modes of timber connections with small diameter fasteners, such as nails, screws or rivets. Mode C (Fig. 2c), namely plug shear, is the most representative. It is defined by the activation of three different failure planes, describing the perimeter of the wood within the fasteners: a head tensile plane H (with an area $A_{t,H} = t_{ef}b_c$), a bottom shear plane B (with an area $A_{v,B} = L_c b_c$) and two lateral shear planes L (with an area $A_{v,L} = L_c t_{ef}$). Mode A (Fig. 2a) and Mode B (Fig. 2b) are variants of plug shear in which the bottom shear B and the lateral shear planes L , respectively, are not activated.

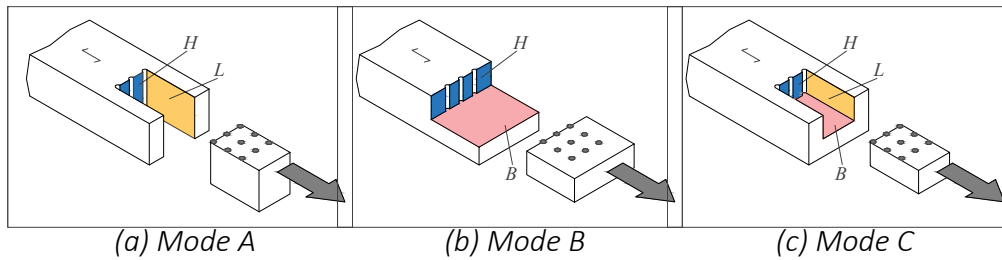


Figure 2. Failure modes with their loading planes (lateral shear L , bottom shear B and head tensile H).

Table 1. Summary of the existing brittle models for connections with small diameter fasteners.

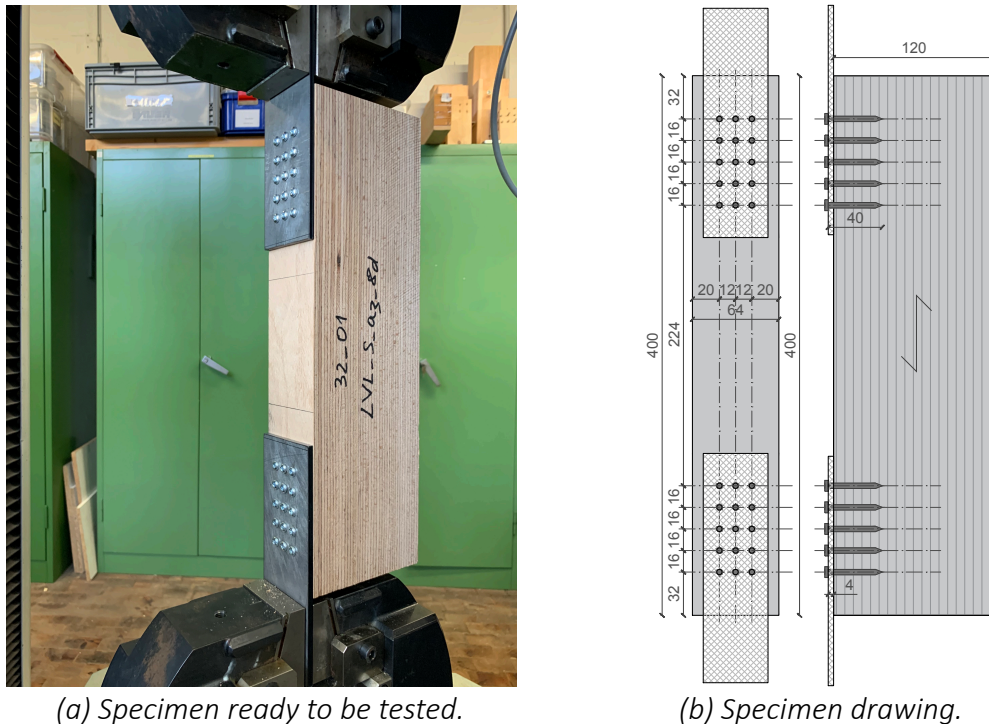
Model	Mode A	Mode B	Mode C
<i>Stahl et al.</i> (2004)	$A_{v,L}f_v + A_{t,H}f_{t,0}$	$A_{v,B}f_v + A_{t,H}f_{t,0}$	$(A_{v,L} + A_{v,B})f_v + A_{t,H}f_{t,0}$
<i>Eurocode 5</i> (2004)	$\max \begin{cases} 1.5A_{t,H}f_{t,0} \\ 0.7A_{v,L}f_v \end{cases}$	—	$\max \begin{cases} 1.5A_{t,H}f_{t,0} \\ 0.7(A_{v,L} + A_{v,B})f_v \end{cases}$
<i>Kangas and Vesa</i> (1998)	—	—	$A_{v,B}f_v + A_{t,H}f_{t,0}$
<i>Johnsson and Parida</i> (2013)	—	—	$\max \begin{cases} A_{t,H}f_{t,0} \\ A_{v,B}f_v \end{cases}$
<i>Quenneville and Zarnani</i> (2017)	Stiffness approach	Stiffness approach	Stiffness approach

Not all the existing models dealing with plug shear (Annex A from the *Eurocode 5* (2004), *Quenneville and Zarnani* (2017), *Kangas and Vesa* (1998), *Johnsson and Parida* (2013) and *Stahl et al.* (2004)) consider the three possible failure modes. All the models share the definition of the load-carrying capacity of each failure plane as its area multiplied by the corresponding strength (tensile parallel-to-grain f_t for the head tensile plane H , and shear strength f_v for the lateral and bottom shear planes). The difference between models consists on how the brittle capacity is obtained: in most cases, the load-carrying capacities of some or all failure planes are added. Table 1 provides an overview of the considered failure modes and the related failure planes by the existing models.

In the case of *Quenneville and Zarnani* (2017), a stiffness model considering those of each involved failure plane is used to obtain the load carrying capacity of the connection. In addition, they consider that both a brittle or a mixed failure can be achieved, depending on whether the crack of the wood happens before or after the yielding of the fastener. For that reason, a different effective thickness of the timber element t_{ef} , that defines the depth of the head tensile H and the lateral L shear planes, is considered in both situations.

3 Materials and methods

A total of 34 different configurations (3 replicates per configuration, that is, 102 single tests) have been performed. Fig. 3 depicts one specimen ready to be tested (Fig. 3a) with its corresponding geometry (Fig. 3b). All the specimens were designed with two symmetrical timber-to-steel connections. In all the connections, 15 fasteners were distributed in 3 rows and 5 columns, as depicted in the connection in Fig. 1. The combination of different materials and variations of the connection geometry were used



(a) Specimen ready to be tested.

(b) Specimen drawing.

Figure 3. Test setup: example of an specimen of configuration LVL_S_a3_8d.

in order to study the influence of several parameters: timber product, fastener type, fastener slenderness L_p/d , steel plate thickness t_p , timber thickness t , distance to the lateral edge a_4 , distance to the end-loaded edge a_3 and the influence of pre-drilling the fasteners' holes.

With this purpose, two timber products were used: glulam GL28h and beech laminated veneer lumber LVL80S. Table 2 includes the material properties used in the research. The characteristic values were obtained from *EN14080* (2013) and *EN14374* (2005) for GL28h and LVL80S, respectively. The given mean values, which were used for a pre-design of the specimens and to compare the obtained test results and the existing models (Section 5), were obtained following the procedure explained by *Jockwer et al.* (2018) and *Cabrero, Honfi, et al.* (2019), and based on the probabilistic model for timber proposed by the *Joint Committee on Structural Safety* (2006). The COVs used for this purpose are 15% for GL28h and 9% for LVL80S (average value of COV from several works (Aydm et al., 2004; Knorz and Van De Kuilen, 2012; Dill-Langer and Aicher, 2014; Purba et al., 2019). The measured average timber density ρ_m (438 -COV = 6.1%- and 813 -COV = 2.3%- kg/m³ for GL28h and LVL80S, respectively) is in good agreement with the values given in the standards.

The two different timber products were combined with two types of fasteners: nails and screws. To assess the influence of the fastener type, both types of fasteners were intended to be as similar as possible, both in length L (40, 60 and 75 mm for nails, and 40, 60 and 70 mm for screws) and nominal diameters $d = 4$ mm (the screws had a core and outer diameters of 3 and 5 mm, respectively). The yield moment M_y provided

Table 2. Material properties of the used timber products. Characteristic and mean values are given.

Timber product	$f_{t,0}$ [N/mm ²] ^a	f_v [N/mm ²] ^a	E_0 [N/mm ²] ^b	G [N/mm ²] ^b	ρ [kg/m ³] ^b
Characteristic level					
GL28h	22.3	3.5	10500	540	425
LVL80S	60	8	14900	630	730
Mean level					
GL28h	30.4	4.6	12600	650	460
LVL80S	70.6	9.2	16800	760	800

^a Mean level obtained by applying the parameters from Joint Committee on Structural Safety, 2006.

^b Mean level given in standards EN14080, 2013; EN14374, 2005.

from the manufacturer (6 500 N/mm for nails and 5 417 N/mm for screws) was considerably lower than the obtained experimental values (following the *EN409* (2009)): 8 490 -COV = 2.5%- and 7 090 -COV = 2.2%- N/mm. Some authors already noticed that the actual yield strength may be higher than the one given by the manufacturers (*Sandhaas et al.* (2013); *Blaß and Colling* (2015)). All the steel plates were made of steel S235. According to the classification from the *Eurocode 5* (2004), two types of steel plates were used: thin plates $-t_p/d \leq 0.5-$ ($t_p = 2$ mm) and thick plates $-t_p/d \geq 1-$ ($t_p = 4$ mm for GL28h and $t_p = 5$ mm for LVL80S).

The described materials were combined between them and with several geometrical variations, leading to 34 configurations expected to fail under plug shear. The geometrical and material properties of all the configurations are given in Table 3.

The connections were tested under tension parallel-to-the grain. The tension tests were performed following the standard *ISO6891–1983* (1983). As shown in Fig. 3a, two lines were drawn on each connection (one in the steel plate and another in the timber element) to measure the slip by means of an optical control system.

4 Test results

The main failure mode of all the tested specimens was, as expected, plug shear. Fig. 4 shows some of the test results. The obtained experimental values are given in Table 3. For each configuration, average values and the corresponding COV are given for the maximum load-carrying capacity F_T , the stiffness K_{ser} and the ductility D_f .

As each test included two symmetrical connections but commonly only one failed, the F_T values have been corrected by applying probabilistic model in which each test is considered as a two component Weibull system, as already done by *Yurrita, Cabrero, and Quenneville* (2019). The stiffness has been calculated by means of the slope of the load-slip curve between the 10% and the 40% of the maximum load.

Finally, the ductility D_f is defined by the ratio $D_f = \delta_f/\delta_y$ (the yield displacement δ_y and the displacement of the point of the graphic where the maximum load F_T has been reached) as defined in *EN12512* (2001), and used by several authors such as *Ottenhaus et al.* (2018), *Jorissen and Fragiaco* (2011) or *Yurrita, Cabrero, and Quenneville*

Table 3. Material and geometrical properties of the tested configurations.

Configuration	Geometrical and material properties										Test Results									
	n_r	n_c	d [mm]	Fastener	L [mm]	Pre-drill	Timber	t_p [mm]	t [mm]	b [mm]	a_1/d	a_3/d	a_2/d	a_4/d	Aver. F_T [kN] ^a	COV	Aver. k_{ser} [kN/mm]	COV	Aver. D_f	COV
GL_N td_40	3	5	4	Nails	40	Yes	GL28h	4	120	64	4	12	3	5	28.25	5.2%	13.52	32.6%	1.56	9.3%
GL_N td_60	3	5	4	Nails	60	Yes	GL28h	4	120	64	4	12	3	5	36.8	5%	13.48	14.2%	1.91	40.5%
GL_N td_75	3	5	4	Nails	75	Yes	GL28h	4	120	64	4	12	3	5	36.87	5.6%	12.35	12.1%	1.55	13.1%
GL_N td_thin_40	3	5	4	Nails	40	Yes	GL28h	2	120	64	4	12	3	5	27.19	4%	15.4	3%	3.26	15%
GL_N td_thin_60	3	5	4	Nails	60	Yes	GL28h	2	120	64	4	12	3	5	35.92	3.6%	15.22	18.8%	3.25	35.7%
GL_N td_Np_40	3	5	4	Nails	40	No	GL28h	4	120	64	4	12	3	5	22.66	0.3%	11.23	17.7%	3.56	26.8%
GL_N td_Np_60	3	5	4	Nails	60	No	GL28h	4	120	64	4	12	3	5	27.06	2.6%	10.13	18.4%	2.1	13.9%
GL_N td_Np_75	3	5	4	Nails	75	No	GL28h	4	120	64	4	12	3	5	32.4	5.7%	11.51	17.5%	1.76	8.3%
GL_S td_40	3	5	4	Screws	40	Yes	GL28h	4	120	64	4	12	3	5	35.25	6.5%	19.99	25.7%	3.47	38.8%
GL_S td_60	3	5	4	Screws	60	Yes	GL28h	4	120	64	4	12	3	5	40.38	3.8%	15.97	21.5%	3.11	31.8%
GL_S td_70	3	5	4	Screws	70	Yes	GL28h	4	120	64	4	12	3	5	42.46	6.8%	17.23	17.5%	3.04	40.3%
GL_S td_thin_40	3	5	4	Screws	40	Yes	GL28h	2	120	64	4	12	3	5	35.25	5.5%	29.76	34.9%	6.16	43.8%
GL_S td_thin_60	3	5	4	Screws	60	Yes	GL28h	2	120	64	4	12	3	5	37.5	6.7%	17.9	30.3%	3.47	8%
GL_S td_Np_40	3	5	4	Screws	40	No	GL28h	4	120	64	4	12	3	5	28.63	3.3%	20.91	31.3%	3.58	37.7%
GL_S td_Np_60	3	5	4	Screws	60	No	GL28h	4	120	64	4	12	3	5	37.74	2.3%	24.95	31.4%	5.15	27%
GL_S td_Np_70	3	5	4	Screws	70	No	GL28h	4	120	64	4	12	3	5	42.28	13.7%	24.09	18.1%	4.47	36.5%
GL_N hw_60	3	5	4	Nails	40	No	GL28h	4	60	64	4	12	3	5	23.02	6.6%	12.44	12.4%	1.93	33.8%
GL_N hw_90	3	5	4	Nails	40	No	GL28h	4	90	64	4	12	3	5	23.12	14.6%	11.67	17%	2.41	49.1%
GL_S hw_60	3	5	4	Screws	40	No	GL28h	4	60	64	4	12	3	5	29.83	5.1%	15.09	20.9%	3.11	21.2%
GL_S hw_90	3	5	4	Screws	40	No	GL28h	4	90	64	4	12	3	5	31.6	1.1%	26.46	20.4%	3.92	38.4%
LV_N td_40	3	5	4	Nails	40	Yes	LV180S	5	120	64	4	12	3	5	57.38	0.8%	31.91	18.6%	1.99	14.2%
LV_N td_60	3	5	4	Nails	60	Yes	LV180S	5	120	64	4	12	3	5	63.21	2.8%	17.65	26.5%	2.19	36.3%
LV_N td_75	3	5	4	Nails	75	Yes	LV180S	5	120	64	4	12	3	5	62.5	51.7%	22.18	9.2%	2.39	34.1%
LV_S td_40	3	5	4	Screws	40	Yes	LV180S	5	120	64	4	12	3	5	64	1.1%	39.25	9.3%	2.73	27.7%
LV_S td_60	3	5	4	Screws	60	Yes	LV180S	5	120	64	4	12	3	5	68.16	6.3%	34.29	28.5%	2.34	2.4%
LV_S td_75	3	5	4	Screws	70	Yes	LV180S	5	120	64	4	12	3	5	72.49	2.7%	28.55	17.8%	2.38	31.1%
LV_N a_4_7d	3	5	4	Nails	40	Yes	LV180S	5	120	80	4	12	3	7	58.23	3.5%	21.09	10.1%	1.65	16.6%
LV_N a_4_9d	3	5	4	Nails	40	Yes	LV180S	5	120	80	4	12	3	9	56.85	3.2%	22.53	7.3%	1.27	10.2%
LV_S a_4_7d	3	5	4	Screws	40	Yes	LV180S	5	120	80	4	12	3	7	67.2	8.4%	41.24	45.8%	2.27	28.8%
LV_S a_4_9d	3	5	4	Screws	40	Yes	LV180S	5	120	96	4	12	3	9	65.91	1.6%	25.66	28.3%	1.99	31.2%
LV_N a_3_8d	3	5	4	Nails	40	Yes	LV180S	5	120	64	4	8	3	5	54.07	7.3%	22.35	10.8%	1.47	25.9%
LV_N a_3_16d	3	5	4	Nails	40	Yes	LV180S	5	120	64	4	16	3	5	60.79	2.1%	21.01	13.7%	1.75	36.4%
LV_S a_3_8d	3	5	4	Screws	40	Yes	LV180S	5	120	64	4	8	3	5	59.93	5.9%	28.43	21.3%	1.75	10.7%
LV_S a_3_16d	3	5	4	Screws	40	Yes	LV180S	5	120	64	4	16	3	5	64.89	0.5%	27.38	14.7%	2.21	7.5%

^a Corrected value according to the Weibull probabilistic model that considers the existence of two connections per test.

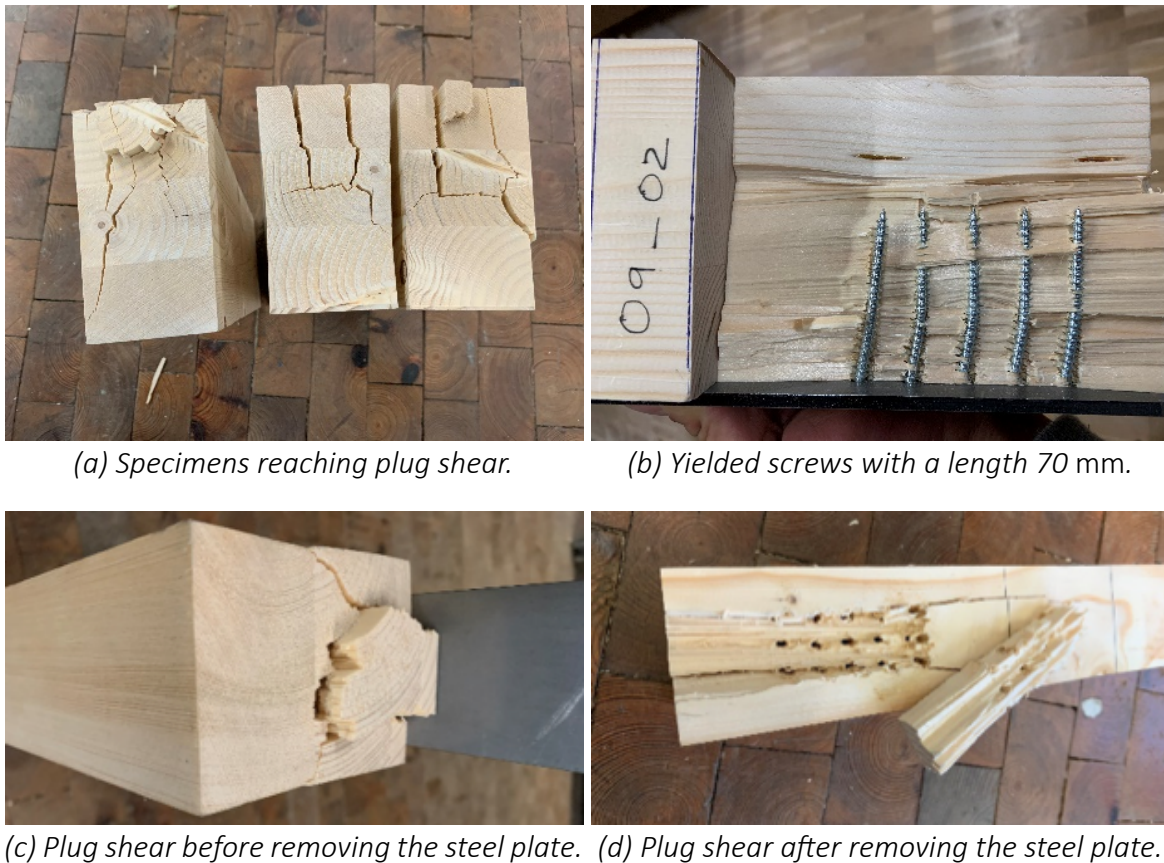


Figure 4. Images of the reached plug shear in the tested specimens

Table 4. Average values of load carrying capacity, stiffness and ductility of the performed test, and the % of cases for each ductility range (Smith et al. (2006)).

Tests studied	Aver. Load F_T [kN]	Aver. Stiffness K_{ser} [kN/mm]	Aver. Ductility D_f	Ductility ranges [%]			
				Brittle	Low duct.	Moderate duct.	Ductile
Tests with GL28h	32.03	15.57	3.08	25.8%	46.8%	17.7%	3.2%
Tests with LVL80S	61.02	26.57	2.03	57.5%	42.5%	0.0%	0.0%
Tests with Nails	40.29	16.24	2.13	47.6%	27.0%	3.2%	0.0%
Tests with Screw	47.71	23.93	3.15	23.1%	76.9%	23.1%	5.1%

(2019). Table 4 provides a brief overview of all these parameters. Four groups of configurations are given according to the two timber products and fastener types. In parallel, Fig. 5 plots the relation between the load carrying capacity of the single tests with the stiffness K_{ser} (Fig. 5a) and the ductility D_f (Fig. 5b). In these graphics, the tests are divided into four groups corresponding to the combination of the two timber products with the fastener types.

It may be noticed how the tests with LVL80S reach in average higher load-carrying capacities and stiffness, but are more brittle (less ductility) than those with GL28h. Regarding the used fasteners, connections with screws withstand more load, are stiffer and, at the same time, are more ductile than the comparable ones with nails.

A classification of the tests regarding their ductility is also given in Table 4 and in (Fig. 5b). As depicted in Fig. 4b, in some cases, plug shear is combined with the yielding of the fasteners, which implies a mixed failure, as reported by *Zarnani and Quenneville* (2014).

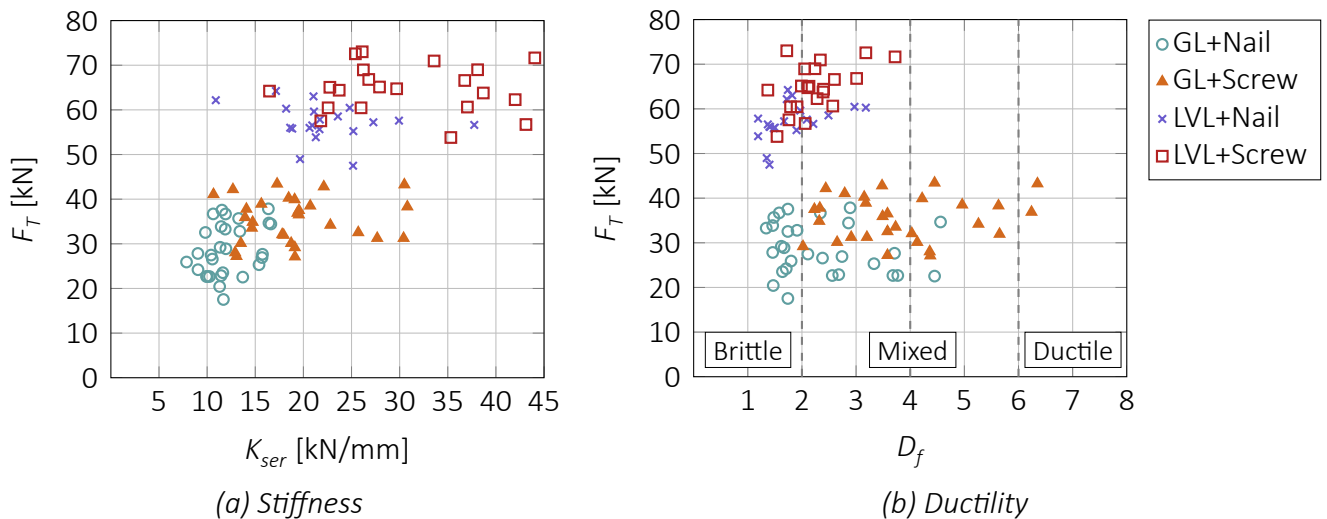


Figure 5. Analysis of the stiffness and ductility obtained in the tests. The test have been divided in 4 groups considering the 4 combinations of timber product and fastener type.

The classification of failure related to the achieved ductility proposed by *Smith et al.* (2006) is used. According to this scale, brittle failure implies a ductility $D_f \leq 2$, and ductile behaviour is considered when $D_f > 6$. In between, two intermediate stages, that can be considered as mixed failure, may be described: low ductility ($2 < D_f \leq 4$) and moderate ductility ($4 < D_f \leq 6$). This classification is given by means of vertical dashed lines in Fig. 5b. Most of the tests fall within the brittle (40.2%) and the low ductility (47.1%) ranges. The moderate ductility range gathers 10.8% of the tests specimens and only 2% of the test can be classified as ductile.

Regarding the failure process, it was noticed that not all the failure planes were activated simultaneously. Usually, the two lateral shear planes L started to fail first. Some of the tests even failed already at this initial stage, but most of them were able to withstand more load, until the head tensile H and bottom shear B planes failed, leading to the final failure of the connection. This process is similar to the one described by *Kangas and Vesa* (1998) and *Johnsson and Parida* (2013).

The analysis of the studied parameters is given in Fig. 6. Each subfigure plots several groups of configurations (two or four, depending on the case) that include the variation of the studied parameter. The analysed parameter is plotted in the abscissas axis, while the load-carrying capacity is given in the ordinates axis.

The fastener penetration length L_p , or the fastener slenderness L_p/d , is studied both in Fig. 6a and Fig. 6b. In general terms, the trend is clear: the load carrying capacity increases when the penetration length is increased. However, the observed non-linear tendency implies the necessity of defining an effective thickness t_{ef} that should consider both the elastic and plastic ranges of the fastener deformation for brittle and mixed failure, respectively.

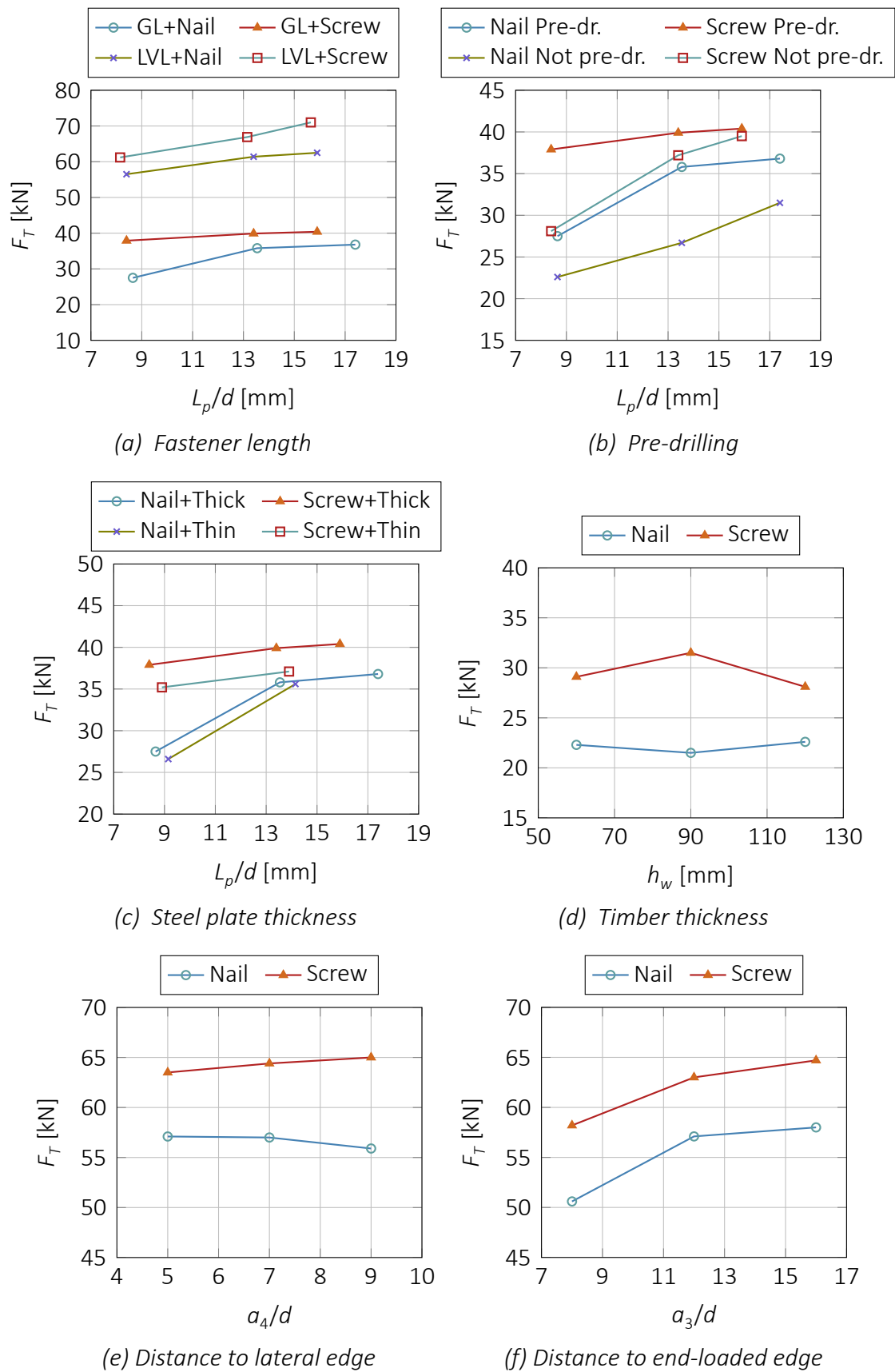


Figure 6. Analysis of the influence of the parameters considered in the tests.

Fig. 6b also includes, by means of the plotted series, the influence of the pre-drilling of the fastener holes. When the pre-drilled and not pre-drilled series of each type of fasteners are compared, it may be seen how the pre-drilled cases (specially in stocky fasteners) reach a higher load-carrying capacity. As studied by *Blaß and Uibel* (2009), this could be explained by the fact that the wood in between the fasteners becomes pre-stressed when there is no pre-drilling.

The influence of the steel plate thickness t_p is studied in Fig. 6c, where configurations with thin and thick plates are plotted. Those cases with thick plates obtain slightly higher load capacities (around 3.5% for screws and 7.0% in nails). This variation is not so relevant to consider the steel plate thickness as a main parameter influencing in plug shear. In fact, *Görlacher* (1995) demonstrated how the yielding behaviour of nails was always the expected for the cases of thick plates, no matter the used steel plate thickness.

The influence of the timber thickness t variation (keeping the same fastener penetration length L_p) is given in Fig. 6d. The minimum variation of the load-carrying capacity between the three tested cases (timber thickness of 60, 90 and 120 mm) suggests that the timber thickness is not a relevant parameter when the fastener penetration is kept the same.

Similar conclusions can be obtained from Fig. 6e, where the influence of the distance to the lateral edge of the timber a_4 is studied. No clear trend (and low variation of results) may be noticed among the series of $5d$, $7d$ and $9d$. Therefore, a significant role of the distance a_4 in the load carrying capacity is discarded. It may only be relevant in order to avoid the failure mode in which the lateral shear planes are not activated (Fig. 2b).

Finally, the influence of the distance to the loaded timber end a_3 is analysed in Fig. 6f, considering cases of $8d$, $12d$ and $16d$. As expected, it is noticed that the increase of the a_3 distance implies an increase of the load-carrying capacity.

5 Performance of the existing models

A brief comparison of the test results with the load-carrying capacity predicted by the existing models has been performed (considering, as explained, the mean level of the material properties).

The prediction accuracy of the five models is plotted in Fig. 7, by comparing the tested load-carrying capacity F_T (abscissas axis) with the predicted load F_p (ordinates axis). The ideal ratio $F_p/F_T = 1$ is given as a reference by means of a dashed line. A fitted linear regression passing through the origin of coordinates is provided, with the corresponding slope m coefficient of correlation R^2 .

The slope closest to $m = 1$ is reached by the Annex A from the *Eurocode 5* (2004) (9.1% above), followed by the model from *Quenneville and Zarnani* (2017) (32.6% below) with coefficients of correlation R^2 of 0.65 and 0.50, respectively. *Kangas and Vesa* (1998) and

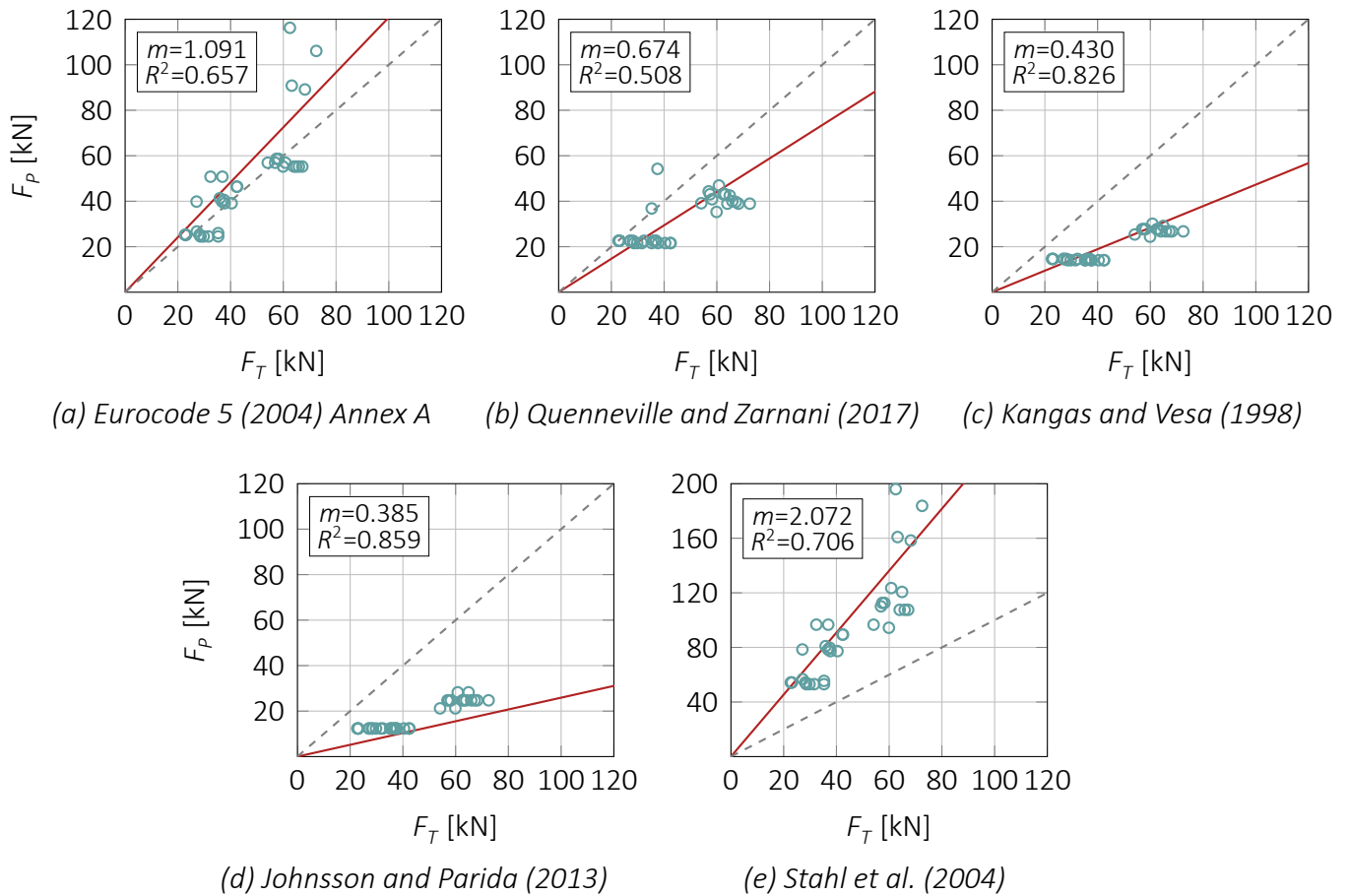


Figure 7. Comparison between the load capacity values obtained from the tests F_T and the corresponding theoretical values F_p predicted by the existing models.

Johnsson and Parida (2013) predict conservative average values (slopes of $m = 0.473$ and $m = 0.259$, respectively), while an opposite trend is provided by Stahl et al. (2004) ($m = 2.270$).

In Fig. 8, a boxplot considering the ratio between the predicted and the tested load carrying capacity F_p/F_T of each model is used to make a more direct comparison of the models' accuracy. Again, the ideal ratio $F_p/F_T = 1$ is given as a reference by means of a dashed line. In this case, both median (thick black lines) and average (crosses) values from the Annex A in the Eurocode 5 (2004) are the closest to the ideal ratio $F_p/F_T = 1$ with values around 1.12. However, this model has several outliers above the superior whisker. Quenneville and Zarnani (2017) provides average values around $F_p/F_T = 0.75$ and less scattered results (only one outlier). The scatter from both Kangas and Vesa (1998) and Johnsson and Parida (2013) is very low, but their average values are under $F_p/F_T = 0.5$. Finally, Stahl et al. (2004) obtains average and mean values above $F_p/F_T = 2$ and the largest box and whiskers (highest scatter).

6 Conclusions and future work

An experimental test campaign of timber-to-steel connections with small diameter fasteners loaded in tension parallel-to-grain has been conducted in order to study brittle

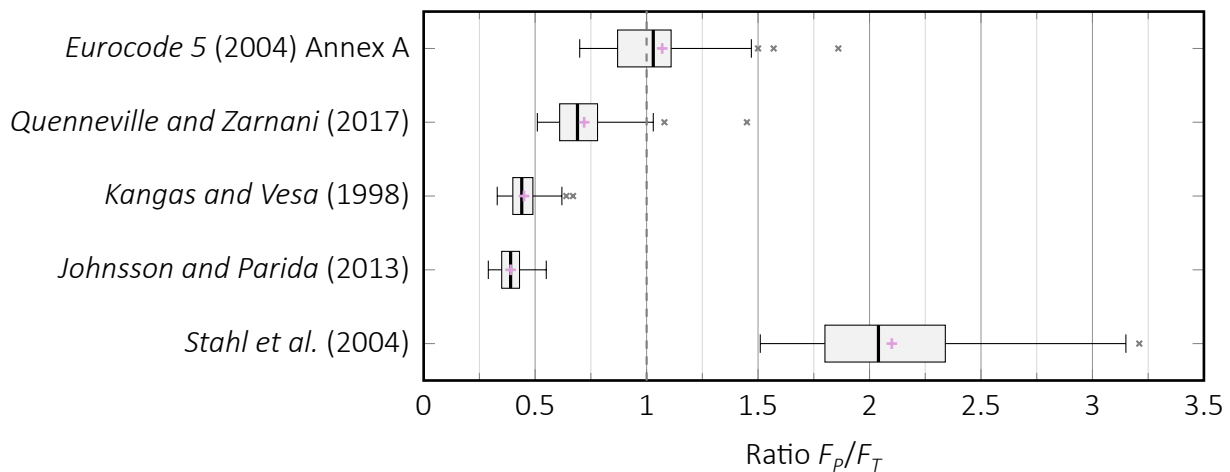


Figure 8. Boxplot considering the accuracy of the predicted ratio between the predicted failure load F_p and the tested failure load F_T .

failure (plug-shear). Different materials (timber -GL28h and LVL80S- and fasteners -nails and screws-) and geometries are combined to identify the main parameters that have an influence on the load-carrying capacity of the connection.

The obtained test results confirmed plug shear as the main failure mode. It is noticed that the failure of all the loading planes does not happen at the same time: first, the lateral shear planes L are activated; and then, only if the connection is able to withstand more load, the head tensile H and the bottom B shear planes fail.

Regarding the ductility D_f , both brittle and mixed failure are reached. The least brittle cases usually correspond to configurations that combine screws with GL28h. Configurations with screws combined with LVL80S usually reach both the highest average load-carrying capacity and stiffness values.

The analysis of the test results provides information on the influence of different parameters. Some of them are confirmed to have an influence (such as timber product, fastener type, spacings, fastener slenderness, or the pre-drilling of the holes), while others seem not to have a clear influence (steel plate thickness and timber thickness).

Finally, the comparison of the test results with the predicted values from the existing models dealing with plug-shear helps to identify some aspects to be improved. With all this new knowledge, further work would try to provide a new model which could improve the prediction accuracy by including the analysed influencing parameters.

7 Acknowledgements

The research has been performed thanks to the network formed within the COST Action FP1402. The first author is supported by a PhD fellowship from the Programa de Becas FPU del Ministerio de Educación y Ciencia (Spain) under the grant number FPU15/03413. He would also like to thank the Asociación de Amigos (University of Navarra) for their help with a fellowship in early stages of this research. The stay of the

first author in the Karlsruhe Institute of Technology has been supported by a fellowship from Gobierno de Navarra. All the authors would like to acknowledge the contribution of the Holzbau und Baukonstruktionen from the Karlsruhe Institute of Technology for funding and performing the tests.

8 References

- Aydm, I., Çolak, S., Çolakoglu, G., and Salih, E. (2004). “A comparative study on some physical and mechanical properties of Laminated Veneer Lumber (LVL) produced from Beech (*Fagus orientalis* Lipsky) and Eucalyptus (*Eucalyptus camaldulensis* Dehn.) veneers”. In: *Holz als Roh - und Werkstoff* 62.3. doi:10.1007/s00107-004-0464-3, pp. 218–220. ISSN: 00183768.
- Blaß, H. J. and Colling, F. (2015). “Load-carrying capacity of dowelled connections”. In: *International Network Timber Engineering Research*. Šibenik, Croatia, Paper 48–7–3.
- Blaß, H. J. and Uibel, T. (2009). *Spaltversagen von Holz in Verbindungen - Ein Rechenmodell für die Rissbildung beim Eindrehen von Holzschrauben*. German. Tech. rep. doi:10.5445/KSP/1000009896. Karlsruher Institut für Technologie (KIT). 180 pp.
- Cabrero, J. M. and Yurrita, M. (2018). “Performance assessment of existing models to predict brittle failure modes of steel-to-timber connections loaded parallel-to-grain with dowel-type fasteners.” In: *Engineering Structures* 171. doi:10.1016/j.engstruct.2018.03.037, 895-910 (INTER version 51–7–12).
- Cabrero, J. M., Honfi, D., Jockwer, R., and Yurrita, M. (2019). “A probabilistic study of brittle failure in dowel-type timber connections with steel plates loaded parallel to the grain”. In: *Wood Material Science & Engineering* 14.5. doi:10.1080/17480272.2019.1645206, pp. 298–311.
- Choquette, J. (2016). “Évaluation d’une nouvelle méthode de calcul des assemblages de bois à l’aide de connecteurs de petits diamètres”. MA thesis. Université Laval, Québec, Canada.
- Dill-Langer, G. and Aicher, S. (2014). “Materials and Joints in Timber Structures: Recent Developments of Technology”. In: *RILEM Bookseries* 9. doi:10.1007/978-94-007-7811-5, pp. 603–613. ISSN: 22110844.
- EN12512 (2001). *Timber structures. Test methods. Cyclic testing of joints made with mechanical fasteners*. Comité Européen de Normalisation.
- EN14080 (2013). *Timber structures - Glued laminated timber and glued solid timber - Requirements*. Comité Européen de Normalisation.
- EN14374 (2005). *Timber structures - Structural laminated veneer lumber - Requirements*. Comité Européen de Normalisation.
- EN409 (2009). *Timber structures - Test methods - Determination of the yield moment of dowel type fasteners*. Comité Européen de Normalisation.
- Eurocode 5 (2004). *CEN:EN 1995-1-1:2004 - Eurocode 5: Design of timber structures - Part 1-1: General - Common rules and rules for buildings*. CTN.

- Foschi, R. O. and Longworth, J. (1975). “Determining embedment response parameters from connector tests”. In: *Journal of the Structural Division* 101, pp. 2537–2555.
- Görlacher, R. (1995). “Load-carrying capacity of steel-to-timber joints with annular ringed shank nails”. In: *CIB-W18 Timber Structures*. Copenhagen, Denmark, Paper 28–7–3.
- ISO6891–1983 (1983). *Timber structures – Joints made with mechanical fasteners – General principles for the determination of strength and deformation characteristics*. ISO/TC 165.
- Jockwer, R., Fink, G., and Köhler, J. (2018). “Assessment of the failure behaviour and reliability of timber connections with multiple dowel-type fasteners”. In: *Engineering Structures* 172. doi:10.1016/j.engstruct.2018.05.081, pp. 76–84.
- Johnsson, H. and Parida, G. (2013). “Prediction model for the load-carrying capacity of nailed timber joints subjected to plug shear”. In: *Materials and Structures* 46.12. doi:10.1617/s11527-013-0030-8, pp. 1973–1985. ISSN: 1359-5997.
- Joint Committee on Structural Safety, ed. (2006). *Probabilistic Model Code*. JCSS. Chap. 3.5. Properties of Timber.
- Jorissen, A. J. and Fragiacomio, M. (Nov. 2011). “General notes on ductility in timber structures”. In: *Engineering Structures* 33.11. doi:10.1016/j.engstruct.2011.07.024, pp. 2987–2997. ISSN: 01410296.
- Kangas, J. and Vesa, J. (1998). “Design on timber capacity in nailed steel-to-timber joints”. In: *CIB-W18 Timber Structures*. Savonlinna, Finland, Paper 31-7–4.
- Knorz, M. and Van De Kuilen, J. W. (2012). “Development of a high-capacity engineered wood product - LVL made of European beech (*Fagus Sylvatica* L.)” In: *World Conference on Timber Engineering 2012, WCTE 2012*. July. Auckland, New Zealand, pp. 487–495. ISBN: 9781622763054.
- Ottenhaus, L.-M., Li, M., Smith, T., and Quenneville, P. (2018). “Mode cross over and ductility of dowelled LVL and CLT connections under monotonic and cyclic loading”. In: *Journal of Structural Engineering* 144.7. doi:10.1061/(ASCE)ST.1943-541X.0002074.
- Purba, C. Y. C., Pot, G., Viguier, J., Ruelle, J., and Denaud, L. (2019). “The influence of veneer thickness and knot proportion on the mechanical properties of laminated veneer lumber (LVL) made from secondary quality hardwood”. In: *European Journal of Wood and Wood Products* LVL. doi:10.1007/s00107-019-01400-3. ISSN: 1436736X.
- Quenneville, P. and Zarnani, P. (2017). *Proposal for the Connection Chapter of the New Zealand Design of Timber Structures*. Unpublished.
- Sandhaas, C., Ravenshorst, G. J. P., Blass, H. J., and Van De Kuilen, J. W. G. (2013). “Embedment tests parallel-to-grain and ductility aspects using various wood species”. In: *European Journal of Wood and Wood Products* 71.5. doi:10.1007/s00107-013-0718-z, pp. 599–608. ISSN: 00183768.
- Smith, I., Asiz, A., Snow, M., and Chui, Y. H. (2006). “Possible Canadian/ISO approach to deriving design values from test data”. In: *CIB W18 Timber Structures*. Florence, Italy, Paper 39–17–1.

- Stahl, D. C., Wolfe, R. W., and Begel, M. (2004). "Simplified analysis of timber rivet connections". In: *Journal of Structural Engineering* 130.August, pp. 1272–1279. ISSN: 0733-9445. DOI: 10.1061/(ASCE)0733-9445(2004)130:8(1272).
- Yurrita, M. and Cabrero, J. M. (2020). "New design model for brittle failure in the parallel-to-grain direction of timber connections with large diameter fasteners". In: *Engineering Structures* 217. doi:10.1016/j.conbuildmat.2019.04.100, (INTER version 52–7–7).
- Yurrita, M. and Cabrero, J. M. (2019). "Effective thickness of dowel-type fasteners at the elastic range for steel-to-timber connections under brittle failure mode in the parallel-to-grain direction: a new method based on a beam on elastic foundation". In: *Engineering Structures* 209. doi:10.1016/j.engstruct.2019.109959, (INTER version 52-7–5).
- Yurrita, M., Cabrero, J. M., and Quenneville, P. (May 2019). "Brittle failure in the parallel-to-grain direction of multiple shear softwood timber connections with slotted-in steel plates and dowel-type fasteners". In: *Construction and Building Materials* 216. doi:10.1016/j.conbuildmat.2019.04.100, pp. 296-313 (INTER version 51–7–10).
- Zarnani, P. (2013). "Load-Carrying Capacity and Failure Mode Analysis of Timber Rivet Connections". PhD thesis. University of Auckland, p. 225.
- Zarnani, P. and Quenneville, P. (2014). "Strength of timber connections under potential failure modes: An improved design procedure". In: *Construction and Building Materials* 60. doi:10.1016/j.conbuildmat.2014.02.049, pp. 81–90. ISSN: 09500618.

Discussion

The paper was presented by M Yurrita

P Dietsch suggested that work should focus on improving existing models.

F Lam received confirmation that the COV of the data was low and commented that higher COV is expected for brittle wood failure modes. M Yurrita said that the specimens were chosen carefully to avoid major defects in the connections.

P Quennville commented about the assessment of test configuration on the results as the use of short specimens might create a dominant single shear plane that would influence the bottom shear plane.

M Yurrita responded that other tests also showed one shear plane. P Quennville was not sure all models had been developed with consideration of this test configuration. Using test configuration that differed from other research might influence the results. M Yurrita agreed and will examine this issue.

C Sigrist commented on the last slide which showed a big difference between brittle and mixed failure and asked whether this is because of penetration length and location of shear plane. M Yurrita responded this was not the case in general and showed that the overall data did not have this issue. The last slide showed the difference between two tested materials.

G Fink asked about the conversion of the material properties for Beech LVL from characteristic properties for model input. M Yurrita will look into this further.

A Ceccotti requested that the ductility definite be consistent between static and seismic considerations.

R Brandner stated that Beech LVL properties need many size effect adjustments and asked if this was considered. M Yurrita said this was not done in this study. R Brandner commented further that the depth of LVL and secondary layer effect in LVL would also need to be considered.

Fatigue Behaviour of Notched Connections for Timber-Concrete-Composite Bridges

Simon Mönch, M.Sc., Scientific Researcher

Prof. Dr.-Ing. Ulrike Kuhlmann, Head of Institute

Institute of Structural Design, University of Stuttgart, Germany

Keywords: Timber-Concrete-Composite Bridges, Notched Connections, Fatigue

1 Introduction

Timber-concrete-composite (TCC) road bridges are an economical solution for one- or two-lane single span bridges with spans between 10 and 30 m. Approximately 50 % of all existing road bridges in Germany have spans ranging from 5 to 30 m (Schmitt et al., 2003), which shows the big market. Because traffic is representing a variable cyclic load, fatigue verifications of all structural members including the shear connectors are required for the design. However, design rules for fatigue verifications of TCC bridges and of appropriate connectors are not given in the standards

Within the development of the new Eurocode generation meanwhile, a Technical Specification (TS) (Dias et al. (2020)), has been developed for the verification of TCC structures for multi-storey and industrial buildings. This also covers basic rules for the design of notched shear connector, see Fig.1.1. This TS will probably be used as a basis for a new Part 3 of Eurocode 5 for the design of TCC-constructions. However, fatigue verification is not yet covered.

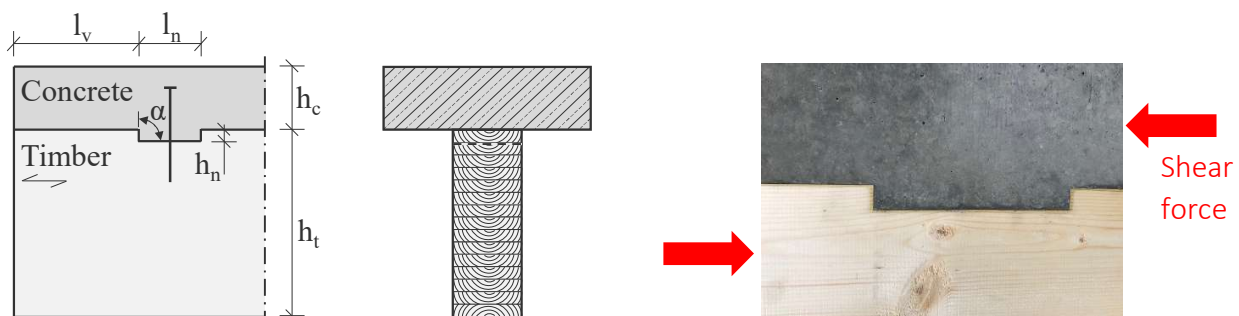


Figure 1.1. Notched connection with geometrical parameters: h_n = notch depth, l_n = notch length, l_v = timber length in front of the notch, h_t = timber thickness, h_c = concrete thickness, α = notch inclination of the edge and screws for preventing uplift (left), notched connection test (right)

Especially for road bridges, compared to pedestrian bridges, the verification of sufficient fatigue strength under frequently recurring traffic loads is required. EN 1995-2 (2004), Annex A specifies the fatigue verification for timber structures. To what extent this procedure may also be applied for TCC-constructions and especially for the design of TCC-shear connectors needs clarification, especially in view of the new generation of Eurocodes, where at the moment prEN 1995-2 is under development.

Two TCC-bridges in an integral construction method, with notches and glued-in steel rods as connecting elements, were constructed in Schwäbisch Gmünd (Southern Germany) in 2012 (see Figure 1.2 (left)). Since these are pedestrian bridges, only statically acting live loads had to be considered for the design. Usually, loads that have to be applied to pedestrian bridges, e.g. from cleaning or emergency vehicles, are only considered as quasi-permanent loads in the design. This is reasonable due to a limited frequency of occurrence (see EN 1995-2 (2004)). In order to be able to use TCC-bridges in road traffic, the fatigue strength under frequently recurring traffic loads needs to be considered. In Germany, the first TCC-road-bridge for heavy traffic loading was built at Wippra in 2008 (Rautenstrauch & Müller (2012)). Thereby, the composite action is achieved by notches with inserted steel plates with welded-on shear studs, see also (Müller (2014)). Other possible connection types for TCC-road-bridges are e.g. HBV system (Bathon & Bletz-Mühldorfer (2014)), where a design approval (Z-9.1-557 (2015)) exist, or X-connectors (Kuhlmann & Aldi (2010)). Figure 1.2 (right) shows a TCC-road-bridge in Lohmar (Germany) with 28 m span. Thereby the HBV system according to Z-9.1-557 (2015) was used to achieve the composite action.



Figure 1.2. TCC-bridge with 27.7 m span in Schwäbisch Gmünd, Germany build in 2012 (left) and TCC-bridge with 28 m span in Lohmar, Germany build in 2014 (right), sources: IB Miebach and M. Gerold

Within a currently ongoing research project (Kuhlmann et al. (2020)), the fatigue behaviour of notched connections and self-tapping fully-threaded screws for use as fasteners in TCC-beams is investigated in order to develop a scientific basis for the fatigue design. This cooperative research project of the Institute of Structural Design at the University of Stuttgart and the Institute of Building Construction and Timber Structures at the Technical University of Braunschweig (Prof. Dr.-Ing. Mike Sieder) aims at design rules which can directly be used for the further development of Eurocode 5.

In the context of this paper, results from the already completed tests are presented. The static tests focus on the evaluation of the stiffness, load bearing capacity and failure mode of the notched connection. In the cyclic tests with single amplitude load spectrum, for notched TCC-connections first S-N-curves representing the fatigue strength are derived for the two investigated stress ratios of $R = 0.1$ and $R = 0.4$ (where $R = \sigma_{\min} / \sigma_{\max}$). This is followed by an overview of additional test series that are currently being carried out.

2 State of research

Extensive investigations on notched TCC-connections in both push-out and TCC-beam tests have been carried out among others, see Boccadoro (2016), Simon (2008), Schönborn (2006), Grosse (2005), Dias (2005), by the Institute of Structural Design at the University of Stuttgart in the last few years. This has mainly been focussed on the static behaviour of the notched connection. In addition to a variation of the concrete cam geometry and the orientation of the timber lamellae (see Kuhlmann & Mönch (2018)), tests with reinforced timber in front of the loaded edge of the notch (see Kudla (2017)) and tests with varied timber length in front of the loaded edge of the notch were carried out. The results of these tests have also been included in the Technical Specification for TCC structures for multi-storey and industrial buildings (Dias et al. (2020)). They indicate for small depth h_n and long timber length in front of the loaded edge of the notch l_v (see Fig. 1.1) a ductile compression failure initiating a secondary concrete failure. In contrast, notches with a depth of h_n about 40 mm, which may serve as connectors for road bridges due to their high shear strength and stiffness, tend to a more brittle shear failure.

Initial tests on notches under cyclic loading were already carried out by Kuhlmann & Aldi (2010). This allowed the derivation of a first fatigue strength curve, the S-N-curve, for timber shear failure in front of the loaded edge of the notch for a conservative stress ratio of $R = 0.1$ (with $R = \sigma_{\min} / \sigma_{\max}$). The experimentally derived S-N-line is still on the safe side compared to the S-N-line derived from EN 1995-2, A.3 (2004) for timber under shear, however it is based on only a small number of tests. Considering the generally high dispersion in fatigue tests and the diverse influences of several materials for the behaviour of TCC notched connections, there is a need of an improved test basis.

Another short series of experiments on notches under cyclic loading was conducted by Simon (2008). As these tests were conducted under low upper loads F_{\max} , there were only run-outs, which are fatigue tests without rupture. At load cycle numbers of sometimes well over 2 million no failure occurred, so that the respective test had to be stopped before failure. Therefore, these tests without failure, as well as a few tests by Kuhlmann & Aldi (2010), cannot be used to derive S-N-curves.

3 Overview on current TCC fatigue tests with notches at the University of Stuttgart

3.1 Geometry and material of the TCC push-out test specimens

Within the framework of the DFG research project (Kuhlmann et al. (2020)), a total of 34 symmetrical push-out tests and 9 TCC-beam tests are conducted. Figure 3.1 shows a push-out test specimen with identification of the displacement measurement devices and dimensions. All test specimens were made of glued laminated timber out of spruce of quality GL 28h according to EN 14080 (2013) and concrete of quality C 30/37 according to EN 1992-1-1 (2004). The depth of the notch is $h_n = 40$ mm and no screws were placed in the notch. The concrete cam is unreinforced and only the two concrete elements had a minimum reinforcement.

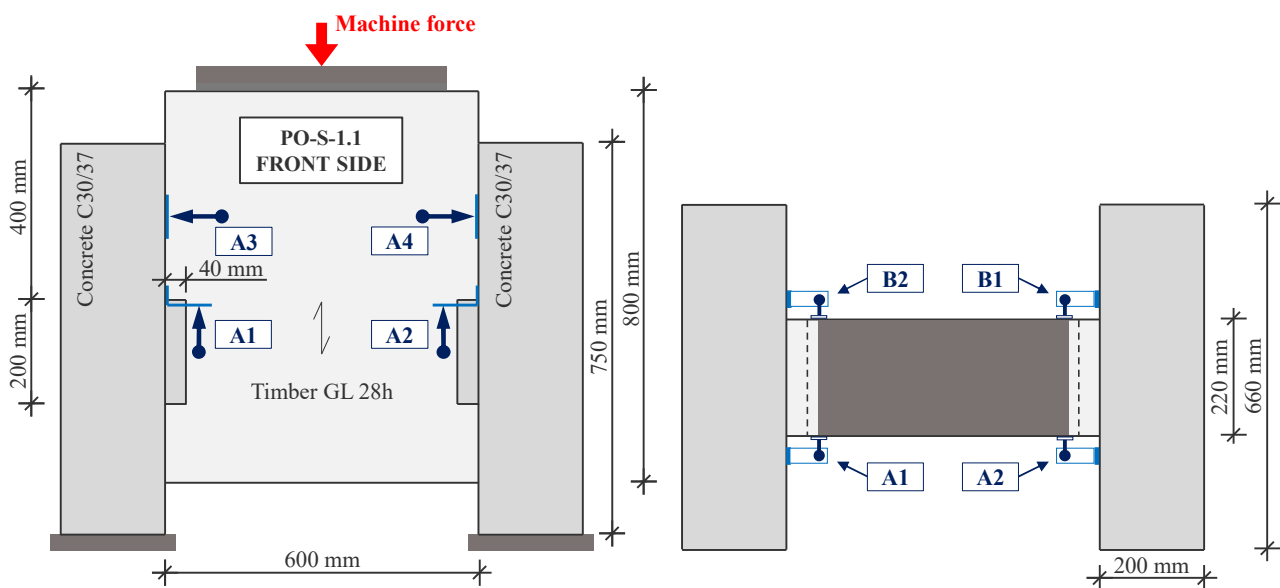


Figure 3.1. Front view (left) and top view (right) of push-out test specimen with identification of displacement measurement devices and dimensions (Kuhlmann et al. (2020))

3.2 Overview on the new test series already conducted in 2019 and 2020

A total of 20 push-out tests (4 static tests, 13 cyclic tests under single amplitude load spectrum and 3 cyclic tests under variable amplitude load spectrum) had already been carried out by April 2020 (see Table 3.1). First the static load bearing capacity was determined with test series PO-S-1. For that a total of 4 test specimens were used, as a certain scattering of results was expected. A reliable mean value (MV) is important, since this is used as an input value for all further test series when determining the upper or lower loads (F_{\max} or F_{\min}) of the cyclic loading according to the respective stress ratio R .

In timber construction, the stress ratio $R = \sigma_{\min} / \sigma_{\max}$ is considered in the fatigue verification according to EN 1995-2, A.3 (2004). The initial tests conducted by Kuhlmann & Aldi (2010) were carried out with a conservative stress ratio of $R = 0.1$. However, both own and comparative calculations by Kuhlmann & Aldi (2010) and

Kudla (2017) show that for TCC-road-bridges a (more favourable) stress ratio in the range of $R = 0.4$ is more realistic.

Table 3.1. Overview on conducted static and cyclic push-out test series with varied parameters

Series number	Number of specimens	Stress ratio $R = \sigma_{\min} / \sigma_{\max} [-]$	Maximum load $F_{\max} [\text{kN}]$	Frequency $F [\text{Hz}]$
PO-S-1	4	-	F_{Ult}	static loading
PO-C-1	2	0.1	$0.75 \cdot F_{\text{Ult}}$	2.5
PO-C-2	2	0.1	$0.50 \cdot F_{\text{Ult}}$	2.5
PO-C-3	3	0.4	$0.75 \cdot F_{\text{Ult}}$	2.5
PO-C-4	3	0.4	$0.60 \cdot F_{\text{Ult}}$	2.5
PO-C-5	3	0.1	$0.35 \cdot F_{\text{Ult}}$	2.5
PO-C-6	3	0.1	$0.35 \cdot F_{\text{Ult}}$ and $0.50 \cdot F_{\text{Ult}}^*$	2.5

* Conducted as two-step variable amplitude load spectrum test
(Constant change of 3800 times $F_{\max} = 0.35 \cdot F_{\text{Ult}}$ and 1000 times $F_{\max} = 0.50 \cdot F_{\text{Ult}}$)

For the five test series (PO-C-1 to PO-C-5) Figure 3.2 shows as a load protocol the amplitudes of the cyclic loads applied with $f = 2.5$ Hz for the different upper loads carried out with stress ratios of $R = 0.1$ (left) and $R = 0.4$ (right).

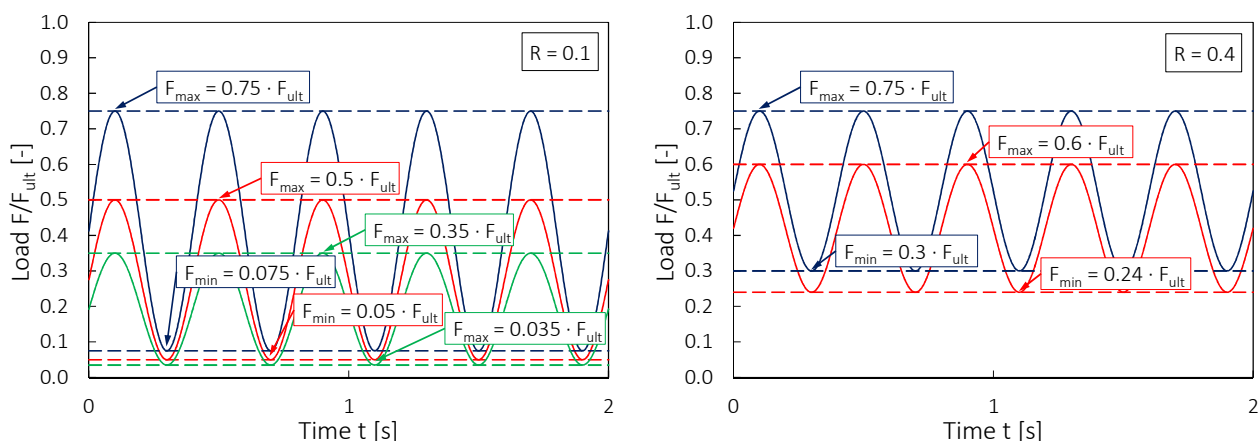


Figure 3.2. Load protocol of the cyclic load for a stress ratio of $R = 0.1$ (left) and for a stress ratio of $R = 0.4$ (right), each shown for all tested upper loads F_{\max}

Test series PO-C-1 to PO-C-5 were conducted as single amplitude load spectrum tests. The aim was to derive S-N-curves for both investigated stress ratios R . Test series PO-C-6 was performed as a variable amplitude load spectrum test with pre-set automatically changing upper loads. The purpose of this test series was to carry out an orientational study for the application of the Palmgren and Miner rule (linear damage accumulation hypothesis) according to Miner (1945).

4 Results from the conducted push-out test series

4.1 Results of the static tests: failure mode, stiffness and load bearing capacity

All four static tests within test series PO-S-1 were evaluated according to EN 26891 (1991). The load was applied in a displacement controlled mode at a speed of $v = 0.8$ mm/min.

Also all cyclic tests were first statically preloaded in several stages, so that the static stiffness K_{ser} could also be derived from these tests. Table 4.1 shows the stiffness resulting from 13 evaluated tests together with results from comparable tests N1 to N3 conducted by Kuhlmann & Aldi (2010).

Table 4.1. Comparison of the mean values (MV) of the stiffness K_{ser} of the notch of the own tests carried out in 2019 and 2020 with the tests by Kuhlmann & Aldi (2010)

Series number	Tests conducted in	Total number of specimens	Mean value K_{ser} [kN/mm/m]	Standard deviation [kN/mm/m]	Coefficient of variation [-]
PO-S-1 and PO-C-1 to PO-C-4	2019 and 2020	13	2355	335.5	0.14
N1 to N3	2010	3	1792	376.3	0.21

All static tests, as well as the cyclic tests discussed in Section 4.2, failed due to a brittle shear failure of the timber in front of the loaded edge of the notch (see Figure 4.1). This occurred when the vertical displacement at the notch was between 0.4 mm and 1.8 mm (see Table 4.2). None of the tests described showed cracks in the concrete or in the concrete cam. Previous investigations at the University of Stuttgart (Kuhlmann & Mönch (2018)) showed that the length of the timber in front of the loaded edge of the notch l_v as a function of the notch depth h_n has a great influence.

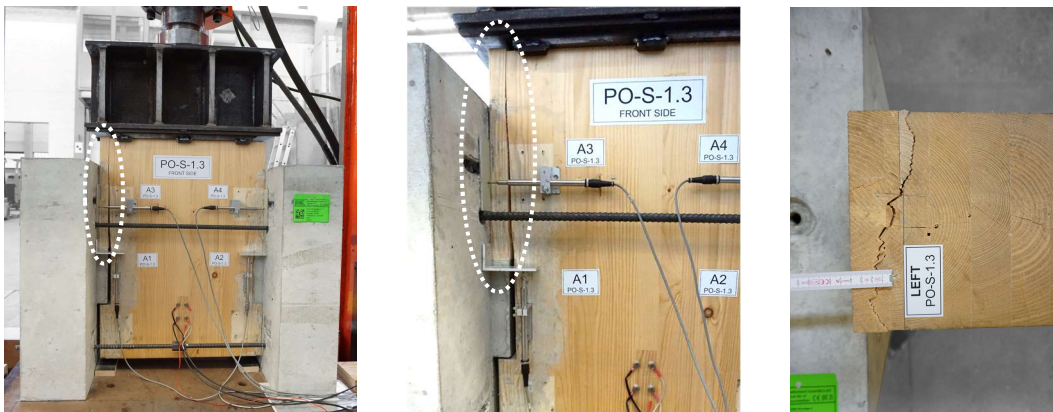


Figure 4.1. Push-out specimen PO-S-1.3 after timber shear failure (left), detail timber in front of the loaded edge of the notch (middle), timber shear failure top view (right) (Kuhlmann et al. (2020))

For the current tests carried out within the framework of the DFG research project (Kuhlmann et al. (2020)), a unique, clearly definable failure is aimed in order to allow the determination of a definite fatigue strength. Thus, after the occurrence of the failure, the number of load cycles before failure can be determined in order to derive S-N-curves (see Section 4.2). Therefore, the timber length in front of the loaded edge of the notch was chosen to $l_v = 10 \cdot h_n$ in order to achieve shear failure of the timber in front of the loaded edge of the notch instead of timber pressure.

Table 4.2 shows the mean values of the achieved maximum loads F_{ult} for the static tests of test series PO-S-1 and for the static tests N1 to N3 performed by

Kuhlmann & Aldi (2010) together with the respective standard deviations and coefficients of variation. These are in a similar range and also the mean value (MV) of the displacements at the notch, at the abrupt, brittle timber shear failure, is roughly in the range of around 1.0 mm.

Table 4.2. Mean Values calculated out of maximum forces F_{ult} obtained from tests conducted by Kuhlmann et al. (2020) and Kuhlmann & Aldi (2010)

Series / Test number	Maximum load F_{ult} [kN/0.44 m]	Standard deviation [kN/0.44 m]	Coefficient of variation [-]	Displacement at timber shear failure [mm] (MV)
PO-S-1 (2019) (4 tests)	507.0	80.4	0.16	1.20
N1 to N3 (2010) (3 tests)	527.0	43.4	0.08	0.76

The values given for F_{ult} refer to a width of 0.44 m. This is corresponding to the sum of the width of the two notches of the symmetrical push-out test specimens (two times 0.22 m). The machine load was applied in the middle of the timber element via a steel beam for the load distribution. A steel plate (shorter than the timber width) was placed between the steel beam and the timber element (end grain surface) in order to allow for the shear failure of the timber in front of the loaded edge of the notch (see Figure 4.1 (left)).

4.2 Results of cyclic test series PO-C-1 to PO-C-5 with single amplitude load spectrum and derived S-N-curves

The mean value of the maximum load $F_{ult} = 507$ kN (determined from the static push-out test series PO-S-1) was used as an input value to determine the upper load F_{max} of the cyclic test series PO-C-1 to PO-C-6. Taking into account the respective stress ratio R of 0.1 or 0.4, the lower load F_{min} of the corresponding amplitude had been fixed as given in Figure 3.2.

To derive S-N-curves representing resistance functions, linear regression and in particular the method of least squares was used. The applied loads F_{max} / F_{ult} as well as the logarithmic values of the number of load cycles N from the cyclically loaded test series and also the results from the static tests were considered.

In the next step, characteristic S-N-curves with 95% survival probability (5% fractile) were derived from S-N-curves with 50% survival probability. The characteristic S-N-curves (5% fractile) were determined with the prediction interval (predictive method of fractile estimation) based on the Student's t-distribution. This procedure also corresponds to Annex D in EN 1990 (2002), (see also worked example in Drebenstedt & Euler (2018)).

Figure 4.2 shows the S-N-curves determined for a stress ratio of $R = 0.1$ and Figure 4.3 for a stress ratio of $R = 0.4$. In order to determine the S-N-curves for $R = 0.1$, also results from tests by Kuhlmann & Aldi (2010) were considered in addition to the current test results.

In addition to the S-N-curves, which represent the corresponding mean values of the test results of the 5% fractile value resulting from statistical evaluation, the characteristic S-N-curve for timber on shear according to EN 1995-2, A.3 (2004) is shown.

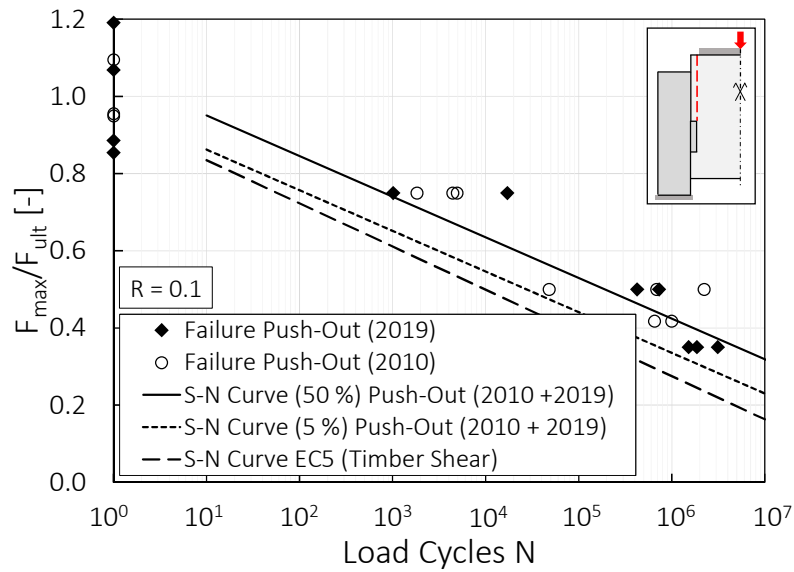


Figure 4.2. S-N-curves for notched TCC-connections for a stress ratio of $R = 0.1$ derived from the current tests (2019-2020) together with results of the tests conducted by Kuhlmann & Aldi (2010)

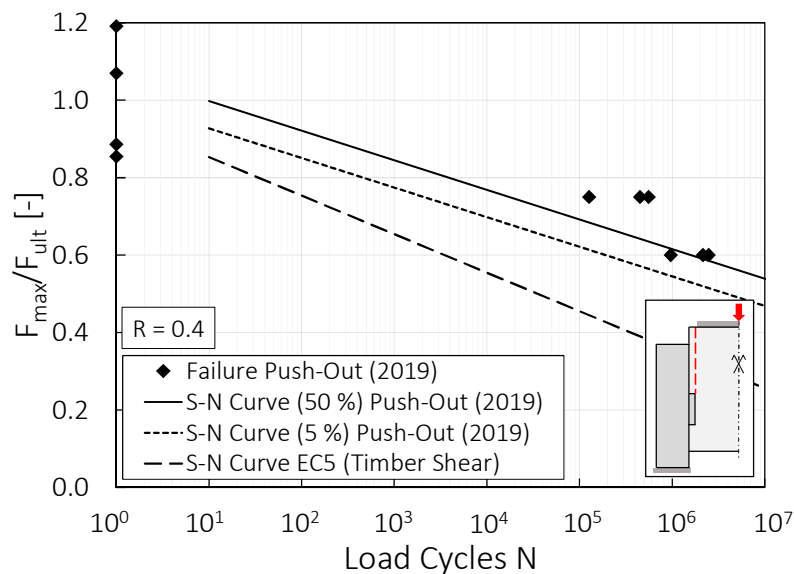


Figure 4.3. S-N-curves derived from the current tests (2019-2020) with a stress ratio of $R = 0.4$

Comparing the results for $R = 0.1$ and $R = 0.4$ it is obvious that the fatigue strength increases with increasing R value. For both investigated stress ratios R it is shown that the statistically evaluated S-N-curves (5% fractile values) resulting from tests are above and thus on the safe side of the characteristic S-N-curves according to EN 1995-2, A.3 (2004). Therefore, the design for timber under cyclic shear stress, which is already defined in EN 1995-2, A.3 (2004), may be applied with sufficient safety for the fatigue design of timber elements of TCC-bridges with notched connections. For realistic R values of 0.4 the tests results seem to indicate that the fatigue strength of EN 1995-2, A-3 could even be improved.

4.3 Results of cyclic test series PO-C-6 with various amplitude load spectrum

Based on the static and cyclic push-out test series already conducted in single amplitude load spectrum, further cyclic test series have been conducted since the beginning of 2020. According to EN 1995-2 (2004) a linear damage accumulation according to Palmgren and Miner (Miner (1945)) may be assumed for the fatigue design of timber subjected to a various amplitude load spectrum. However, this was originally developed only for an aluminium alloy under certain boundary conditions (see Miner (1945)) and is also common practice for the fatigue design in steel constructions according to EN 1993-1-9 (2005), where the underlying assumptions that the load sequence does not play a role and the fatigues strength is only dependent on the stress range and not on the mean stress are usually met. For timber at least the last condition is not fulfilled. However, all load cycle counting methods for transferring the real variable traffic load into a single amplitude load spectrum are based on the linear damage accumulation according to Palmgren and Miner. Therefore, it is crucial to show that this rule may also be applied for the fatigue verification of timber within EN 1995-2 (2004).

The purpose of test series PO-C-6 was to carry out an orientational study on the applicability of the Palmgren and Miner rule. Test series PO-C-6 was performed as a variable amplitude load spectrum test with pre-set automatically changing upper loads (see Figure 4.4 (left) or Table 3.1). The load was applied in two alternation steps (constant change of 3800 times $F_{max} = 0.35 \cdot F_{ult}$ and 1000 times $F_{max} = 0.50 \cdot F_{ult}$). These two upper loads F_{max} have already been investigated individually in the single amplitude load spectrum tests of test series PO-C-2 and PO-C-5. So the maximum number of cycles N_f before failure are known. A proportion of the maximum number of cycles n_i should have a proportional damage n_i/N_f .

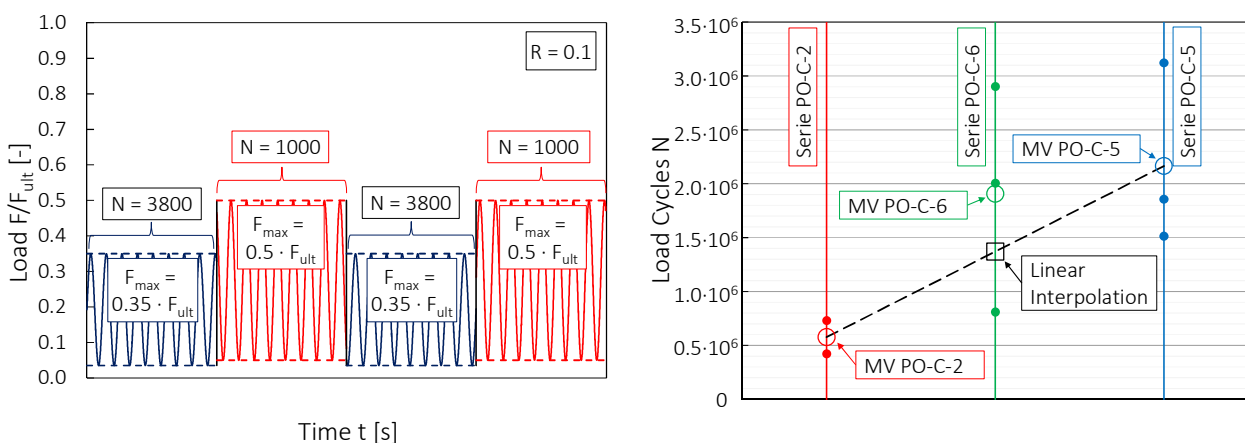


Figure 4.4. Load protocol of the two step variable amplitude load spectrum test series PO-C-6 (left) and comparison of the number of load cycles before failure of test series PO-C-6 with the results of test series with comparable upper loads F_{max} conducted with single amplitude load spectrum (right)

Figure 4.4 (right) shows the results from test series PO-C-6 together with results from the single amplitude load spectrum tests which are mathematically comparable based on the linear damage accumulation hypothesis according to Palmgren and Miner. In order to be able to compare the results simply and clearly, the ratio of the respective

applied load cycles per amplitude of 1.0 to 3.8 was chosen. The reason for this is that the mean value (MV) of the number of load cycles to failure of test series PO-C-5 ($F_{\max} = 0.35 \cdot F_{\text{ult}}$) was about 3.8 times higher than the mean value of test series PO-C-2 ($F_{\max} = 0.50 \cdot F_{\text{ult}}$).

The individual number of load cycles before failure are shown as small filled-in point in Figure 4.4 (right). The respective mean value (MV) resulting from the corresponding test series is also shown as a large circle. The middle vertical line shows the number of load cycles before failure from the two-step variable amplitude load spectrum tests of test series PO-C-6. In addition, the interpolated mean value, which is calculated using 50% of the average load cycles from test series PO-C-5 with $F_{\max} = 0.35 \cdot F_{\text{ult}}$ (representing 50% damage) and 50% of the average load cycles from test series PO-C-2 with $F_{\max} = 0.50 \cdot F_{\text{ult}}$, (representing another 50% damage theoretically) is shown as an un-filled square.

It is shown that the interpolated mean value corresponding to the linear damage accumulation hypothesis according to the Palmgren and Miner rule is below the actual average of load cycles before failure in test series PO-C-6 and thus on the safe side. But this is only a single series of tests, which should not be considered as a complete validation of the Palmgren and Miner rule for fatigue testing of timber, which however gives a positive indication.

5 Further planned test series

Based on the static test series already performed and the cyclic test series with single amplitude load spectrum, further static and cyclic test series have been carried out since spring 2020. In the first step it has been investigated whether notched connections still have a residual static load bearing capacity in the size of the original load bearing capacity after a certain number of previous load cycles or whether the cyclic loading causes a pre-damage that reduces the static load bearing capacity.

Within the DFG research project (Kuhlmann et al. (2020)), the fatigue behaviour of fully threaded screws (SPAX) with cylinder head according to ETA-12/0114 (2017) is currently being investigated at the Technical University of Braunschweig (Germany) for different load directions to define basic rules for the fatigue strength. These findings will be used in a series of tests on notched connections that are being conducted at the University of Stuttgart, where the timber in front of the loaded edge of the notch is reinforced by these fully threaded screws. This investigation will show whether and to what extent fully threaded screws in the timber in front of the loaded edge of the notch have an influence on the fatigue behaviour of the notch.

While all previous and currently ongoing tests were carried out on symmetrical push-out tests, TCC beams with notched connections will also be tested cyclically starting in autumn 2020. The stress ratio of $R = 0.4$, which has already been investigated by means of push-out test series (PO-C-3 and PO-C-4), will also be applied on the beam test specimens that resemble more the actual geometry of real TCC-bridges in practice. The aim

here is, as for the comparable push-out test series, which have already been carried out, to contribute to the determination of the S-N-curves.

6 Summary and Outlook

In this paper experimental investigations on symmetrical TCC push-out test specimens with notches as connections were discussed. These were conducted under both static and cyclic loads at the University of Stuttgart since 2019.

S-N-curves representing the fatigue strength of the TCC notched connections were derived from the test results and statistically evaluated to determine 5% fractile values for a timber shear stress of the notched connections. These were compared to the characteristic S-N-curves according to EN 1995-2, A.3 (2004). The comparison showed that the fatigue verification for timber in shear, already implemented in EN 1995-2, A.3 (2004), may also be applied with sufficient safety for the fatigue verification of the notched connections in TCC-bridges.

Thus, in the future, TCC-bridges with notched connections subjected to recurring traffic loads may be designed economically and safely with already standardised fatigue verification procedures. The results of this test programme may contribute to the future development of Eurocode EN 1995-2 in view of TCC-bridges and allow for an increased application in the field of road bridges.

7 Acknowledgements

The investigations are funded by the German Research Foundation (DFG) – project number 397985109. This support is gratefully acknowledged.

We extend our appreciation to our DFG project partner, the Institute of Building Construction and Timber Structures at the Technical University of Braunschweig (Prof. Dr.-Ing. Mike Sieder and Peter Niebuhr, M.Sc.) for their good cooperation.

Moreover, we thank SPAX International GmbH & Co. KG for providing screws for the specimens and MPA Stuttgart for their great support in conducting the tests.

8 References

- Bathon, L.; Bletz-Mühldorfer, O. (2014):* Fatigue Design of Wood-Concrete-Composite System. In: World Conference on Timber Engineering, WCTE (Québec City, Canada).
- Boccardo, L. (2016):* Timber-concrete composite slabs made of beech laminated veneer lumber with notched connection. ETH Zürich, Switzerland, PhD thesis, 2016.
- Dias, A. (2005):* Mechanical Behaviour of Timber-Concrete Joints. Technical University of Delft, Netherlands, PhD thesis, 2005.
- Dias, A.; Fragiaco, M.; Harris, R.; Kuklík, P.; Rajcic, V.; Schänzlin, J. (2020):* CEN/TC 250, Eurocode 5: Design of Timber Structures – Structural design of timber-concrete composite structures – Common rules and rules for buildings, CEN-Technical Specification, March 2020.

- Drebenstedt, K.; Euler, M. (2018):** Statistical Analysis of Fatigue Test Data according to Eurocode 3. In: 9th International Conference on Bridge Maintenance, Safety and Management – IABMAS 2018, Melbourne, Australia, 9.-13. July 2018.
- Grosse, M. (2005):** Zur numerischen Simulation des physikalisch nichtlinearen Kurzzeittragverhaltens von Nadelholz am Beispiel von Holz-Beton-Verbundkonstruktionen (in German). Institute of Structural Engineering, Bauhaus-Universität Weimar, PhD thesis, 2005.
- Kudla, K. (2017):** Kerven als Verbindungsmittel für Holz-Beton-Verbundstraßenbrücken (in German). Institute of Structural Design, University of Stuttgart, Mitteilung No. 2017-02, PhD thesis, 2017.
- Kuhlmann, U.; Aldi, P. (2010):** Fatigue strength of timber-concrete-composite bridges: Determination of a S-N-line for the grooved connection and the „X-connector“. In: World Conference on Timber Engineering, WCTE, Trento, Italy, 20-24. June 2010.
- Kuhlmann, U.; Mönch, S. (2018):** Design Parameters of Notched Connections for TCC Structures as Part of Eurocode 5. In: International Network on Timber Engineering, INTER 2018, Tallinn, Estonia, 13.-16. August 2018.
- Kuhlmann, U.; Sieder, M.; Mönch, S.; Niebuhr, P. (2020):** Ermüdungsverhalten von Kerven und selbstbohrenden Vollgewindeschrauben für die Anwendung als Verbindungsmittel bei Holz-Beton-Verbundträgern (in German). University of Stuttgart, Institute of Structural Design and Technical University Braunschweig, Institute of Building Construction and Timber Structures, DFG Research Project, Project number: 397985109, 2018-2020.
- Miebach, F.; Niewerth, D.; Wolf, F.; Laraki, J. (2018):** Holz-Beton-Verbundbrücken – Erfahrungen und Perspektiven (in German). Qualitätsgemeinschaft Holzbrückenbau e.V.
- Miner, A. (1945):** Cumulative Damage in Fatigue. In: Journal of Applied Mechanics 12 (1945), pp. 159 – 164.
- Müller, J. (2014):** Trag- und Verformungsverhalten spezieller Verbundelemente für Holz-Beton-Verbundstraßenbrücken unter Kurzzeit-, Ermüdungs- und Langzeitbeanspruchung (in German), Institut für Konstruktiven Ingenieurbau, Bauhaus-Universität Weimar, PhD thesis, 2014.
- Rautenstrauch, K.; Müller, J. (2012):** Trag-, Verformungs- und Ermüdungsverhalten spezieller Verbundelemente für Holz-Beton-Verbundstraßenbrücken (in German). Forschungsvorhaben AiF/iVTH 16266 BR, Bauhaus Universität Weimar, Research report.
- Schmitt, V. et al. (2003):** Statistische Grundlage zum Forschungsprojekt: Untersuchungen zum verstärkten Einsatz von Stahlverbundkonstruktionen bei Brücken kleiner und mittlerer Stützweiten (in German). Research project FOSTA P 629 / Schmitt Stumpf Frühauf und Partner Ingenieurgesellschaft für Bauwesen mbH, Munich.
- Schönborn, F. (2006):** Holz-Beton-Fertigteilelemente (in German). Leopold-Franzens-Universität Innsbruck, PhD thesis, 2006.

- Simon, A. (2008):** Analyse zum Trag- und Verformungsverhalten von Straßenbrücken in Holz-Beton-Verbundbauweise (in German). Institute of Structural Engineering, Bauhaus-Universität Weimar, PhD thesis, 2008.
- EN 14080 (2013):** Timber structures – Glued laminated timber and glued solid timber – Requirements. European Committee for Standardization (CEN), Brussels.
- EN 26891 (1991):** Timber Structures – Joints made with mechanical fasteners – General principles for the determination of strength and deformation characteristics. European Committee for Standardization (CEN), Brussels.
- EN 1990 (2002):** Eurocode: Basis of structural design. European Committee for Standardization (CEN), Brussels.
- EN 1992-1-1 (2004):** Eurocode 2: Design of concrete structures – Part 1-1: General rules and rules for buildings. European Committee for Standardization (CEN), Brussels with corrections and amendments + AC:2010.
- EN 1993-1-9 (2005):** Eurocode 3: Design of steel structures – Part 1-9: Fatigue. European Committee for Standardization (CEN), Brussels with corrections and amendments + AC:2009.
- EN 1995-2 (2004):** Eurocode 5: Design of timber structures – Part 2: Bridges. European Committee for Standardization (CEN), Brussels.
- ETA-12/0114 (2017):** European Technical Assessment ETA-12/0114 of 12/10/2017. SPAX self-tapping screws – Screws for use in timber constructions, ETA-Denmark.
- Z-9.1-557 (2015):** Allgemeine bauaufsichtliche Zulassung Z-9.1-557: Holz-Beton-Verbundsystem mit eingeklebten HBV-Schubverbindern (in German). Deutsches Institut für Bautechnik, Berlin.

Discussion

The paper was presented by S Mönch

G Montgomery received clarification that the rebar in the test set up had slack and did not influence the test. It was used as a safety measure in case the specimen tipped over. G Montgomery commented that during his testing with CLT/glulam with inclined screws eccentricity was encountered under high load had created tensile stress orthogonal to the loaded direction and split the glulam specimen.

S Aicher commented about the S/N curve comparison between the test results and Eurocode and asked how was the 5th percentile curve obtained from the mean curve based on mean values. S Mönch responded that he used all the data values and performed statistical evaluation to obtain the 5th percentile S/N curve. S Aicher commented the slope of the 5th percentile S/N might be higher for better fit.

G Ravenshorst received confirmation of the load path of the test specimen and the possible failure modes and only compression loads were applied.

P Dietsch commented that the paper should end with clear proposals for implications to standards.

Quality assurance and design of timber structures in varying climates

Marcus Schiere, Bern University of Applied Sciences, Biel, Switzerland

Bettina Franke, Bern University of Applied Sciences, Biel, Switzerland

Steffen Franke, Bern University of Applied Sciences, Biel, Switzerland

Keywords: timber structures, moisture content, Service Class, moisture induced stress, FEM simulations, climate

1 Introduction

1.1 Wood and moisture

Wood as a hygroscopic material adapts to variations of relative humidity and temperature of its surrounding environment: it either releases moisture in a drying process or adsorbs it during wetting process. Moisture content (MC) affects mechanical properties of wood below the fibre saturation point (FSP). Variations of MC lead to the shrinkage and swelling of wood.

The design standard SN EN 1995-1-1:2014 (Eurocode 5) considers the hygroscopic behaviour by suggesting three Service Classes (SC) based principally on the relative humidity of the surrounding air:

- SC1 for timber elements located in relative humidity that exceed a value of 65% for only several weeks per year,
- SC2 for timber elements located in relative humidity exceed a value of 85% only several weeks per year, and
- SC3 for conditions exceeding the climate mentioned under SC2.

The corresponding average moisture content in the SC1 and SC2 should not exceed the 12 M% and 20 M% (softwood), respectively. Assignment of the correct SC to a structure is one of the first important decisions a structural engineer needs to make when starting the design of a timber structure.

1.2 Damage in timber structures related to moisture

The distribution of MC across load bearing elements like glulam is normally non-uniform (Dietsch et al. 2015, Franke et al. (2018), Fortino et al. 2019). The subse-

quent hygro-expansion and (constrained) swelling and shrinkage generates moisture induced stresses (MIS). These stresses can exceed the allowable strength perpendicular to the grain and generate either cracks or delamination of glue lines. Both reduce the load-carrying capacity and visible appeal of timber structures. Structures are built throughout the year and building processes span multiple months until a building envelope is closed. Damage is already initiated before the building is opened for its intended use.

The importance of the relation between MC and structural health was quantified in two assessment studies: (1) High MC, low MC, or MC variations could implicitly be related to almost half of the evaluated cases of structural damage or failure (Frese and Blass, 2011) and (2) MC variations could be related to about one third of these damages (Dietsch et al. 2018).

1.3 Paper contents

This paper summarises data from 30 different buildings (Figure 1) monitored in two MC monitoring campaigns (Dietsch et al. 2015, Franke et al. 2019). As the structures were monitored over at least a year, annual average MC and MC variations are calculated. Based on the observations, finite element modelling (FEM) methods are used to simulate developments MC and MIS in glulam beams according to construction taking place in summer (July) or winter season (January).

2 Moisture content monitoring and moisture induced stresses

2.1 Moisture content monitoring campaigns

Measurement campaigns are normally initiated for quality assurance or structural health purposes. Leakage of water through asphalt decks of timber bridges was detected in Franke et al. (2014). Cables were embedded into substitute dowels to monitor MC in a pedestrian bridge in Birschke et al. (2008). The Norwegian Public Roads Administration conducts MC measurements in timber bridges (Norsk Treteknisk Institut, 2013).



Figure 1: Example of an ice rink 'B2' monitored in Dietsch et al. (2015) (left) and cable car station 'Schneehüenerstock' during its construction in Franke et al. (2019) (right)

The second reason to perform MC monitoring campaigns is to investigate the relation between moisture and climate in different building types (Dietsch et al., 2015). Franke et al. (2019) and Simon et al. (2017) investigated MC developments in timber bridges.

2.2 Moisture content measurements

2.2.1 Electric resistance method

The MC data reported in this paper was measured using the electric resistance and the sorptive method. Moisture content u is expressed as a mass percentage (M%) and calculated by using the wet and dry mass of wood, m_{wet} and m_{dry} , respectively:

$$u = (m_{wet} - m_{dry}) / m_{dry} \times 100 \quad (1)$$

The electric resistance can be measured between (partially insulated) electrode pairs and translated into a MC (Figure 2). Depending on the wood species, accuracies range from 1 M% to 2 M% below the FSP (Forsén and Tarvainen, 2000). Uncertainties related to grain orientation between the electrodes, type of electrodes (nails or screws), material density and temperature do exist (Skaar, 1989), but all -except for temperature- are not significant (Forsén and Tarvainen, 2000).

Temperature and moisture gradients can negatively affect the measured value of resistance between the electrodes (Skaar, 1989 and Niklewski, 2018). When analyzing in-situ measurements, averaging MC measurements over at least 24 hours is recommended (Franke et al., 2019).

2.2.2 Sorption method

The sorption method is an indirect method of MC measurement. It relies on the relation between relative humidity and temperature of the surrounding air and the corresponding moisture of wood. The climate is measured in a cavity in the wood (Figure 2). Melin et al. (2016) claims it is a more exact measuring method than the electric resistance. It is better suitable than the electric resistance method at sub-zero temperatures (Björngrim et al. 2017). Conversion from measured relative humidity and temperature to MC can be made using equations as suggested by Simpson (1973). Melin et al. (2016) uses temperature-dependent adsorption and desorption isotherms along with so-called moisture scanning curves.



Figure 2: Partially Teflon coated GANN electrodes (left), partially insulated screws (middle) and CMOS relative humidity and temperature sensor (right).

2.3 Moisture induced stresses

2.3.1 Wetting and drying of glued laminated timber

Section 1.2 mentioned examples where the moisture variation lead to damage in timber structures. Möhler and Steck (1980) were able to generate cracks perpendicular to the grain during laboratory experiments where glulam beams were subjected to MC variations. Experimental studies of moisture induced stresses are performed in step climates, i.e. a sudden change in surrounding relative humidity (Jönsson, 2004 and Angst and Malo, 2013). The studies focus on the generation of stresses perpendicular to the grain by drying or by wetting loads, where tensile stresses are generated either in the surface or midplane of the cross sections (Figure 3).

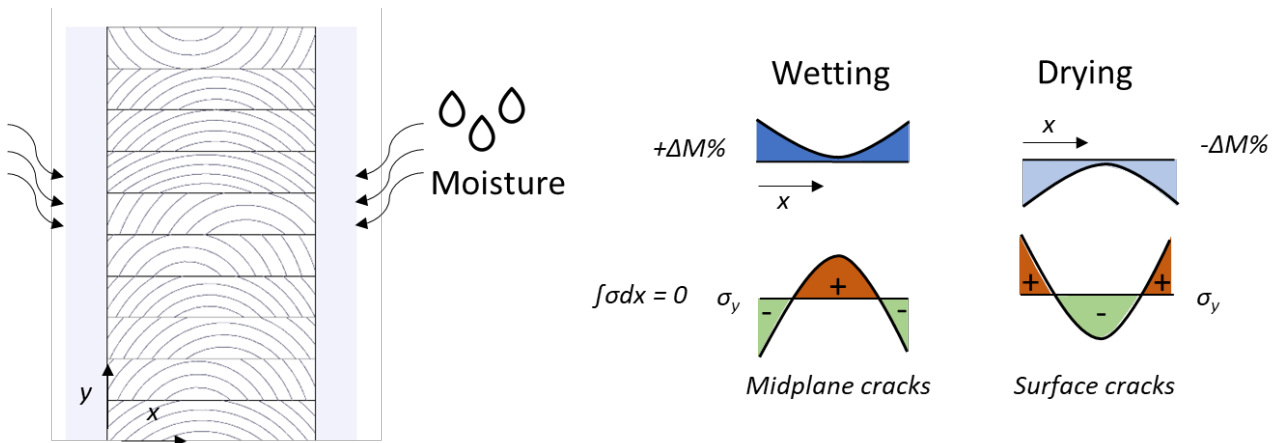


Figure 3: Tensile stresses generated in the cross section midplane due to wetting (left) and in the surface due to drying (right)

2.3.2 Moisture content diffusion

MC distributions in timber cross sections can be simulated using either a single-Fickian (Angst and Malo 2010, Niklewski 2018) or the multi-Fickian model (Frandsen et al. 2007, Fortino et al. 2019). The single-Fickian approach is used in this work:

$$\delta u / \delta t = D \delta^2 u / \delta x^2 \quad (2)$$

where the single derivative of moisture to time is a function of the double derivative of moisture to space times the diffusion parameter D . Literature (Hanhijärvi (1995), Aicher and Dill-Langer (1998), and Olek et al. (2005)) suggests several values of the diffusion parameter, but the one given by Angst and Malo (2010) is used here being $3.0 \text{ m}^2/\text{s}$ for both radial and tangential direction.

The boundary condition at the surface of the glulam element is set to be equal to that of the theoretical equilibrium MC of the surrounding air. Hysteresis effect or surface emission resistance was not accounted for in this model (Angst and Malo, 2013).

2.3.3 Moisture induced stresses

The moisture induced stresses are calculated using the equation presented in Angst and Malo (2013):

$$\varepsilon'_T = \varepsilon'_E + \varepsilon'_S + \varepsilon'_{MS} \quad (3)$$

Where the total strain is the summation of the elastic strain, the hygro-sorptive strain, and the mechano-sorptive strain, all as a derivative to time. The equations were modelled into the Finite Element solver ANSYS (Version 19.2) to analyse of the moisture induced stress developments in the RT-plane (radial-tangential) (Schiere, 2016). The implemented algorithms were validated using measurements of MC and MIS made on glulam cross sections (Jönsson, 2004).

The elastic strain is calculated using the compliance matrix C times the change of elastic stress σ . The compliance matrix is the inverse of the elasticity matrix.

$$\varepsilon'_E = C\sigma' \quad (4)$$

The hygro-sorptive strain is calculated using the hygro-expansion factor α times the change in MC u over time.

$$\varepsilon'_S = \alpha u' \quad (5)$$

The mechano-sorptive strain is calculated using the mechano-sorptive factor m times the elastic stress σ times the MC change u .

$$\varepsilon'_{MS} = m \sigma |u'| \quad (6)$$

3 Data analysis and simplification of measured climate

3.1 Classification of climate

A total of 30 different buildings and structures were arranged into nine different building types, see Table 1. The buildings were monitored over at least a year and all the structural elements were protected from direct impact of rain and sun, i.e. all MC were below FSP. Dietsch et al. (2015) monitored structures in southern Germany, Franke et al. (2019) in Switzerland. Instead of using the SC, their classification was based upon the building envelope and encountered climate:

- Climatized: closed and often thermally insulated building envelope, active climate regulation through heating or dehumidifiers
- Ventilated: closed building envelope without active heating system, however ventilated by (smaller) openings in the building envelope
- Open: Covered structure, free circulation of air, large openings in the building envelope, structural elements are still protected from direct exposure to weather.

Normally, a heated structure would be designed according to SC1, the ventilated and open structure according to SC2.

The measurements of MC were performed using the electric resistance and sorption methods (Section 2.2). In all structures except the bridges and cable car stations, MCs were measured using partially insulated GANN electrode pairs (Figure 2). In the

Table 1: List of monitored structures

Building/Structure	Dietsch et al., (2015a) Climatized/Ventilated/Open	Franke et al. (2019) Climatized/Ventilated/Open
Swimming pools	2/-/-	-/-/-
Sports halls	3/-/-	-/-/-
Production halls	2/-/-	-/-/-
Ice rinks	2/2/-	1/-/2
Riding halls	-/3/-	-/1/-
Agricultural buildings	-/3/-	-/-/-
Storage halls	-/3/-	-/-/-
Ski stations/cable car	-/-/-	-/3/-
Bridges	-/-/-	-/-/3
Total	9/11/-	1/4/5

bridges, partially insulated screws were used. The cable car stations were monitored using climate sensors, i.e. sorption method, due to the extended periods of sub-zero temperatures they were exposed to during winter.

The resistances between electrodes were measured using the Scanntronik Gigamodul and logged with either Thermofox or the Materialfox. Climate was measured using temperature and relative humidity sensors and logged using the Thermofox modules. The measured resistance was converted to MC using the SoftFox software (Scanntronik Mugrauer GmbH).

The analysed glulam cross-sections in Section 4.1 are between 160 mm and 240 mm wide in Dietsch et al. 2015) and 280 mm to 480 mm wide in Franke et al. (2019). All presented data concerns measurements in reference locations at 15 mm depth.

3.2 Data analysis

The relative humidity of the air and MC at a maximum depth of 15 mm are converted into so-called envelopes. The data is filtered using a moving average. Then one or two maxima or minima are omitted to exclude single, perhaps unlikely events (Figure 4). The result is a box of which the boundaries are set by relative humidity (horizontal axis) and measured MC (vertical axis). The sorption isotherm is plotted, too (Simpson, 1973).

The used measurements spanned at least a year of continuous monitoring. They concern measurements made in reference locations, i.e. locations that are representative for the general climate in the structure. Four different variables are obtained from the data: Average MC \bar{u} , the difference between minimum and maximum MC Δu_{15mm} , equilibrium MC at the surface $\Delta u_{surface}$, and the ratio $r_{u,15mm}$ between MC at the surface $\Delta u_{surface}$ and the amplitude at 15 mm depth Δu_{15mm} .

$$\Delta u_{15mm} = \max(u_{15mm}) - \min(u_{15mm}) \quad (7)$$

$$\Delta u_{surface} = \max(u_{surface}) - \min(u_{surface}) \quad (8)$$

$$r_{u,15mm} = \Delta u_{surface} / \Delta u_{15mm} \quad (9)$$

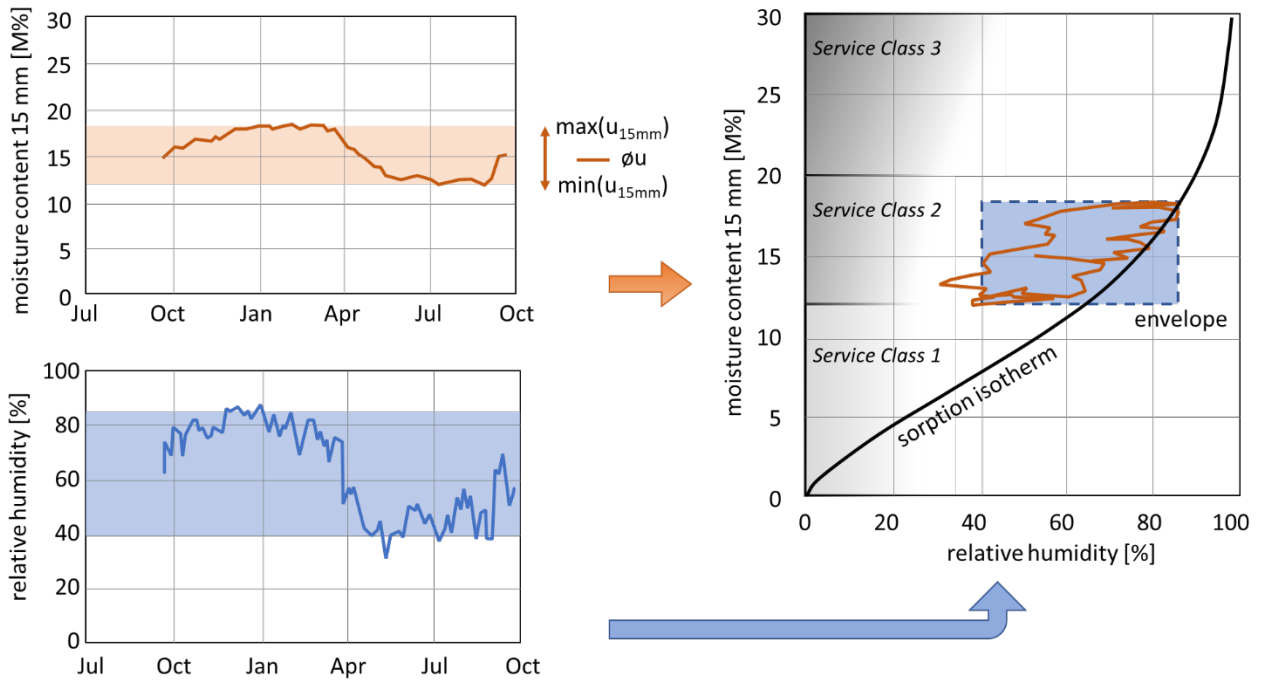


Figure 4: Signal analysis of measured relative humidity and moisture content (left), and conversion into envelopes (right)

The value r_u can be used to calculate a moisture gradient when divided over the depth of the electrode from the surface (Dietsch et al. 2015, Fortino et al. 2019).

3.3 Model winter and summer moisture content variations

Heated structures are typically dry in winter and relatively humid in summer. In winter, relative humidity outside is high, but absolute humidity is low. When cold air from outside the building enters a warmer environment in the building, the relative humidity will drop. As shown later in Section 4.1, relative humidities of 30% or lower are easily encountered in heated structures. On the other hand, ventilated structures are humid in winter and dryer in summer. A close look at the central European climate reveals that autumn and spring are the wettest and driest period, respectively (Schiere et al. 2018b). However, the driest and wettest period will be referred to as summer (1 July) and winter (1 January). The following equation for MC variations in a heated structure (SC1) and ventilated structures (SC2) are proposed (Figure 5):

$$u(t)_{SC1} = \varnothing u - \Delta u_{surface}/2 \cos(2\pi t/365) \quad (10)$$

$$u(t)_{SC2} = \varnothing u + \Delta u_{surface}/2 \cos(2\pi t/365) \quad (11)$$

The equations are used to calculate MIS in a glulam cross section in the process of transfer from a production facility at a MC of 12 M% into the heated or ventilated building, SC1 or SC2 respectively, and consecutive operation in normal use:

- SC 1 with an average MC $\varnothing u$ of 9 M% and an amplitude in MC variations (amplitude) of 2 M% at the surface of the beam ($\Delta u_{surface} = 4 \text{ M\%}$). A scenario is calculated for construction in winter and summer.

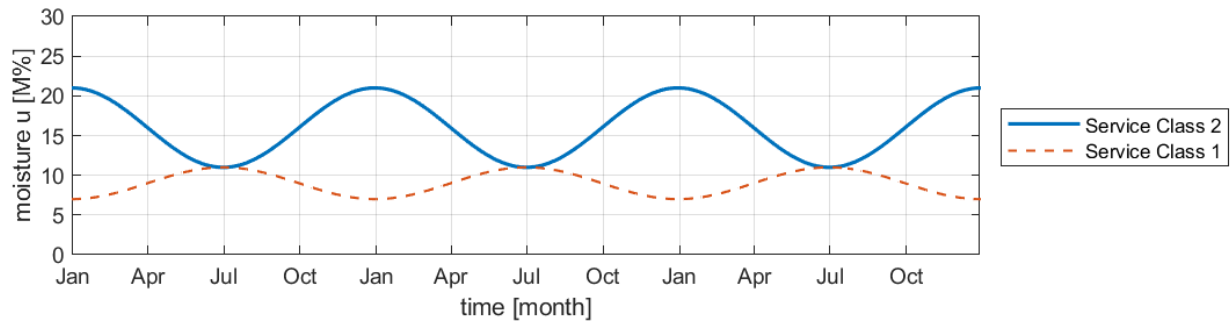


Figure 5: Model climate for Service Class 1 and Service Class 2 conditions

- SC 2 with an average MC \bar{u} of 16 M% and a variation (amplitude) of 5 M% at the surface of the glulam beam ($\Delta u_{surface} = 10 M\%$). A scenario is calculated for construction in winter and summer.

A cross section of a glulam beam (200 mm wide and 800 mm high) is modelled in a layup of ideally arranged lamellas with a pith location in the midplane of a beam (Figure 6). In more realistic layups with a spread in pith locations, MIS tend to reduce in the midplane and increase at the surface of the glulam beam (Schiere et al. 2018a). The material properties (radial-tangential) are modelled using cylindrical coordinates. The input parameters to the model are listed in Table 2.

beam width 200 mm

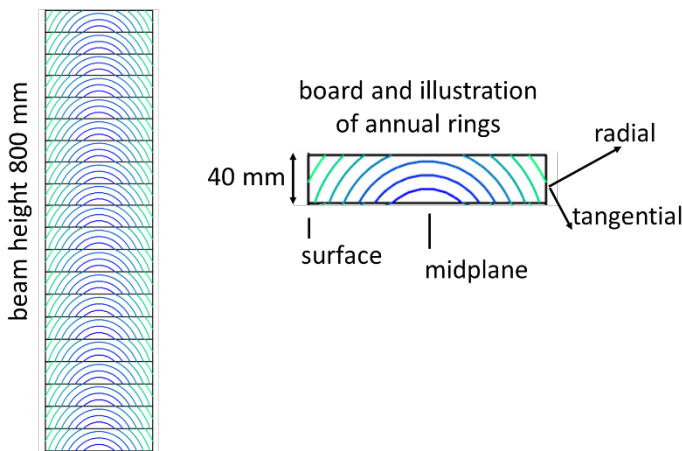


Figure 6: Illustration of board layout of numerical model, the coordinate system, and the layout of the modelled glulam beam

Table 2: Parameters used in the FE model to calculate the moisture induced stresses (Angst and Malo (2013) and Fortino et al. (2009))

Property	Value	Unit	Property	Value	Unit
E_R	$467 \cdot 10^6$	N/m^2	m_R	0.15	mm^2/N
E_T	$216 \cdot 10^6$	N/m^2	m_T	0.20	mm^2/N
G_{RT}	$41 \cdot 10^6$	N/m^2	m_{RT}	0.40	mm^2/N
ν_{RT}	0.5	-	μ_{RT}	0.75	-
α_R	0.13	$\%/M\%$	μ_{TR}	0.75	-
α_T	0.27	$\%/M\%$			

4 Results

4.1 Measured moisture contents and moisture content variations

The measured variations in relative humidity and MC are plotted in Figure 7. The average MCs, the average difference per maximum and minimum MC, and the ratio between difference in equilibrium MC and measured MC is plotted as well. The swimming pools and the ice rinks were climatized using dehumidifiers. Per diagram, only one climate type listed in Section 3.1 was plotted.

The figure clearly shows the difference between the climatized, ventilated and open structures. This leads to the following relevant observations:

- In climatized structures, average MC $\bar{\rho}u$ varies between 6.2 M% and 12.0 M% and Δu_{15mm} varies between 1.6 M% and 2.8 M% (smallest variations).

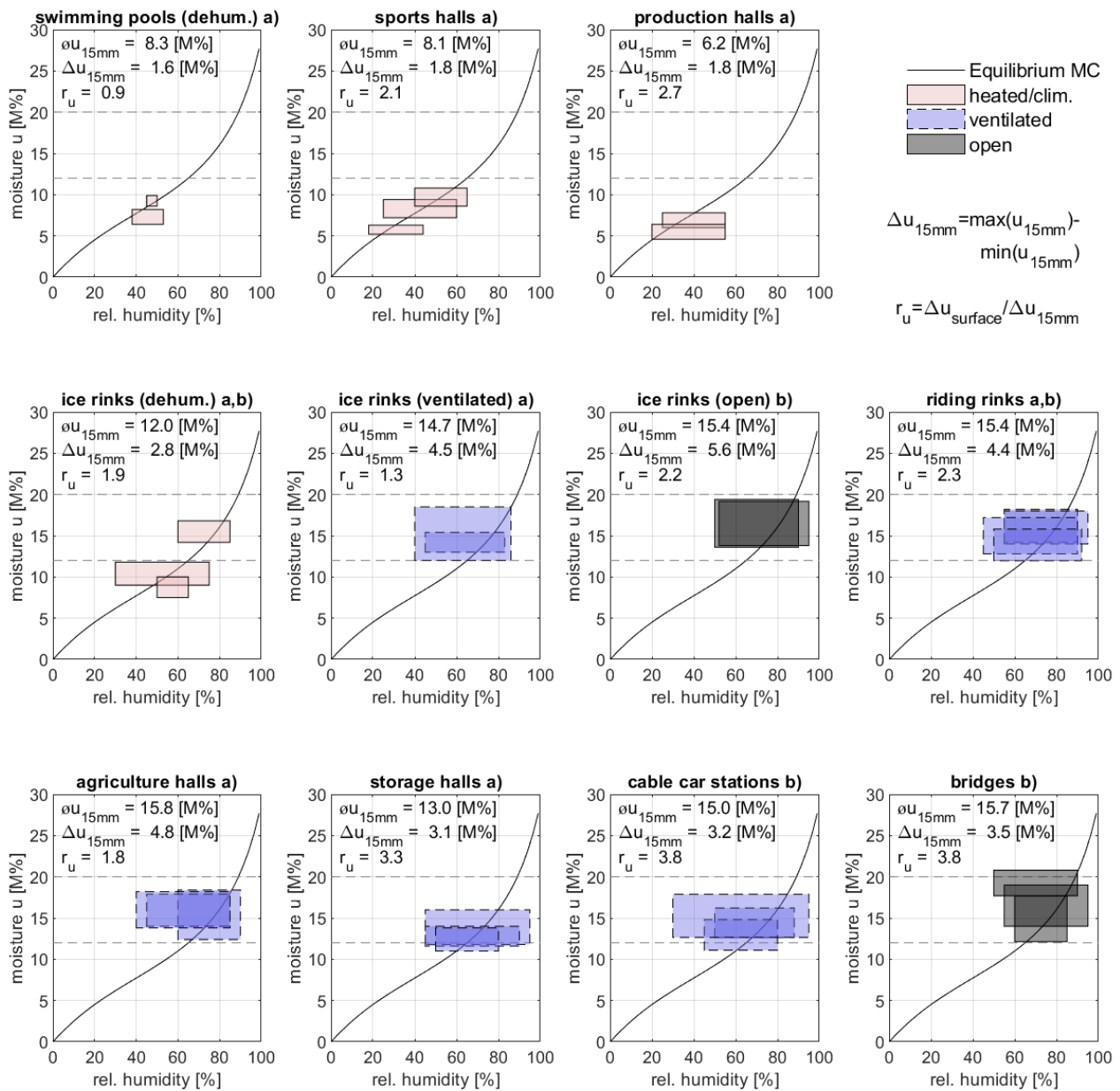


Figure 7: envelopes of measured relative humidity and corresponding moisture content in 30 different large-span structures: a) Dietsch et al. (2015) and b) Franke et al. (2019)

- In ventilated structures, average MC ϕ_u varies between 13.0 M% and 15.8 M% and Δu_{15mm} varies between 3.1 M% and 4.8 M%.
- In open structures, average MC ϕ_u varies between 15.7 M% and 16.5 M% and Δu_{15mm} varies between 3.5 M% and 5.6 M% (highest variations).

The figure shows that the choice of SC is evident for most structures, except for ice rinks. The highest MCs as well as MC variations are found in the open and well-ventilated structures.

The highest average values of r_u are found in the cable car stations. It is noted that the climate on average is quite stable, except for an incidental peak in relative humidity caused by local climate conditions.

The plotted data concern measurements at reference locations. Building physics affect the relative humidities in buildings which in turn affect MC of structural elements as well. In the dehumidified swimming pools, a cooler façade or opening in the building skin can change SC conditions from SC1 to SC2. Outage of dehumidifiers in ice rinks have also been known to lead to rapid increases of relative humidity. In ventilated and open ice rinks, high MC over the ice-surface have led to ‘soaked’ timber elements, forcing authorities to temporarily close facilities due to reduced load bearing capacity and stiffness of the roof structure.

4.2 Simulated moisture content variations and moisture induced stresses in 200 mm wide cross sections

4.2.1 Short term developments

The MC variations, deformation, and MIS following construction time and beyond are observed in Figure 8. The SC1 condition is plot in the right column and the SC2 condition is plot in the left column.

Beams entering SC1 conditions suffer a large decrease of MC in winter (January). Straight out of the production facility at 12 M%, the beam is subjected to conditions that represent an equilibrium MC of 7 M%. Following the drying of the surface, tensile stresses at the surface will develop rapidly. Compression stresses in the cross section’s midplane will develop only slowly.

In the case of the structural element entering the SC2 conditions in winter, the MC at the surface will increase after leaving the production facility. This results in tensile stresses in the midplane of the cross section which will gradually increase, and compression stresses at the surface of the cross-section which will increase rapidly.

In this example, elements entering the construction site in summertime (July) are subjected to small MC variations and development of MIS in SC1 and SC2.

It is noted that the duration of transfer from production facility to construction site is an idealised scenario: transfer of the building element to the construction site, installation on site (without any protection from sun or rain), closing of the building envelope and other climate scenarios until use are not included. Such conditions like en-

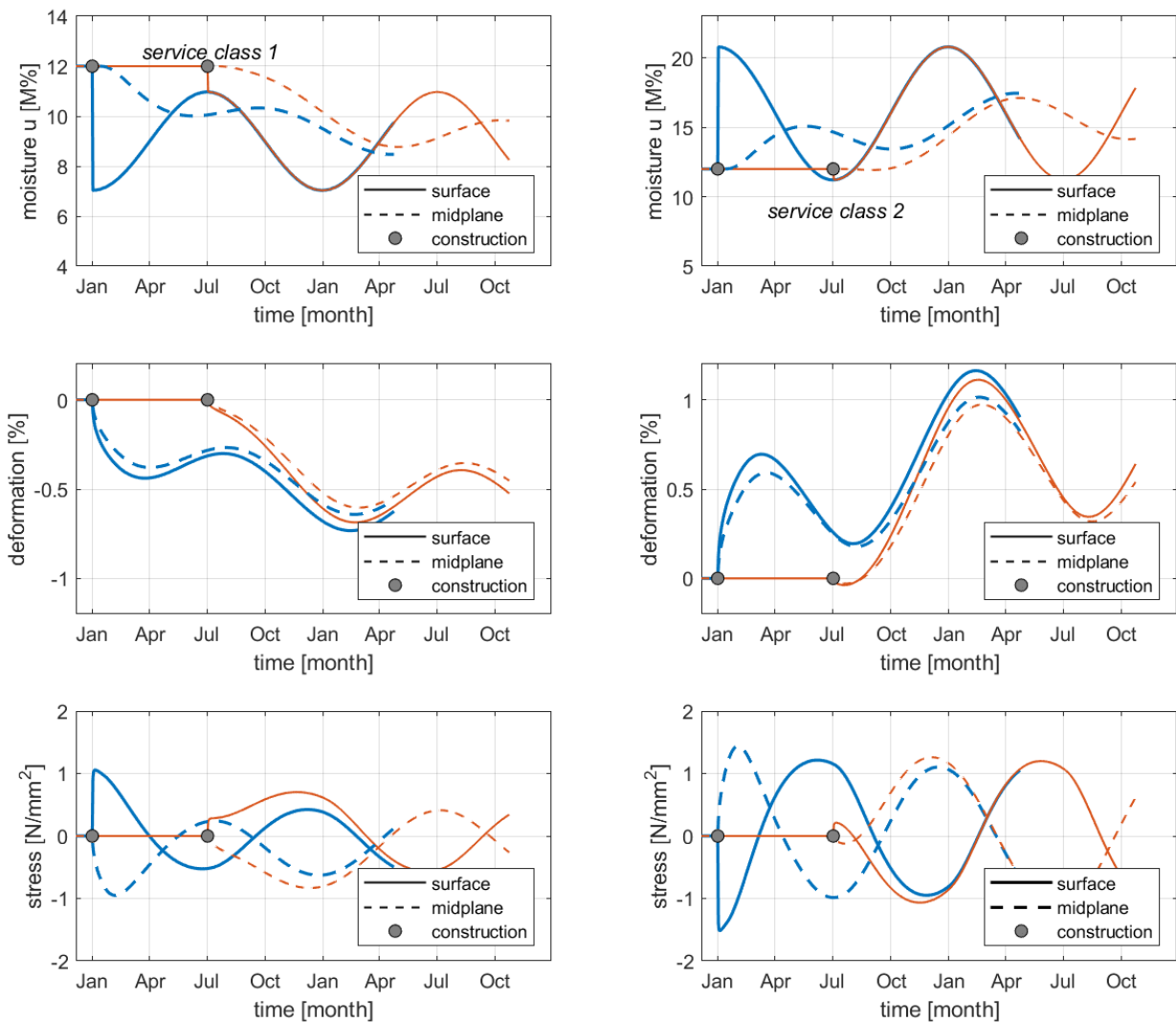


Figure 8: Illustration of moisture content (upper) and moisture induced stresses (bottom) for both SC1 and SC2 conditions.

countered in the application of screed have not been documented: timber elements were exposed to a high relative humidity of 90% at temperatures of 20 °C for weeks, followed by a dry period where temperatures up to 35 °C and relative humidities of 30% were measured. Cracks in timber had appeared already before the building was in use.

4.2.2 Long term developments

The length of the simulations represents 1.5 year after construction. The development of MC at the midplane of the cross section show that it takes at least 1.5 years to approach the average annual MC, i.e. 9 M% or 16 M% in SC1 and SC2 respectively. The amplitudes of the MIS in the SC1 conditions decrease with compared to the ones developed after construction. Those in SC2 conditions achieve approximately equal levels as those found at the start of the construction period.

Although simulated with simplified climate profiles and modelling, the MIS still support the need for extra measures during construction or repair of buildings.

5 Conclusions and recommendations

The evaluated MC in the studied structures establish a basis for design of future buildings. Special conditions can be anticipated to by the designing engineers: single events, change of building use, and so on. Despite the observed trends, the responsible structural engineer should verify if the designed structure will encounter similar conditions as those of the monitored buildings.

In ice rinks, expected MC depends on the building envelope and the use of dehumidifiers. Experience shows that high MC is easily achieved, either above the ice-surface or during an outage of the climate control equipment. Generally, elements exposed to weather experience higher MC as well. Leakage of sealings or roofs are to be avoided, just as much as high relative humidities developing in connections with little ventilation. If structures are exposed to wet conditions for extended periods of time, sufficient drying/ventilation should be assured to reduce average moisture contents. Moisture content monitoring has proven to contribute to quality assurance and structural health monitoring of buildings and structures. Affordable solutions that increase the possibility of detecting anomalies in an early stage, thereby avoiding high repair costs, are available.

Variation of MC in load-bearing elements imposes change in dimensions and can lead to the development of (high) moisture induced stresses, already during construction of the building. Winter conditions are demanding for the timber and measures should be pursued that reduce moisture content variations. In the simulated SC1 conditions, the MC decreases from 12 M% to 7 M% at the surface of the glulam beam. These are conditions where cracks perpendicular to grain develop in the surface of timber elements. According to the simulations, summer offers a much milder climate for timber construction. In the simulated SC2 conditions, MCs in January will increase from 12 M% to 21 M%.

Acknowledgements

The work was supported by the Federal Office for the Environment (FOEN) under project number 2013.06 and 2016.17. Industry partners Roth AG, Makiol Wiederkehr AG, and Tiefbauamt des Kantons Bern, WaltGarmarini AG, Pirmin Jung Ingenieure AG, Büro für Projektleitungen und Baufragen, Henkel & Cie. AG, SFS Unimarket AG, and Würth AG Schweiz. Research partners Technical University of Munich and Lund University are also acknowledged for their contribution.

6 References

Aicher S, Dill-Langer G, Ranta-Maunus A (1998), Duration of load effect in tension of glulam in different climates, Holz als Roh- und Werkstoff 56, p. 295-305

- Angst V Malo KA (2010), Moisture induced stresses perpendicular to the grain in glulam: a review and evaluation of the relative importance of models and parameters, *Holzforschung* 64 (5), p. 609–617
- Angst V Malo KA (2013), Moisture-induced stresses in glulam cross sections during wetting exposures, *Wood Sci Technology* 47, p. 227–241
- Birscke C, Rapp AO, Bayerbach R, Morsing N, Fynholm P, Welzbacher C (2008): Monitoring the “material climate” of wood to predict the potential for decay: Results from in situ measurements on buildings, *Building and Environment* 43, p. 1575–1582
- Björngrim N, Fjellström PA, Hagman O (2017), Resistance measurements to find high moisture content inclusions adapted for large timber bridge cross-sections, *BioResources* 12 (2), pp. 3570-3582
- Dietsch P, Gamper A, Merk M, Winter S (2015), Monitoring building climate and timber moisture gradient in large-span timber structures, *Journal of Civil Structural Health Monitoring* 5 (3), p. 153–165
- Dietsch P. and Winter S. (2018), Structural failure in large-span timber structures: A comprehensive analysis of 230 cases, *Journal of Structural Safety* 71, p. 41-46
- SN EN 1995-1-1:2014, Eurocode 5: Bemessung und Konstruktion von Holzbauten-Teil 1-1: Allgemeine Regeln und Regeln für den Hochbau (inkl. A1:2008 und A2:2014), SIA Zurich, Switzerland
- Forsén H and Tarvainen V (2000), Accuracy and functionality of hand-held wood moisture content meters, Technical Research Centre of Finland, VTT Publications 420, Espoo, Finland
- Franke B, Franke S, Müller A (2014), Case studies: long-term monitoring of timber bridges, *Journal of Civil Structural Health Monitoring* 5 (2), p. 195-202
- Franke B, Franke S, Schiere M, Müller A (2019), Moisture content and moisture-induced stresses of large glulam members: laboratory tests, in-situ measurements and modelling, Volume 14 (4), p. 243-252
- Franke B, Franke S, Schiere M, Müller A (2014), Quality assurance of timber structures, research report, Bern University of Applied Sciences, Switzerland, ISBN 978-3-906878-04-1
- Frandsen H, Damkilde L, Svensson S (2007), A revised multi-Fickian moisture transport model to describe non Fickian effects in wood, *Holzforschung* 61, p. 563-572
- Frese M. and Blass H.J. (2011), Statistics of damages to timber structures in Germany, *Engineering Structures* 33 (11), p. 2969–2977
- Fortino S, Mirianon F, Toratti T (2009), A 3D moisture-stress FEM analysis for time dependent problems in timber structures, *Mechanical Time-Dependent Materials* 13, p. 333–356

- Fortino S, Hradil P, Genoese A, Genoese A, Pousette A (2019), Numerical hygro-thermal analysis of coated 412 wooden bridge members exposed to Northern European climates, *Construction and Building Materials* 208, p. 413 492–505
- Hanhijärvi A (1995), Modelling of creep deformation mechanisms in wood, Dissertation Helsinki University of Technology, Espoo, Finland
- Jönsson J (2004), Internal stresses in the cross-grain direction in glulam induced by climate variations, *Holzforschung* 58, p.154–159
- Melin C, Gebäck T, Heintz A, Bjurman J (2016), Monitoring dynamic moisture gradients in wood using inserted relative humidity and temperature sensors, *e-Preservation Science*, 1581-9280 (eISSN) 13, p. 7-14
- Mohler and Steck (1980), Untersuchungen über die Rissbildung in Brettschichtholz infolge Klimabeanspruchungen, *Bauen mit Holz* 4/80, p. 194-200
- Niklewski J (2018), Durability of timber members: moisture conditions and service life assessment of bridge detailing, Dissertation Lund University, Sweden, ISBN 978-91-87993-11-4
- Norsk Treteknisk Institut (2013), Monitoring five timber bridges in Norway - results 2012, Report no. 310332, Oslo, Norway
- Olek W, Perré P, Weres J (2005), Inverse analysis of the transient bound water diffusion in wood, *Holzforschung*, 444 Vol. 59, pp. 38–45
- Schiere M (2016), Moisture diffusion and moisture induced stresses in glulam cross-sections, MSc Thesis, BFH Bern, Switzerland, thesis no. MHT/PA/MA/045/16/00
- Schiere M, Franke B, Franke S (2018a), Antworten zur Tragfähigkeit infolge dynamischer Klimawechsel, SWIN conference proceedings, Biel, Switzerland
- Schiere M, Franke B, Franke S, Müller A (2018b), Comparison between local versus regional climate using monitoring data of timber structures, WCTE Conference Proceedings, Seoul, South Korea
- Simon A, Jahreis M, Koch J, Arndt R (2017), New design guidelines for structural protected timber bridges, International Conference on Timber Bridges conference proceedings, Skellefteå, Sweden
- Simpson W. (1973), Predicting equilibrium moisture content of wood by mathematical models, *Wood and Fiber*, 5 (1), p. 41-49
- Skaar C (1988): *Wood-water relations*, Springer Verlag, Germany, ISBN 3-540-19258-1

Discussion

The paper was presented by M Schiere

P Dietsch asked if the model climate was compared with real climate conditions. M Schiere replied that this was done in the past where Fourier analysis was used that showed 1st amplitude was governing.

S Aicher commented that the simulation of sinusoidal climate disregarded contribution of singular events. Based on his experience singular climate events contribute significantly to damage and should be considered as climatic variation. M Schiere agreed that singular climate events as well as location of timber elements within a building should be considered. S Aicher added that time dependent damage model would be appropriate.

P Dietsch asked about the influence of the laying of screed for floors. M Schiere responded that data showed that it could cause change in relative humidity and temperature experienced by the floor and be treated as a singular climate event.

Shrinkage behaviour of reinforced glulam members

Martin Danzer*, Philipp Dietsch** and Stefan Winter*

* Chair of Timber Structures and Building Construction, Tech. University of Munich

** Department of Structural Engineering and Material Sciences, Unit of Timber Engineering, University of Innsbruck

Keywords: timber, glulam, reinforcement, wood moisture, shrinkage, holes, notches

1 Introduction

As a hygroscopic material, wood adapts its moisture content to the climatic conditions of the environment (temperature and relative humidity). It reacts with swelling in the case of an increase and with shrinkage in the case of a decrease of wood moisture content. Due to its comparatively low strength properties with regard to shear and especially tension perpendicular to the grain, reinforcing elements are often arranged in timber members to increase their load-carrying capacity. This positive effect of the reinforcement is, however, in conflict with its effect of restraining the free swelling or shrinkage behaviour of wood. Regarding this restraining effect shrinkage is considered the more critical case, because of the resulting stresses in tension perpendicular to the grain. This situation can occur in drying processes, e.g. from the moisture content at production to the equilibrium moisture content in low relative humidities, which are typical for insulated, heated buildings [Dietsch et al. (2015)]. So far, there are only few experimental studies available on this topic [Ehlbeck et al. (1992), Blaß & Krüger (2010), Wallner (2012)]. In most cases, the test specimens were exposed to climatic cycles of rather short duration with abrupt, significant changes in relative humidity, a climatic situation which cannot directly be transferred to environmental conditions occurring in practice. From the results of these investigations, it is not possible to distinguish whether the cracks were caused by the high moisture gradient across the cross section or whether they were actually caused by the restraining effect of the reinforcing elements. Hence, the extent to which cracks are induced as a result of the latter effect and the resulting consequences to the

load-carrying capacity of such members are still unclear. In Dietsch (2017) the restraining effect of the reinforcement was investigated by implementing the change of moisture content not in form of a climatic cycle but by an equivalent deformation applied to the reinforcement.

2 Experimental investigations

2.1 Test programme

To clarify the abovementioned question, the restraining effect of typical applications of reinforcing elements was quantified for three groups of glulam members (homogeneous arrangements over a section of the beam as well as local arrangements at holes and notches), see Figures 1-3.

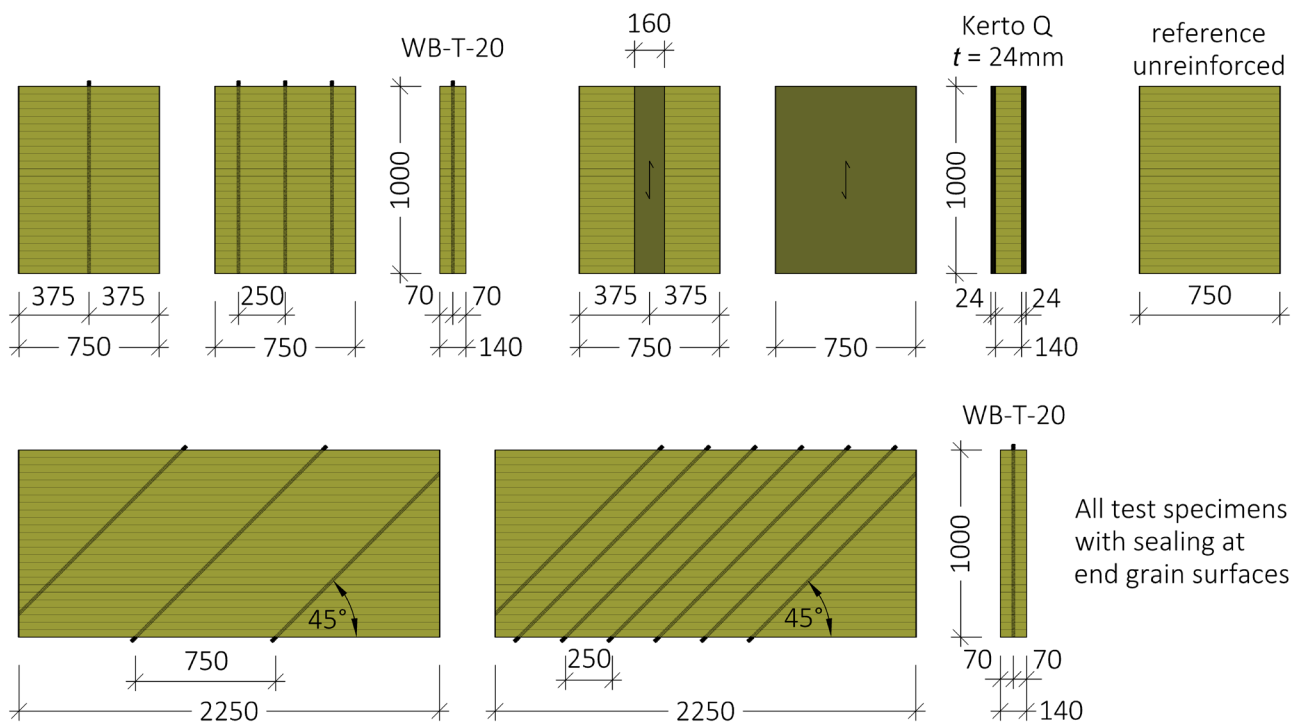


Figure 1: Configurations of homogeneous arrangements of reinforcement

The glulam specimens (declared as GL28c) were obtained from two manufacturers, A and B. Each configuration consisted of four specimens, two from manufacturer A and B, respectively. The types of reinforcement used were drilled-in, internal (fully-threaded screws $d = 13\text{ mm}$ / threaded rods $d = 20\text{ mm}$) as well as glued-on, external reinforcing elements (LVL $t = 24\text{ mm}$, PRF adhesive).

All reinforced test specimens were first exposed to a slow drying process over a period of 410 days to mirror the climatic conditions in insulated, heated buildings. Starting from a level of 60% RH, the relative humidity was decreased by 5%/month and then kept constant in a range of 30% - 35% RH.

After climate storage destructive tests were realized on all test specimens with holes and notches. During climate storage, one side of the otherwise symmetrically manufactured beams with holes and notches remained unreinforced. After climate storage, the unreinforced sides were reinforced in the same way to the opposite side and the load-carrying capacities of both sides (with / without restraining effect of reinforcement due to shrinkage) were determined by 3-point bending tests in a two-stage test procedure, see Figure 2. To determine the load-carrying capacities of the sides without restraining effect ("Test 2") the cracked parts of the sides with restraining effect ("Test 1") also had to be reinforced.

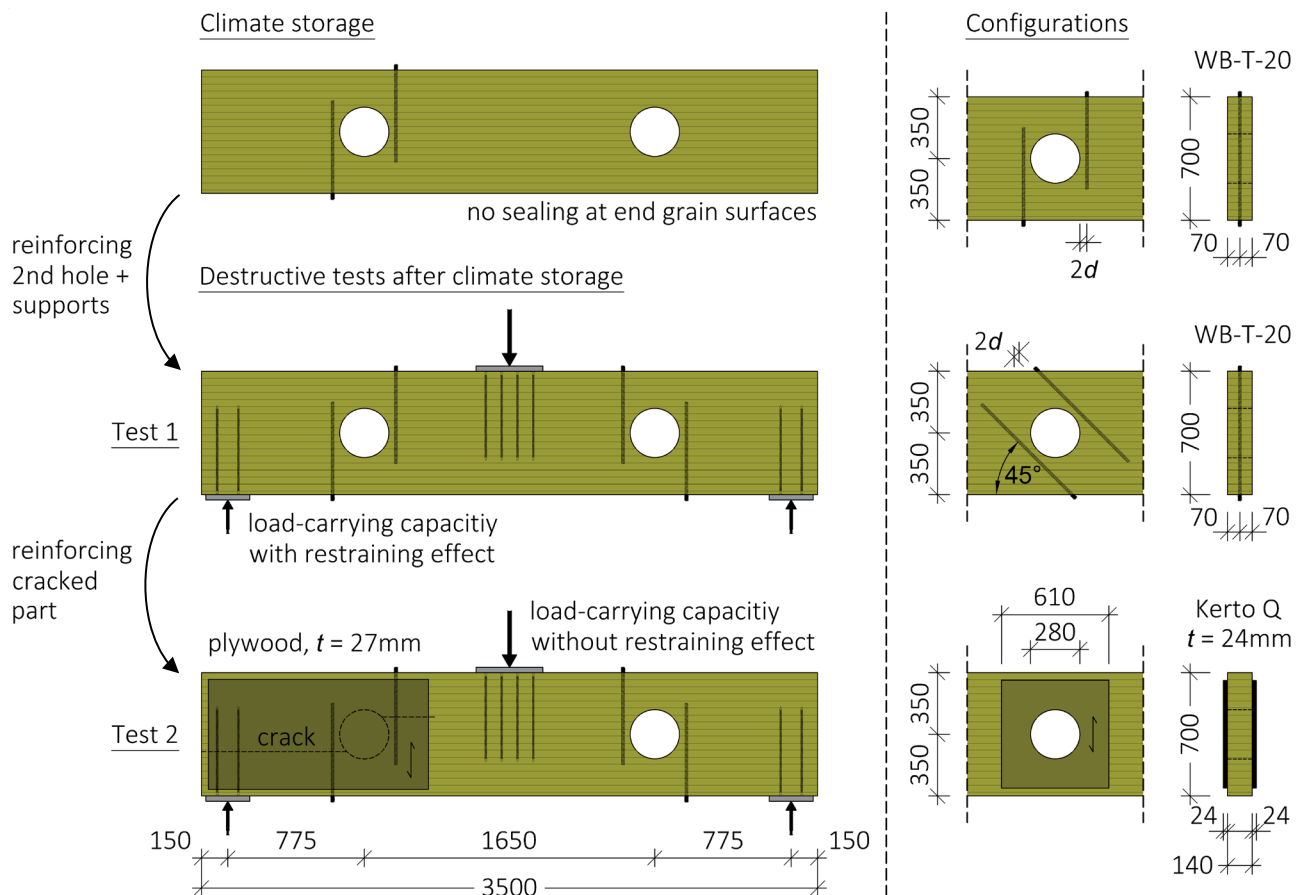


Figure 2: Test programme and configurations of beams with holes

In case of the beams with notches, the procedure was performed in an analogous manner, due to the page limitations of the paper Figure 3 contains only the last step "Test 2".

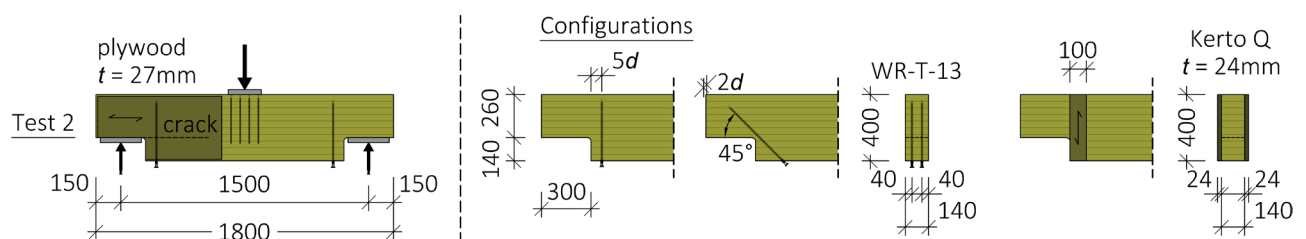


Figure 3: Test programme and configurations of beams with notches

2.2 Results

2.2.1 Distribution of wood moisture

The initial wood moisture contents before the application of the reinforcing elements and starting the drying process were determined on all specimens by resistance measurements at different depths (15 mm/25 mm/40 mm). Differentiating between the three groups of glulam members and the two manufacturers, the following mean values of the moisture contents were obtained (see also Table 1):

manufacturer A: $u_0 = 10.2\% - 11.5\%$

manufacturer B: $u_0 = 13.2\% - 13.6\%$

As a result of the different initial wood moisture contents, the shrinkage behaviour on the test specimens of the two manufacturers differed significantly, so that a manufacturer-specific evaluation was necessary.

During the drying period the distribution of wood moisture content in the test specimens across the cross-sectional width as well as in fibre direction in the vicinity of unsealed end grain surfaces was determined over time by resistance measurements on several specimens, see Figure 4 (top). In addition, the distribution of wood moisture content across the cross-sectional width was determined by the kiln-drying method. To this end, slices of additional test specimens were prepared with a sealing on four sides and stored in the same climate chamber. At specific points in time, in the beginning once a week, in the end every four weeks, specimens from this series were taken from the climate chamber and analysed according to Figure 4 (bottom).

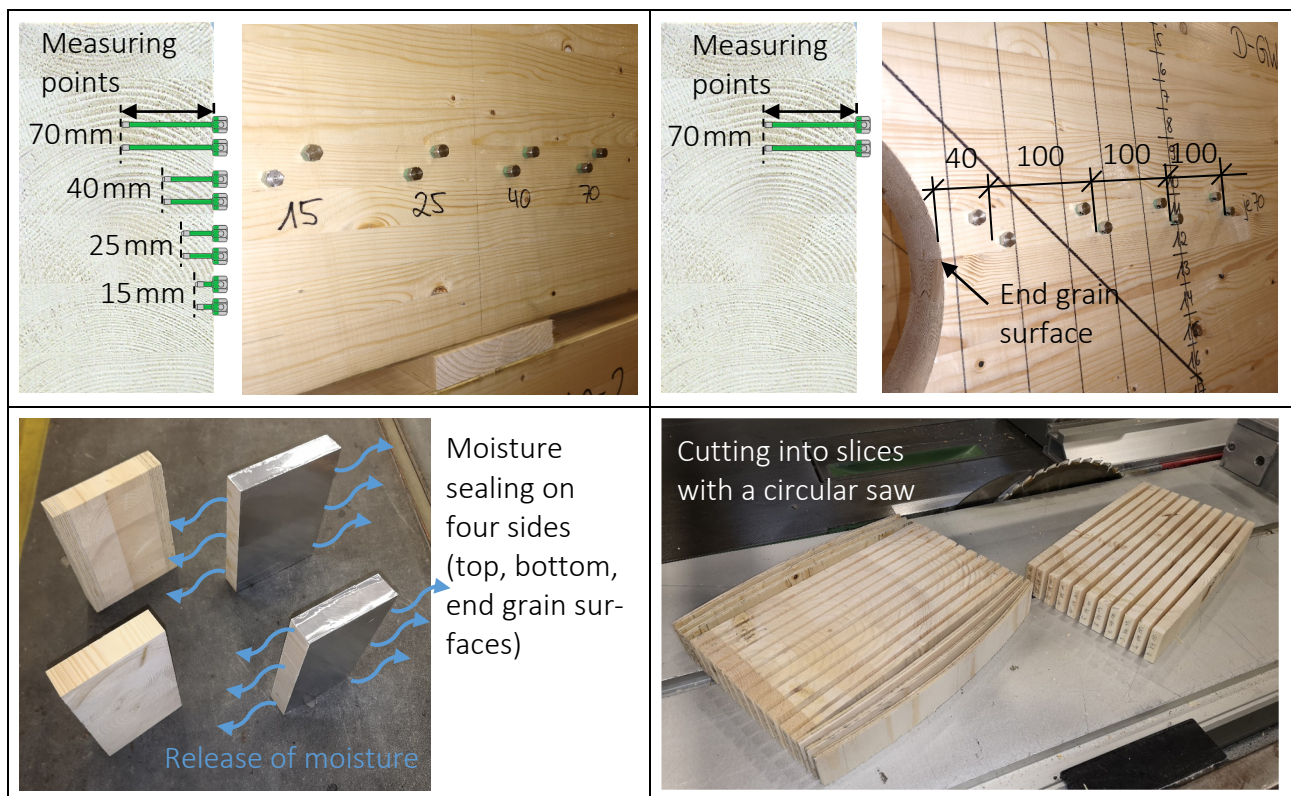


Figure 4: Resistance measurements (top) and kiln-drying method (bottom)

In Figure 5, the distribution of wood moisture content over time in the test specimens of manufacturer B is illustrated (averaged over the measured specimens). The data sets “N”, “H” and “HA” represent the initial wood moisture contents of the groups of glulam members “notches”, “holes” and “homogeneous arrangements”.

With regard to the distribution across the cross-sectional width a moisture gradient was formed in the first few months accompanied by a continuous decrease in wood moisture. In the range of months 8 - 10, the process slowed down before the moisture content could be lowered again in the last months.

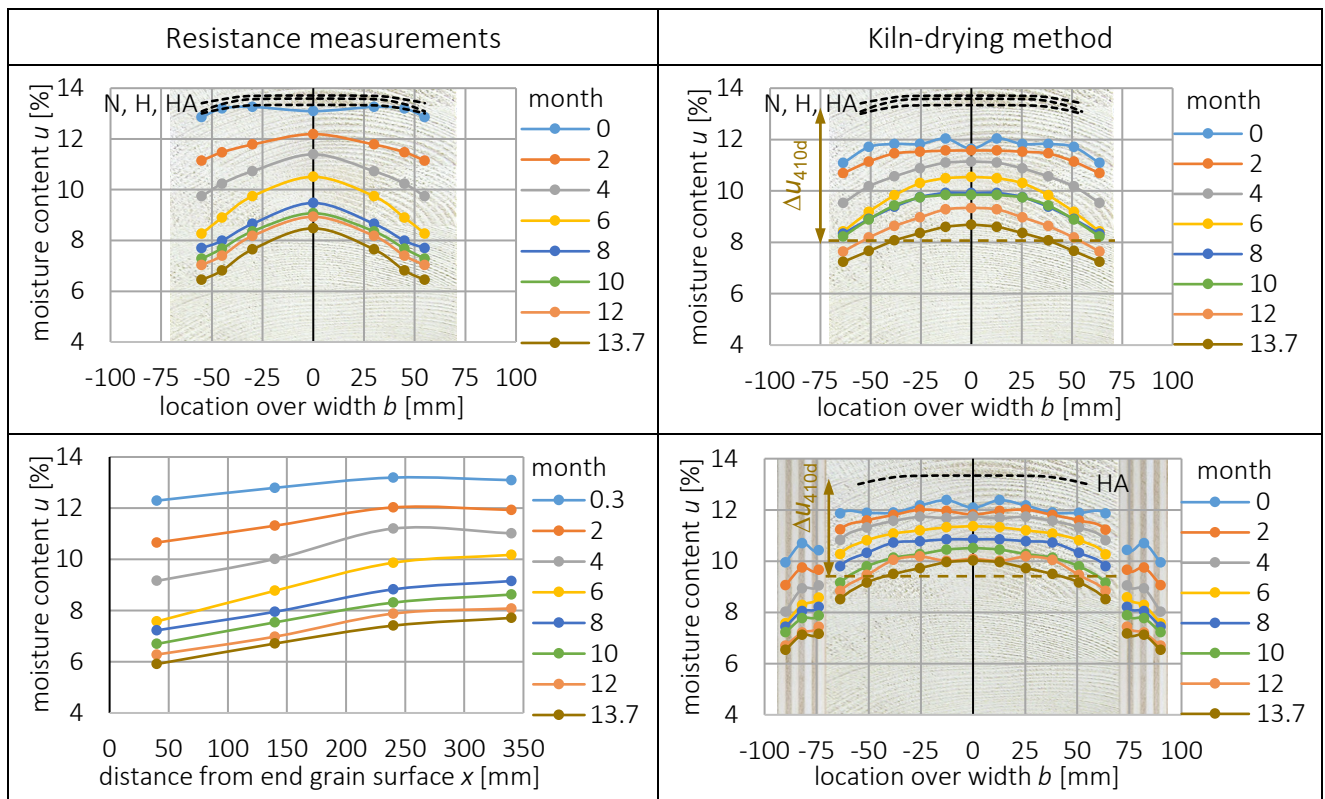


Figure 5: Distribution of wood moisture content in test specimens of manufacturer B

With increasing time of climate storage, a comparison of the kiln-drying method with the resistance measurements showed continuously increasing deviations. At the end of climate storage, the deviations of the measurements near the surface could be quantified up to $\approx 1\%$ in the case of specimens of manufacturer B and up to $\approx 1.5-2\%$ in the case of specimens of manufacturer A. With an accompanying study [Pommer (2019)] fundamental sources of error could be excluded by a comparison of these two methods applied on the same material. As a consequence of the described deviations, only the results of the kiln-drying method formed the basis for all further evaluations. However, in case of the specimens of manufacturer B in the first 4 - 5 months results of the resistance measurements had to be used, because of deviations between results of the kiln-drying method and the initial wood moisture content, determined by resistance measurements. The reason for that is assumed in an influence at the time of preparing the comparatively thin slices (cutting out of larger specimens, sealing, labelling) in the environment of normal climate.

In Table 1 the differential moisture contents Δu_{410d} at the end of the climate storage are summarized with respect to the initial moisture contents. The differential moisture content Δu_{410d} is defined as the difference between initial wood moisture content and wood moisture content after 410 days, both situations considered as averaged values of the distributions across the cross-sectional width of the glulam part, see Figure 5.

Table 1: Differential moisture contents at the end of the climate storage

Group of glulam member	manufacturer A		manufacturer B	
	u_0	Δu_{410d}	u_0	Δu_{410d}
Homogeneous arrangement (no external reinforcement)	10.6	2.8	13.2	5.1
Homogeneous arrangement (external reinforcement)	10.6	2.0	13.2	3.8
Holes	10.2	2.4	13.4	5.3
Notches	11.5	3.7	13.6	5.5

According to the results of the kiln-drying method the maximum difference in moisture content between inner part of the cross section and the area close to the surface occurred after round about 6 months and had a magnitude of $\approx 2.5\% - 3.0\%$ (specimens of manufacturer B). This was significantly below the magnitude of $\approx 4\% - 5\%$, which in investigations of Möhler & Steck (1977) was found to be the critical difference, where cracks are to be expected in unreinforced test specimens. The objective of avoiding the occurrence of cracks close to the surface due to an excessively pronounced moisture gradient was thus achieved.

With regard to the distribution in direction of the grain, a difference of up to $\Delta u \approx 2.5\% - 3\%$ (specimens of manufacturer B) could be noted over the measured length. The wood moisture content at the end grain surface reaches values similar to those at the side faces of the distribution across the cross-sectional width. As a result, there is a spatial distribution in the end grain region, i.e. larger differences in wood moisture content occur at this location at an earlier point in time.

2.2.2 Crack formation

In order to quantify the restraining effect, the formation of cracks on all specimens was recorded once a week in terms of time, quantity, position and extent over time. Based on this approach critical differential moisture contents at time of crack formation are illustrated in Figure 6 and Figure 7 for the three groups of glulam members. Mean values are only stated if cracks appeared in both specimens of a configuration from the same manufacturer. In addition, the differential moisture contents at the end of the drying period according to Table 1 are shown.

It is obvious that the behaviour between the specimens of the two manufacturers differs significantly. While only very few cracks were detected on test specimens from manufacturer A (differential moisture content $\Delta u < 3\%$ in most cases at the end of the drying period), cracks were found on most specimens from manufacturer B in the

range of a differential moisture content $\Delta u \approx 3\% - 5.5\%$. It can be seen that the differential moisture content of the specimens from manufacturer A ($\Delta u_{410d} = 2.8\%$) is only slightly below the critical range of differential moisture content mentioned above. An inclined arrangement of the reinforcing elements proved to be consistently more favorable with regard to the restraining effect than comparable arrangements perpendicular to the grain.

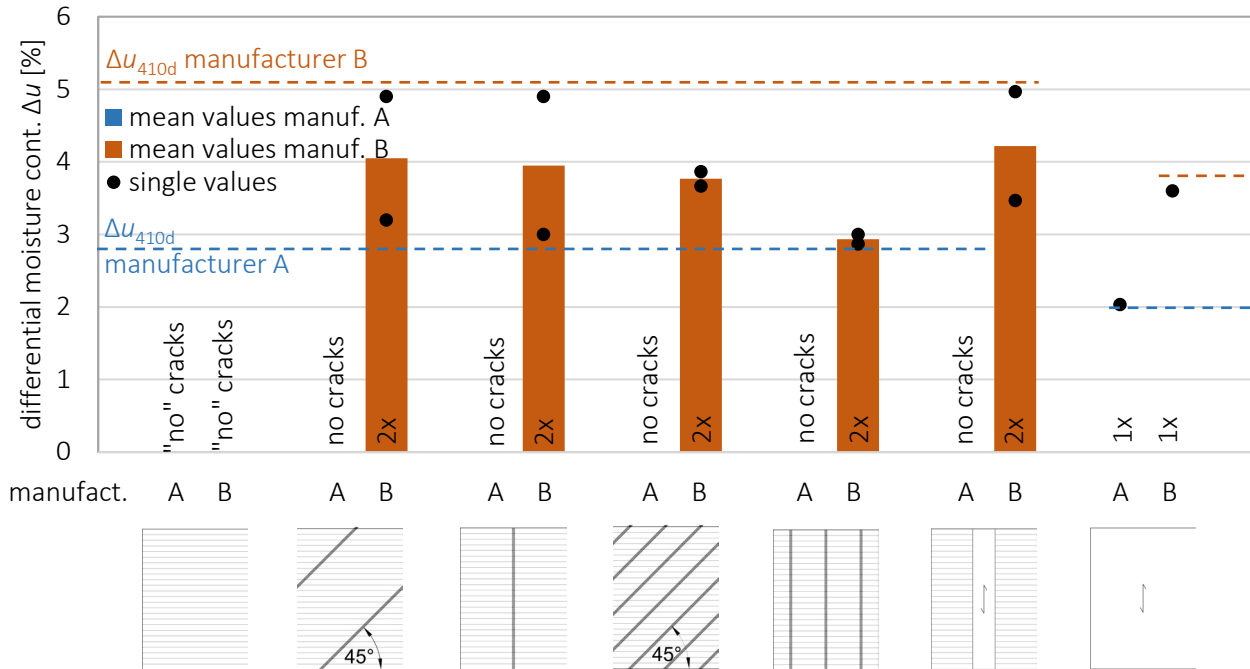


Figure 6: Differential moisture content at time of crack formation (homogeneous arrangement)

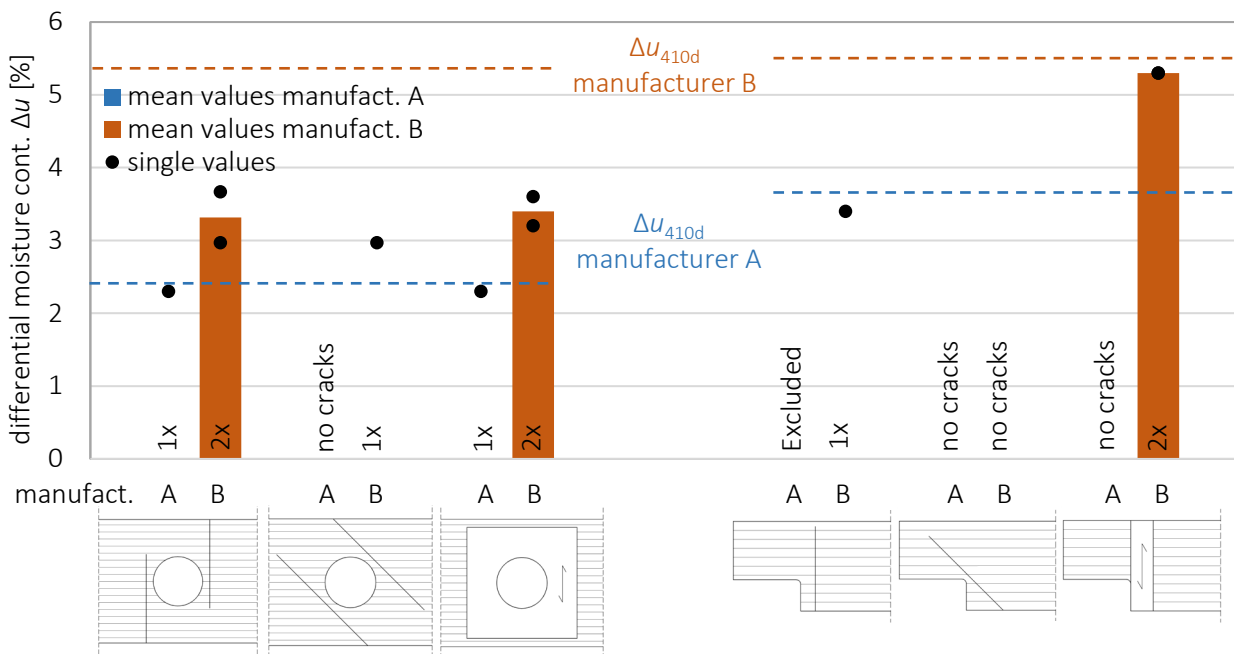


Figure 7: Differential moisture content at time of crack formation (left: holes; right: notches)

The term “no” cracks in case of the unreinforced specimen (homogeneous arrangement) means that cracks were recorded, but they were very thin ($\leq 0,25\text{ mm}$) and locally limited to the surface, so that they were neglected. The results of the two specimens with notches from manufacturer A with internal reinforcement at $\alpha = 90^\circ$ were

excluded, as these showed a pronounced formation of cracks from the beginning, but in areas where it was not to be expected. For example, already after 28 days on the unreinforced side of the beam, in the area of edge lamellas or generally in areas without reinforcement.

2.2.3 Shrinkage deformations

To further quantify the restraining effect, shrinkage deformations over time were recorded once a week on test specimens of the group "homogeneous arrangements". For this purpose a digital calliper (accuracy 0.07 mm) was used to record changes in height between upper and lower edges at defined distances to the reinforcing elements, see Figure 8. In the case of an external reinforcement, the jaws were placed at the upper and lower end faces of the LVL panel.

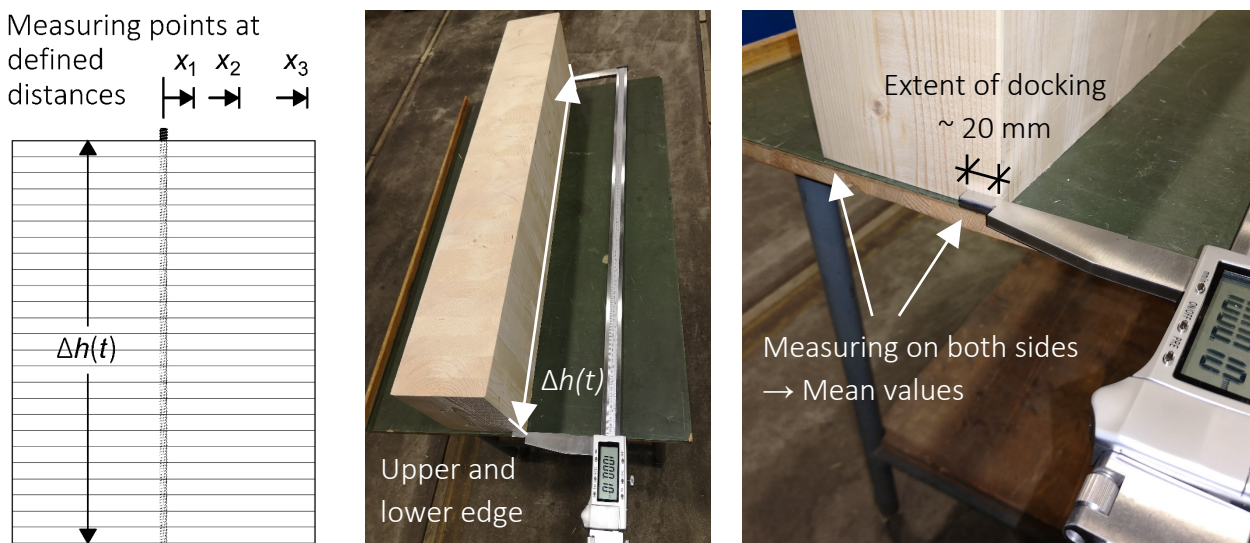


Figure 8: Measuring shrinking deformations between upper and lower edges

As a result of the different initial wood moisture contents, the shrinkage behaviour on the test specimens of the two manufacturers differed significantly. With the onset of crack formation, a quantitative comparability is not possible any more. Because of that results presented here are related solely to specimens of manufacturer A (only very few cracks), see Figure 9. For the full results, the interested reader is referred to the final report [Danzner et al. (2019)].

The shrinkage deformations measured on the specimens with internal reinforcement of different arrangement show similar behaviour when compared to the results obtained during the monitoring of crack formation, see Figure 6. Thus, these investigations confirm the different degrees of restraining effect of the reinforcement depending on the geometry of arrangement.

An inclined arrangement of the reinforcing elements resulted consistently in larger shrinkage deformations (i.e. smaller restraining effect) compared to arrangements perpendicular to the grain. At a higher degree of reinforcement the difference tends to be more pronounced compared to a lower degree of reinforcement.

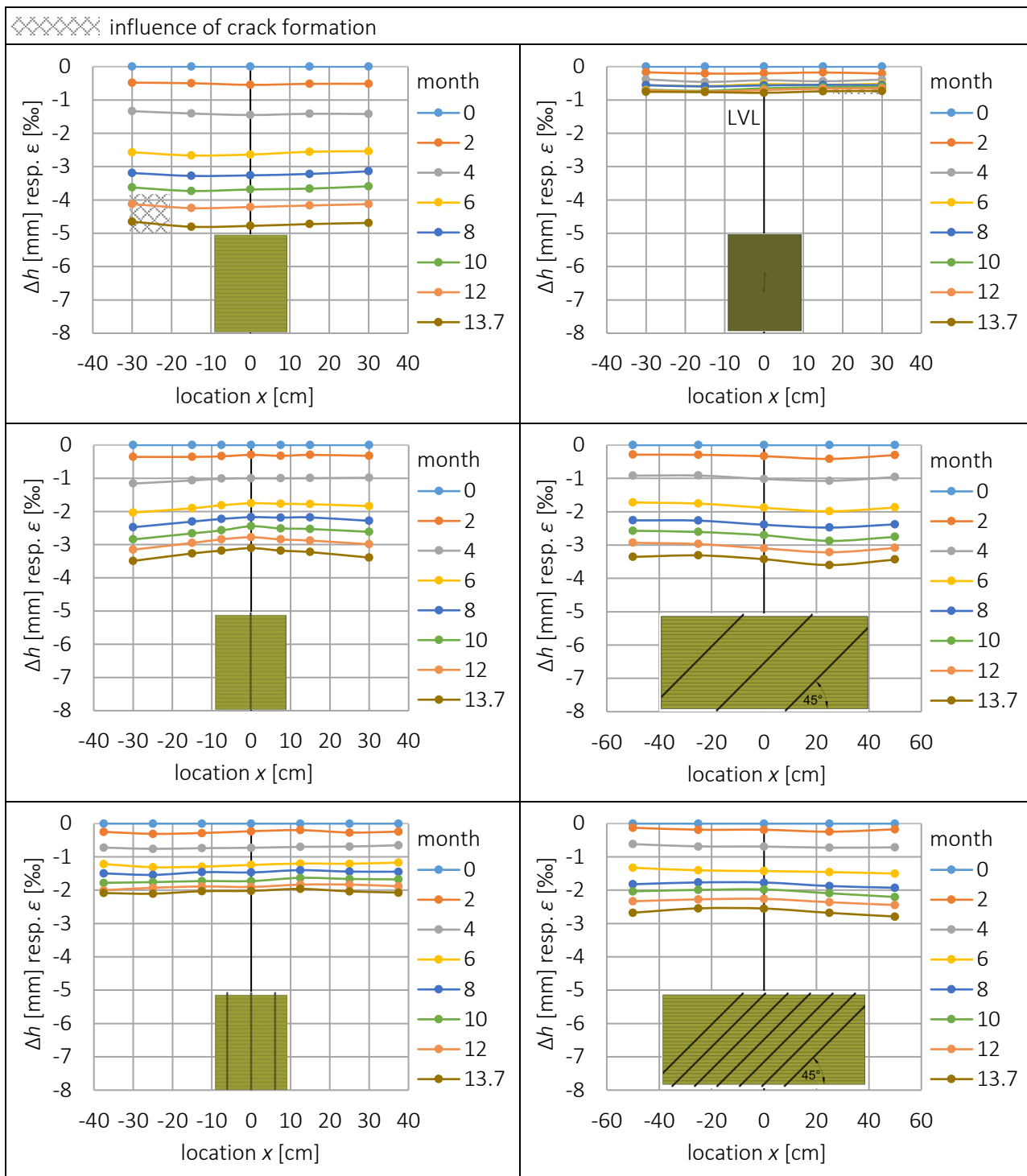


Figure 9: Measured shrinking deformations on specimens of manufacturer A

2.2.4 Load carrying capacities after climate storage

In Figure 10 and Figure 11 the load-carrying capacities of the destructive tests after climate storage are illustrated for the beams with holes and notches, respectively. In both cases load-carrying capacities are stated as shear stresses related to the respective net cross-sections (holes: $V/A_{net} = V/[b \cdot (h-h_d)]$; notches: $V/A_{net} = V/(b \cdot h_{ef})$). Regarding the differing restraining effect in dependence of the respective initial wood moisture contents the evaluation was carried out separately (A, B) as well as across manufacturers (A+B). Test results in detail can be found in Danzer et al. (2019).

- Beams with holes

All specimens with the exception of one failed first on the side, which was reinforced during climate storage. As a result, the restraining effect - with the exception of the inclined arrangement on test specimens from manufacturer A - led to a significant reduction in the load-carrying capacity.

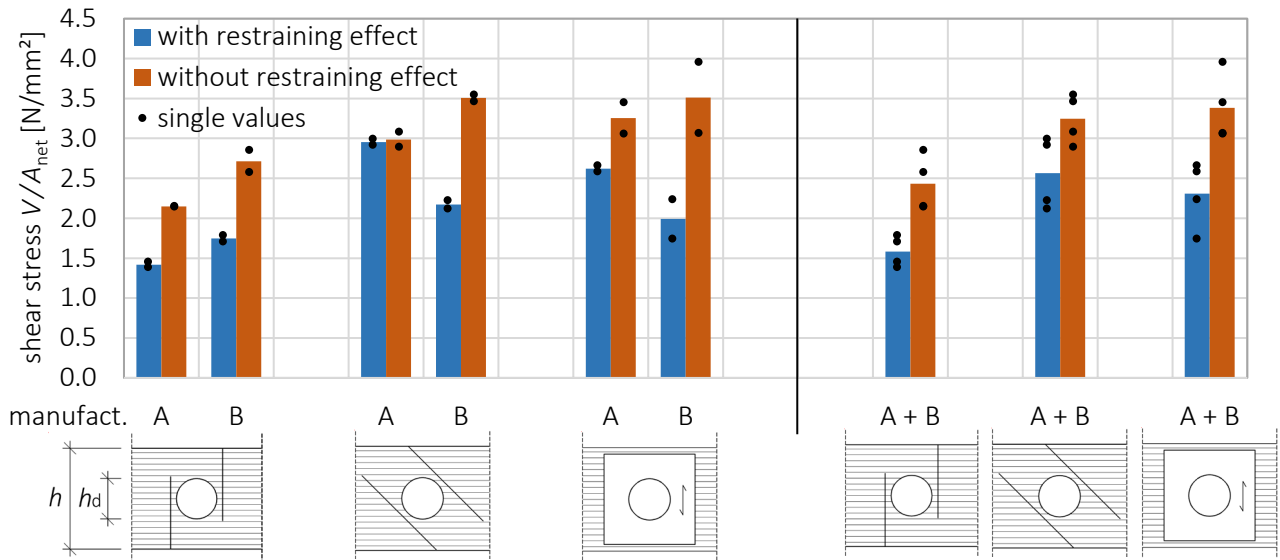


Figure 10: Load-carrying capacities of beams with holes, $A_{net} = b \cdot (h - h_d)$

On basis of the separate evaluation, the ratios "with/without restraining effect" show that the reduction of the load-carrying capacity on test specimens from manufacturer B is consistently higher in relative terms. This indicates that the higher differential moisture content compared to test specimens from manufacturer A has led to higher drying-induced stresses perpendicular to the grain and consequently has reduced the load-carrying capacity in shear more significantly.

From the results of the evaluation across manufacturers, the data set "without restraining effect" indicates a descending load-carrying capacity in the order of the configurations external reinforcement, internal reinforcement $\alpha = 45^\circ$, internal reinforcement $\alpha = 90^\circ$. The load-carrying capacity due to the restraining effect of the reinforcement was reduced to 65% with internal reinforcement at $\alpha = 90^\circ$, to 68% with external reinforcement and to 79% with internal reinforcement at $\alpha = 45^\circ$. In relative as well as absolute terms, the inclined arrangement provides the highest load-carrying capacities for the case "with restraining effect", whereby the differences are small compared to the external reinforcement, but large compared to the internal reinforcement under $\alpha = 90^\circ$.

Tests were carried out exclusively on beams with reinforced holes. The load-carrying capacity of comparable holes in the unreinforced state could therefore only be estimated in a theoretical way. A comparison of test results to such estimated load-carrying capacities of unreinforced holes showed that the reinforcing effect was neutralized to a large extent in the case of an internal reinforcement arranged perpendicular to the grain, for detailed information see Danzer et al. (2019).

- Beams with notches

All specimens with the exception of two failed first on the side, which was reinforced during climate storage. Similar to the specimens with holes, the existing restraining effect, with the exception of the inclined arrangement on test specimens from manufacturer B, resulted in a mostly significant reduction in load-carrying capacity.

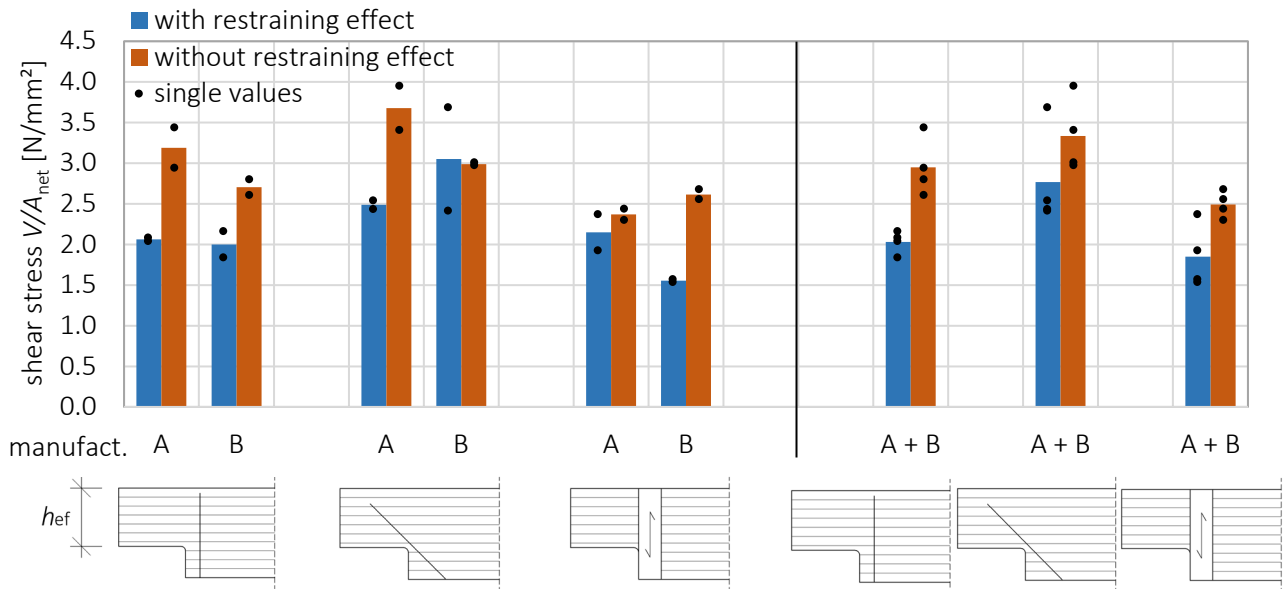


Figure 11: Load-carrying capacities of beams with notches, $A_{net} = b \cdot h_{ef}$

Based on the results of the evaluation across manufacturers, in the data set "without restraining effect" a descending load-carrying capacity can be identified in the order of the configurations internal $\alpha = 45^\circ$, internal $\alpha = 90^\circ$, external. Taking into account the restraining effect, the internal, inclined configuration again provided the highest load-carrying capacity. As a result of the restraining effect, the load-carrying capacities were reduced to 69% for internal reinforcement at an inclination $\alpha = 90^\circ$, to 74% for external reinforcement and to 83% for internal reinforcement at an inclination $\alpha = 45^\circ$. Overall, similar correlations can be observed in comparison to beams with holes, however, the reductions in relative terms are somewhat smaller. This could be related to the lower member height and the associated lower restraining effect.

In analogy to beams with holes, no tests were carried out on beams with unreinforced notches. Therefore, the load-carrying capacity was estimated based on the design format in DIN EN 1995-1-1:2010 without considering a reduced cross-sectional width due to possible shrinkage cracks (coefficient k_{cr}). A comparison of this estimated load-carrying capacity with the test results shows that – despite the restraining effect – for notches a considerable reinforcing effect is apparent compared to the unreinforced state. On the one hand this is due to the fact that for notches generally higher reinforcing effects can be achieved compared to holes. On the other hand, the lower beam height leads to a less reduction of the load-carrying capacity in relative terms due to the restraining effect.

3 Numerical investigations

3.1 Numerical model

In addition to the experimental investigations, numerical investigations were carried out on the three groups of glulam members to determine critical differential moisture contents for an onset of cracking. The investigations were based on three-dimensional simulation models within the FEM-program ANSYS, considering the lamella structure of glulam as well as the polar orthotropy of the wood structure with a distinction between longitudinal, radial and tangential directions. The material behaviour was assumed to be linear elastic, the material properties of wood were adopted from Neuhaus (1981) as follows:

$$\begin{array}{lll}
 E_L = 12000 \text{ N/mm}^2 & E_R = 820 \text{ N/mm}^2 & E_T = 420 \text{ N/mm}^2 \\
 G_{LR} = 625 \text{ N/mm}^2 & G_{LT} = 745 \text{ N/mm}^2 & G_{RT} = 42 \text{ N/mm}^2 \\
 \nu_{LR} = 0.055 & \nu_{LT} = 0.035 & \nu_{RT} = 0.311
 \end{array}$$

For simulating the reaction of wood regarding changes in wood moisture content the hygroexpansion coefficients $\alpha_L = 0.01 \text{ \%/\%}$, $\alpha_R = 0.16 \text{ \%/\%}$, $\alpha_T = 0.32 \text{ \%/\%}$ were used. To account for relaxation effects during the restrained shrinkage the listed values have been halved.

With respect to external reinforcing elements the material properties of the glued-on LVL panels were adopted from the technical approval Z-9.1-847. The bond between LVL panel and glulam member was not modelled explicitly but in a simplified way by full constraint. Internal reinforcing elements like fully-threaded screws and threaded rods were modelled as cylindrical steel bars with a linear elastic, isotropic material behavior ($E = 210000 \text{ N/mm}^2$, $\nu = 0.3$). Stiffness parameters for the withdrawal stiffness were adopted from the technical approval ETA-12/0062 in case of the fully-threaded screws and derived from test results obtained by Blaß & Krüger (2010), Stamatopoulos & Malo (2016) and Graule (2018) in case of drilled-in threaded rods. The bond between internal reinforcement and glulam was modelled by a tubular bond layer. For glued-in situations a linear elastic, isotropic material behavior ($E = 3000 \text{ N/mm}^2$, $\nu = 0.4$) was used, for drilled-in situations the withdrawal stiffness was converted in elastic stiffness parameters, so that the bond layer represented the compliance of the withdrawal behaviour.

Based on the analogy between the physical phenomena diffusion and heat transfer a change in wood moisture content was implemented in the form of a change in temperature, the hygroexpansion coefficients were assigned to the thermal expansion coefficients. Figure 12 illustrates the simplified assumptions regarding the modelling of a change in moisture for different sections in a member. In order to represent a drying scenario realistically, the change in moisture was applied as a combined quantity. It consists of a constant component across the cross-sectional width Δu_{const} and a variable component Δu_{width} , which was approximated in the form of a quadratic parabola, see Figure 12.

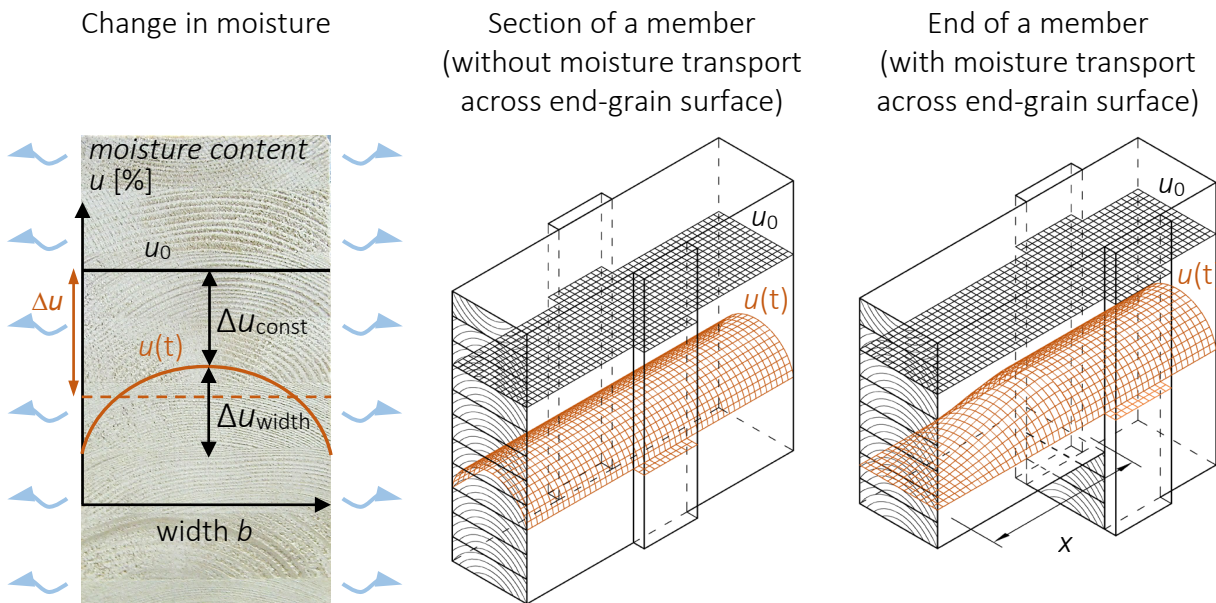


Figure 12: Simplified assumptions regarding the modelling of a change in moisture

This combined character led to the consequence that several calculations were required, which afterwards had to be interpolated. If the variable component Δu_{width} is fixed and the constant component Δu_{const} is varied, the linear scalability, which would affect both components, is no longer given. Following the results due to the climatic scenario of the experimental investigations in section 2.2.1 the variable component Δu_{width} was continuously set to 3% for the parameter study. The constant part Δu_{const} was varied until the tensile strength perpendicular to the grain was reached.

The determination of critical differential moisture contents was based on an integrative, probability-based evaluation of all elements stressed in tension perpendicular to the grain on the basis of the theory of Weibull (1939). The assumed strength in tension perpendicular to the grain regarding the reference volume $V_0 = 0.01 \text{ m}^3$ was $f_{t,90,\text{mean}} = 0.90 \text{ N/mm}^2$, see Danzer et al. (2019) for a detailed explanation.

All test configurations with apparent cracks on both specimens of a manufacturer were modelled and the numerical results compared to test results. This comparison showed sufficient agreement, see Danzer et al. (2019).

3.2 Parameter study

In Figure 13 critical differential moisture contents are illustrated exemplarily for a homogeneous arrangement of the reinforcement in sections of glulam members with a reference length of 2250 mm. The stated results represent an averaged constant value of the variable distribution across the cross-sectional width, see Figure 12.

The parameter study showed that the onset of cracking is influenced in particular by the quantity of reinforcement, the inclination of reinforcement to grain direction, the member height and the withdrawal stiffness of the reinforcement. All four influencing factors have a negative effect on the formation of cracks with increasing magnitude. With regard to the inclination, it can be concluded that the difference in results seems to increase with increasing quantity and stiffness of the reinforcement. In case

of drilled-in reinforcing elements the critical difference in moisture content of an inclined arrangement was up to 20 %- 25 % higher than with a comparable arrangement at $\alpha=90^\circ$, in case of glued-in reinforcing elements up to 35 %. On beams with holes and notches, the difference between an arrangement at $\alpha=90^\circ$ and $\alpha=45^\circ$ was even more pronounced compared to the homogeneous arrangement.

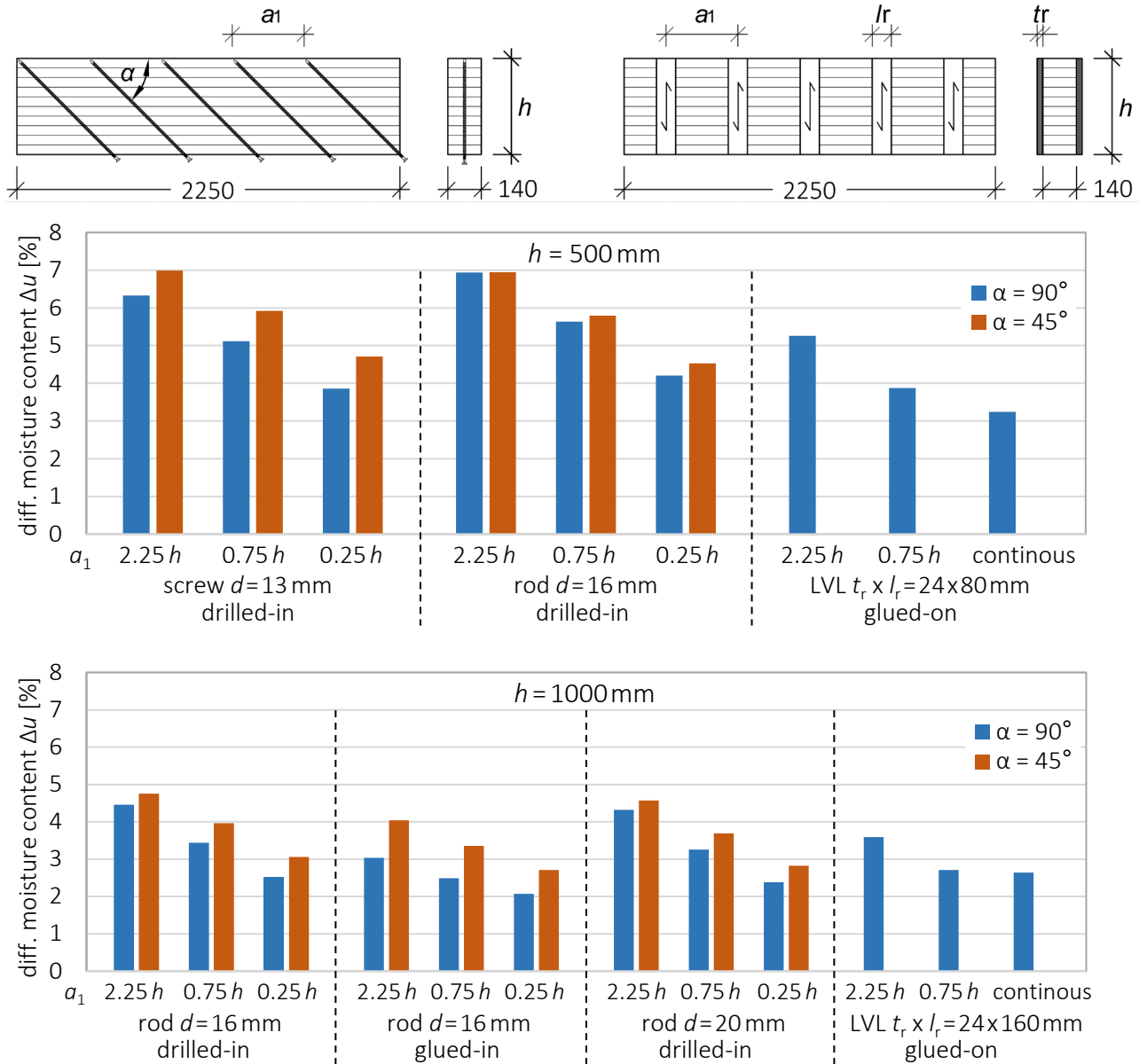


Figure 13: Results for homogeneous arrangement of reinforcement

In addition, the general influence of the member height was investigated using the configuration of a glued-in threaded rod $d=16$ mm according to Figure 14.

It can be seen that a change in member height has a significant effect on the critical differential moisture content especially at small heights. With increasing member height this influence decreases. This behavior can be explained by the distribution of tensile stresses perpendicular to the grain. Starting from the upper and lower edges of the member, the tensile stresses increase over a height marked h_1 , see Figure 14. Beyond this height, however, the tensile stresses in the intermediate member regions hardly change at all, even with increasing member height. This means that the

decrease of the differential moisture content at larger member heights in particular is related to the volume effect of the Weibull theory. For smaller member heights, in addition, the lower level of the tensile stresses leads to a more pronounced effect.

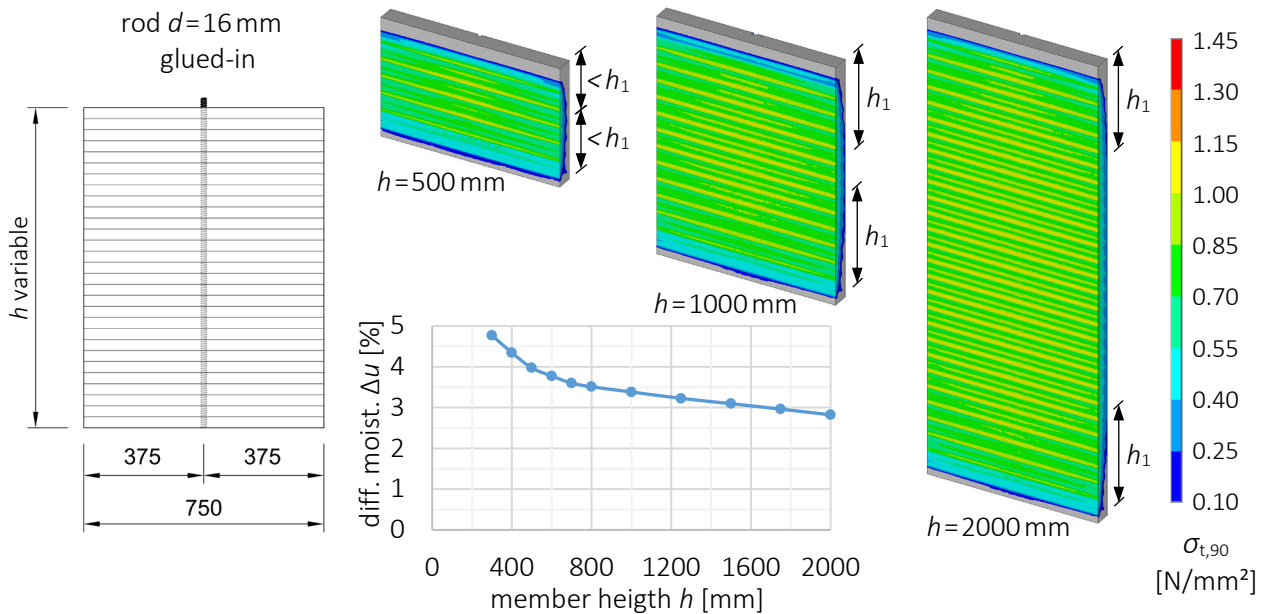


Figure 14: Configuration and results with varying member height (one half of the FE-model)

4 Conclusion

The objective of the research project was to investigate whether and to what extent reinforcing elements have a negative impact on the structural behaviour of glulam members due to their potential of restraining the free shrinkage behaviour of wood. In experimental investigations specimens of three groups of reinforced glulam members (homogeneous arrangements, holes, notches) were first exposed to a slow drying process over a period of 410 days. Cracks developed at differential wood moisture contents $\Delta u \approx 3\% - 5.5\%$. An inclined arrangement proved to be consistently more favourable with regard to the restraining effect than comparable arrangements perpendicular (i.e. 90°) to the grain. This conclusion was confirmed by a comparison of the measured shrinkage deformations. In destructive tests after climate storage on reinforced members with holes and notches it was found that load-carrying capacities decreased to around $65\% - 83\%$ due to the restraining effect of the reinforcement compared to specimens reinforced after climate storage. In all cases, inclined, internal arrangements resulted in the least reduction of load-carrying capacities. In absolute terms, an inclined arrangement of internal reinforcement, compared to an arrangement perpendicular to the grain, also resulted in higher load-carrying capacities of beams with holes or notches due to the simultaneous reinforcing effect with regard to tension perpendicular to the grain and shear.

The experimental results were confirmed by numerical investigations, showing that the onset of cracking is influenced in particular by the quantity of reinforcing ele-

ments, their inclination to grain direction, the member height and the axial withdrawal stiffness of the reinforcement. All four influencing factors have a negative effect on the formation of cracks with increasing magnitude.

5 References

- Blaß, H.J., Krüger, O. (2010): Schubverstärkung von Holz mit Holzschrauben und Gewindestangen. (Forschungsbericht). Karlsruher Berichte zum Ingenieurholzbau 15. KIT Lehrstuhl für Ingenieurholzbau und Baukonstruktionen, Universität Karlsruhe.
- Danzer, M., Dietsch, P., Winter, S. (2019): Verhalten verstärkter Brettschichtholzbauteile unter Schwindbeanspruchung. (Forschungsbericht). Lehrstuhl für Holzbau & Baukonstruktion, TU München.
- Dietsch, P., Gamper, A., Merk, M., Winter, S. (2015): Monitoring building climate and timber moisture gradient in large-span timber structures. *Journal of Civil Structural Health Monitoring*, Vol. 5, 153-165.
- Dietsch, P. (2017): Effect of reinforcement on shrinkage stresses in timber members. *Construction and Building Materials*, Vol. 150, 903-915.
- Ehlbeck, J., Belchior-Gaspard, P., Gerold, M. (1992): Eingeleitete Gewindestangen unter Axialbelastung bei Übertragung von großen Kräften und bei Aufnahme von Quersugkräften in Biegeträgern – Teil 2: Einfluß von Klimaeinwirkung und Langzeitbelastung. (Forschungsbericht). Versuchsanstalt für Stahl, Holz und Steine, Universität Karlsruhe.
- ETA-12/0062 (18.06.2012): SFS selbstbohrende Schrauben WR. SFS intec AG. Österreichisches Institut für Bautechnik, Wien.
- Graule, A. (2018): Axiale Verbundsteifigkeit eingedrehter Gewindestangen. (Masterarbeit). Lehrstuhl für Holzbau & Baukonstruktion, TU München.
- Möhler, K., Steck, G. (1977): Rissbildung in Brettschichträgern durch Trocknung oder durch Trocknung nach vorheriger Feuchtigkeitszunahme. (Forschungsbericht). Versuchsanstalt für Stahl, Holz und Steine, Universität Karlsruhe (TH).
- Neuhaus, H. (1981): Elastizitätszahlen von Fichtenholz in Abhängigkeit von der Holzfeuchtigkeit. (Dissertation). In: Technisch-wissenschaftliche Mitteilungen, Mitteilung Nr. 81-8. Institut für konstruktiven Ingenieurbau, Ruhr-Universität Bochum.
- Pommer, M. (2019): Vergleich verschiedener Holzfeuchtemessverfahren. (Seminararbeit). Lehrstuhl für Holzbau & Baukonstruktion, TU München.
- Stamatopoulos, H., Malo, K.A. (2016): Withdrawal stiffness of threaded rods embedded in timber elements. *Construction and Building Materials*, Vol. 116, 263-272.
- Wallner B. (2012): Versuchstechnische Evaluierung feuchteinduzierter Kräfte in Brettschichtholz verursacht durch das Einbringen von Schraubstangen. (Masterarbeit). Institut für Holzbau und Holztechnologie, TU Graz.
- Weibull, W. (1939): A statistical theory of the strength of materials. *Proceedings of the Royal Swedish Institute of Engineering*, No. 151. Stockholm.
- Z-9.1-847 (07.05.2014): Furnierschichtholz "Kerto-S" und "Kerto-Q" nach EN 14374. Metsä Wood, Building & Industry. DIBt, Berlin.

Discussion

The paper was presented by M Danzer

E Serrano asked about the reverse finding for inclined reinforcement cases of A and B. M Danzer responded that the differential moisture content was not as high for A compared to B and large scatter was found in the results.

R Jockwer commented that use of external reinforcement per Eurocode 5 can slow down moisture diffusion. He asked would you recommend using external reinforcement. M Danzer said that the results would be the same if the time for test were longer. So it would only be a question of time. Moisture transfer speed may be higher in direction of the grain which may be the case if the ends were not sealed. In the end it would be a question of the stiffness of the reinforcement. P Dietsch added the tests were conducted in a slow drying process. In practice more rapid drying condition might exist where external reinforcement might be valuable. S Winter agreed with P Dietsch and stated if we were able to quantify damping effect (relaxation) then external reinforcement would be beneficial.

T Ehrhart stated why would we take it for granted that we have large differential moisture content. Timber should be dried to proper moisture content appropriate to its end use. M Danzer agreed in general if the end use condition was known. P Dietsch agreed that this point is covered in the standard and cost of drying may be a hindering issue. Drying the timber to within 3% moisture content of the expected end use conditions would avoid the problem. S Winter stated that the standard is an idealized situation. The industry practice during construction, scheduled maintenance of say swimming pools and conditions of long term use of structure would need to be considered as well.

S Aicher stated that the influence of the use of LVL as external reinforcement might be over interpreted. He asked whether the LVL used had any cross bands. Without cross bands the LVL might have been too stiff and could affect the results. P Dietsch confirmed that the LVL had cross bands. S Aicher stated he would refrain from penalizing the external reinforcement technique as based on his experience damping of the drying procedure and relaxation appearing with external reinforcement would be a better way to avoid formation of cracks.

T Ehrhart added that the industry would not know the end use condition of the beams as it should be the responsibility of the engineer to specify the right moisture condition for the beam end use condition. R Brandner questioned the sampling procedure as only two producers were considered. M Danzer responded that the number of specimen was a question of available space and testing resources, the observed scatter in the data of the specimen was already high and agreed that a larger number of specimens would be better.

Fracture Mechanics Based Design of CLT-plates – Notches at Supports and Half-and-Half Joints

Erik Serrano, Division of Structural Mechanics, Lund University

Henrik Danielsson, Division of Structural Mechanics, Lund University

Keywords: Cross laminated timber, CLT, notch, FE-analysis, fracture mechanics

1 Introduction

1.1 Background and aim

Geometric discontinuities such as notches should, if possible, be avoided since they introduce high stress (strain) gradients and reduce considerably the load bearing capacity of the members (see *e.g.* Gustafsson, 1988). Nevertheless, notches are frequently used as a means to create simple joints between CLT-plates: half-and-half joints as seen in Figure 1a. Such joints are typically situated along the main direction of the CLT-plate, and are assumed to transfer zero or only limited amount of shear force. In reality, however, shear forces will be transferred by such joints, and possibly also bending moments. Another situation is shown in Figure 1b: a notched support.

For half-and-half joints in a 5-layer CLT-plate (Figure 1a), crack initiation and propagation in the mid layer would take place due to a combination of tension perpendicular to the grain and *rolling* shear. For 3- and 7-layer plates the crack propagation would take place due to a combination of tension perpendicular to the grain and *longitudinal* shear.

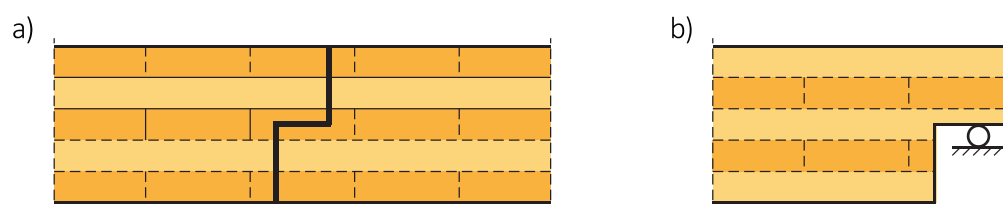


Figure 1: a) A half-and-half joint for CLT-plates, b) A CLT-plate with a notch at the support.

The aim of the present work is to further develop the knowledge about notched CLT-plates and support the development of reliable and rational design approaches. The paper presents numerical results to complement previous findings (Serrano, 2018; Serrano *et al.*, 2019; Nairn, 2020) and also presents new test results, including notch orientations relevant for half-and-half joints for 5-layer plates.

1.2 Previous work

The mechanical behaviour of notched CLT-plates has been studied experimentally in Friberg (2017), and those results were further discussed and analysed in Serrano (2018) and Serrano *et al.* (2019), where different modelling approaches based on fracture mechanics were evaluated. In the work of Nairn (2020), further developments were presented, including taking into account the influence of residual stresses (*e.g.* due to moisture changes) and the effect of crack closure/contact. In these previously published works the same conclusion has been drawn: a design approach based on beam theory such as the one proposed in Gustafsson (1988) is indeed both relevant and convenient and such an approach can be calibrated to reasonable accuracy towards experimental results.

2 Materials and methods

2.1 Testing material and specimen preparation

CLT plates with a 5-layer uniform layup were used. The layers were 20 mm thick and thus the plate thickness was 100 mm. All laminations were 150 mm wide. The material was provided by a Swedish manufacturer, and originated from cut-outs for door openings. Consequently, the plates delivered to the laboratory were approximately 2 m long and 1 m wide, with the outer layers being oriented in the longer of these directions. The laminations were of quality C24 and were not structurally edge glued. The CLT was produced using a polyurethane adhesive for the face gluing.

Prismatic beam-like specimens with a square cross section of 100×100 mm² were cut from the CLT plates. Beams were cut in two directions relative to the surface layer laminations: both along and across. Thus, the resulting beams had the outer laminations oriented either along the beam axis (denoted type 0°) or oriented in the beam width direction (denoted type 90°). The cutting of the beams from the plate was done centrally with regards to the width direction of the longitudinal laminations. Thus, in the beam specimens, only one lamination was present in each longitudinal layer. Each beam was cut to 800 mm length and at each end a rectangular notch was cut. Directly after testing the specimens, the moisture content (MC) in the vicinity of the notch was measured using an electric moisture meter (model “606-2”, by *testo SE & Co. KGaA*). The average MC for all specimens was 10.1%, with a standard deviation of 0.6%.

2.2 Test method

The test set-up of the three-point bending tests, the geometry of the specimens and the two different orientations investigated are depicted in Figure 2. In total eight different notch geometries were tested, four each for the type 90° (series A-D) and 0° (series E-H), cf. Figure 2.

Testing was performed in a MTS 810 servo-hydraulic testing machine under displacement control, where the cross-head speed was varied between 2-5 mm/min for the various tests, including first tests where the speed was adjusted. Most of the tests were performed using a load speed of 2 or 3 mm/min and maximum load was typically reached within 3 minutes. The load was monitored via a 100 kN load cell and displacement was measured with the built-in LVDT of the piston. Load and displacement were logged at a frequency of 5 Hz.

Steel plates of size 50×100 mm² were placed at the supports and at the loading point to reduce indentation.

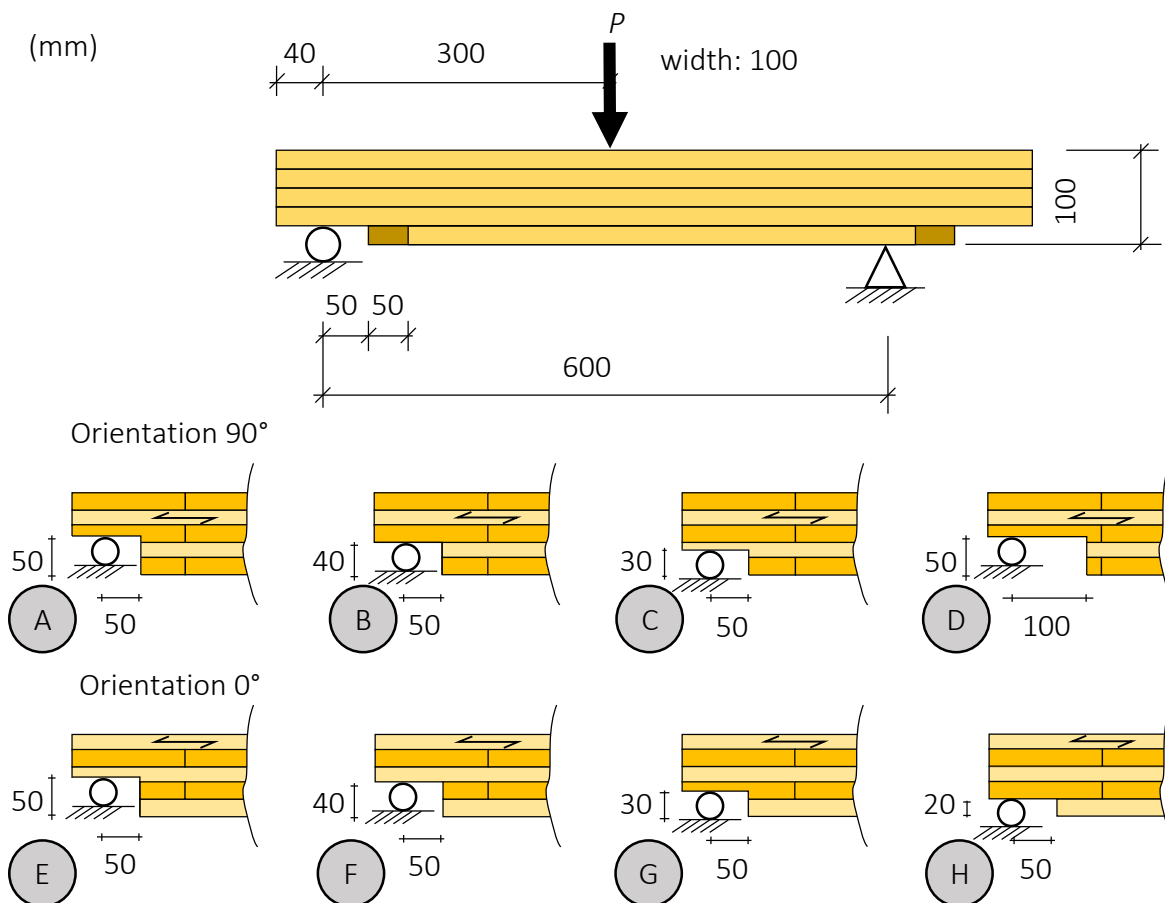


Figure 2. Test-setup used, CLT-orientations and notch geometries for the different test series A-H.

2.3 Calculation models

Three different calculation models were used to model the tests performed: a) analytical beam theory similar to the approach of EC5 (Eurocode 5, 2004), b) FE-based structural element approach, c) 2D-continuum finite element approach. All these approaches are based on linear elastic fracture mechanics using the compliance method (Serrano & Gustafsson, 2006). Within that framework, a general expression for the failure load (shear force) is:

$$V_f = \sqrt{\frac{2bG_c}{\partial C / \partial(\beta h)}} \quad (1)$$

with G_c being the critical energy release rate at crack propagation and with b being the width of the beam. The term $\partial C / \partial(\beta h)$ denotes the derivative of the compliance, C , of the structure with respect to the crack length, βh , see Figure 3.

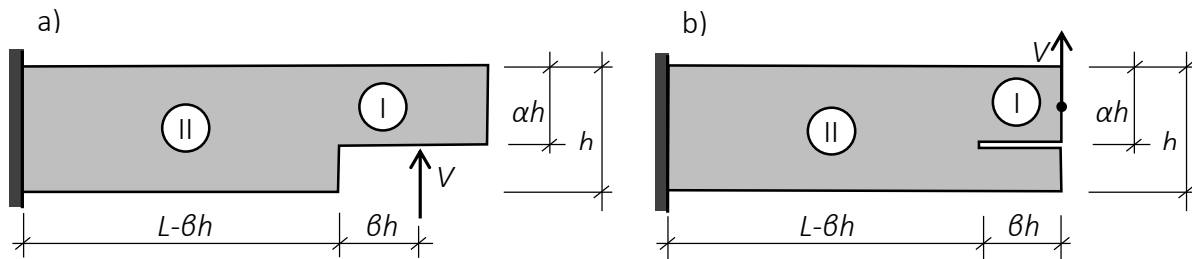


Figure 3. a) Notched beam with notation defining geometry. b) Equivalent slit cut beam.

The material parameters used were for consistency chosen to be the same as those used in Serrano *et al.* (2019), and thus no calibration of the models in relation to the test results was done. The values adopted are presented in Table 1.

Table 1. Material properties assumed in the analyses.

Parameters	Values	Description
$E_0 ; E_{90}$	12 000 ; 500	MOE along grain; perp. grain [MPa]
$G_{0,90} ; G_{90,90}$	600 ; 75	Shear modulus, longitudinal; rolling shear [MPa]
$\nu_{0,90} ; \nu_{90,90}$	0.3 ; 0.3	Poisson's ratios [-]
G_c	400	Critical energy release rate (Mode I) [J/m ²]

2.3.1 Analytical beam theory approach

The beam theory method used in Serrano *et al.* (2019) was adopted also in this study. It is based on the so-called Gustafsson approach (Gustafsson, 1988), which was developed based on Timoshenko beam theory for homogeneous beams, see Figure 3. The method uses the concept of linear elastic fracture mechanics and the compliance method, thus making use of Eq. (1).

In its current implementation, the shear stiffness of the cross sections was also calculated using Timoshenko beam theory, however accounting for the layered structure of the CLT. Although the beam theory approach is denoted analytical, it should be

emphasised that the cross section shear stiffness in general cannot be calculated using closed form expressions suitable for hand calculation. Here, the algorithm given in Wallner *et al.* (2013) was adopted.

The expression for the failure load, expressed as shear force, V_f , is given by:

$$V_f = \frac{\sqrt{2bG_c}}{\sqrt{1/(KGA)_I - 1/(KGA)_{II} + \beta h \sqrt{1/(EI)_I - 1/(EI)_{II}}}} \quad (2)$$

where b is the beam width, G_c is the critical fracture energy during crack propagation, $(KGA)_i$ and $(EI)_i$ denote the shear stiffness and the bending stiffness of the notched and full cross sections (Timoshenko beam theory), respectively, cf. also Figure 3.

The expression in Eq. (2) is based on the assumption of a compliant connection (a rotational spring) with stiffness denoted k_θ between parts I and II. A convenient choice of that stiffness is made according to (Gustafsson, 1988):

$$k_\theta = 1 / \sqrt{(1/(KGA)_I - 1/(KGA)_{II})(1/(EI)_I - 1/(EI)_{II})} . \quad (3)$$

For a more detailed discussion on such choices, and the derivation of Eq. (2), see Serrano *et al.* (2019). In the following, the approach based on Eq. (2) and using the definition according to Eq. (3) is denoted “Analytical/EC5”.

If the rotational spring is assumed to be infinitely stiff, the expression for the failure load becomes:

$$V_f = \frac{\sqrt{2bG_c}}{\sqrt{1/(KGA)_I - 1/(KGA)_{II} + (\beta h)^2(1/(EI)_I - 1/(EI)_{II})}} \quad (4)^1$$

which is an expression that typically would give results on the unsafe side in relation to Eq. (3).

Using Eq. (4), the term (βh) can be adjusted such that an additional (fictitious) crack length is assumed. This would add compliance to the structure, compensating for the infinitely stiff rotational spring. In addition, such an adjustment could be used for calibration of the model. Thus,

$$V_f = \frac{\sqrt{2bG_c}}{\sqrt{1/(KGA)_I - 1/(KGA)_{II} + (\beta h + \Delta a)^2(1/(EI)_I - 1/(EI)_{II})}} \quad (5)$$

where the value of the additional crack length, Δa , could be used for calibration, see *e.g.* Serrano *et al.* (2019) and Danielsson & Gustafsson (2015).

¹ Corresponds to Eq (8) in Serrano *et al.* (2019), where the expression includes an error: the square of $(\beta h)^2$ is missing.

2.3.2 Structural element approach

The structural element approach was implemented as described in Serrano *et al.* (2019), thus including the use of Timoshenko beams for the two parts of the structure, with the possibility to include also a rotational spring connection, as depicted in Figure 4.

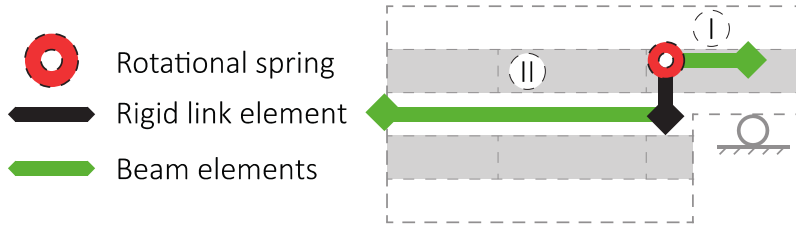


Figure 4. A beam model for analysis of notched CLT-plates.

It should be pointed out that this approach can be made identical to the above-mentioned analytical beam theory approach. The main reason for including the structural element approach is, however, that it is more general than the analytical beam theory approach. Parameter choices for *e.g.* the rotational spring stiffness, k_{θ} , and/or shear stiffness can be tested without the need for finding closed form solutions corresponding to Eq. (2) or Eq. (3). Also, it could be possible to use other higher order shear deformation beam theories, such as the so-called zig-zag theory in formulating the structural element stiffness matrices, see *e.g.* Tessler *et al.* (2009).

In this study, the structural element approach was implemented by using an infinitely stiff rotational spring and adjusting the crack length according to Eq. (5). The additional crack length was set to be equal to the notch depth, *i.e.* $\Delta a = (1 - \alpha)h$. In the following, the approach based on Eq. (5), in combination with this particular choice of Δa is denoted “Structural elements”

2.3.3 2D finite element approach based on LFM

The third modelling approach used in this paper is based on 2D, plane stress models, assuming linear elastic behaviour, and assuming pre-defined crack paths based on experimental evidence. Thus, it was assumed that cracking starts from the re-entrant corner of the notch and a) propagation takes place at 45° orientation in a transverse layer until reaching the longitudinal lamination above or/ followed by b) propagation along the grain in a longitudinal layer/at the interface of a longitudinal layer.

The FE-models had a fine mesh in the region of interest, *i.e.* in the zone at the notched end, and a coarser mesh in other parts. Typically, 25 000–35 000 first order plane stress elements were used, with an element size of 0.125 mm side length in the area with the dense mesh. An example of a FE-model used in the analyses is shown in Figure 5, showing also a detail of the notch corner ($\alpha = 0.5$) in the deformed state, for a crack length of 7 mm. For these analyses, the FE-code ABAQUS was used (Dassault, 2018).

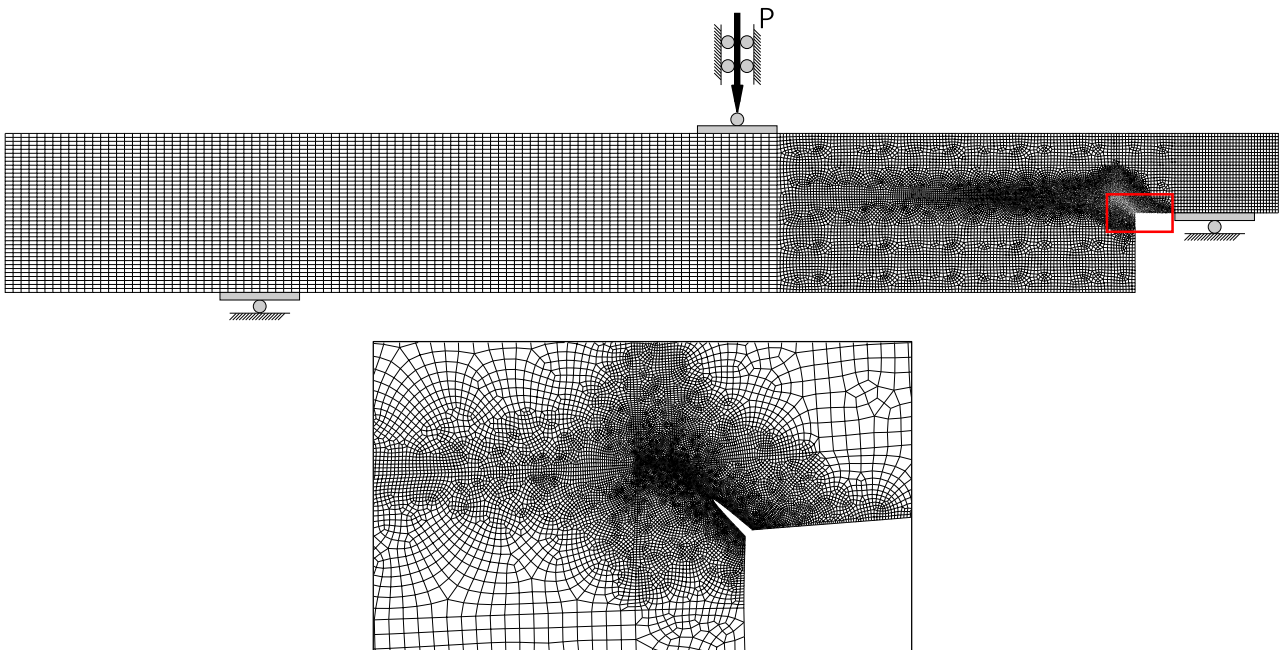


Figure 5. Example of FE-mesh and detail of the mesh at the corner of the notch (deformed state). In this example, $\alpha=0.5$ and the crack length is 7 mm. The plates at the support and loading points were modelled by applying kinematic constraints.

3 Results and discussion

3.1 Test results and general observations

Test series specifics and test results and are summarised in Table 2 and some examples of failed specimens are shown in Figures 6 and 7.

The original test plan included 8 nominally equal tests for test series A-H.

In test series C, only four notches were tested. Firstly, it turned out that failure was heavily influenced by rolling shear failure in the mid transverse layer and secondly, the crack propagation was sudden and extensive, with the crack propagating beyond the loading point. Thus, it was not possible to test the other ends of the specimens.

In test series E one notch test was excluded, since it was not possible to perform that test after extensive cracking had already taken place while testing the first end of the specimen.

It should be noted that the *full* cross section of the specimens would experience a maximum *rolling shear stress* of 0.12 and 0.23 MPa per kN of shear force, for the 0° and 90° specimens, respectively (according to beam theory and assuming the transverse MOE to be zero). Specimens in series C failed due to rolling shear, which would be expected since the mean failure load corresponds to $9.05 \times 0.23 \approx 2.1$ MPa. At the notched end, stress transfer is complex and compression perpendicular to the beam axis increases the shear capacity considerably.

Table 2. Shear force capacity from tests. N =number of tested notches, COV = coefficient of variation. α and β are defined in Figure 3.

Series	Lay-up	Orientation	α	β	N	$V_{f, mean}$ (kN)	COV	Specimens rejected due to
A	5×20	90°	0.5	0.5	8	3.20	0.133	
B	5×20	90°	0.6	0.5	8	3.31	0.108	
C	5×20	90°	0.7	0.5	4	9.05	0.178	Rolling shear, ext. cracking
D	5×20	90°	0.5	1.0	8	2.58	0.107	
E	5×20	0°	0.5	0.5	7	5.16	0.189	Extensive cracking
F	5×20	0°	0.6	0.5	8	11.3	0.094	
G	5×20	0°	0.7	0.5	8	10.6	0.169	
H	5×20	0°	0.8	0.5	8	10.0	0.244	

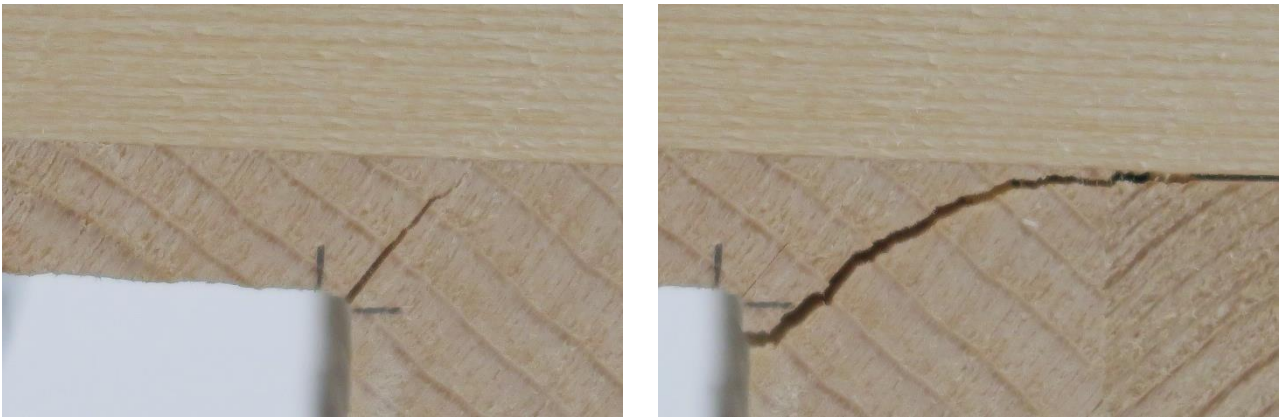


Figure 6. Example of cracking at notch corner for one of the specimens in series A. Left: Crack initiation and propagation. Right: Final crack pattern.

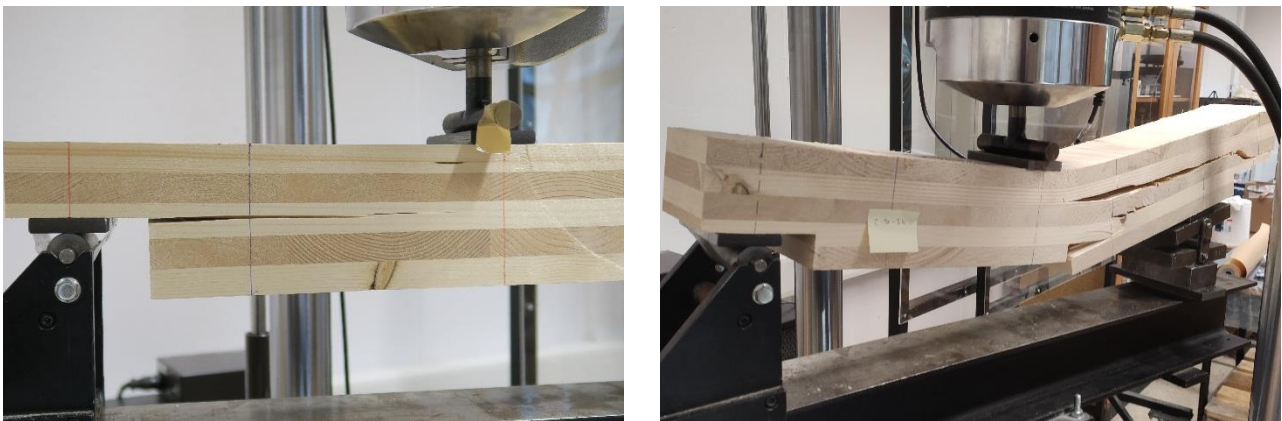


Figure 7. Left: Example of cracking at notch corner for a specimen in series E. Right: Example of specimen from series C only possible to test in one end. Due to the severe cracking when testing the first end, failure at the notch was not achieved when testing the second end.

3.2 Model results and general observations

The beam theory approach with the rotational stiffness determined according to Eq. (3), leads in some cases to unphysical results. The reason is that a complex value of the rotational spring stiffness can be obtained, as was observed already in Serrano *et al.* (2019).

As regards the structural element approach, the specific choices of $k_{\theta} = \infty$ and $\Delta a = (1 - \alpha)h$ adopted in the present study give the same results as the approach based on Eq. (5) would do.

The 2D-FE approach gives results in terms of crack propagation load as a function of crack length, see Figure 8. In determining the load bearing capacity it is thus essential to define also a load capacity criterion. Here, the load bearing capacity was determined by the local maximum of the load versus crack length response from the analyses. For cases C and E, where such a local maximum was not found, the load bearing capacity corresponding to a crack length of 12 mm was instead used. This choice of crack length is based on fracture mechanics considerations, as explained in Serrano *et al.* (2019).

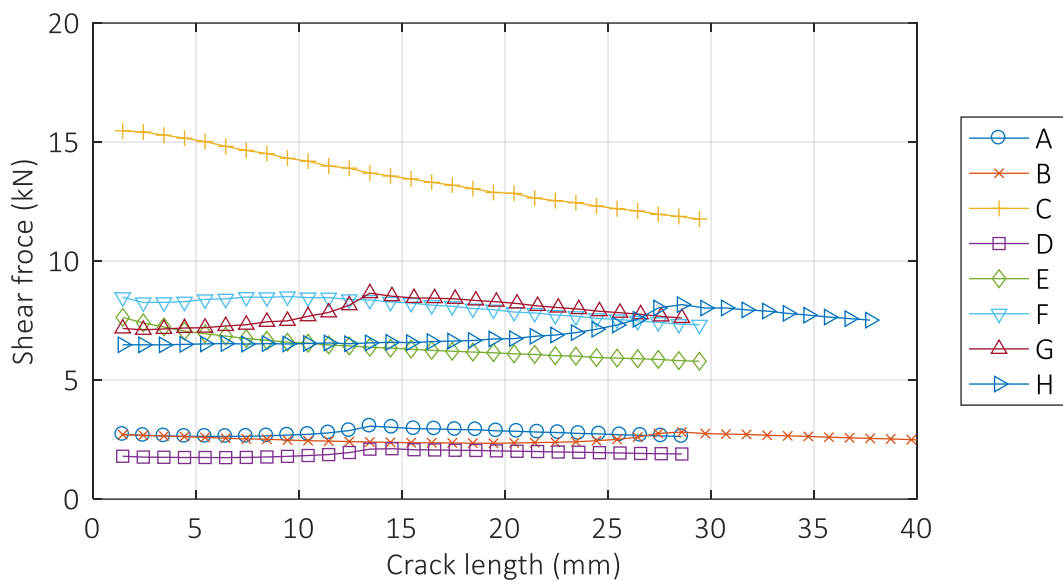


Figure 8. Shear force at crack propagation versus crack length as predicted by 2D-FEM analyses.

Applying the models described above, making use of the material parameters given in Table 1 the predictions shown in Table 3 were found.

Table 3. Shear force capacity, V_f , for different models. Results in boldface italics are the real part of the complex (and non-physical) result from the use of the analytical EC5-approach.

Series	Shear force capacity (kN)			Remark
	Analytical EC5	Structural elements	2D FEM	
A	<i>5.15</i>	3.51	3.06	
B	<i>5.30</i>	4.51	2.82	
C	9.27	10.8	13.9	2D-FEM: at 12 mm crack
D	<i>3.13</i>	2.29	2.11	
E	5.96	6.47	6.45	2D-FEM: at 12 mm crack
F	7.88	9.00	8.51	
G	8.06	9.50	8.65	
H	8.44	10.3	8.17	

3.3 Comparison of model predictions and recommendations for EC5

Apart from the above-mentioned results, also the tests reported in Friberg (2017) are used for comparison with the calculated predictions.

As regards the tests by Friberg (2017), similar tests as those reported here were performed. Thus, the test specimens were cut from 5-layer CLT plates in the shape of 100 mm wide beams which were tested in three-point bending. All specimens were cut with the same orientation: with the outer laminations along the length of the beam specimens. The CLT used was 160 mm thick, with a 40-20-40-20-40-layup and the material was C24, without structural edge bonding between the laminations. The results are summarised in Table 4.

Table 4. Shear force capacity from experiments reported in (Friberg, 2017).

Series	Notch depth (mm)	α	β	N	Shear force (kN)	COV
J	40	0.75	0.3125	6	15.0	0.11
K	60	0.625	0.3125	7	14.4	0.12
L	80	0.5	0.3125	6	8.9	0.15
M	100	0.375	0.3125	8	5.5	0.15
N	120	0.25	0.3125	8	5.3	0.12

Several adjustments (calibrations) of the analytical model and of the structural element model were tested, in order to find well-performing formulation based on Eqs. (2)-(5). A reasonable minimum requirement on such a formulation would be that it should give good fits to test results, without producing any complex solutions. Thus, at least for the layups/geometries examined until now, it seems that the structural elements approach ($k_{\theta} = \infty$ and $\Delta a = (1 - \alpha)h$, cf. Eq. (4)) is the best candidate among

the ones examined so far. A comparison of the different models' capabilities to predict the load bearing capacity is given in Figure 9, where the results (Tables 2-4) are normalised with respect to the results corresponding to test series H. It should again be emphasised that the EC5-approach gave non-physical results for series A, B and D, although when considering only the real part, the results look reasonable for series D. Also note that the tests in series C were very much influenced by rolling shear failure. Thus, the good predictions by the EC5-approach and the structural elements approach are coincidental, and the poor prediction of the 2D-FEM approach is of no concern, since the failure mode obtained in the tests is not included in any of the modelling approaches.

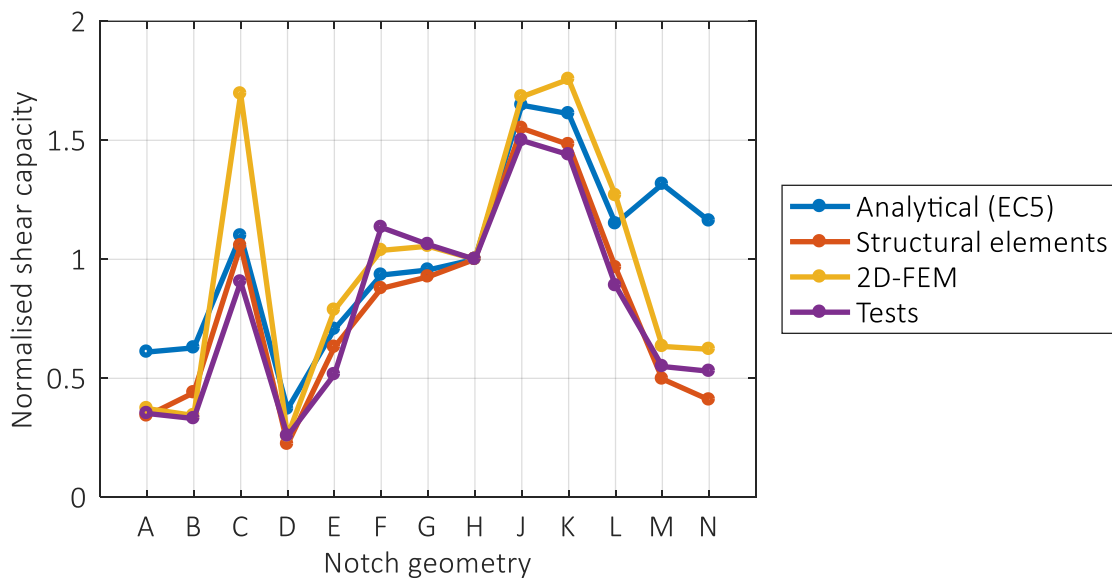


Figure 9. Comparison of predicted shear force capacity from different modelling approaches and experimental results. Notch geometries and CLT-layups A-N are defined in Tables 3 and 4. Each curve is normalised with respect to its value for series H.

It should be emphasised that for all the model implementations presented, material data has been chosen without any detailed calibration. Bearing in mind the relatively high variability in some of the test series, and bearing in mind the very limited amount of test data available, it is, however, of little use at this time, to fit the models by further fine tuning of material parameters.

4 Conclusions, relation to EC5 and outlook

4.1 General conclusions and relation to EC5

The following conclusions are drawn from the research presented in this paper:

- The prediction of shear force capacity of notched CLT plates can be done by use of a fracture mechanics approach.

- A direct and consistent application to CLT of the current EC5-approach for solid timber beams can give unphysical results in some cases. Such an approach is therefore not a candidate for inclusion in design codes.
- For codification, it is recommended to use an approach which handles the influence of compliance between the full cross section and the notched part in a simplified manner, *e.g.* by adding an additional length to the notch length βh .
- A reasonable approach for a design formula could be assuming $k_{\theta} = \infty$ and adjusting the notch length by an amount of $\Delta a = (1 - \alpha)h$, cf. Eq. (5).

4.2 Further work – Testing and modelling

As already pointed out, there is a severe lack of test data for notched CLT plates. Although the present work presents additional test data, the openly available database is much too limited to serve as a basis for codification. It is thus essential that additional test programmes are initiated.

Such test programmes should first and foremost focus on extending the test results data base with additional lay-ups, notch geometries and timber qualities. Another parameter that could be of interest to investigate is the possible influence of edge gluing on the load bearing capacity, in particular in combination with the influence of the width-to-thickness ratio of the laminations.

CLT is a complex product, being non-homogeneous in terms of traditional wood material features (*e.g.* knots and grain deviation), in terms of material orientations and in terms of structure (*e.g.* the position of an individual board in relation to the notch). Thus, as regards further modelling, it would be of interest to perform analyses with models including a higher degree of detailing such as annual ring orientation and non-edge glued boards. Such modelling could furthermore be used for parametric studies including stochastic approaches (Monte Carlo) to verify the influence of the CLT build-up on the variability of bearing capacity.

5 Acknowledgements

The support from Södra Building Systems, providing the test material used in this work, is hereby gratefully acknowledged.

This research has been supported by the Swedish Research Council FORMAS through grant 2019-01354, and by Vinnova, FORMAS and the Swedish Energy Agency under the umbrella of ERA-NET Cofund ForestValue (project *InnoCrossLam*). ForestValue has received funding from the EU Horizon 2020 research and innovation programme under grant agreement N° 773324. The financial support from these organisations is gratefully acknowledged.

6 References

- Danielsson, H. & Gustafsson, P. J. (2015): A beam theory fracture mechanics approach for strength analysis of beams with a hole. In: International Network on Timber Engineering Research – Proceedings Meeting 48, Paper INTER/48-19-1, Šibenik, Croatia.
- Dassault (2018): Dassault Systemes Simulia Corp. ABAQUS/CAE, Version 2019.
- Eurocode 5 (2004): EN 1995-1-1:2004, Eurocode 5: Design of timber structures – Part 1-1: General – Common rules and rules for buildings.
- Friberg, A. (2017): Bärförmåga för KL-trä med urtag – Provning och beräkningsmetoder (in Swedish). (Load-bearing capacity of CLT with notches – Testing and calculation methods). Bachelor thesis, Report THID-5526, Division of Structural Mechanics, Lund University.
- Gustafsson, P. J. (1988): A study of strength of notched beams. In: Proceedings CIB-W18 Meeting 21, Paper CIB-W18/21-10-1, Parksville, Canada.
- Nairn, J. A. (2006): On the calculation of energy release rates for cracked laminates with residual stresses, *International Journal of Fracture*, 139, 267–293.
- Serrano, E. (2018): Cross Laminated Timber Plates with Notches – Analyses based on fracture mechanics. In: *Timber – Bonds, Connections and Structures*. G. Dill-Langer (Ed.), ISBN 978-3-946789-01-7, MPA University of Stuttgart, Stuttgart.
- Serrano, E. & Gustafsson, P. J. (2006): Fracture mechanics in timber engineering – Strength analyses of components and joints. *Materials and Structures*, 40:87–96.
- Serrano, E., Gustafsson, P. J. and Danielsson, H. (2019): Prediction of load-bearing capacity of notched cross laminated timber plates. In: International Network on Timber Engineering Research – Proceedings Meeting 52, Paper INTER/52-12-2, Tacoma, USA.
- Tessler, A., Di Sciuva, M., Gherlone, M. (2009): Refined zigzag theory for laminated composite and sandwich plates. NASA/TP-2009-215561.
- Wallner-Novak, M., Koppelhuber, J. & Pock, K. (2013): *Brettsperrholz Bemessung – Grundlagen für Statik und Konstruktion nach Eurocode*. ProHolz Austria, Immenstadt, Austria.

Discussion

The paper was presented by E Serrano

P Dietsch and E Serrano discussed scaling of the test specimens in relation to the dimensions of the specimen that one can handle in the lab.

S Aicher stated that the material tested had unusual aspect ratio of the thickness to width of the laminae which could have suppressed rolling shear failures. Typical material would see more rolling shear failure. E Serrano stated that the material was obtained from Swedish industries. He stated that the Rolling shear failure load occurred at a level 3 times of that for the 90 degree orientation; hence, rolling shear failure should not happen in the typical cases. S Aicher said he agreed with the statement for the material tested.

G Hochreiner asked about the combined effect of tension perpendicular to grain and shear strains. E Serrano responded that in the past nonlinear fracture mechanics approach with combined mode were considered. This could handle the combined stress case.

G Hochreiner stated that there might be different effects at the mean and 5th percentile level. E Serrano said that this is an issue of variability as well as codification of the results which have not been investigated here.

P Dietsch quoted S Winter in that a proposal for Eurocode 5 consideration should be submitted by April 2021.

Prediction of Torsional Stress at In-plane Shear Loading of Cross Laminated Timber

Henrik Danielsson, Division of Structural Mechanics, Lund University, Sweden

Mario Jeleč, Department of Materials and Structures, University of Osijek, Croatia

Erik Serrano, Division of Structural Mechanics, Lund University, Sweden

Keywords: Cross laminated timber, CLT, in-plane shear, FM III, models, FE-analysis

1 Background and aim

In-plane shear loading is a basic mode of loading for cross laminated timber (CLT). For design, three shear failure modes (FM) are in general of interest:

- Shear failure mode I – Gross shear failure
- Shear failure mode II – Net shear failure
- Shear failure mode III – Shear failure by torsion over the crossing areas

For design with respect to shear FM III, there are several different models available for calculations of the design-relevant torsional stress. These models yield in many cases significantly differing results, see e.g. Danielsson & Serrano (2019) for a comparison of model predictions for CLT composed of three layers (CLT 3s) and five layers (CLT 5s).

The main aim of this paper is to extend the discussion from the previously mentioned study, to also include CLT composed of seven layers (CLT 7s). The focus is here on models for prediction of the torsional stress acting in the crossing areas between laminations of adjacent layers. Predictions according to proposed design models are compared to results of finite element (FE) analysis. The study presented concerns the influence of the element lay-up in terms of the thickness of the longitudinal and transversal layers, respectively.

In a wider perspective, the aim of this paper is to contribute to the development of consistent design approaches for CLT at *pure in-plane shear loading* and *in-plane beam loading* conditions, giving similar but not identical internal force distributions.

2 Analytical models for in-plane shear FM III

Four design models for prediction of torsional stress are included in the comparison. The models are here denoted Models A–D and are described in Sections 2.1–2.4. These are the same models as are included in the comparison for CLT 3s and 5s, as presented in Danielsson & Serrano (2019).

An element with symmetric lay-up in the thickness direction and loaded in pure shear, $v_{xy} = v_{yx}$ (N/m), according to Figure 2.1 is considered. The longitudinal and transversal layers are assumed to be composed of laminations of widths b_x and b_y , respectively. The element is assumed to have no edge-bonding, meaning that the narrow faces of the laminations are traction-free. The lay-up is defined by the longitudinal layer thicknesses $t_{x,k}$ and the transversal layer thicknesses $t_{y,k}$. The longitudinal and transversal net cross section thicknesses are hence given by $t_x = \sum t_{x,k}$ and $t_y = \sum t_{y,k}$, and the gross cross section thickness by $t_{CL} = t_x + t_y$.

For elements without edge-bonding, torsional moments and stresses appear in the crossing areas between laminations of adjacent layers, see Figure 2.1. The torsional moments are in the considered design models assumed to give a shear stress distribution corresponding to that of relative rigid body rotation over a shear compliant medium.

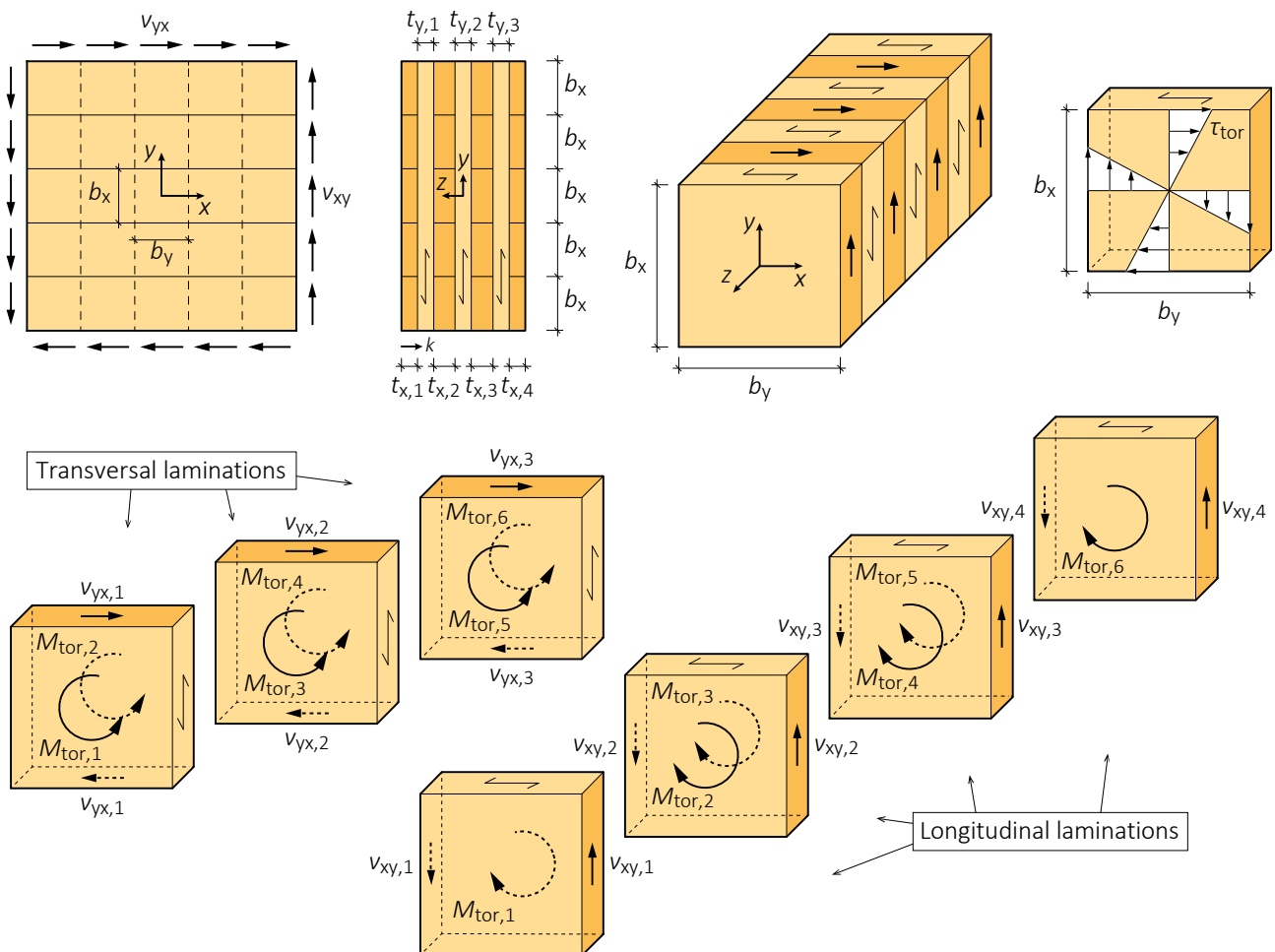


Figure 2.1. Definitions of geometry and load parameters.

The design-relevant maximum torsional stress is for the models presented below hence assumed according to

$$\tau_{\text{tor}} = \frac{M_{\text{tor}} b_{\text{max}}}{I_{P,CA} 2} \quad \text{where} \quad I_{P,CA} = \frac{b_x b_y}{12} (b_x^2 + b_y^2) \quad (1)$$

and where $b_{\text{max}} = \max(b_x, b_y)$. For $b_x = b_y = b$, Equation (1) can be simplified to

$$\tau_{\text{tor}} = \frac{3 M_{\text{tor}}}{b^3} \quad (2)$$

2.1 Model A

The maximum torsional stress is in the Representative Volume Sub-Element (RVSE) approach, as presented by Bogensperger et al. (2010), given by

$$\tau_{\text{tor}} = \frac{3 v_{xy} \max(t_j^*)}{b \sum t_j^*} \quad (3)$$

where $\max(t_j^*)$ represents the maximum RVSE thickness and $\sum t_j^*$ represents the sum of the RVSE thicknesses. The definition of the RVSE thicknesses t_j^* are given in Bogensperger et al. (2010), and are also found in Danielsson & Serrano (2019).

2.2 Model B

The maximum torsional stress can according to the Austrian CLT handbook by Wallner-Novak et al. (2013) be calculated as

$$\tau_{\text{tor}} = \frac{3 v_{xy}}{b} \frac{1}{n_{CA}} \quad (4)$$

where n_{CA} is the total number of crossing areas in the element width direction.

2.3 Model C

The maximum torsional stress should according to ÖNORM B 1995-1-1 /A:2018-11 (2018) be determined according to

$$\tau_{\text{tor}} = \frac{3 v_{xy}}{2 b} \frac{t_{\text{max}}}{\min(t_x, t_y)} \quad (5)$$

where t_{max} refers to the maximum individual layer thickness. Also in the draft version of design of cross laminated timber for a revised Eurocode 5 (CEN/TC 250/SC5, 2020), an approach according to Equation (5) is suggested.

2.4 Model D

Model D is based on equilibrium considerations and assumptions of distributions of the total shear flows, v_{xy} and v_{yx} (N/mm) to the shear flows in the respective layers, $v_{xy,k}$ and $v_{yx,k}$, see e.g. Danielsson & Serrano (2019) and Danielsson et al. (2019). The torsional moments $M_{\text{tor},k}$ are in this approach determined based on static equilibrium of parts of the individual longitudinal and transversal laminations, as illustrated in Figure 2.1.

The narrow faces of the laminations are assumed to be traction-free, meaning that at sections corresponding to gaps between adjacent laminations in the same layer, the

shear flow is carried by either the longitudinal layers only ($v_{xy} = \sum v_{xy,k}$) or by the transversal layers only ($v_{yx} = \sum v_{yx,k}$). At these sections, the shear flow in the individual laminations may be assumed according to

$$v_{xy,k} = \beta_{x,k} v_{xy} \quad (6)$$

$$v_{yx,k} = \beta_{y,k} v_{yx} \quad (7)$$

where the dimensionless weighting factors here are defined as $\beta_{x,k} = t_{x,k}/t_x$ and $\beta_{y,k} = t_{y,k}/t_y$, respectively. The force distribution between the respective layers is hence assumed according to the relative layer thicknesses, but other choices are also possible.

Considering rotational equilibrium about the z-axis for the individual parts of the longitudinal and transversal laminations, see Figure 2.1, the respective torsional moments may for symmetric element lay-ups be expressed as

$$M_{\text{tor},1} = M_{\text{tor},6} = v_{xy} b_x b_y \beta_{x,1} \quad (8)$$

$$M_{\text{tor},2} = M_{\text{tor},5} = v_{xy} b_x b_y (\beta_{y,1} - \beta_{x,1}) \quad (9)$$

$$M_{\text{tor},3} = M_{\text{tor},4} = v_{xy} b_x b_y \left(\frac{1}{2} - \beta_{y,1}\right) \quad (10)$$

which for the case of equal lamination widths, $b_x = b_y = b$, gives a maximum torsional stress according to

$$\tau_{\text{tor}} = \frac{3 v_{xy}}{b} B_{\text{max}} \quad \text{where } B_{\text{max}} = \max \left\{ \begin{matrix} \beta_{x,1} \\ \beta_{y,1} - \beta_{x,1} \\ \frac{1}{2} - \beta_{y,1} \end{matrix} \right\} = \max \left\{ \begin{matrix} \frac{t_{x,1}}{t_x} \\ \frac{t_{y,1}}{t_y} - \frac{t_{x,1}}{t_x} \\ \frac{1}{2} - \frac{t_{y,1}}{t_y} \end{matrix} \right\} \quad (11)$$

Further comments regarding CLT 3s and 5s are given in Danielsson & Serrano (2019).

3 Finite element model

Full 3D linear elastic FE-analyses were performed using the software Abaqus/CAE 2019 (2018). The same modelling approach and stiffness parameters were used for this study as for the study presented in Danielsson & Serrano (2019). The individual laminations were modelled as 3D solids, considering orthotropic stiffness properties according to Table 3.1. Rectilinear material principal directions were used with the longitudinal (L) direction oriented in the length direction of the laminations, the tangential (T) direction oriented in the lamination width direction and the radial (R) direction oriented in the lamination thickness direction. A gap of 0.2 mm was modelled between adjacent laminations within the same layer.

The flat-side adhesive bonding between the laminations of adjacent layers was modelled using a combination of hard contact in compression and linear elastic response

in tension and in the two in-plane shear directions. The stiffness parameters of this elastic response were assigned as $K_{nn} = K_{ss} = K_{tt} = 1000 \text{ N/mm}^3$. Linear 8-node brick elements with full integration (denoted C3D8 in Abaqus) were used consistently. The elements were close to cubical in shape with a side length of approximately 6 mm.

Pure shear loading was introduced by applying shear forces at the end-faces of the individual laminations. The distribution of the total applied shear forces between the individual laminations was according to Equations (6) and (7). Results regarding lamination shear forces and crossing area torsional moments were evaluated at the centremost part in the x - and y -directions of the FE-model, consisting of five laminations in each layer, as illustrated in Figure 2.1.

Previous parameter studies, using the same modelling approach as described above, have shown that modification of the elastic stiffness parameters within practically relevant ranges of values has only minor influence on the results in terms of the internal force distribution, see e.g. Jeleč et al. (2018), Jeleč et al. (2019) and Danielsson et al. (2019). Previous studies regarding the influence of the distribution in the element width direction of the applied shear loading have, likewise, been found to have only a very small influence on the internal forces at the location for evaluation, see e.g. Danielsson & Serrano (2019).

Table 3.1. Lamination stiffness parameters used for FE-analyses.

E_L	E_T	E_R	G_{LT}	G_{LR}	G_{TR}	ν_{LT}	ν_{LR}	ν_{TR}
[MPa]	[MPa]	[MPa]	[MPa]	[MPa]	[MPa]	[-]	[-]	[-]
12 000	400	600	750	600	75	0.50	0.50	0.33

4 FE-results and model comparisons

The parameter study presented here concerns the element lay-up and the influence of the relative layer thicknesses on the distribution of shear forces in the element width direction and the maximum torsional stress. The parameters considered are:

- The ratio between the net cross section thicknesses: t_x/t_y
- The ratio between the longitudinal layer thicknesses: $t_{x,2}/t_{x,1} (= t_{x,3}/t_{x,4})$
- The ratio between the transversal layer thicknesses: $t_{y,2}/t_{y,1} (= t_{y,2}/t_{y,3})$

The results presented relate to elements with a gross cross section thickness $t_{CL} = 240 \text{ mm}$, shear loading $v_{xy} = v_{yx} = 240 \text{ N/mm}$ and equal longitudinal and transversal laminations widths, $b_x = b_y = b = 150 \text{ mm}$.

Results regarding the distribution of the total shear flow between the individual longitudinal and transversal layers are presented in Figure 4.1, presented as normalized with respect to the total applied shear flow $v_{xy} = v_{yx} = 240 \text{ N/mm}$. Results from the FE-analyses are compared to distributions according to Equations (6) and (7).

The left column of subfigures in Figure 4.1 shows the influence of the ratio between the net cross section thicknesses, t_x/t_y , for three different ratios of $t_{x,2}/t_{x,1}$ and a fixed ratio $t_{y,2}/t_{y,1} = 1.0$. The FE-analyses showed that the ratio between the net cross section thicknesses does not influence the distribution of the shear flow between the individual longitudinal and transversal layers. The shear flows $v_{xy,k}$ and $v_{yx,k}$ according to Equations (6) and (7) are also not affected by the ratio t_x/t_y , for fixed ratios $t_{x,2}/t_{x,1}$ and $t_{y,2}/t_{y,1}$. The results of the FE-analyses and Model D were, however, in full agreement only for the specific case $t_{x,2}/t_{x,1} = 2.0$, i.e. for lay-ups with internal longitudinal layers ($t_{x,2}$ and $t_{x,3}$) of twice the thickness as the external longitudinal layers ($t_{x,1}$ and $t_{x,4}$) and for equal thickness of the three transversal layers ($t_{y,1} = t_{y,2} = t_{y,3}$).

The middle and right columns of subfigures in Figure 4.1 show the influence of the ratio between the internal and external longitudinal layers thicknesses, $t_{x,2}/t_{x,1}$, and the ratio between the transversal layer thicknesses, $t_{y,2}/t_{y,1}$, for a fixed ratio $t_x/t_y = 1.0$. Also here, it can be seen that the model predictions according to Equations (6) and (7) are in full agreement only for the specific case $t_{x,2}/t_{x,1} = 2.0$ and $t_{y,2}/t_{y,1} = 1.0$.

Results regarding the predicted *maximum* torsional stress τ_{tor} according to the FE-analyses and according to Models A–D are presented in Figures 4.2, 4.3 and 4.4. The results from the FE-analyses are based on resulting torsional moments acting over the crossing areas, determined by integration of the shear stress components τ_{zx} and τ_{zy} , and subsequent calculation of the torsional stress according to Equation (2).

Results for predicted *maximum* torsional stress τ_{tor} as influenced by the ratio between the net cross section thicknesses, t_x/t_y , are presented in Figure 4.2. The FE-analyses showed almost no influence of the ratio t_x/t_y on the maximum torsional stress for the nine different combinations of fixed ratios $t_{x,2}/t_{x,1}$ and $t_{y,2}/t_{y,1}$ considered here. Model D, likewise, also predict no influence of the ratio t_x/t_y on the maximum torsional stress, however overestimating the maximum value of τ_{tor} to some extent for all considered lay-ups except the specific case of $t_{x,2}/t_{x,1} = 2.0$ and $t_{y,2}/t_{y,1} = 1.0$. For this lay-up, the predictions of all considered models – except Model C – agreed very well with the FE-results regarding the influence of the ratio t_x/t_y .

The influence of the lay-up parameters $t_{x,2}/t_{x,1}$ and $t_{y,2}/t_{y,1}$ on the predicted maximum torsional stress is illustrated in Figures 4.3 and 4.4, respectively. Results are presented for two fixed ratios of t_x/t_y (1.00 and 1.86) and six combinations of ratios $t_{x,2}/t_{x,1}$ and $t_{y,2}/t_{y,1}$. Models A–D show large differences regarding predicted maximum torsional stress for the range of lay-ups considered in this comparison. The maximum torsional stress according to Model D is for all considered lay-ups equal to, or greater than, the maximum torsional stress according to the FE-analyses.

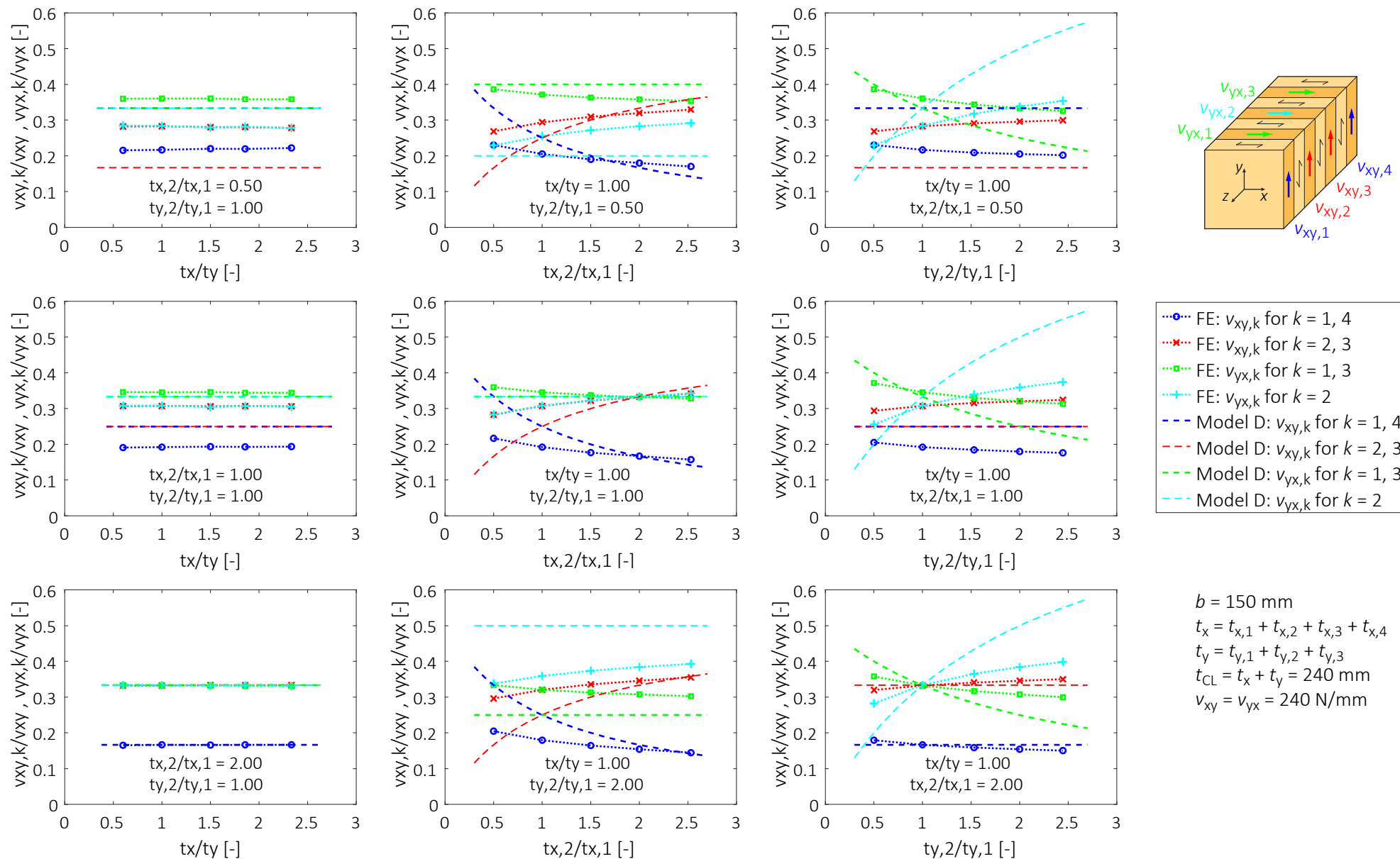
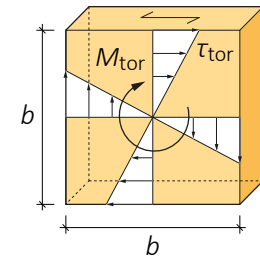
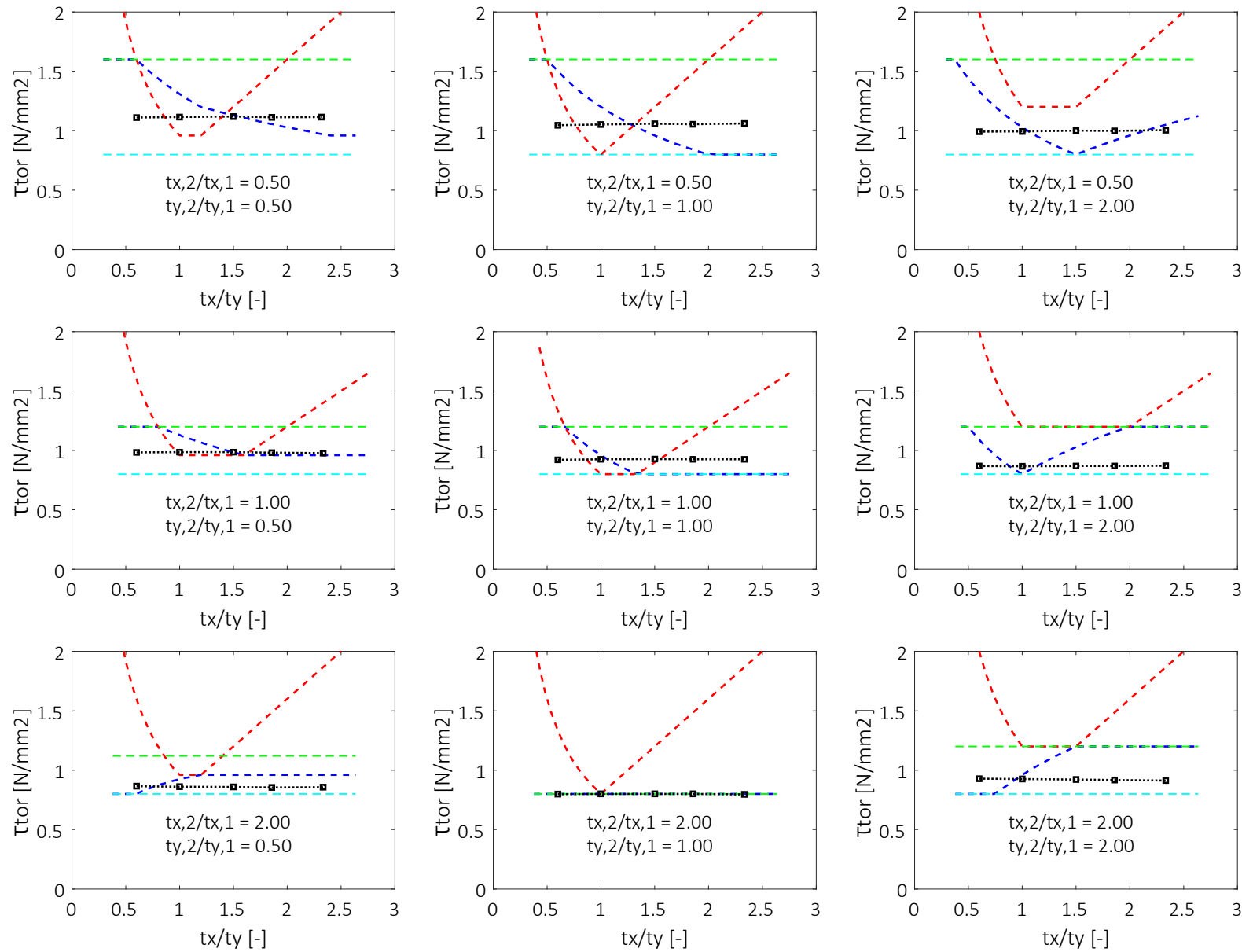


Figure 4.1. Shear flow distributions vs. t_x/t_y , $t_{x,2}/t_{x,1}$ and $t_{y,2}/t_{y,1}$, respectively, according to FE-analyses and according to Model D.



- - - Model A
- - - Model B
- - - Model C
- - - Model D
- - - FE-results

$b = 150 \text{ mm}$
 $t_x = t_{x,1} + t_{x,2} + t_{x,3} + t_{x,4}$
 $t_y = t_{y,1} + t_{y,2} + t_{y,3}$
 $t_{CL} = t_x + t_y = 240 \text{ mm}$
 $v_{xy} = v_{yx} = 240 \text{ N/mm}$

Figure 4.2. Maximum torsional stress τ_{tor} vs. t_x/t_y , for nine different combinations of fixed ratios $t_{x,2}/t_{x,1}$ and $t_{y,2}/t_{y,1}$.

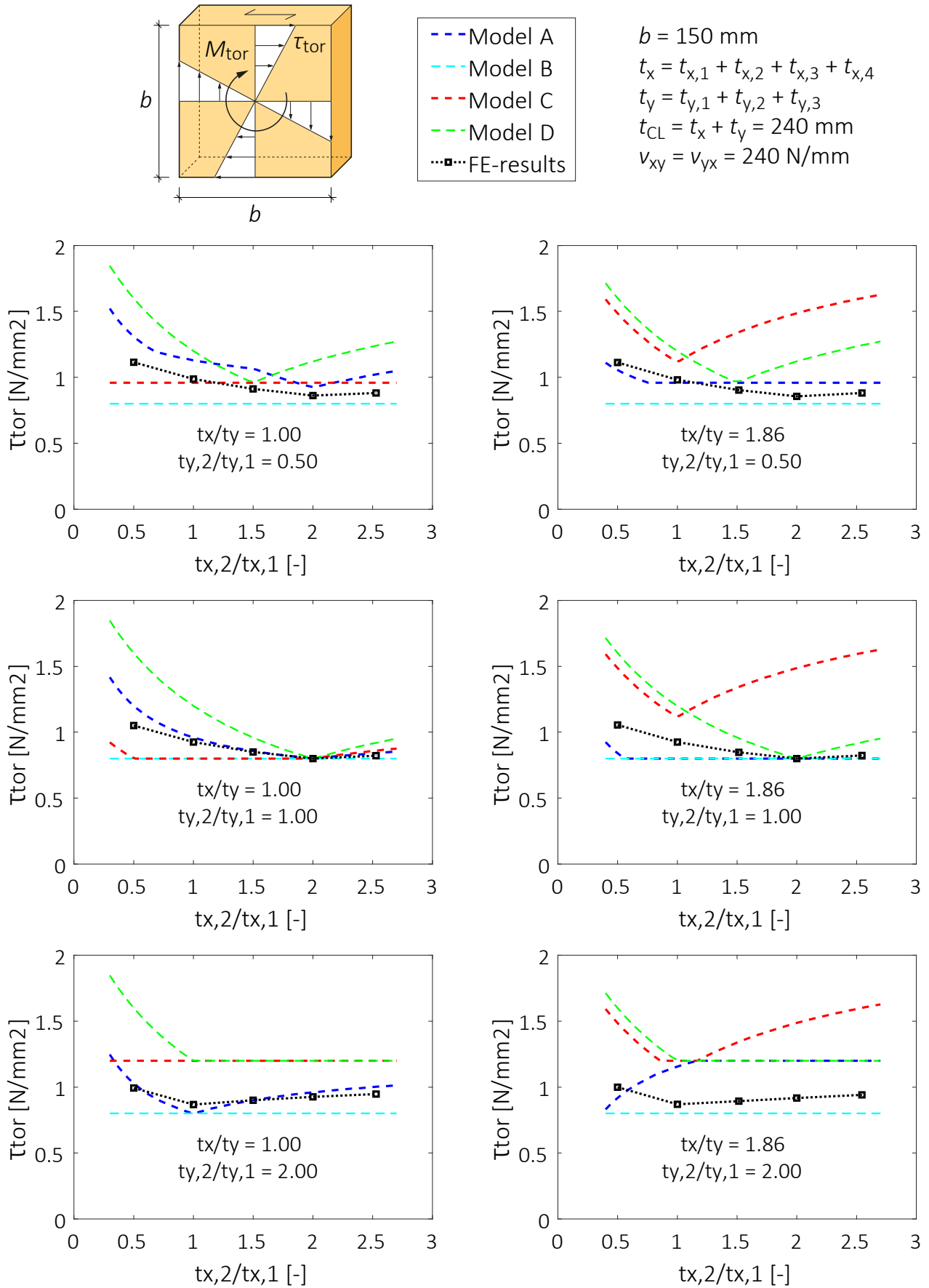


Figure 4.3. Maximum torsional stress τ_{tor} vs. $t_{x,2}/t_{x,1}$, for six different combinations of fixed ratios t_x/t_y and $t_{y,2}/t_{y,1}$.

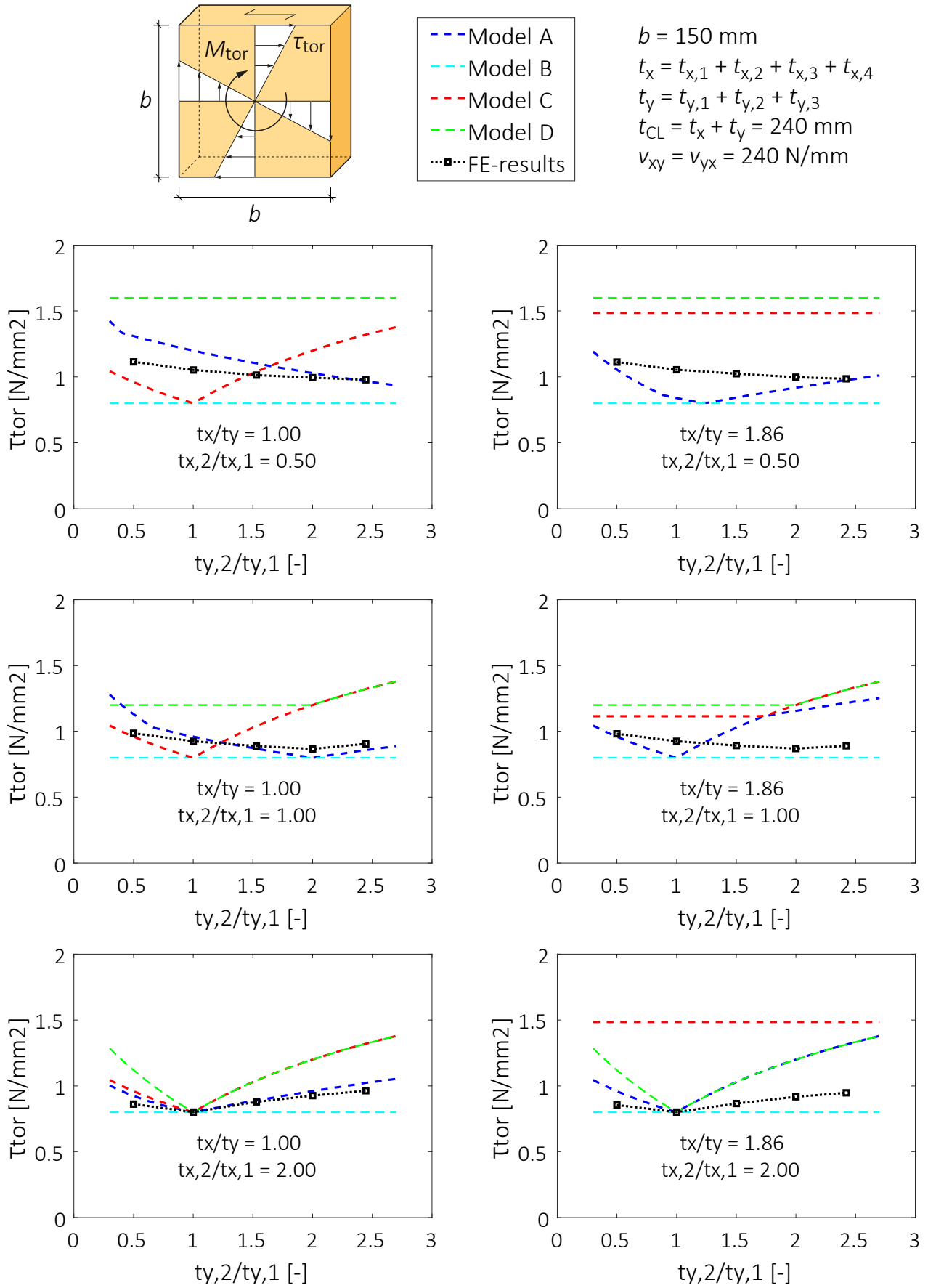


Figure 4.4. Maximum torsional stress τ_{tor} vs. $t_{y,2}/t_{y,1}$, for six different combinations of fixed ratios t_x/t_y and $t_{x,2}/t_{x,1}$.

5 Discussion

The results of the FE-analyses presented in Section 4 are in general in-line with the results of FE-analyses for CLT 3s and 5s presented in Danielsson & Serrano (2019). The distribution of the total shear flow ($v_{xy} = v_{yx}$) between the individual longitudinal and transversal layers according to Model D, Equations (6) and (7), agreed very well with the FE-results for lay-ups having ratios $t_{x,2}/t_{x,1} = 2.0$ and $t_{y,2}/t_{y,1} = 1.0$. Consequently, also the predictions of the maximum torsional stress agreed very well for these lay-ups, irrespective of the ratio between the net cross section thicknesses, t_x/t_y . The FE-analyses predicted equal torsional moments for all six crossing areas in the element width direction for these lay-ups. Equal torsional moments for all crossing areas in the element width direction also yields the lowest possible value of the maximum torsional stress, according to Model D.

For the case of pure in-plane shear loading of CLT 5s, equal torsional moments for the four crossing areas in the element width direction are in Danielsson & Serrano (2019) reported for lay-ups having a ratio $t_{x,2}/t_{x,1} = 2.0$, irrespective of the ratio between the net cross section thicknesses, t_x/t_y . For CLT 3s, the shear flow in the two longitudinal layers and the torsional shear stress in the crossing areas, respectively, are always equal irrespective of the element lay-up, due to symmetry. As is shown in Danielsson & Serrano (2019), models A, B and D all predict shear flows and torsional stresses in very close agreement with the FE-results for CLT 3s.

Results from FE-analyses of CLT 5s at *in-plane beam loading* conditions, presented in Danielsson et al. (2017), Jeleč et al. (2018), Jeleč et al. (2019) and Danielsson et al. (2019), have shown the same response; equal torsional moments for all crossing areas in the element width direction for $t_{x,2}/t_{x,1} = 2.0$ and non-uniform distribution of the torsional moments for $t_{x,2}/t_{x,1} \neq 2.0$. For the beam loading case, Model D with weighting factors $\beta_{x,k}$ based on the relative layer thicknesses also gives slightly higher maximum torsional stress for $t_{x,2}/t_{x,1} \neq 2.0$, compared to FE-results.

Hence, Model D seems to give very accurate predictions of the distribution of the shear flow between the individual layers and of the crossing area torsional moments for the following element lay-ups:

- CLT 3s: all lay-ups,
- CLT 5s: lay-ups with $t_{x,2}/t_{x,1} = 2.0$,
- CLT 7s: lay-ups with $t_{x,2}/t_{x,1} = 2.0$ and $t_{y,2}/t_{y,1} = 1.0$.

Common for these lay-ups is that they represent *repetitive symmetric* parts of an infinite element with consistent thicknesses of the longitudinal and transversal layers, respectively, for any ratio of net cross section thicknesses, t_x/t_y , see Figure 5.1. For this situation, the average shear stress in the respective longitudinal and transversal layers should, due to the repetitive symmetry, be equal for all longitudinal and transversal layers, respectively.

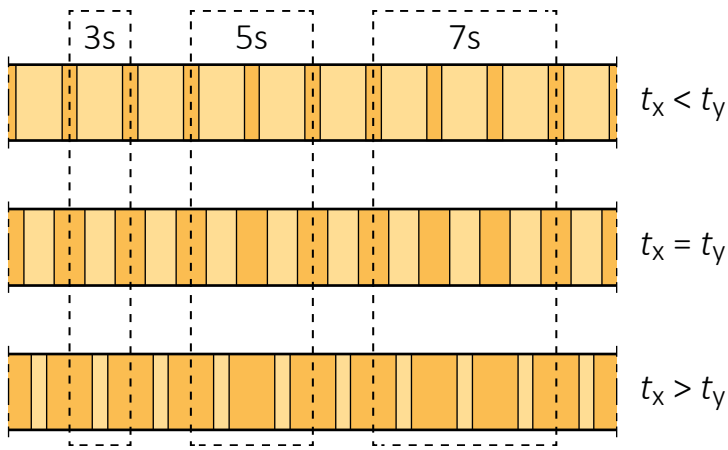


Figure 5.1 Illustration of repetitive symmetries for CLT 3s, 5s, and 7s lay-ups.

The discrepancies between the predictions of the maximum torsional stress according to Model D and the results of the FE-analyses relate to the discrepancies regarding the distribution of the shear flow between the individual longitudinal and transversal layers. Model improvements could hence possibly be obtained by a better understanding of this distribution and a refined formulation of Equations (6) and (7). This type of reformulation could be found by consideration of different shear deformation modes, and associated stiffness measures, e.g. in-line with the model for in-plane shear stiffness of CLT as discussed by Moosbrugger et al. (2006) and Bogenberger et al. (2010). Another option for modification of Model D is to determine weighting factors $\beta_{x,k}$ and $\beta_{y,k}$ by curve-fitting to FE-results, in a similar fashion as reported in e.g. Danielsson et al. (2019) for CLT at in-plane beam loading conditions. Modifications such as these could lead to more accurate predictions compared to FE-results, but would however most likely result in more complicated design equations.

A general limitation of the study of CLT 7s presented here, and the study of CLT 3s and 5s presented in Danielsson & Serrano (2019), relate to the considered element lay-ups. Both studies are limited to consideration of the element lay-ups in terms of the relative net cross section thicknesses, t_x/t_y , and of the relative longitudinal and transversal layer thicknesses, $t_{x,2}/t_{x,1}$ and $t_{y,2}/t_{y,1}$, respectively. Equal lamination widths, $b_x = b_y = b = 150$ mm, were considered for all laminations. The lamination width may have some influence on the internal force distribution and hence on the predicted maximum torsional stress. The limited parameter study of the influence of lamination widths on the shear force distribution in the element width direction for in-plane beam loading of CLT elements presented in Jeleč et al. (2019), however, suggests that this influence is relatively small. The lamination width is still of general interest for design with respect to shear FM III according to Models A–D, since the predicted torsional stress is proportional to $1/b$ which means that the capacity is proportional to b .

6 Concluding remarks

Comparison of model predictions for the maximum torsional stress at in-plane shear loading of CLT elements with seven layers (CLT 7s) has been presented. Predictions according to four models (Models A–D) have been compared to results of full 3D FE-analyses of CLT elements with different lay-ups, considering the ratios t_x/t_y , $t_{x,2}/t_{x,1}$ and $t_{y,2}/t_{y,1}$.

From the comparison of FE-results and predictions according to the considered analytical models (Models A–D), the following conclusions were drawn:

- None of the analytical models gave predictions of the maximum torsional stress in *full* agreement with the FE-results for the complete range of lay-ups considered in this study.
- Predictions from Models A, B and D agreed very well with the FE-results for the specific case of lay-ups with layer thicknesses according to ratios $t_{x,2}/t_{x,1} = 2.0$ and $t_{y,2}/t_{y,1} = 1.0$, irrespective of the ratio t_x/t_y .
- Model A gave predictions which in an overall sense appear to best resemble the FE-results. Model A gave very accurate predictions for the specific lay-ups mentioned above, with $t_{x,2}/t_{x,1} = 2.0$ and $t_{y,2}/t_{y,1} = 1.0$. For other lay-ups, Model A predicted both greater and lesser values of the maximum torsional stress compared to the FE-results.
- Model D gave results which are either accurate (for the specific case of $t_{x,2}/t_{x,1} = 2.0$ and $t_{y,2}/t_{y,1} = 1.0$) or conservative (for all other considered lay-ups) compared to the FE-results.

Although not in perfect agreement with results of FE-analysis, Model D could be considered for potential inclusion in design codes, such as Eurocode 5. The model is fairly simple and based on a rational mechanical background. The results presented here suggest that Model D is accurate or conservative for pure in-plane shear loading of CLT 7s and results presented in Danielsson & Serrano (2019) suggest the same response for CLT 3s and 5s.

Furthermore, Model D is based on the same rational mechanical background as the design proposals for shear FM III of CLT at *in-plane beam loading* conditions as presented in Jeleč et al. (2018) and Jeleč et al. (2019). Hence, consistent design approaches could be formulated for the two cases using these suggested models for the case of in-plane shear loading conditions *and* in-plane beam loading conditions.

7 Acknowledgements

The financial support from FORMAS for the project *Strength and fracture analysis of cross laminated timber* (grant 2019-01354) and financial support for the project *InnoCrossLam* is gratefully acknowledged. The project *InnoCrossLam* is supported under the umbrella of ERA-NET Cofund ForestValue by Vinnova, FORMAS and the Swedish Energy Agency. ForestValue has received funding from the European Union's Horizon 2020 research and innovation programme under grant agreement N° 773324.

8 References

Abaqus/CAE 2019 (2018), Dassault Systèmes.

Bogensperger T, Moosbrugger T, Silly G (2010): Verification of CLT-plates under loads in plane. In: Proc. WCTE, Riva del Garda, Italy.

CEN/TC 250/SC5 (2020): Working draft of design of cross laminated timber, LVL, solid wood panels (SWP) and wood fibre insulation boards as sheeting for timber frame members in a revised Eurocode 5-1-1, Version: 2020-02-11, N1203.

Danielsson H, Serrano E, Jeleč M, Rajčić V (2017): In-plane loaded CLT beams – Tests and analysis of element lay-up. In: Proc. INTER, INTER/50-12-2, Kyoto, Japan.

Danielsson H, Jeleč M, Serrano E, Rajčić V (2019): Cross laminated timber at in-plane beam loading – Comparison of model predictions and FE-analyses. *Engineering Structures* 179:246–254.

Danielsson H, Serrano E (2019): Cross laminated timber at in-plane shear loading – Comparison of model predictions. In: Proc. INTER, INTER/52-12-2, Tacoma, USA.

Jeleč M, Danielsson H, Serrano E, Rajčić V (2018): Cross laminated timber at in-plane beam loading – New analytical model predictions and relation to EC5. In: Proc. INTER, INTER/51-12-5, Tallinn, Estonia.

Jeleč M, Danielsson H, Rajčić V, Serrano E (2019): Experimental and numerical investigations of cross-laminated timber elements at in-plane beam loading conditions. *Construction and Building Materials* 206:329–346.

Moosbrugger T, Guggenberger W, Bogensperger T (2006): Cross-laminated timber wall segments under homogeneous shear – with and without openings. In: Proc. WCTE, Portland, USA.

ÖNORM B 1995-1-1 /A:2018-11 (2018): Eurocode 5: Design of timber structures – Part 1-1: General – Common rules and rules for buildings – National specifications for the implementation of ÖNORM EN 1995-1-1, national comments and national supplements (Amendment), Austrian Standards International.

Wallner-Novak M, Koppelhuber J, Pock K (2013): *Brettsper Holz Bemessung – Grundlagen für Statik und Konstruktion nach Eurocode*. ProHolz Austria, Druck Eberl Print, Immenstadt, Austria.

Discussion

The paper was presented by H Danielsson

P Dietsch commented that this work could contribute towards working group 1 for Eurocode 5 on CLT design.

R Tomasi questioned whether model D, which is based on equilibrium, considered different torsional moments through the thickness of the panel. H Danielsson stated that yes and the layup and thickness of the laminae would make a difference. R Tomasi discussed past test results with 3 and 5 layers CLT where internal layer thickness had an effect. H Danielsson said this would agree with the model prediction.

Assessment of seismic design factors and proposal of modification to Chilean seismic building design standard (NCh 433) for mid-rise wood light-frame buildings

Hernán Santa María, UC Timber Innovation Center, Chile.

Ángela Salinas, Bio-Bio University, Chile.

Jairo Montaña, UC Timber Innovation Center, Chile.

Juan Jose Ugarte, UC Timber Innovation Center, Chile.

José Luis Almazán, UC Timber Innovation Center, Chile.

Pablo Guindos, UC Timber Innovation Center, Chile.

Alexander Opazo, Bio-Bio University, Chile

Franco Benedetti, Bio-Bio University, Chile

Victor Rosales, UC Timber Innovation Center, Chile.

Xavier Estrella, UC Timber Innovation Center, Chile.

Felipe Guiñez, UC Timber Innovation Center, Chile.

Sebastián Berwart, UC Timber Innovation Center, Chile.

Sebastián Cárcamo, UC Timber Innovation Center, Chile.

Alan Jara, Bio-Bio University, Chile.

Keywords: wood light-frame, buildings, seismic factors, mid-rise structures, FEMA P-695.

1 Introduction

The Chilean forestry industry has increased its productivity and today constitutes, after mining, the second highest exporting sector of the country's economy. The managed forests planted in Chile cover 2.414.208 hectares (INFOR, 2017). However, despite all this potential, the volume of timber residential construction in Chile is much lower than other forested countries in the Americas like the United States and Canada. In these

countries, wood construction is used for more than 90% of the total residential construction, while for the year 2017, it represented only 18% of residential construction in Chile (Cámara Chilena de la Construcción 2014). In addition, unlike those other countries where wood light-frame system construction can be used in buildings up to six stories, in Chile it is used for only one- to two-story dwelling houses, thus the Chilean society is missing the advantages of this timber construction system in much of the potential applications.

In recent years, governmental institutions considering the potential of the Chilean forest products industry have supported the development of timber buildings. This within the context of increasing concern about global warming, and as a possible strategy for moving forward on addressing the challenge of providing sustainable alternatives for the future built environment.

However, considering the Chilean high seismic risk, it was necessary to improve comprehension of the seismic behaviour of mid-rise wood-frame systems. In order to increase the allowable building height of wood light-frame structures from two- up to six-stories in the Chilean market, it was required to establish a response modification factor (R-factor) calibrated for mid-rise wood-frame system and the performance expectations of the Chilean standard. This due to uncertainties whether current R-factor in the Chilean seismic design standard was adequate for six-story buildings. Therefore, a project was conducted to determine the most suitable R-factor for wood light-frame building construction up to six-stories in height.

This manuscript summarizes the main issues addressed for the assessment of the seismic performance factor. This investigation involved: (i) develop a set of building configurations for wood light-frame archetype buildings, (ii) structural design of the building archetypes, (iii) conduct monotonic and cyclic tests of shear wall elements, (iv) sub-assembly level tests: framing-to-sheathing connection tests, wood structural panel sheathing mechanical property tests, nail tests, and testing of wood frame elements to determine their mechanical properties, (v) numerical modelling using the test results as input parameters to complete shear wall and building archetypes models, (vi) non-linear time history dynamic analysis simulation, and (vii) evaluation of seismic performance factor. The procedure for quantitatively establishing the seismic performance factors with consideration for the performance expectations provided in the Chilean seismic design standard followed the FEMA P-695 guidelines (FEMA, 2009). Thus, a response modification factor (R-factor) for use in force-based design procedures was estimated.

2 Provisions of the Chilean seismic design standard, NCh-433 Of.1996 Mod. 2012/DS61.

The NCh-433 - Building seismic design standard (INN, 2009) defines a response modification factor R-Factor of $R=5.5$ for timber light-frame shear walls.

One provision included in NCh 433 with relevant impact in the structural design of the wood light-frame buildings is the maximum inter-story drift. It is defined in Section 5.9.2 and states that: *“the maximum relative displacement between two consecutive stories, measured at the centre of mass in each direction of analysis, must not be greater than the story height multiplied by $\Delta = 0.002$ (0.2%)”* (INN, 2009). This inter-story drift requirement is to be determined for the forces associated with the design spectrum reduced by R-factor. No deflection amplification factor (C_d) is defined or required to be used. This is essentially the major difference in the Chilean performance requirements when compared to the common performance requirements in other countries.

The disadvantage regarding the maximum inter-story drift provision is that was originally set to control the performance of reinforce concrete buildings, but actually this provision governs all construction materials equally. Therefore, due to the inherent lower lateral stiffness of timber structures, it is difficult to achieve the high lateral stiffnesses required to control the inter-story drifts. Thus, wood light-frame structural systems are at a disadvantage when compared to other materials. For this reason, this research project also focused on trying to find a maximum drift limit value more suitable to this timber system.

3 Structural archetypes of buildings configurations

A series of structural archetypes were developed with the aim of covering as wide of range of possible configurations for wood light-frame buildings according to FEMA P-695 guidelines. Four building archetypes were designed considering the most representative characteristics observed in the Chilean building stock (Cárcamo S., 2017): two configurations representing social housing, and two configurations representing the private market buildings. First, extensive research on residential timber buildings built with the wood light-frame system internationally was completed. Later, extensive research of the most typical construction typologies in reinforced concrete and masonry residential buildings currently being built for the five- and six-story real estate market in Chile was completed. These investigations provided information required to set the different space distributions, symmetries, maximum spans, different tributary areas, simple and complex perimeters, discontinuities, among others for the four archetypes developed. Two of these four archetypes used in the investigation are shown in Figure 1.

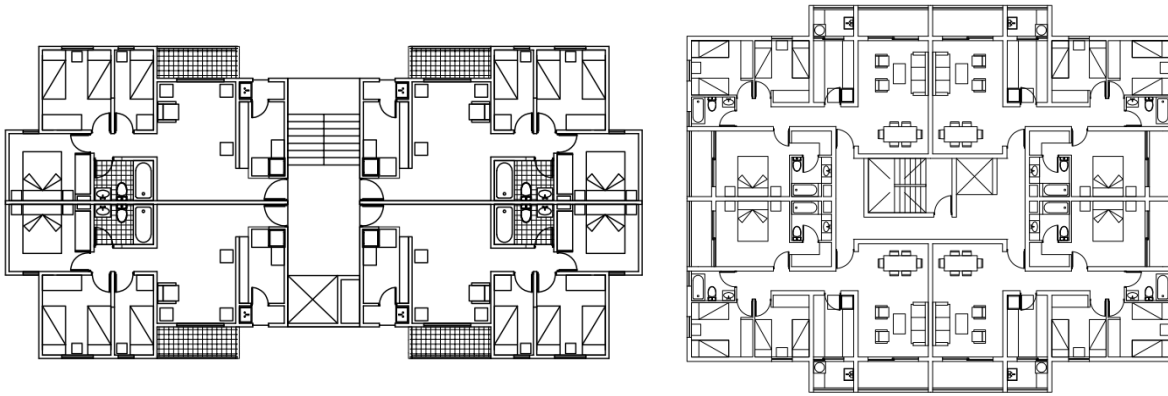


Figure 1. Some buildings configurations, "Type A" (Left) and "Type B" (Right).

These four building configurations were designed using the Equivalent Lateral Force and Modal Response Spectrum analysis procedures following the provisions of the NCh 433 design standard for various locations throughout Chile. The matrix of archetypes includes buildings located at Seismic Zones 1 ($A_0 = 0.2g$) and 3 ($A_0 = 0.4g$), and located on Soil Types A, B, C, and D. Four different heights of buildings were considered: three-, four-, five- and six-stories.

For the structural design of the building configurations archetypes, the following standards, papers and guidelines were considered: AWC-SDPWS American Wood Council, (2015), NCh 1198 standard INN, (2014), S. Rossi et al., (2015), NBCC, (2005), Nassani D.E., (2014), BSSC, (2003), CECOBOIS, (2015), Newfield, G et al., (2013), Newfield, G et al., (2015), Leung T. et al, (2010) and APEGBC, (2011).

According to the main purpose of this investigation, regarding the determination of a more suitable R-Factor for the wood light-frame system up to six-stories height in Chile, several trial R-Factors were considered for the structural designs. A set of four seismic design factors were considered: $R = 5.5$, $R = 6.0$, $R = 6.5$, $R = 7.0$.

Also, different maximum inter-story drifts were considered for the structural designs, because as mentioned on Section 2, it is a key performance parameter. In this sense, the following trial drift limits were considered: $\Delta = 0.002$ (0.2%), $\Delta = 0.003$ (0.3%) and $\Delta = 0.004$ (0.4%).

Regarding anchorage devices for the wood light-frame shear walls buildings, the Hold-Down (HD) devices were considered for the structural designs of the 3-, 4- and 5-story buildings. On the other hand, Anchor Tie-down System (A.T.S.) devices were implemented for the structural designs of the 5- and 6-story wood light-frame buildings.

Additionally, the structural designs of buildings were considered varying the mechanical structural grade of the shear wall studs and sole plates. Therefore, shear walls with a timber frame made of C16 and MGP10 Radiata Pine sawn timber were considered for the building's structural archetypes.

Carrying out all the permutations and combinations between all the different variables described above, the resulting matrix consisted of more than 1.000 different structural building designs. Afterwards all this work, the structural design archetypes associated

with the combination of parameters: R-Factor & Δ , of greatest interest were selected to perform the FEMA P-695 analysis methodology (FEMA, 2009). Thus, only 201 archetypes considering the actual NCh 433 standard provisions: $R = 5.5$ & $\Delta = 0.002$ (0.2%), together with the interest combination given by: $R = 6.5$ & $\Delta = 0.004$ (0.4%), were selected for the collapse assessment process of the FEMA P-695 methodology.

This resulted in a manageable number of idealized non-linear models to sufficiently represent the range of intended applications for a proposed system being achieved.

4 Experimental program

The experimental program developed for this research project involved testing of shear walls, their sub-assembly components, elements, materials, and relevant connections. Two different anchorage conditions were tested: Hold-Downs (HD) anchor devices and Anchor Tie-down System (A.T.S.).

The shear walls tests were divided into 3 Phases:

Phase 1 included shear walls tests subjected to monotonic and cyclic loading for walls with different aspect ratios (Height / Length), different edge nail spacings, but using the same HD devices. The configurations of the test specimens are shown in Table 1.

Phase 2 also involved shear walls tests with cyclic loading, HD anchors, different edge nail spacings and different wall lengths. However, additional gravity load and overturning moment forces were added. This was done in order to characterize the response of the shear walls of the first story of wood light-framed buildings to the action of tractions and compressions that the overturning moment subjected to them. The additional compression load from the overturning moment could cause a compression failure at the post-studs or buckling of the OSB sheathing panel. On the other hand, the additional tensile load due to the overturning moment action on the shear wall specimens, could cause a HD failure due to a state of greater stress than generated by the traction from the cyclic shear loading alone. The configuration of these test specimens are shown in Table 2.

Phase 3 included tests of shear wall specimens tests subjected to cyclic shear loading with the same aspect ratio, but different nail spacings. However, the main difference is the anchorage condition provided by the A.T.S. These shear wall tests with this anchorage were carried out in specimens of one- and two-story heights. Which were necessary to characterize the response of six-story building models using this type of anchorage, which conceptually works very differently than the traditional HD anchor. The configurations of the test specimens are shown in Table 3.

Thirty-two shear walls subjected to monotonic and cyclic loading were tested during this research program. The details of the specimen's configurations are shown in Tables 1 to 3. All the sawn timber used on the project for studs and sole-plate was 2x6"

with exact dimensions of 35 x 138 mm. All the wood frame elements used in constructing the shear walls consisted of mechanically graded, Chilean MGP10 (Australian structural grade) Radiate Pine. The wood framing elements were donated by Arauco. The wood structural panel sheathing used throughout the project was 11.1 mm thick OSB rated sheathing panels, which were installed on both sides of the walls. The OSB panels were donated by Louisiana Pacific. One type of nail was used throughout the project, it was 70 mm long with a nominal diameter of 3.3 mm helical nails installed with pneumatic gun.

The HD and A.T.S. anchoring devices were all donated by Simpson Strong-Tie Company. The HD used on Phase 1 and 2 were HD12. The A.T.S. rod’s diameters were used on the shear walls specimens as indicated in Table 3. Shrinkage compensation devices were implemented according to the rod’s diameter.

Table 1. Test configuration specimens for shear walls – Phase 1.

Notation	Loading Protocol	Length [mm]	Edge Nailing Spacing [mm]	Anchor Device
M120-10-01	Monotonic	1200	100	Hold-Down
M120-10-02	Monotonic	1200	100	Hold-Down
M120-05-01	Monotonic	1200	50	Hold-Down
M120-05-02	Monotonic	1200	50	Hold-Down
M240-10-01	Monotonic	2400	100	Hold-Down
M240-10-02	Monotonic	2400	100	Hold-Down
M240-05-01	Monotonic	2400	50	Hold-Down
C120-10-01	Cyclic	1200	100	Hold-Down
C120-10-02	Cyclic	1200	100	Hold-Down
C120-05-01	Cyclic	1200	50	Hold-Down
C120-05-02	Cyclic	1200	50	Hold-Down
C240-10-01	Cyclic	2400	100	Hold-Down
C240-10-02	Cyclic	2400	100	Hold-Down
C240-05-01	Cyclic	2400	50	Hold-Down
C240-05-02	Cyclic	2400	50	Hold-Down
C360-10-01	Cyclic	3600	100	Hold-Down
C360-10-02	Cyclic	3600	100	Hold-Down
C70-10-01	Cyclic	700	100	Hold-Down
C70-10-02	Cyclic	700	100	Hold-Down

NOMENCLATURE:

M-120-10-0X: Type of test (M = Monotonic test; C = Cyclic test) – shear wall length – edge nail spacing – No. of specimen test”

Table 2. Test configuration specimens for shear walls with axial load and moment - Phase 2.

Notation	Loading Protocol	Length [mm]	Edge Nailing Spacing [mm]	Anchor Device
C120-10-01	Cyclic	1200	100	Hold-Down
C120-10-02	Cyclic	1200	100	Hold-Down
C120-05-01	Cyclic	1200	50	Hold-Down
C240-10-01	Cyclic	2400	100	Hold-Down
C240-10-02	Cyclic	2400	100	Hold-Down
C240-05-01	Cyclic	2400	50	Hold-Down
C360-10-01	Cyclic	3600	100	Hold-Down
C360-10-02	Cyclic	3600	100	Hold-Down

Table 3. Test configuration specimens for shear walls with A.T.S. - Phase 3.

Notation	Loading Protocol	Length [mm]	Edge Nailing Spacing [mm]	Anchor Device
C240-10-01	Cyclic	2400	100	A.T.S. SR4
C240-10-02	Cyclic	2400	100	A.T.S. SR14
C240-05-01	Cyclic	2400	50	A.T.S. SR10
C240-05-02	Cyclic	2400	50	A.T.S. SR14
Story 1 = C240-10	Cyclic	2400	50	A.T.S. SR14
Story 2 = C240-05			100	A.T.S. SR10

The monotonic tests were conducted by applying a linear increasing load until the shear wall failure was observed. The CUREE-Caltech reversible displacement protocol (Krawinkler H, et al. 2001) was used for the cyclic tests. The cyclic protocol was calibrated based on the results from the initial monotonic tests. Additional information about this experimental campaign results and all the sub-assembly level tests such as: framing-to-sheathing connection tests, panel sheathing mechanical properties tests, nails tests, and testing of wooden frame elements to determine the mechanical properties can be found in Guiñez F, (2019) and Estrella X, (2020).

This experimental campaign was designed to fulfill three fundamental objectives: (1) to prove that structural wood light-frame systems provide adequate lateral resistance for buildings up to 6-stories located in areas of high seismicity in Chile, (2) verify that the SDPWS-2015 design standard (American Wood Council, 2015), can be homologated for use in Chile utilizing Chilean materials and meeting the national constructive practices, and (3) develop reliable characterization variables to use in numerical models.

In this context, it was possible to verify that the light-frame system has an adequate response to cyclic loads. It was also possible to verify that this structural system has a high deformation capacity without losing its structural integrity, and that this system

responds in a ductile failure mode. Photos of the shear walls tests described earlier are presented in Figures 2 and 3.



Figure 2. Shear walls tests specimens subjected to cyclic shear plus gravity load and overturning moment action.



Figure 3. Shear walls tests specimens with A.T.S., one story test (Left), two stories test (Right).

5 Numeric Modelling

Numerical models of the tested shear walls specimens were developed in order to simulate the behaviour of these elements when subjected to large deformations within the non-linear range. The mechanical behaviour of the shear walls is simulated using non-linear springs that were calibrated using the reversed cyclic testing of shear walls and their key connections. Several detailed models of shear walls tested were developed using the Matlab program M-CASHEW developed by Pang W & Hassanzadeh S, (2012). This made it possible to extrapolate the results obtained at the laboratory to other shear wall dimensions that were not tested, providing valuable information used to develop and analyse archetype buildings. A model for wood light-framed shear walls was developed, consisting of: (1) Euler-Bernoulli frame two-node elements with 3-DOFs per node to represent the studs and sole plate, (2) Sheathing OSB panels were modelled using rectangular shear-panel elements with 5 DOFs, and (3) two-node-link

elements to represent both sheathing-to-framing and Hold-Down connections. A schematic of the developed shear wall model is shown in Figure 4. The mechanical properties of the shear wall components were taken from sub-assembly level tests results as indicated in Estrella X, (2020).

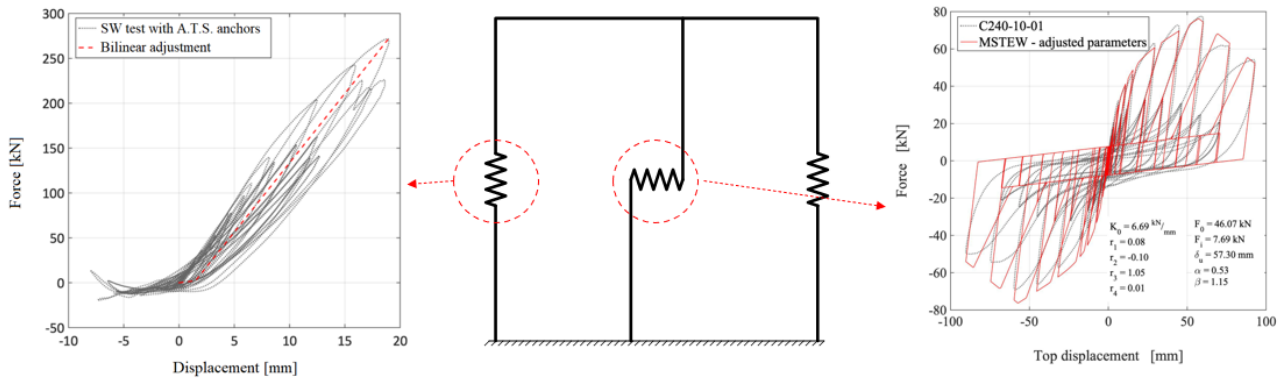


Figure 4. Representation of wood-framed shear walls non-linear model.

The results of the model predictions versus cyclic and monotonic shear walls test results with different aspect ratios are shown in Figure 5. It can be seen good agreements between the model and the experimental responses in terms of maximum force, maximum displacement, initial stiffness, ultimate displacement, ductility, and energy dissipation. The average model errors when predicting each of the aforementioned parameters are 0.8%, 2.3%, 6.9%, 6.8%, 3.8% and 9.3%, respectively. These levels of error were considered admissible for non-linear models.

6 Modelling and nonlinear analysis

The FEMA P-695 presents a rational methodology for the quantification of seismic design factors for structural systems. Non-linear analyses are used in the P-695 methodology to evaluate the buildings capacity in terms of an acceptably low probability of collapse for seismic demands of different intensities. For this, non-linear models were developed for each one of the 201 structural archetypes described earlier.

A 3D nonlinear model was developed for each building archetype. As proposed by Pei and van de Lindt (2009), wood-frame shear walls were modelled using nonlinear spring elements which connect two consecutive floors. The hysteretic behaviour of each wood-frame shear wall was modelled using the Modified-Stewart (MSTEW) model proposed by Folz and Filiatrault (2001). More detailed information about the model formulation proposed for the wood-frame shear walls and the mid-rise building archetypes can be found in Estrella X. et al., (2019a, 2020).

Once the structural nonlinear models for the structural system archetypes were complete, static pushover analyses were carried out for each of the buildings archetypes.

This was to study their maximum resistance, maximum deformation capacity, initial stiffness, and quantify their ductility. The archetypes response was analysed for loading in both directions separately by applying a monotonically increasing lateral load pattern distribution. The load pattern was associated with the first mode of vibration.

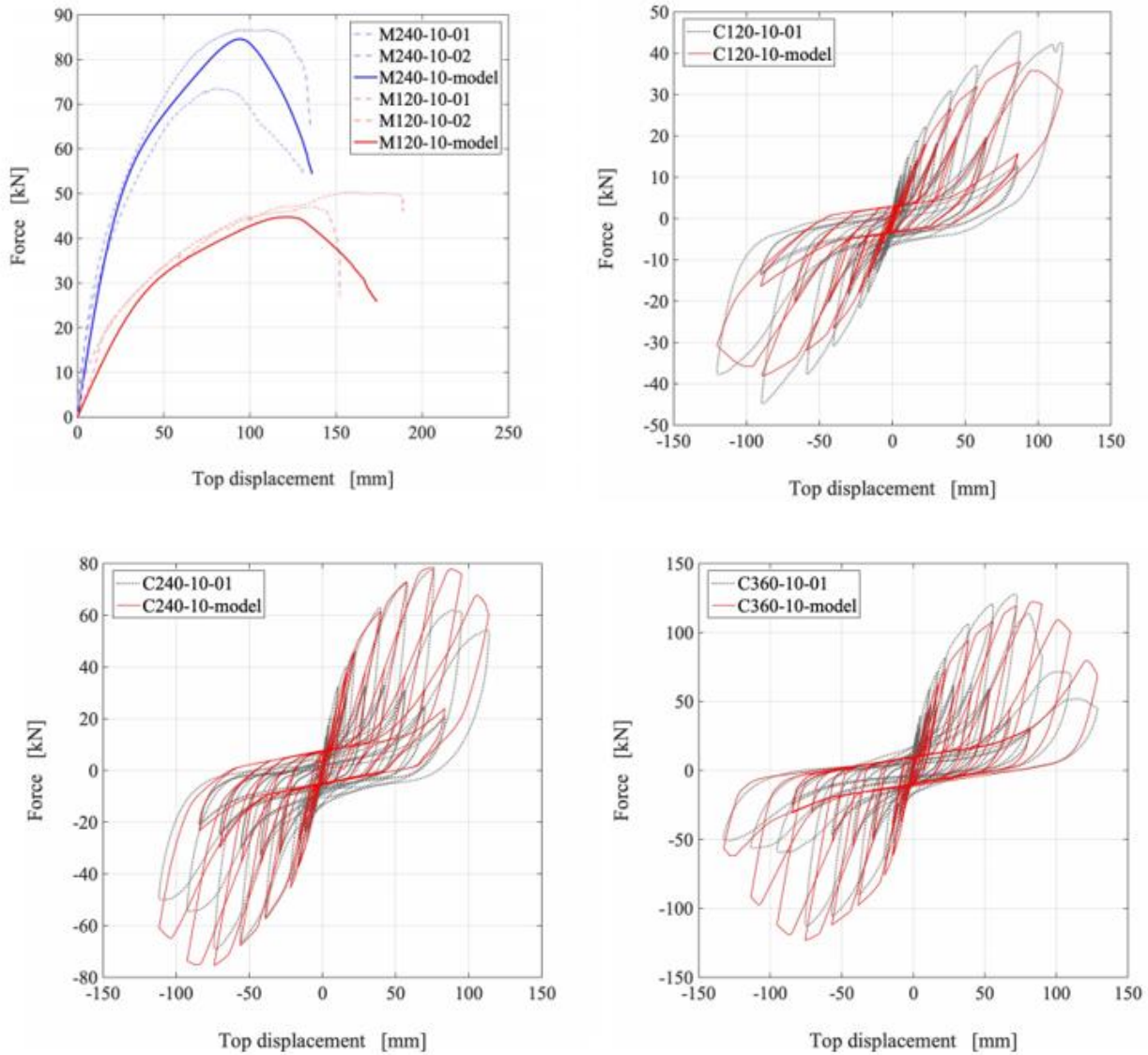


Figure 5. Comparison between shear walls tests and proposed numerical model predictions.

An example the response results for the X-X direction of archetype “Type A” located in Seismic Zone 1, Soil Type B, and structurally designed using both of the interest parameter combinations (R-Factor & Δ) are shown in Figure 6. When analysing the building model response for the X-X direction, it was noted that the strength of the building model falls by 24.8% when the archetype is structurally designed using the combination of parameters given by $R = 6.5$ & $\Delta = 0.004$, while the initial stiffness decreases only 7.8%. There are no notable changes in the building ductility (displacement capacity).

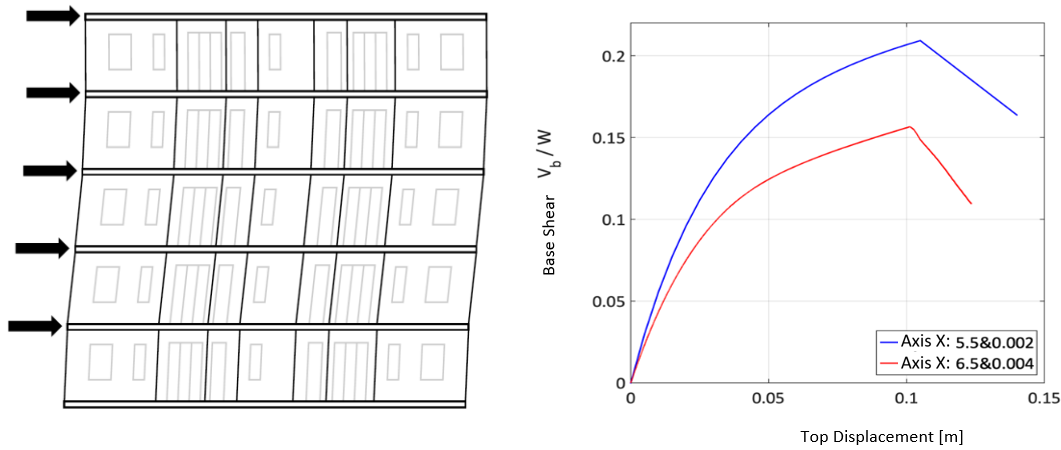


Figure 6. "Type A" building archetype model results for Static-Pushover analysis using the two interest combinations of parameters of seismic design factors and inter-story admissible drifts.

Subsequently, bidirectional Incremental Dynamic Analyses (IDA) were performed for each principal direction of the building archetype models using a set that includes 26 pairs of ground motions records (horizontal components) selected particularly for this study. Thus, for the X-X and Y-Y building main directions, a total of 52 analyses resulted for each combination of design factor and admissible inter-story drift parameters. To compute the collapse capacity of each building archetype, bidirectional IDA analyses were conducted employing the software SAPWood V2.0 developed by Pei and van de Lindt, (2009).

Detailed information about ground motion selection such as: earthquake magnitude, fault type, distance to the fault, record components, intensity measures, number of records per earthquake, accelerogram correction, soil conditions, among others, can be found in Estrella X, (2019b).

The ground motions were monotonically and systematically scaled to the earthquake intensity that caused the collapse of an archetype model. For this research, the collapse of the structure was established as an equivalent drift of 3% of the story height as per FEMA 356 (FEMA, 2000). The scaling protocol followed, for progressively increasing the ground motion record intensities until the structure reached the limit state, is described in detail in Estrella X, (2019b).

It is known that the calculation of the collapse capacity of structural systems through IDA analyses is influenced by the spectral shape of the ground motions. The approach followed for this research project is described in Estrella X, (2019b).

The FEMA P-695 methodology defines collapse level ground motions as the intensity that would result in median collapse of the seismic-force-resisting system. The median collapse occurs when one-half of the structures exposed to this intensity of ground motion would have some form of life-threatening collapse (FEMA, 2009).

The 52 IDA response curves for the previously presented building archetype (5-story "Type A" building, located at Seismic Zone 1 and Soil Type B) are provided in Figure 7.

The IDA response curves are plotted for the two combinations of parameters of interest. The resulting median of the collapse level ground motions Sa_{COLL} was determined for the 3% inter-story drift for the 5%-damped design level spectral acceleration and the 5%-damped of the Maximum Credible Earthquake (MCE) Sa_{MCE} spectral acceleration. The MCE ground motions is defined as 1.2 times the design earthquake according to the NCh-433 standard.

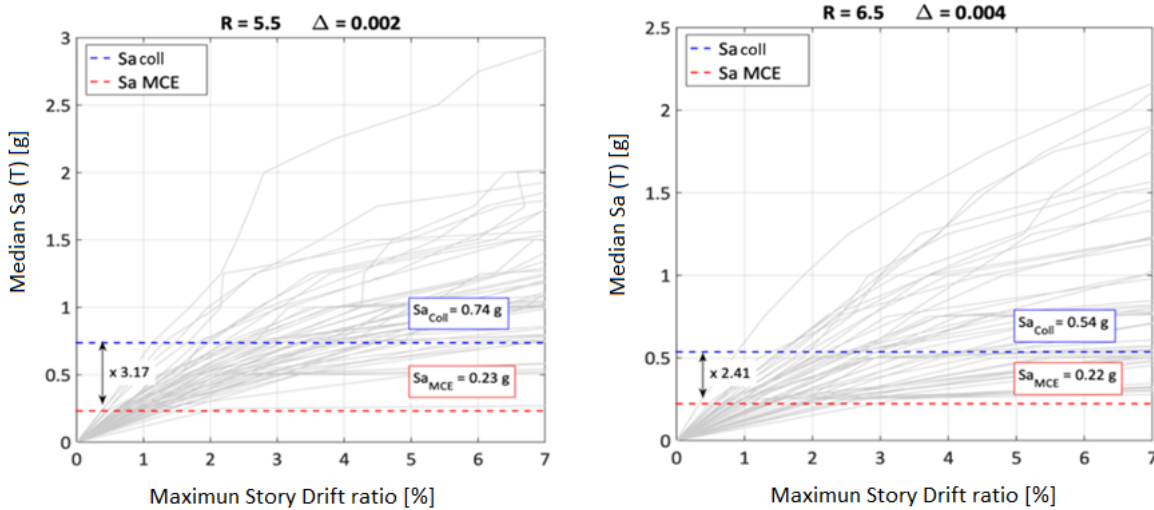


Figure 7. IDA curves responses of “Type A” building archetype model for the two interest combinations of parameters, current NCh-433 standard parameters (Left), proposed modified parameters (Right).

The Collapse Margin Ratio calculated as $CMR = Sa_{COLL} / Sa_{MCE}$ for the cases shown in Figure 7 are 3.17 and 2.41 for the current and proposed NCh-433 parameter values, respectively. Subsequently, the Adjusted Collapse Margin Ratio (ACMR) is calculated, which is obtained by adjusting the CMR by the Spectral Shape Factor (SSF) that depends on the set of seismic records used, and by a factor of 1.2 that is applied when performing bidirectional dynamic analyses ($ACMR = CMR \times SSF \times 1.2$) (FEMA 2009). Detailed information about the determination of SSF factors can be found in Estrella X, (2019b).

The ACMRs calculated for each case are presented in Table 4. There was a 25% decrease in the ACMR when the proposed NCh-433 modified parameters ($R = 6.5$ & $\Delta = 0.004$) were compared to the current parameters.

Section 7.1.2 of the FEMA P-695 methodology defines the collapse performance objectives as: (1) a conditional collapse probability of 20% for all individual wood light-frame archetypes, and (2) a conditional collapse probability of 10% for the average of each of the performance groups of wood light-frame archetypes. The Collapse Margin Ratios computed (CMR), the period-based ductility (μ_T), the Spectral Shape Factors (SSF), and the Adjusted Collapse Margin Ratio (ACMR) are presented in Table 4. Two individual archetypes (incorporating low aspect ratio shear walls) shown in Table 4 pass the acceptable criteria of Adjusted Collapse Margin Ratio performance objective, given

by and $ACMR_{20\%}$ of 1.49. The $ACMR_{10\%}$ for the performance objective of the average of each of the performance groups is 1.84.

Table 4. Adjusted Collapse Margin Ratios and Acceptable Collapse Margin Ratios for individual wood-frame archetypes performance objective.

Archetypes	Stories	Comb. of Parameters	CMR	μ_{τ}	SSF	ACMR	$ACMR_{20\%}$	Acceptance Check
C	5	2400	3.17	4.15	1.17	4.86	1.49	Pass
C	5	2400	2.41	4.02	1.51	3.64	1.49	Pass

The aforementioned procedure is equivalent for all the other 201 combinations of structural archetypes, soil types and seismic zones. The complete results considering the 201 structural archetypes, the performance groups, the buildings located in Seismic Zone 1, 3, and Soil Types A, B, C and D are summarized in the Figure 8. Further details regard the seismic performance evaluation, the total system collapse uncertainty and the robustness of the analysis can be found in Estrella X, (2019b and 2020).

It can be seen in Figure 8 that the structural system of wood light-frame shear walls fulfills the acceptance criteria of FEMA P-695.

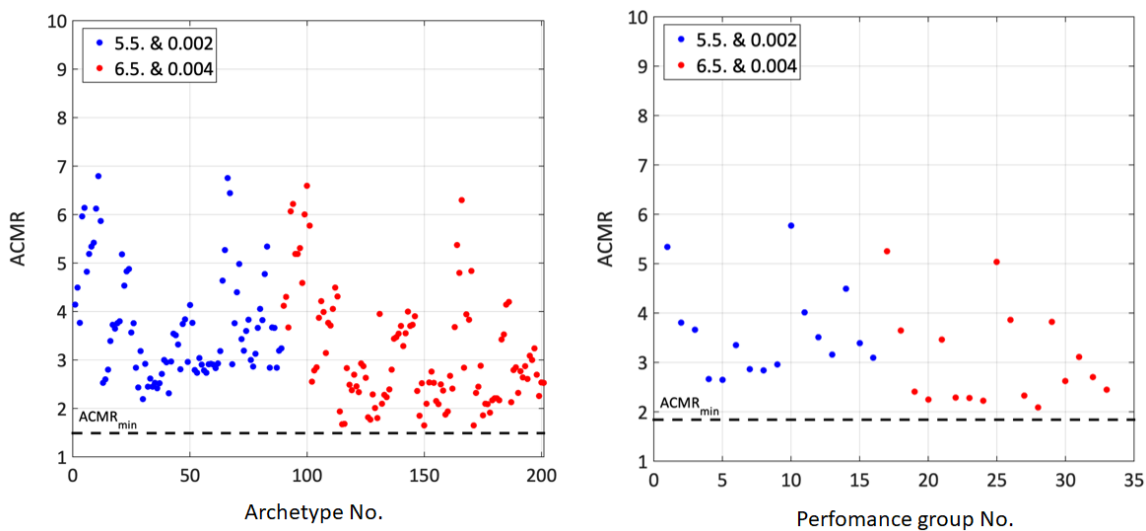


Figure 8. ACMR results for the buildings archetype and performance group analysed.

7 Conclusion

The following conclusions can be drawn, based on the analyses presented:

1. The current seismic provisions included in the NCh 433 standard assumes that an R-Factor of $R=5.5$ provides an acceptable level of collapse safety. However, the results of this research reveal that $R=6.5$ also meet the collapse performance

- objectives of the FEMA P-695 methodology. Therefore, this new R-Factor could be approved as the design seismic factor for the studied structural system. Therefore, this research project recommends a $R=6.5$ value for R-Factor in Chile.
2. It was found that the maximum inter-story drift included in NCh 433 standard had a significant impact in the structural design of the wood light-framed buildings. Two interest combinations of parameters for R-Factor & Δ were studied in detail. The results show that the combination of current NCh433 standard parameters $R = 5.5$ & $\Delta = 0.002$ leads to safe, but conservative and stiff buildings.
 3. It was also verified that the structural archetype designs for a maximum inter-story drift limit of 0.004 (0.4%) also met the collapse evaluation methodology limits. As a result, it was possible state that building designs are safe for up to 6-stories in height. Therefore, the maximum inter-story drift limit of 0.004 could be implemented for structural designs of the wood light-frame systems studied, as long as non-structural elements in buildings construction are protected and properly designed for the seismic forces at their interface with the main structure.

8 References

- INFOR - Instituto Forestal, (2017): El sector forestal chileno 2017 - Chilean forestry sector 2017. <https://simef.minagri.gob.cl/bibliotecadigital/handle/123456789/15910>.
- Cámara Chilena de la Construcción, (2014): “Balance de la Vivienda en Chile”. Disponible en: <http://www.cchc.cl/wp-content/uploads/2014/07/Balance-de-la-Vivienda-2014.pdf>
- FEMA, (2009): Quantification of Building Seismic Performance Factors. Federal Emergency Management Agency, Washington, D.C.
- INN - Instituto Nacional de Normalización, (2009): NCh 433 Of96 Mod2009, Diseño Sísmico de Edificios.
- Krawinkler H, Parisi F, Ibarra L, Ayoub A, Medina R, (2001): Development of a Testing Protocol for Woodframe Structures. CUREE Report W-02, Task 1.3.2, Consortium of Universities for Research in Earthquake Engineering. Richmond, California.
- Guiñez, F., Santa-Maria, H., Almazán, J., (2019): Monotonic and Cyclic Behaviour of Wood Frame Shear Walls for Mid-Height Timber Buildings. *Engineering Structures*. 189. 100-110. [10.1016/j.engstruct.2019.03.043](https://doi.org/10.1016/j.engstruct.2019.03.043).
- American Wood Council, (2015): Special Design Provisions for Wind and Seismic, ANSI/AWC SDPWS-2015, Leesburg, VA.
- Pang W, Hassanzadeh S. (2012): Corotational model for cyclic analysis of light-frame wood shear walls and diaphragms. *J Struct Eng*;139:1303–17. [doi:10.1061/\(asce\)st.1943-541x.0000595](https://doi.org/10.1061/(asce)st.1943-541x.0000595).

- Cárcamo S., (2017): Informe Nº 7 – Configuraciones arquitectónicas propuestas, Proyecto Corfo 16BPE-62260. Centro de Innovación en Madera CIM-UC.
- Instituto Nacional de Normalización. NCh 1198: Madera - Construcciones en Madera – Cálculo. 2014, Santiago.
- Rossi S, et al., (2015): Seismic Elastic Analysis of Light Timber-Frame Multi-Storey Buildings: Proposal of an Iterative Approach, *Constr. Build. Mater.* <http://dx.doi.org/10.1016/j.conbuildmat.2015.09.037>
- NBCC, (2005): National Building Code of Canada. Part 4: Structural Design. Canadian Commission on Building and Fire Codes, National Research Council of Canada (NRCC), Ottawa, Canada.
- Nassani D, (2014): A Simple Model for Calculating the Fundamental Period of Vibration in Steel Structures. Hasan Kalyoncu University. Turkey.
- BSSC, (2003): FEMA 450: Recommended Provisions for Seismic Regulations for New Buildings and Other Structures. Building Seismic Safety Council, National institute of building sciences, Washington DC.
- Centre d'expertise sur la construction commerciale en bois (CECOBOIS), (2015): Guide technique sur la conception de bâtiments de 5 ou 6 étages à ossature légère en bois - Volume 2: Exemple de calcul d'un bâtiment de six étages à ossature légère en bois. Dépôt légal Bibliothèque nationale du Québec.
- Newfield, G., Ni, C., Wang, J., (2013): A Mechanics-Based Approach for Determining Deflections of Stacked Multi-Story Wood-Based Shear Walls. FPInnovations, Vancouver, B.C. and Canadian Wood Council, Ottawa, Ont.
- Newfield, G., Ni, C., Wang, J., (2015): Design Example: Design of Stacked Multi-Storey Wood-Based Shear Walls Using a Mechanics-Based Approach. FPInnovations, Vancouver, B.C. and Canadian Wood Council, Ottawa, Ont.
- Leung T. et al, (2010): "Predicting Lateral Deflection and Fundamental Natural Period Of Multi-Storey Wood Frame Buildings". Paper for the world conference on timber engineering WCTE-10.
- APEGBC, (2011): Structural, Fire Protection and Building Envelope Professional Engineering Services for 5 and 6 Storey Wood Frame Residential Building Projects (Mid-rise buildings). APEGBC Technical and Practice Bulletin. Professional Engineers and Geoscientists of BC. Canadá.
- Pei S, van de Lindt J W., (2009): Coupled Shear-Bending Formulation for Seismic Analysis of Stacked Wood Shear Wall Systems. *Earthquake Engineering And Structural Dynamics*. 38: 1631-1647.
- Folz, B., Filiatrault, A. (2001): Cyclic Analysis of Wood Shear Walls. *Journal of Structural Engineering*, 127(4): 433–441.
- Estrella, X., Almazán, J., Guindos, P., Santa María, S., and Malek, S. (2019a): Seismic Design Factors for Wood Frame Buildings. IV Latin American Conference on Timber Structures, Montevideo, Uruguay.

- Estrella, X., Guindos, P., Almazán, J.L., Malek, S., (2020): Efficient Nonlinear Modeling of Strong Wood Frame Shear Walls for Mid-Rise Buildings. *Engineering Structures* 215, 110670.
- Estrella, Xavier & Guindos, Pablo & Almazán, Jose. (2019b). Ground Motions for FEMA P-695 Application in Subduction Zones. *Latin American Journal of Solids and Structures*. 16. 10.1590/1679-78255848.
- FEMA, (2000): FEMA 356 - Prestandard and Commentary for the Seismic Rehabilitation of 869 Buildings. Federal Emergency Management Agency, Washington, D.C.
- Pei, S, van de Lindt J W. User's Manual for SAPWood for Windows. Version 2.0. Colorado State University. 2010.
- Santa María H, Caicedo N, Montañó J, Almazán J L, (2016): Towards Timber Mid-Rise Buildings in Chile: Structural Design Challenge and Regulations Gaps. In: *World Conference on Timber Engineering*. 2963-2970.

Discussion

The paper was presented by J Montano

D Dolan asked did you only deal with platform frame as he was involved in the design of two balloon frame systems in Chile where lack of proper guidance from code on ductility drove the design towards using of base isolators.

J Montano said that the study did not consider balloon frame construction. D Dolan said that most construction in Chile seemed to be more interested in balloon frame construction. J Montano said survey data showed that platform framing is more popular in Chile.

A Ceccotti asked whether there is a timber design code in Chile dealing with this area. J Montano said there are two codes in Chile related to this. For statics there is a NCH for timber design but it does not cover shear walls. A general design code for seismic design would cover all material including timber. A Ceccotti commented that R factor depends on country structural code and if the code body is very conservative R factor for timber might be very different and more penalizing. D Dolan said R factor of 3 was used for the two buildings that he was involved in. A Ceccotto said R factors should be set for ones' own country.

R Dietsch commented that R factor of 6.5 in the conclusion should be tied to the type of construction and suggested an editorial check for the language of the manuscript.

Fire design model of I-joists in wall assemblies

Katrin Nele Mäger, Tallinn University of Technology

Alar Just, Tallinn University of Technology, RISE Research Institutes of Sweden

Tommy Persson, Masonite Beams AB

Alfred Wikner, Masonite Beams AB

Keywords: fire design, charring, load-bearing capacity, wooden I-joists, buckling

1 Introduction

I-joists are typically used as the load-bearing elements in timber frame assemblies (TFA) which consist of a combination of material layers – sheeting boards (claddings) and cavities which may be partially or completely filled with insulation (see Figure 1). The materials used in conjunction with a timber member in a TFA affect the heating of the timber member.

The behaviour of timber frame assemblies (TFA) with I-joists in fire is quite complex due to the composite action of the flanges and the web of an I-joist. The aim of the ongoing research project is to develop an easy to use, safe and reliable design model for the fire resistance calculations of I-joists in wall and floor assemblies. The new model follows the Effective Cross-Section Method (ECSM) philosophy and will be proposed to be included in the revised Eurocode 5 Part 1-2.

Two phenomena have to be considered according to the ECSM: charring and mechanical resistance. It is assumed that charring of wood is a material characteristic which is not dependent on the orientation of the structure (wall or floor). Charring of the flanges is primarily dependent on the cladding material and thickness. After the failure of the claddings the charring is influenced by cavity insulation. In this paper gypsum plasterboards as cladding and stone wool as cavity insulation have been tested and analysed.

The loss of strength and stiffness seen in wood at elevated temperatures is considered in the ECSM by a zero-strength layer. The zero-strength layer (ZSL) is an additional reduction of the cross-section to compensate for the reduction in strength and

stiffness properties. The development of the expressions to calculate the ZSL depths for compression elements is discussed in this paper.

Schmid et al (2011) proposed a first approach for strength reduction properties for a wall model with I-joists. The test results are included in the analysis of the current study.

The claddings on either side of the I-joist act as bracings against buckling in wall plane. In the fire situation the cladding might fall-off and the flange on the fire exposed side will remain unbraced. Buckling length will increase but the web of the I-joist will provide some stiffness (see Figure 1).

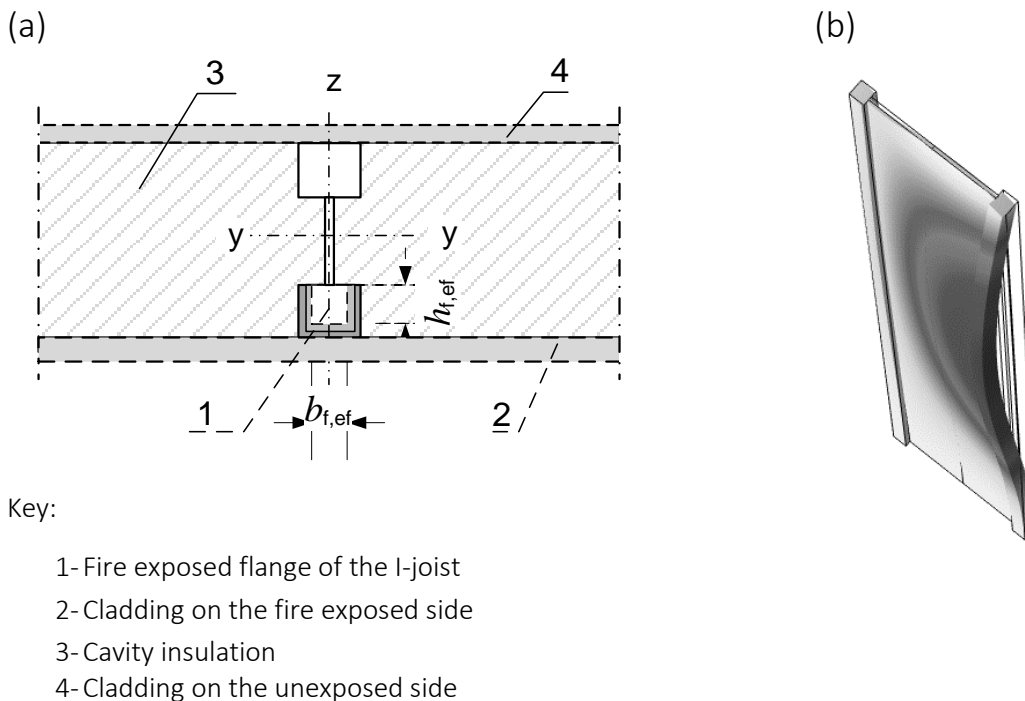


Figure 1. Timber frame assembly with I-joists exposed to fire. Cross-section (a) and the typical buckling mode after fall-off of cladding (b).

This paper includes analysis of performed tests and finite element simulations. Testing of various types of I-joists have been conducted in ambient conditions and in furnaces in standard fire. The ambient tests have provided an insight into the mechanism of buckling of the I-joist with full and reduced cross-sections. The latter was an imitation of the principles of calculation of the ECSM. Additionally, a database of full-scale furnace fire test results has been gathered and is used as verification of the model parameters.

2 Experimental and theoretical investigations

2.1 Model-scale furnace fire tests

A total of 7 horizontal model-scale tests (MST) have been performed with specimens with I-joists in a cubic metre furnace at RISE in Boras (see Table 1). Additionally, the test results by Schmid et al (2011) have been used for further evaluation. All tests followed the ISO 834 standard temperature-time curve according to EN1363. Each test

specimen had two test beams within a frame and featured various insulation materials. The fire exposed side was initially protected by a 15-mm type F gypsum plasterboard. The unexposed side was covered by a wood-based board. All tested cross-sections had a height of 220 mm.

Table 1. Parameters measured from the model scale furnace tests.

Test no	Beam B1		Beam B2		Insulation	t_{ch} [min]		$t_{ch,2}$ [min]		t_f [min]	$t_{ch,w}$ [min]		t_{test} [min]
	Producer	Flange $h_f \times b_f$ [mm]	Producer	Flange $h_f \times b_f$ [mm]		B1	B2	B1	B2		B1	B2	
19-1	1	97x47	1	47x47	GW	25,8	25,8	36,0	33,9	25,8	no	no	46
19-2	1	97x47	1	47x47	SW	29,0	29,3	47,3	52,4	53,2	no	69,6	70
20-1	2	45x36	2	96x39	GW	31,8	31,6	39,1	38,3	38,0	50,7	no	51,8
20-2	2	45x36	2	96x39	SW	29,8	30,9	36,3	35,7	33,7	54,4	no	55,4
20-3	1	97x47	2	96x39	Void	33,7	31,5	34,5	34,4	34,3	34,5	34,4	34,9
20-4	3	47x45	3	97x45	SW	32,8	30,7	40,6	38,9	35,2	61,5	no	63,4
20-5	4	90x39	3	97x45	SW	29,7	27,4	37,1	39,8	34,1	69,1	no	69,3
111*	1	47x47			SW	25,7		-		-			27
112*	1	47x47			SW	23,9		25,3		-			42,2
113*	1	47x47			SW	26,5		27,9		-			48,2
114*	1	47x47			SW	26,1		27,5		50,3			53,2
115*	1	47x47			SW	20,7		22,2		20,7			35,7
116*	1	47x47			SW	16,6		18,3		16,6			26,6
117*	1	47x47			SW	58,5		59,4		71,7			71,7
118*	1	47x47			SW	19,8		21,4		19,8			30,2
119*	1	47x47			SW	25,5		26,9		40,4			40,4

* Test results from Schmid et al (2011) research project. Values for $t_{ch,2}$ have been calculated using the component additive method.

Thermocouples (TC) were installed in various points on the tested I-joists. Each beam had two measurement stations, where the temperature on the exposed side, at 6, 12 and 18-mm depths, in the top corners of the exposed flange and on the web was measured. Additional TCs were applied on the exposed and unexposed side of the insulation layer.

After the test, the specimen was extinguished within 2 minutes. Then, the residual cross-sections were cleaned of loose char with a wire brush and measured. The residual areas of the exposed flange were compared with calculated areas (see 3.1.1).

2.2 Thermal simulations

A large amount of 2D thermal finite element simulations have been conducted using SAFIR v2014a1 software. The thermal properties were taken from Eurocode 5 Part 1-2 (2004) and Schleifer (2009). All structures were exposed to the ISO 834 standard temperature-time curve. The simulated sections were discretised into rectangular elements. The sizes of the elements were varied between 1x1 mm and 5x5 mm. The time steps were kept at maximum 5 seconds. The simulation programme is described in detail by Mäger & Just (2019).

The factors which were varied with each thermal simulation were the size of the flanges (both width and height), the length of the fire exposure (up to 120 minutes) and the thickness and fall-off time of the fire protection system (gypsum board).

2.2.1 Residual cross-section

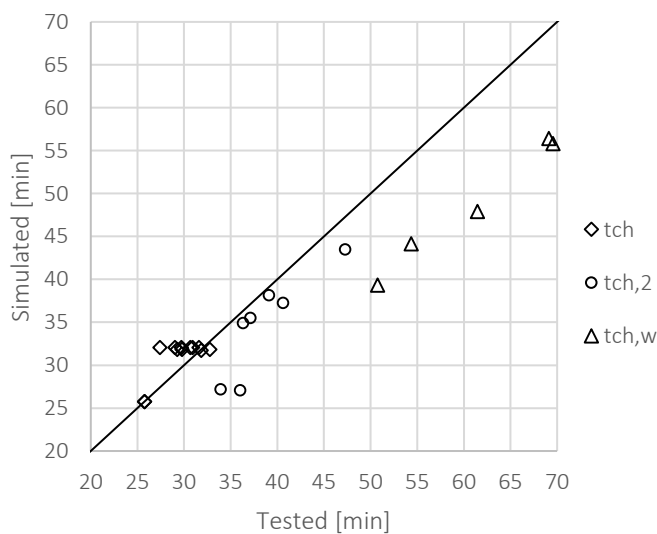
The results of the simulations were temperature distributions in the cross-section for each time step. These were further analysed using a MATLAB script to calculate the residual area (nodes with the temperature below 300°C) of the fire exposed flange for each time step based on summarising the areas of the trapezoidal slices.

The charring coefficients were developed using linear regression of the relative reduction of area. Based on the system of simulations, coefficients which best matched with all simulated configurations were derived. Different charring phases depending on the start time of charring and the failure time of the protective cladding were analysed.

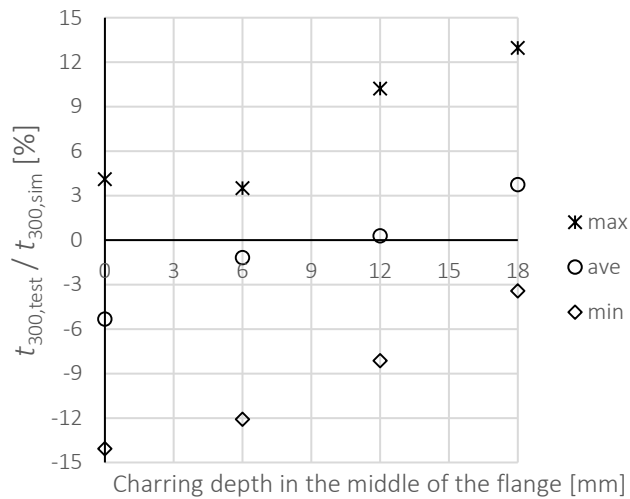
2.2.2 Comparison to MST

The results of the thermal simulations have been compared to MST results. The development of the charring depth in the middle of the flange is very comparable between the simulations and tests. However, some differences were identified, especially in the behaviour of the protective cladding (gypsum plasterboard). The same failure times t_f were induced in the simulations. The start time of charring t_{ch} behind the protective cladding occurred, on average, 5% earlier in the tests (see Figure 2a). This suggests that the generic thermal properties of gypsum plasterboard may be different from the tested products.

The start time of lateral charring $t_{ch,2}$ in simulations is slightly shorter than measured in tests. Additionally, the start time of charring on the web is even more conservative. This would hint to the simulations being more conservative with increased number and thickness of the specimen compared to fire tests.



(a)



(b)

Figure 2. Comparison of start times of charring of the flange, lateral side and web in tests and simulations (a). Comparison of charring depth in the middle of the exposed flange (b).

The comparison of times to reach certain charring depths measured in tests and simulations is shown in Figure 2b. A clear trend towards more conservative values with increasing charring depths can be seen. The start time of charring (at a depth of 0-mm) and charring depth of 6 mm occur on average 5% and 1,3% earlier in tests than in simulations. The results of the thermal simulations are still valid, because the variability of products within the same material type is large and therefore the generic thermal properties may not capture every tested combination of products.

2.2.3 Effective cross-section

The depths of the zero-strength layer (ZSL) have been derived from thermal simulations. The temperature distributions in the cross-section were substituted with reduction factors for strength according to Eurocode 5 Part 1-2 (2004). An assumption has been made that all load is carried by the flanges, which will, depending on the load situation, be in pure compression or pure tension.

Each element of the exposed flange, with an area of 1 mm² was given the average reduction factor for strength of the nodes in its corners (which is also equal to the reduction of the area). After calculating the total resistance by summarising the elements with reduced area, the total effective area could be derived. The effective area is assumed to have the strength of unheated timber.

The depth of the ZSL is the difference between the charred area and the effective area (see Figure 5), assuming that the zero-strength layer depth is the same from the fire exposed side and the lateral sides of the exposed flange and that the charred area is rectangular (calculated according to 3.1 and Mäger & Just (2019)).

Graphs where the ZSL depths from all simulations were plotted as a function of the notional charring depth from the exposed side were analysed to derive the expression for the ZSL. The relationship to the failure time of the cladding was evident as the longer the failure time is, the greater the range of the ZSL.

2.3 Compression tests at ambient temperatures

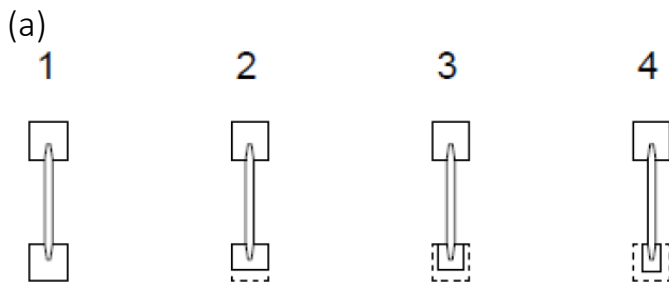
Two series of compression tests were carried out at RISE in Skelleftea in 2019 and 2020 to investigate the buckling behaviour of I-joists.

In test series 1 the effect of the size of flange cross-section on the fire exposed side was studied. Two different cross-section heights of I-joists were tested - originally 200 mm and 500 mm. Two different flange sizes were tested – 47x47 mm and 70x47 mm. All test specimens in test series 1 were loaded in the middle of original cross-section height. The non-exposed flange was braced with a wooden board and fasteners with 200 mm distance between them. The size of the unbraced flange was reduced according to the types shown in Figure 2a.

In test series 2 the effect of load placement and bracing was studied. Three different cross-section heights of I-joists were tested - 200 mm, 300 mm and 400 mm. The test load was placed in the middle of the original cross-section height, on the non-exposed flange and on the exposed flange. The non-exposed flange was braced with wooden board and fasteners with 200 mm distance between them. The exposed flange was unbraced or braced similarly to the non-exposed flange.

The cross-section parameters and results of the tests are presented in

Table 2 and Table 3.



Type	Size of	
	flange height	flange width
1	100%	100%
2	70%	100%
3	70%	70%
4	75%	50%

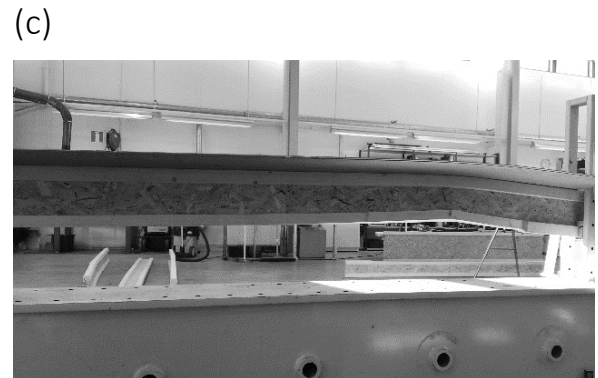
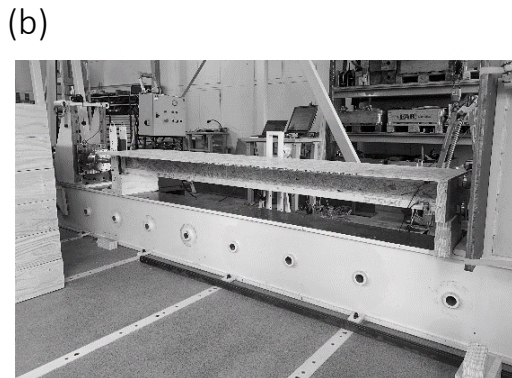
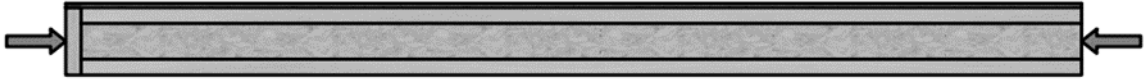
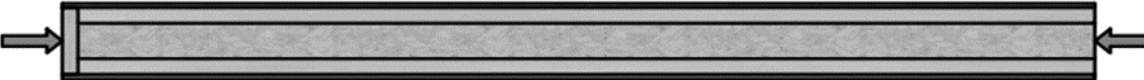
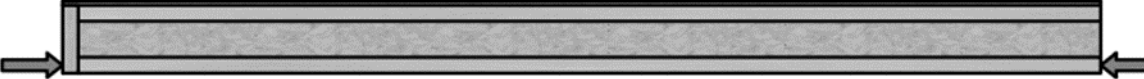
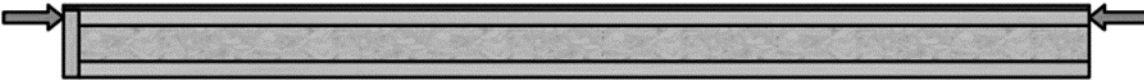


Figure 3. Types of reduced cross-sections of I-joists (a) test setup (b) and typical rupture mode (c).

Table 2. Compression tests at ambient temperature. Series 1.

I-joist	Type of reduced cross-section	Cross-section height	Flange size at fire exposed side $h_f \times b_f$	Maximum load [kN]					
H200	1	200	47x47	74,1	102,2	97,8	78,5	89,7	97,7
H200	2	186	33x47	75,7	77,5	91,8	75,5	90,1	73,0
H200	3	186	33x33	60,2	65,4	69,5	52,2	73,1	75,7
H200	4	176	23x35	49,5	50,2	58,8	57,7	57,8	
HI 200	1	200	47x70	192	154,6	137,5			
HI 200	4	176	35x35	66,5	82,6	90,8			
H 500	1	500	47x47	27,3	55,1	56,6			
H 500	4	476	23x35	33,5	30,8	31,0			

Table 3. Compression tests at ambient temperature. Series 2.

I-joist	Type of reduced cross-section	Cross-section height	Flange size at fire exposed side $h_f \times b_f$	Maximal load [kN]		
						
C201	1	200	47x47	69,7	78,4	78,8
C301	1	300	47x47	44,5	46,9	48,1
C401	1	400	47x47	38,5	39,8	42,5
						
C202	1	200	47x47	80,9	95,8	92,7
C302	1	300	47x47	90,6	72,7	97,8
C402	1	400	47x47	110,5	92,6	104,2
						
O201	1	200	47x47	51,1	43,6	39,9
O301	1	300	47x47	31,6	31,4	27,2
O401	1	400	47x47	27,9	25,8	24,1
						
OP201	1	200	47x47	73,9	76,6	69
OP301	1	300	47x47	54,1	70,1	68,6
OP401	1	400	47x47	67,4	65,7	67,6

Load-bearing capacities of H500 are significantly lower than those of H200. This is caused by the lower stiffness of the web of the H500 allowing buckling under lower load. The load-bearing capacity of the non-braced flange is crucial for the load-bearing capacity of the wall.

In test series 2 the capacities under different load placement were studied. Differences were observed under load placed centrally or one of the flanges. The cases with one or both flanges braced were compared.

Test results show that the load-bearing capacity of I-joists with a 200-mm cross-section height was reduced by 16% when one flange was released. I-joists with a cross-section height of 300 mm and 400 mm lost 47% and 60% of the initial capacity respectively.

Rupture of the test specimens occurred always at the location of a knot in the unbraced flange at approximately 2 to 2,3 m from the support. Buckling occurred in wall plane in all tests.

For the derivation of the design model the unbraced flange is considered as an axially loaded member. The web is considered as a continuous spring support.

Based on the test results the relation between the web stiffness and load-bearing capacity was analysed and the factor k_w for the reduction of buckling length according to the web stiffness was derived. Buckling length of the unbraced flange is considered as a total wall height (L_z) which is reduced according to the stiffness provided by the web ($k_w L_z$). The latter is considered by the spring coefficient for the web.

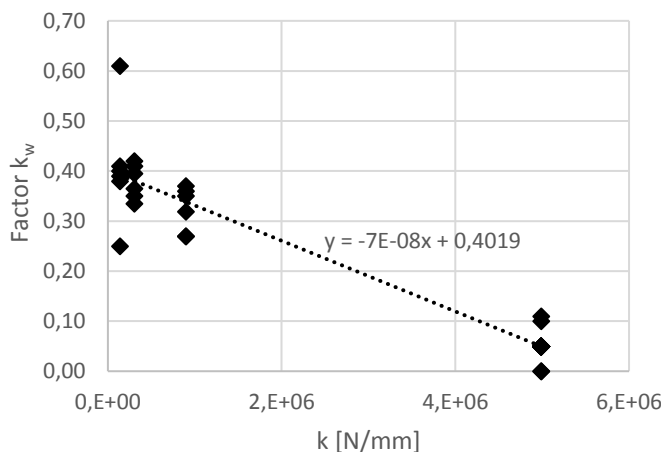
Spring coefficient k for the web as cantilever is derived as follows:

$$k = F/\delta \tag{1}$$

$$\delta = Fh_w^3 / (3E_{web}I_{web}) \tag{2}$$

where $E_{web}I_{web}$ is the bending stiffness of the web around vertical axis (x) with the width of the cross-section taken as the entire height of the column. h_w is the cross-section height of the web (between flanges). Buckling length in wall plane is assumed to be replaced by a fictive buckling length $k_w L_z$, where k_w is a buckling length factor derived from test results (see Figure 4a).

(a)



(b)

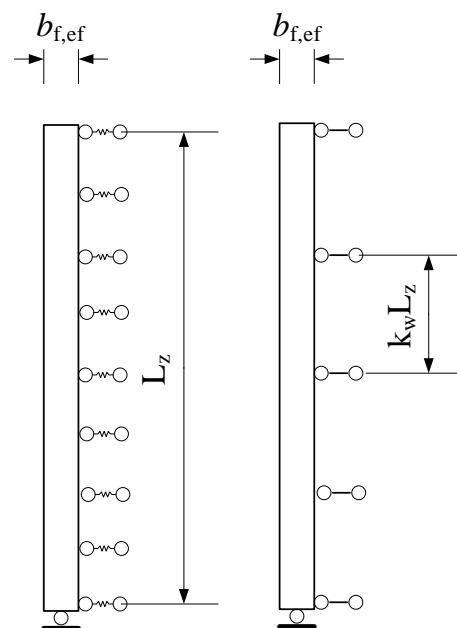


Figure 4. Relation between buckling length factor and web stiffness (a) and application of the fictive buckling length (b).

3 Design model

The following design model is proposed in this paper. The dimensions of the fire exposed flange of the I-joist should be reduced by charring depth and zero-strength layer depth. Then, the buckling analysis should be performed.

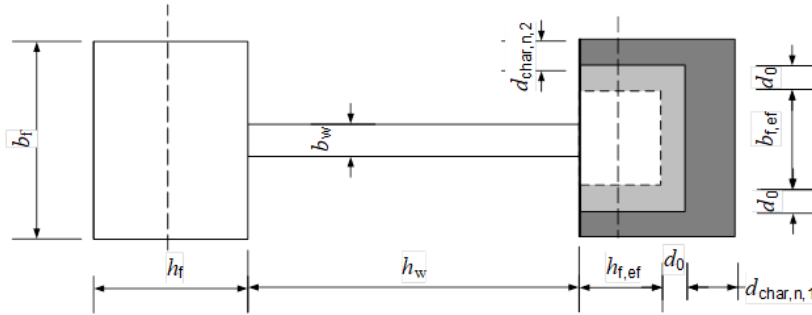


Figure 5. Dimensions of the I-joist

3.1 Charring depth

The calculation model for charring has been described in Mäger & Just (2019). In the following, improved values for charring coefficients are given.

The calculation model for charring is applicable for floor and wall assemblies. The following parameters should be used for timber frame assemblies with I-joists and PL1 cavity insulations (for example stone wool).

The combined conversion and section factor $k_{s,n,1}$ for the fire exposed side should be calculated as:

$$k_{s,n,1} = 9,48 \cdot b_{fl}^{-0,43} \quad (3)$$

The combined conversion and section factor $k_{s,n,2}$ for the lateral sides should be calculated as:

$$k_{s,n,2} = 2,25 \cdot h_{fl}^{-0,13} \quad (4)$$

The post-protection factor k_3 should be calculated as:

$$k_3 = 6,52 - 0,04 \cdot t_f \quad (5)$$

The consolidation time t_a should be calculated as:

$$t_a = 1,04 \cdot t_f \quad (6)$$

The consolidation factor k_4 should be calculated as:

$$k_4 = 0,91 + 0,021 \cdot t_a \quad (7)$$

3.2 Zero-strength layer depth

The other part of the analysis of I-joists in a wall assembly is the analysis of the load-bearing capacity. In fire, it may be a combination of various effects which will be discussed further on.

The design model assumes that load is divided onto the flanges as described before.

For I-joists in wall assemblies, the depth of the zero-strength layer was derived based on the reduction factors for compression strength depending on temperature. These values may be useful also for beams with intermediate supports.

$$d_0 = -\frac{t_f}{1800} \cdot (d_{\text{char},n,1})^2 + \frac{t_f}{60} \cdot d_{\text{char},n,1} + 3,7 \cdot \ln(b_{\text{fl}}) - 4 \quad (8)$$

If the required fire resistance is less than the failure time of fire protection t_f then the required fire resistance time should be used in Formula (8) instead of t_f .

3.3 Stability

There are 3 different cases considering buckling in the walls plane:

- Case 1: Both flanges are braced – there are noggins or boards on the fire exposed side and on the unexposed side.
- Case 2: Both flanges are not braced.
- Case 3: Flange on the fire unexposed side is braced while the flange on fire exposed side is not.

For Case 1 and Case 2 the buckling analysis is made according to EN 1995-1-1 with taking the effective moment of inertia into account.

For Case 3 the buckling out of wall plane is considered with taking into account the whole cross-section. The web dimensions are to be reduced based on the used material.

Buckling analysis in wall plane should be performed for unbraced flange taking into account the coefficient k_w as follows:

$$k_w = 0,4 - 7 \times 10^{-8} k \geq 0,1 \quad (9)$$

where

$$k = 3E_{\text{web}} I_{\text{web}} / h_w^3 \quad (10)$$

$$I_{\text{web}} = L_z \cdot b_w^3 / 12 \quad (11)$$

where

k is a web stiffness;

I_{web} is the moment of inertia of the web;

b_w is the thickness of the web;

h_w is the cross-section height of the web

E_{web} is the modulus of elasticity of the web;

L_z is the buckling length of the I-joist in walls plane.

For Case 3, the distribution of axial load between the flanges is essential.

As a simplified approach, the load should be distributed between the flanges according to the relation between the cross-sectional areas taking into account the eccentricity in the required fire resistance time.

4 Verification

The charred cross-sections calculated using the charring coefficients presented above have been compared with the residual cross-sections measured in model-scale fire tests. Figure 6 shows the comparison of tested and calculated times to reach the residual cross-section from tests. In most cases, the calculated charred cross-section is reached in a shorter time than in the tests, therefore, being conservative.

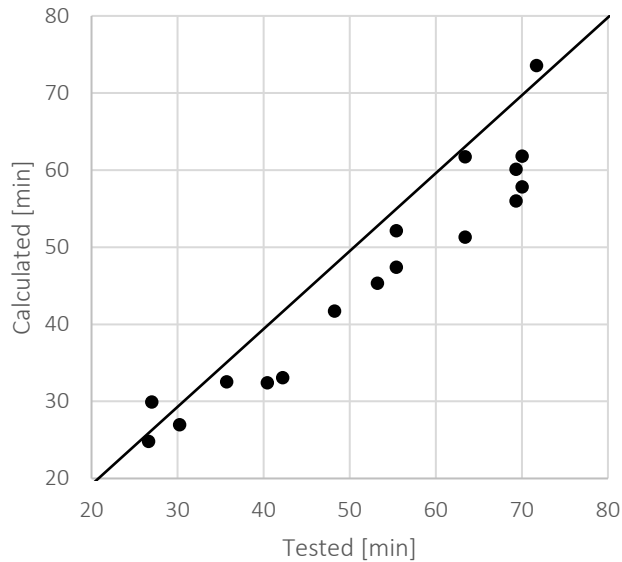


Figure 6. Comparison of calculated and tested times to reach the charred cross-section of the tests. Safe side below the solid line.

The proposed design model has been verified using data from full-scale fire tests provided by industry partners. The parameters of the specimens are described in Table 4. Comparison of tests and calculated fire resistances are shown in Figure 7.

Table 4. Loaded full-scale fire tests of walls.

Test wall	I-joist		Insulation	t_f [min]	t_{test} [min]	Test load [kN/stud]
	Height h	Flange $h_f \times b_f$ [mm]				
W1	250	47x47	WF	61	61	17
W2	200	47x47	SW	21	57	22
W3	200	47x47	WF	77	85	22
W4	200	47x47	GW	47	69	24
W5	200	47x47	WF	27	40	17
W6	200	47x47	WF	102	113	50
W7	250	47x47	WF	66	83	54

The calculation parameters of PL1 insulation were used to describe the tests with stone wool. The other types of insulation were considered using the appropriate parameters developed for rectangular cross-sections by Tiso (2018).

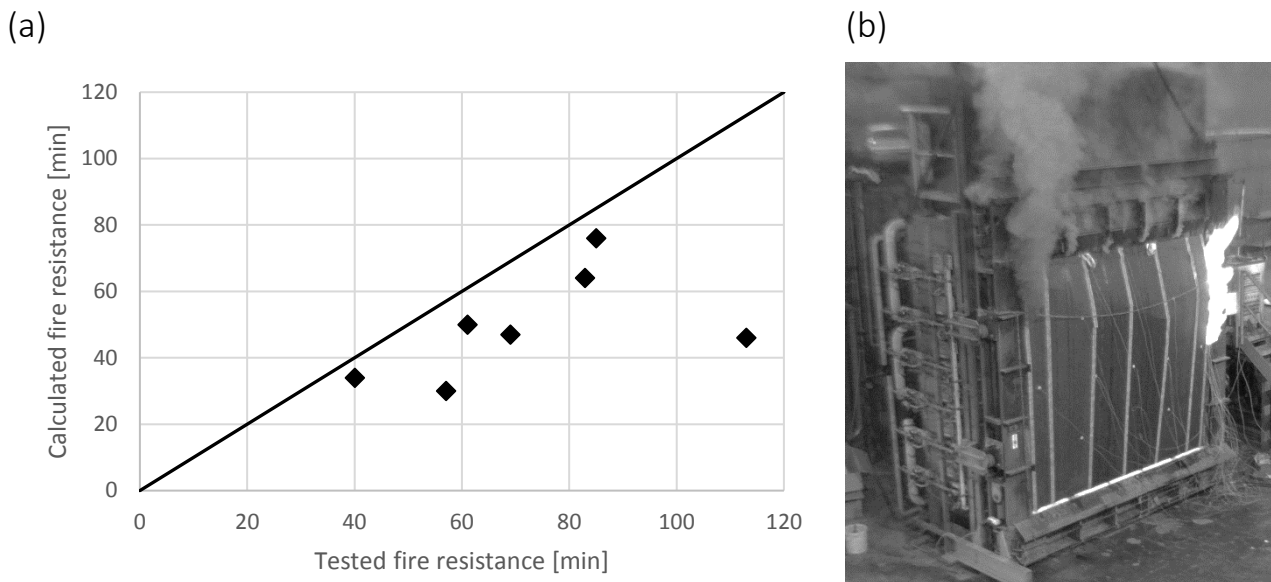


Figure 7. Comparison of calculated and tested fire resistance times (a) and picture from the failure of the wall in loaded full scale fire test (b)

5 Discussion

The research presented in this paper has provided an unexpected and little explored set of challenges. For I-joists, being slender and highly optimised products, every minute of gained fire resistance is important.

The vast amount of thermal simulations that have been analysed to derive the charring coefficients and the expressions for the zero-strength layer have taken the state-of-the-art much further for light timber frame assemblies with I-joists. Many possible approaches to derive the necessary parameter values have been attempted within this project with only the successful results presented here.

The buckling behaviour of I-joists in walls occurs as a complex of phenomena. This paper provides the results of experimental work and analysis of specific compression tests with wood-based I-joists. A relatively simple approach to consider a reduced buckling length for I-joists exposed to fire with one unbraced flange has been developed. Work is continued to further the test results by simulations.

The most important parameter in the fire design of timber frame assemblies with relatively small members is the failure time of the fire protection system. This is considered using 95% guaranteed values in the fire design models for Eurocode. Because of that the other design parameters (charring coefficients) can be determined based on mean values.

The rupture of the load bearing I-joist with relatively small flanges is sensitive to sizes and locations of knots. The reduction of the flange can lead to a different compression strength than the original strength value. For tests at ambient conditions the compression strength based on the relation between bending strength and MOE is used. The MOE of all tested I-joists was determined. Then, some joists were tested in

bending until rupture and the relationship between bending strength and MOE was developed. For fire tests the characteristic strength and MOE values for the declared strength class according to EN 338 (2003) are used for further evaluation. That makes the analysis of the test results slightly uncertain concerning the exact strength values and explaining the bigger safety margin. The relationship of the MOE of the I-joist and the compression and tensile strength of flanges was taken to be the same as for structural strength graded timber according to EN 338 (2003).

In the present study there was always a knot observed at the place where rupture occurred. The location of knots is not controlled while the size and frequency of appearance of the knots are guaranteed by quality control done in the factories. The design model should assume a knot in the most unfavourable location when considering load bearing capacity. The effect of knots should be studied further.

The glue line between the web and flange did not lose its integrity in any of the tests with any of the products that were evaluated. Glue line integrity at elevated temperatures of finger joints is assumed to not be relevant for compression members due to the joint being pushed together regardless of the type of adhesive.

Acknowledgements

The authors would like to thank RISE Research Institute of Sweden, Masonite Beams, James Jones, Metsä Wood and Steico for their material, knowledge and support.

The work was partly supported by the FIREWOOD project (2019-2022) funded by Era-NET cofund Forest Value and Estonian Research Council grant PRG820.

References

- Eurocode 5 (2004): Design of timber structures - Part 1-1: General and rules for buildings. CEN. (EN 1995-1-1).
- Eurocode 5 (2004): Design of timber structures - Part 1-2: General - Structural fire design. CEN. (EN 1995-1-2).
- EN1363-1:2020. Fire Resistance Test – Procedure. CEN.
- Mäger, K N, Just, A (2019): Preliminary design model for wooden I-joists in fire. INTER meeting. Tacoma.
- Schleifer, V (2009): Zum Verhalten von raumabschliessenden mehrschichtigen Holzbauteilen im Brandfall. Thesis (PhD). ETH Zürich.
- Schmid, J, Just, A, König, J (2011): Fire exposed wooden I-joists for wall assemblies. Stockholm: SP Technical Research Institute of Sweden. (SP Report 2011:27).
- Tiso, M (2018): The Contribution of Cavity Insulations to the Load-Bearing Capacity of Timber Frame Assemblies Exposed to Fire. TTÜ Press, Tallinn. (PhD Thesis).
- EN 338 (2003): Structural timber–strength classes. CEN.

Discussion

The paper was presented by K N Mäger

A Frangi asked whether we have the consolidation phase (Phase 4). K N Mäger responded yes. For small rectangular sections we did not have this but for I joist this is possible to be a bit more accurate by adopting a reduced slope. A Frangi commented that Phase 3 is very short. K N Mäger agreed but this is useful for I-Joist considerations. A Frangi asked if the model could be trusted to predict with accuracy one to two minutes differences in view of the complex behaviour. K N Mäger responded that there are difficulties in fire test to take good pictures but the model predicted failure mode is close to reality. Also she is confident with time to failure predictions based on test results comparisons.

BJ Yeh asked why the testing with I joist as wall elements as this application is uncommon in N. America. K N Mäger said in Sweden eight storey buildings have been built with I-joist as wall elements because of thermal efficiency requirements. BJ Yeh commented that in the picture showing the loaded confirmation tests wall sheathing should be placed on the fire side (hot side). K N Mäger responded that the configuration came from industry practice.

S Aicher commented that the effective cross section of the I Joist flange might have been too small. This assumption might contribute to the calculated results being too conservative. K N Mäger agreed but decided not to challenge Eurocode values.

F Lam asked about the variability of the full size wall tests with no replicates. K N Mäger agreed but cost of full scale fire tests are high and small specimen fire tests with replications work well.

Vibrations of floors – Comparison of measured data and suggested design

Patricia Hamm, Biberach University of Applied Sciences, Germany

Julian Marcroft, MiTek Holding, UK

Tomi Toratti, Federation of the Finnish Woodworking Industries, Finland

1. Introduction

This paper analyses the new design rules for the vibration performance of floors which are currently being drafted in CEN TC250/SC5 within WG3 Sub-group 4 “Vibrations”. These rules are being tested against existing timber floors. The hand calculation methods are applicable to timber floors on rigid (wall) supports as well as on flexible (beam) supports, pre-published in [1].

The basic idea was to change the rules in a way, that the perception will be the most important value. Therefore, it was decided to introduce the response factor R . The perception is dependent on the first natural frequency as below:

$$a_{\text{rms}} < \text{Response factor} \times a_{\text{rms,base}} \quad \text{when } f_1 < 8 \text{ Hz}$$

$$v_{\text{rms}} < \text{Response factor} \times v_{\text{rms,base}} \quad \text{when } f_1 \geq 8 \text{ Hz}$$

The equations for the hand calculation of acceleration of the floor due to resonant excitation a_{rms} and the velocity due to a cyclic step load v_{rms} have been developed.

From 2007 to 2009 a lot of wooden floors were measured in order to find suitable evidence and input to the equations given in EC5. As these vibration measurements were conducted in the context of a German research project, most of the floors were located in Germany, some in Austria or Switzerland. Several other studies from Finland and UK have also been considered.

2. Explanation of proof of floor vibration

Figure 1 shows the principle way and the most important equations of the proof.

Table 1 gives the limit values of deflection due to point load and the response factors depending on the performance levels.

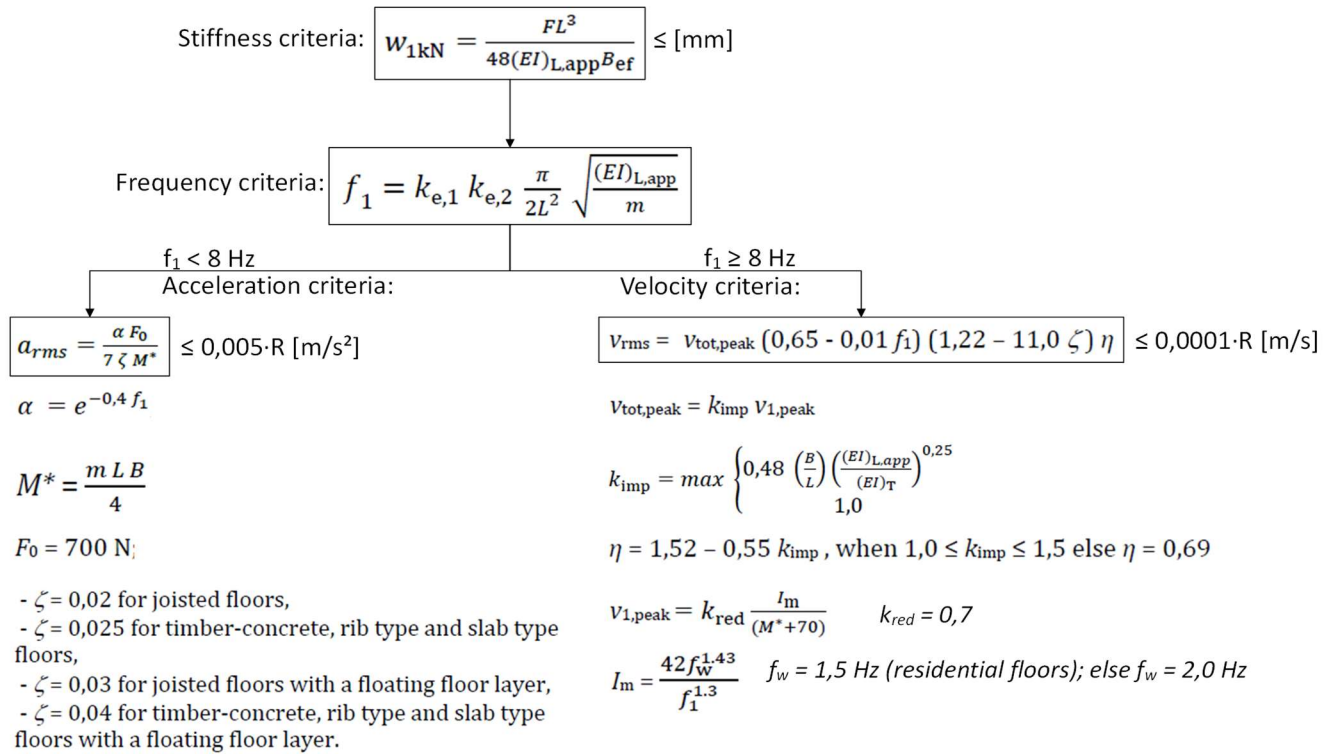


Figure 1. Flowchart and equations of the proof of floor vibration.

Table 1. Limit values and response factor R according to performance level.

Criteria	Floor performance levels					
	Level I	Level II	Level III	Level IV	Level V	Level VI
<u>Stiffness criteria</u> for all floors w _{1kN} [mm] ≤	0,25		0,5	0,8	1,2	1,6
Response factor R	4	8	12	20	30	40
<u>Frequency criteria</u> for all floors f ₁ [Hz] ≥			4,5			
<u>Acceleration criteria</u> for resonant vibration (f ₁ < 8 [Hz]) design situations a _{rms} [m/s ²] ≤			0,005 R			
<u>Velocity criteria</u> for transient vibration (f ₁ ≥ 8 [Hz]) design situations v _{rms} [m/s] ≤			0,0001 R			

3. Application of the equations on measured German floors.

These equations have been applied on the measured floors and compared to the subjective evaluation. Figure 2 shows the coherency between the subjective evaluation and the calculated response factor R due to acceleration of floors with frequency lower than 8 Hz.

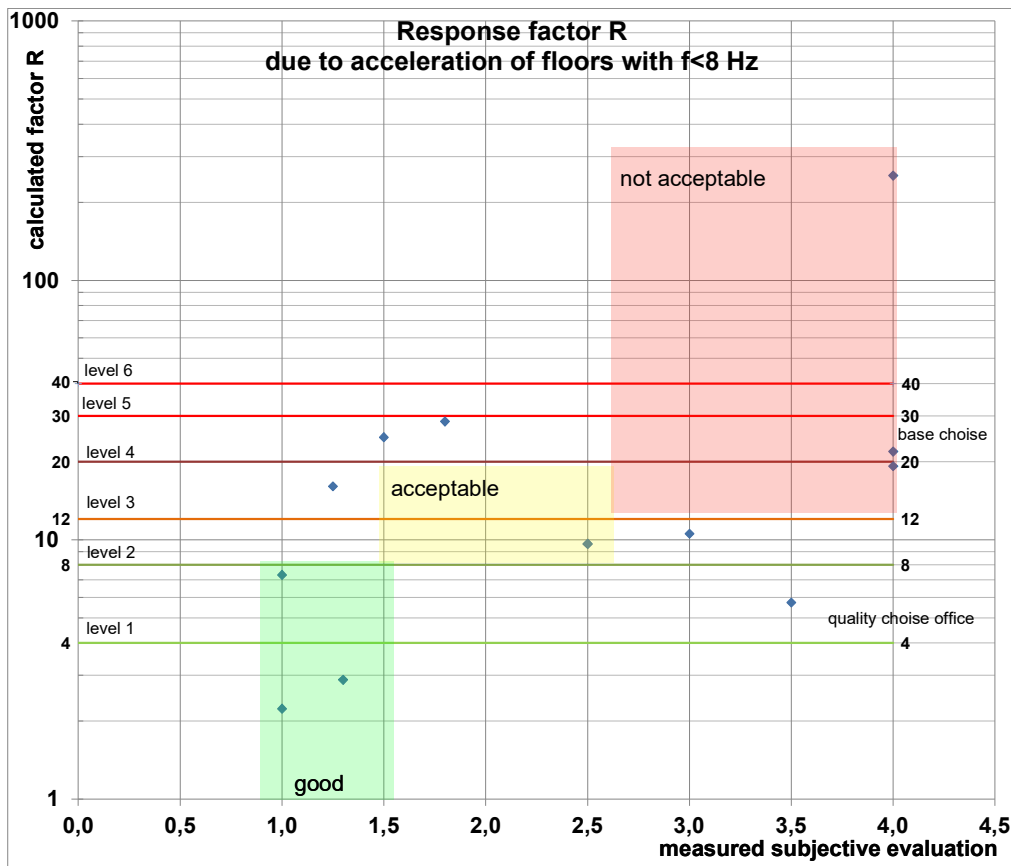


Figure 2. Comparison between evaluation and calculated response factors for low frequency floors (<8 Hz).

Figure 3 shows the same, but there are the floors with frequencies higher than 8 Hz. So, the response factor R was calculated based on velocity.

Marked by the red circle there are several floors with good performance due to calculation ($R < 8$), but not that good by subjective evaluation. This was even worse when all floors were designed with walking frequency $f_w = 1,5$ Hz. In the actual design draft, only residential floors are designed with walking frequency 1,5 Hz, the others with 2,0 Hz. The walking frequency $f_w = 2,0$ Hz leads to a higher impulse and a higher velocity and a better correlation.

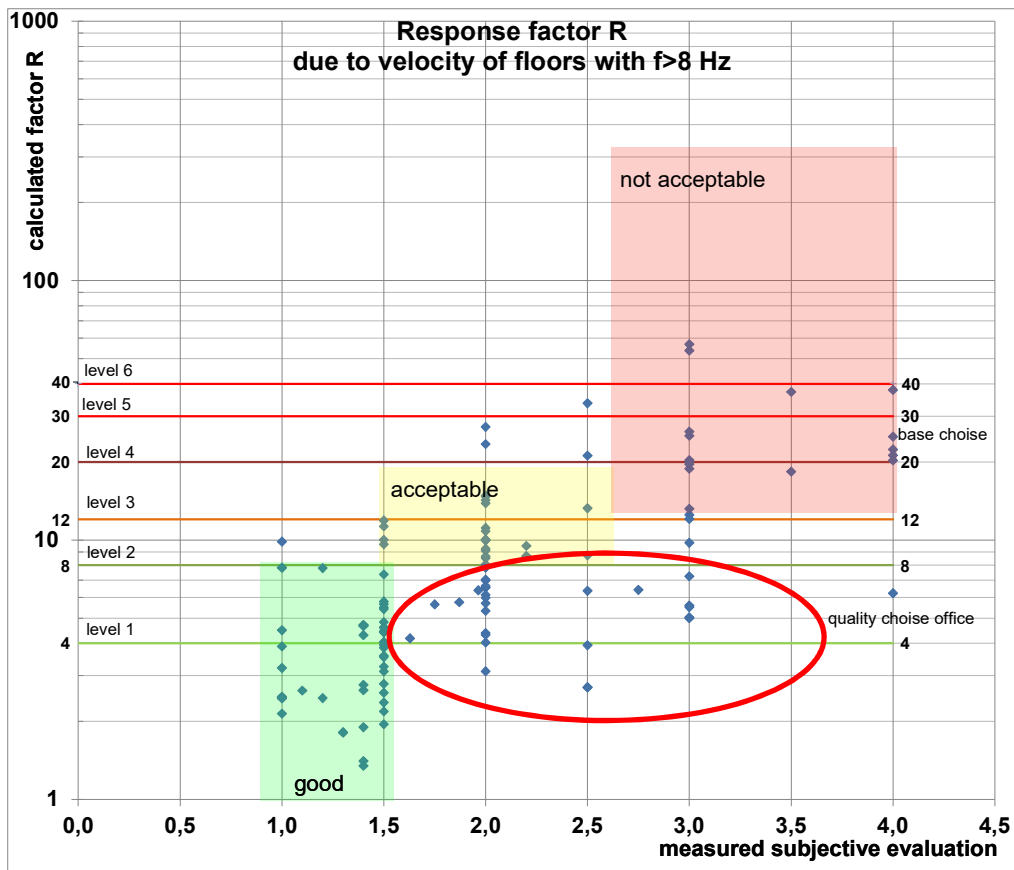


Figure 3. Comparison between evaluation and calculated response factors for higher frequency floors (≥ 8 Hz).

A floor with good response factor may fail the proof of deflection (stiffness criteria). In the next step all floors, which do not fulfil the stiffness criteria, have been deleted, see figure 4.

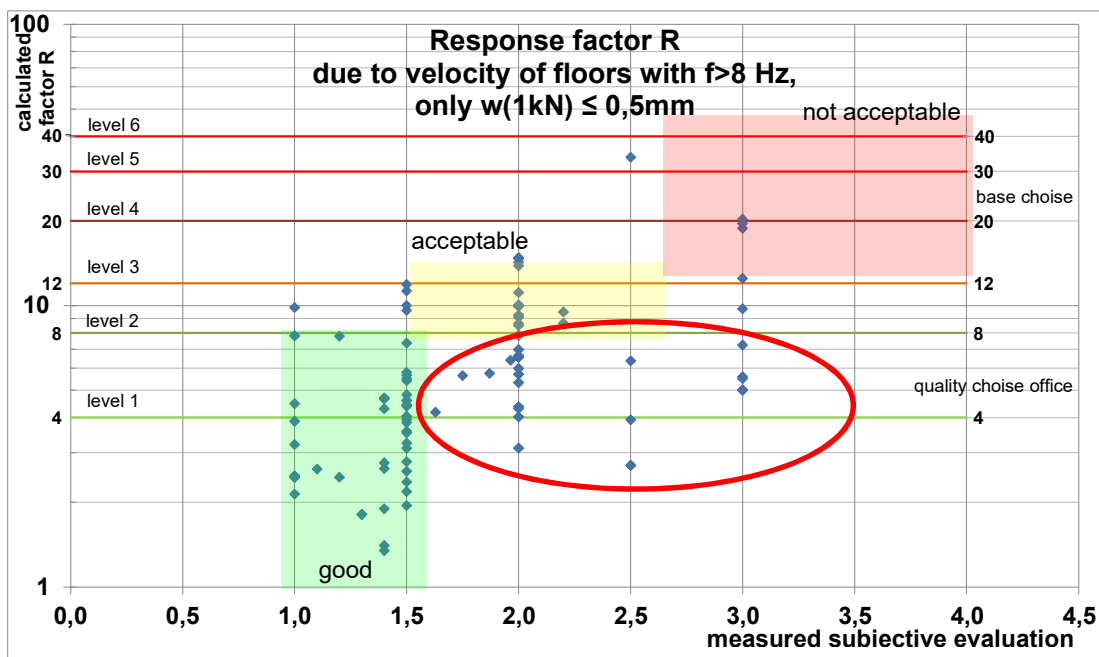


Figure 4. Comparison between evaluation and calculated response factors for higher frequency floors (≥ 8 Hz), floors with $w(1kN) < 0,5mm$ only.

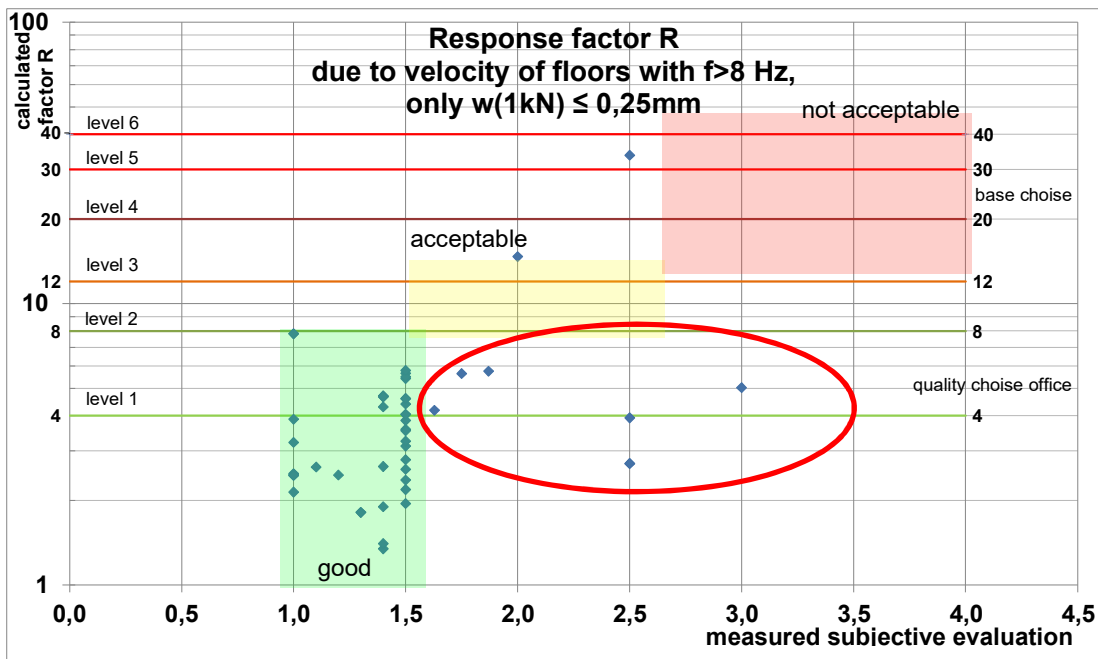


Figure 5. Comparison between evaluation and calculated response factors for higher frequency floors (≥ 8 Hz), floors with $w(1kN) < 0,25mm$ only.

Most of the “wrongly classified” values do not appear in figure 5 when applying the stricter stiffness criteria, here this means $w(1kN) \leq 0,25mm$. This shows that the stiffness criteria is also needed to divide the floors in the evaluation to “good” and “acceptable”.

4. Demands on construction on floor structures

Table 2: Prescriptive demands on floor structures and construction depending on subjective evaluation of behaviour.

demands regarding the vibrations	floors with higher demands	floors with lower demands
Subjective evaluation	1,0 to 1,5	1,5 to 2,5
Timber concrete composite systems	no more demands	no more demands
Massive timber floors, e.g. cross laminated timber or nail laminated timber floors	heavy floating screed on a light or heavy fill	heavy floating screed (fill not necessary)
	light floating screed on a heavy fill	light floating screed on a heavy fill *)
timber beam floors	heavy floating screed on a heavy fill	heavy floating screed (fill not necessary)
	Probably not possible	light floating screed on a heavy fill

*) Heavy fill is at least 60 kg/m^2 , e.g. a 40 mm grit fill.

The demands on construction are described in table 2 and in [2]. Applied on the measured data two more “wrongly classified” values disappear in figure 6.

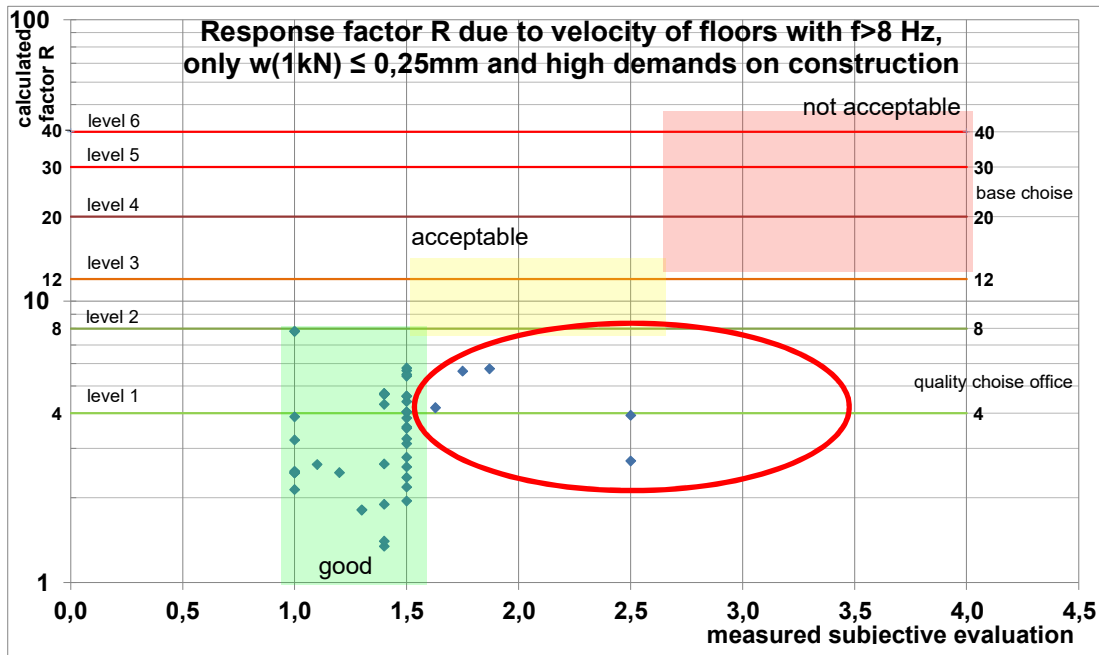


Figure 6. Comparison between evaluation and calculated response factors for higher frequency floors (≥ 8 Hz), floors with $w(1kN) < 0,25mm$ and fulfilling demands on construction.

5. No proof of R factor for floors with $f \geq 8$ Hz

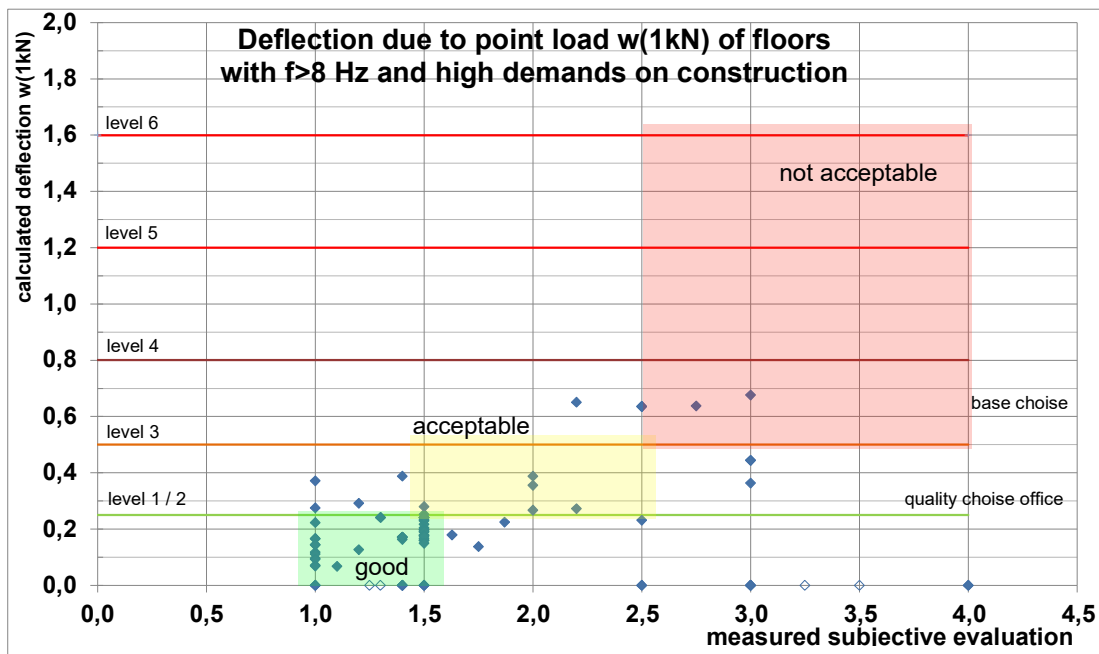


Figure 7. Comparison between evaluation and calculated deflection $w(1kN)$ for higher frequency floors (≥ 8 Hz) and fulfilling demands on construction.

Mark: The dots with value =0 do not fulfil either frequency criteria ($f > 8H$) or demands on construction. They should be ignored in this figure.

Figure 7 shows one more comparison: There is a very good correlation between deflection due to pointload combined with demands on construction and subjective evaluation. Out of this it is inferred, that the proof of resonance factor is not needed for floors which are typically built in Germany, Austria or Switzerland. This proof should be replaced by the demands on construction.

The recommendation for German, Austrian and Swiss floors is shown in figure 8:

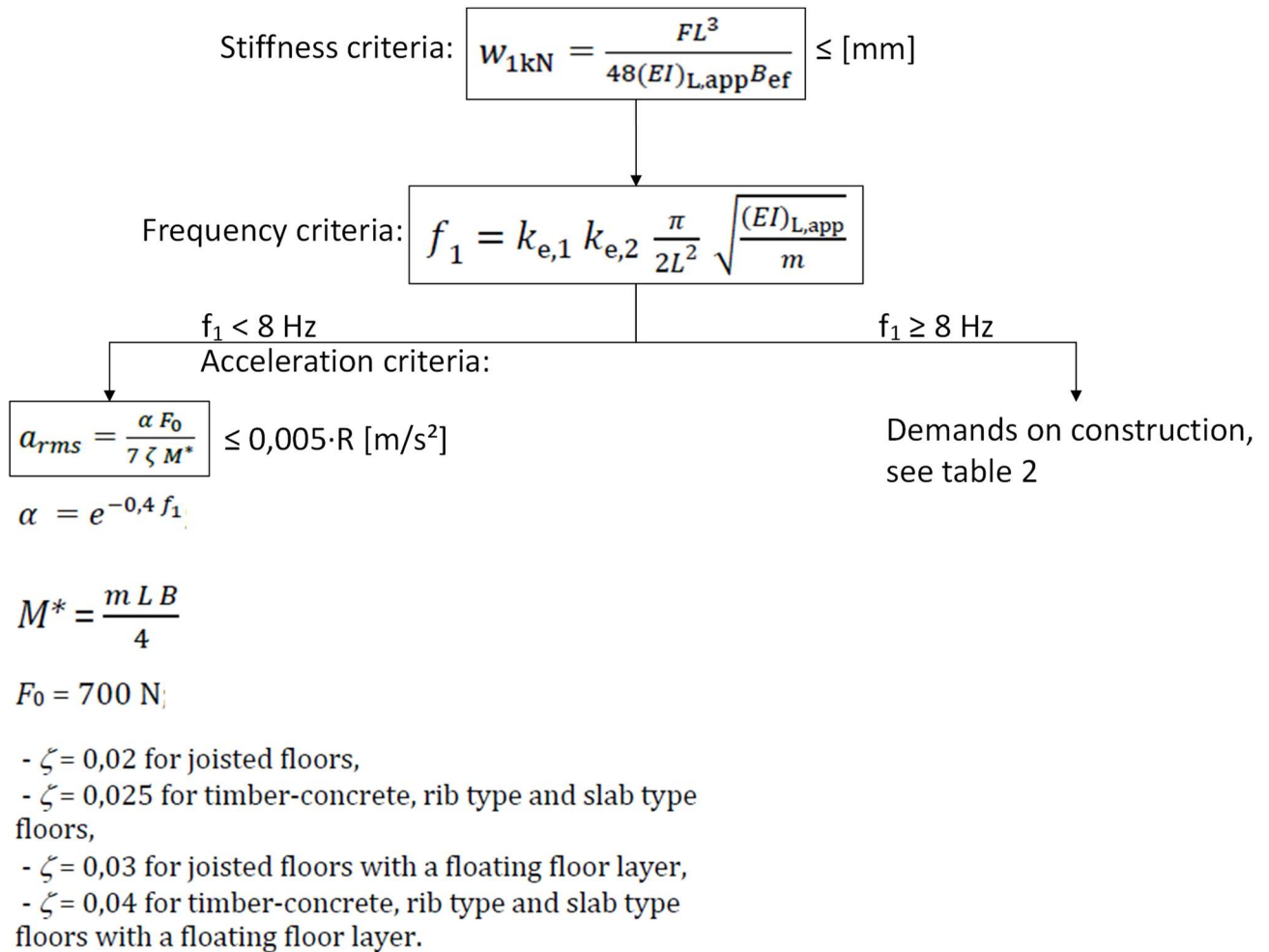


Figure 8. Flowchart and equations of recommended proof of floor vibration for typical German, Austrian, Swiss floors.

6. Comparison of criteria with response factor: acceleration and velocity

If the natural frequency of the floor is close to 8 Hz, there should be not a big difference between results of proofs of acceleration and the proof of velocity: if $f_1 = 8\text{Hz}$, $R(a_{rms}) \approx R(v_{rms})$ should be close to equal.

Acceleration:

$$R(a_{rms}) = \frac{\alpha F_0}{7 \zeta M^*} \cdot \frac{1}{0,005} = \frac{e^{-0,4 \cdot 8 \cdot 700}}{7 \zeta M^*} \cdot \frac{1}{0,005} = \frac{4,08}{\zeta M^*} \cdot \frac{1}{0,005} = \frac{815}{\zeta M^*}$$

If the damping is assumed to be $\zeta = 0,03$, this leads to $R(a_{rms}) = \frac{27000}{M^*}$.

Velocity:

$$R(v_{rms}) = \frac{v_{rms}}{0,0001} = \frac{v_{tot,peak} \cdot (0,65 - 0,01 f_1) \cdot (1,22 - 11,0 \zeta) \eta}{0,0001} = \frac{k_{imp} \cdot v_{1,peak} \cdot 0,57 \cdot 0,89 \cdot \eta}{0,0001}$$

The following assumptions are set: $k_{imp} = 1$; $\eta = 0,97$;

1. Step frequency is chosen for residential $f_w = 1,5\text{ Hz}$:

$$R(v_{rms}) = \frac{1}{0,0001} \cdot \frac{1 \cdot k_{red} \cdot 42 \cdot f_w^{1,43} \cdot 0,49}{f_1^{1,3} \cdot (M^* + 70)} = \frac{0,7 \cdot 5,02 \cdot 0,49}{0,0001 \cdot (M^* + 70)} = \frac{17300}{(M^* + 70)}$$

2. Step frequency is chosen for other kind of use: $f_w = 2\text{ Hz}$:

$$R(v_{rms}) = \frac{1}{0,0001} \cdot \frac{1 \cdot 0,7 \cdot 42 \cdot 2^{1,43} \cdot 0,49}{8^{1,3} \cdot (M^* + 70)} = \frac{26000}{(M^* + 70)}$$

With the second assumption ($f_w = 2,0\text{ Hz}$) there is a very good correlation between the two proofs, assumed that $M^* + 70 \approx M^*$.

7. Proof of vibration is not required for short spans

In the following some numerical examples for small or big rooms are given.

It has been shown that floors with frequency of 8 Hz have a response factor of

$$R(a_{rms}) \approx R(v_{rms}) \approx \frac{26500}{M^*}.$$

To reach a response factor better than 8, the modal mass must be 3300kg.

$M^* = \frac{m \cdot L \cdot B}{4} \geq 3300 \text{ kg}$, m must be 825kg/m² in case of a 4x4 [m²] floor (!) or 366kg/m² in case of a 6x6 [m²] floor.

The other way round: The R factor is high, if there is to less mass.

Table 3 shows the R factor of floors, all with 8 Hz, depending on the dimensions (span and width) and the mass.

Table 3: Response factor of floors with frequency of 8 Hz, step frequency of 1,5 Hz and varying dimensions of span and width.

m [kg/m ²]	L [m]	b [m]	M* [kg]	$R(a_{rms}) \approx R(v_{rms})$
150	3	3	338	79
150	3	4	450	59
150	4	4	600	44
150	4	5	750	35
150	4	6	900	29
150	5	5	938	28
150	5	6	1125	24
150	6	6	1350	20
200	4	4	800	33
200	4	5	1000	27
200	4	6	1200	22
200	4	7	1400	19
200	5	5	1250	21
200	5	6	1500	18
200	5	7	1750	15
200	6	6	1800	15
200	6	7	2100	13
200	7	7	2450	11

Table 3 shows, that also for small floors, which do not have any vibration problems, the response factor is high. This is another reason to vote for the procedure shown in figure 8. In case of floors with big span (and width), there may be enough mass to reach a good response factor. In this case (big span) the frequency often is lower than 8 Hz. Then the R factor has to be calculated based on acceleration.

8. Comparison of equations with measured vibrational behaviour of typical UK lightweight joisted floors

In 2019 measurements of vibration behaviour under footfall were undertaken by Dr. Wen-Shao Chang of Sheffield University on variations of a lightweight wood-based joisted floor typical of those built in the UK for intermediate floors of houses. The floor had overall plan dimensions of 4.8m x 4.8m and was built off 1.2m high timber frame walls. The floor comprised 72mm wide 253mm deep metal-web joists overlaid by a 22mm P5 particleboard deck. No plasterboard ceiling was fixed to enable variations to the floor construction to be expediently carried out.

43 sets of vibration measurements were undertaken on the floor construction to investigate the effects of variations in:

- floor longitudinal stiffness
- floor transverse stiffness
- level of imposed loading on the floor
- support conditions (e.g. beam supports replacing the timber frame walls)
- presence of a stairwell

Each set of vibration measurements contained the following:

- Determination of modal damping ratio and fundamental frequency from a heel-drop test.
- Vibration velocities were determined for a 'slow' walk and a 'fast' walk. As the walking frequencies measured for the slow walk were close in magnitude to the 1.5 Hz stipulated in prEN1995-1-1 for residential floors, the focus has primarily been on the slow walk measurements.
- For each walking speed three sets of measurements were taken with the walker walking parallel to the joists and three sets of measurements were taken with the walker walking perpendicular to grain.
- Average values for both directions were calculated by Dr. Chang for both the peak vibration velocity and the r.m.s vibration velocity. The r.m.s values are 'whole event' (5-7 steps) r.m.s values.

The key objective is to compare vibration velocities calculated using the prEN1995-1-1 procedure with measured vibration velocities, though some elaboration is required

for both the calculated and measured vibration velocities as below. Comparisons are made for both peak vibration velocities and the r.m.s vibration velocities.

Calculated velocities. These were calculated by inserting as appropriate the measured values for walking frequency, weight of walker, longitudinal floor stiffness, modal damping ratio and fundamental frequency into the prEN1995-1-1 equations.

Measured velocities. The comparisons are also only made with the slow walk data. It was found that mostly the 'parallel' and 'perpendicular' velocities are in reasonable agreement and an average value of the two has been compared with the calculated velocity.

This paper is limited to the comparison of calculated and measured vibration velocities for floors on wall supports where the transverse floor stiffness is solely provided by the floor deck with vibration measurements being taken on eight such floors. In table 4 details of these floors are given together with the measured values of damping ratio and fundamental frequency. The following observations are made about table 4:

- All the damping ratios are greater than the 2% value stipulated in prEN1995-1-1 for joisted floors with the lowest value being 2.03% and the average value being 2.84%.
- The fundamental frequencies calculated in accordance with prEN1995-1-1 were on average 8% higher than the measured values with the range being from 2% less to 14% greater. This may be partially explained by the fact that the weight of the person doing the heel-drop was not included in the determination of the measured fundamental frequencies.

In table 5 comparisons are made, for both peak vibration velocity and r.m.s vibration velocity, between the average measured values and the equivalent values calculated in line with prEN1995-1-1. One deviation from the prEN1995-1-1 procedure was the k_{red} factor in equation (9.12) which, because the walker walked close to the receiver sensor, was taken as 1.0 rather than the 0.7 assumed in prEN1995-1-1. In the case of the peak vibration velocities it can be seen that the calculated values are on average 1.43 times the measured values with the minimum ratio being 1.13. However, in the case of the r.m.s vibration velocities the calculated values are on average 2.50 times the measured values with the minimum ratio being 2.01. Whilst the calculated peak vibration velocities might be considered to compare acceptably with the measured values, the calculated r.m.s vibration velocities are unduly conservative. However it should also be noted that there would be closer agreement between calculated and

measured r.m.s vibration velocities if the measured r.m.s values had been calculated as 'single step' values.

From inspection of prEN1995-1-1 it can be seen that the evaluation of r.m.s vibration velocities from peak vibration velocities is done in equations (9.15) and (9.16). In particular it is noticed in equation (9.16) that the value of the factor η is not allowed to be lower than 0.69 as below:

$$\eta = 1,52 - 0,55k_{imp}, \text{ when } 1,0 \leq k_{imp} \leq 1,5 \text{ else } \eta = 0,69 \quad (9.16)$$

The background to the lower limit of 0,69 is not known (perhaps associated with vibration testing done on concrete floors) but certainly prevents the ratio between measured r.m.s and peak vibration velocities being attained by the calculated values for floors where the transverse stiffness is only provided by a floor deck. If the basic equation is equation (9.16) is maintained but a smaller lower limiting value of η allowed as shown below, then it can be seen from table 6 in the case of the r.m.s vibration velocities the calculated values are on average 1.22 times the measured values with the minimum ratio being 0.99. This is similar to the peak vibration velocities where the calculated values are on average 1.43 times the measured values with the minimum ratio being 1.13.

$$\eta = 1,52 - 0,55k_{imp}, \text{ when } 1,0 \leq k_{imp} \leq 2,2 \text{ else } \eta = 0,31 \quad \text{Modified (9.16)}$$

This simple modification to equation (9.16) of prEN1995-1-1 would result in r.m.s vibration velocities calculated in accordance with prEN1995-1-1 having values much closer to the measured values for the very common case of a lightweight joisted floor whose transverse stiffness is only provided by the floor deck.

There is a need to clarify within the EN Standard system whether the r.m.s vibration velocities should be for 'single step' or 'whole event' and contingent on this decision the value of the k_{red} factor in equation (9.12) of prEN1995-1-1 may need to be adjusted.

References:

- [1]: Abeysekera, I.K., Hamm, P.; Toratti, T., Lawrence, A.: Development of a floor vibration design method for Eurocode 5. In: INTER - International Network on Timber Engineering Research. 13. – 16. August 2018, Kap. 51-20-2, 14 S. Tallinn, Estonia. Hrsg.: KIT, Karlsruhe. ISSN 2199-9740.
- [2]: Hamm, P., Richter, A., Winter, S.: Floor Vibrations – New Results. In: WCTE: World Conference in Timber Engineering. 20. – 24. Juni 2010. Riva del Garda, Italy.

TABLE 4 – DAMPING RATIOS AND FUNDAMENTAL FREQUENCIES FOUND FOR LIGHTWEIGHT JOISTED FLOORS.

Test no.	Longitudinal floor construction	Transverse floor construction	Floor longit. stiffness $EI_{L,app}$	Floor transv. stiffness EI_T	Support type at edge	Imposed load	0.7 kN receiver load?	Damping ratio (%)	Measured frequency (Hz)	Calculated frequency (Hz)	$f_{1,calc}$ $f_{1,meas}$
21	72 x 253 posijoists at 600	22 P5 particleboard	1.03E+12	2.66E+09	T-F	0	No	2.56%	13.97	14.91	1.07
20	72 x 253 posijoists at 600	22 P5 particleboard	1.03E+12	2.66E+09	T-F	0.15	Yes	3.04%	9.86	11.17	1.13
8	72 x 253 posijoists at 300	22 P5 particleboard	2.02E+12	2.66E+09	T-F	0	No	3.51%	15.53	17.45	1.12
5	72 x 253 posijoists at 300	22 P5 particleboard	2.02E+12	2.66E+09	T-F	0.15	Yes	3.44%	13.67	14.52	1.06
13	72 x 253 posijoists at 600	22 P5 particleboard	1.02E+12	2.66E+09	Masonry	0	No	3.12%	13.67	14.91	1.09
12	72 x 253 posijoists at 600	22 P5 particleboard	1.02E+12	2.66E+09	Masonry	0.15	Yes	2.61%	9.77	11.09	1.14
33	72 x 253 posijoists at 600	22 P5 particlebd (glued)	1.06E+12	2.66E+09	T-F	0	No	2.03%	15.23	14.90	0.98
34	72 x 253 posijoists at 600	22 P5 particlebd (glued)	1.06E+12	2.66E+09	T-F	0.15	Yes	2.45%	10.64	11.17	1.05
								Mean	2.84%	Mean	1.08
								Min	2.03%	Min	0.98
								Max	3.51%	Max	1.14

TABLE 5 – COMPARISON OF MEASURED VIBRATION VELOCITIES AND VIBRATION VELOCITIES CALCULATED TO prEN1995-1-1.

Test no.	Longitudinal floor construction	Transverse floor construction	Support type at edge	Imposed load	0.7 kN receiver load?	PEAK VIBRATION VELOCITIES			RMS VIBRATION VELOCITIES		
						Measured unfiltered	Calculated	Calcul. Unfilt.	Measured unfiltered	Calculated	Calcul. Unfilt.
21	72 x 253 posijoists at 600	22 P5 particleboard	T-F	0	No	0.0164	0.0214	1.30	0.0027	0.0071	2.60
20	72 x 253 posijoists at 600	22 P5 particleboard	T-F	0.15	Yes	0.0176	0.0224	1.27	0.0037	0.0075	2.01
8	72 x 253 posijoists at 300	22 P5 particleboard	T-F	0	No	0.0139	0.0201	1.45	0.0026	0.0057	2.20
5	72 x 253 posijoists at 300	22 P5 particleboard	T-F	0.15	Yes	0.0095	0.0185	1.94	0.0019	0.0060	3.10
13	72 x 253 posijoists at 600	22 P5 particleboard	Masonry	0	No	0.0119	0.0238	2.00	0.0025	0.0074	2.99
12	72 x 253 posijoists at 600	22 P5 particleboard	Masonry	0.15	Yes	0.0216	0.0253	1.17	0.0036	0.0090	2.51
33	72 x 253 posijoists at 600	22 P5 particlebd (glued)	T-F	0	No	0.0172	0.0194	1.13	0.0025	0.0063	2.57
34	72 x 253 posijoists at 600	22 P5 particlebd (glued)	T-F	0.15	Yes	0.0175	0.0206	1.18	0.0036	0.0072	2.02
						Mean	1.43		Mean	2.50	
						Min	1.13		Min	2.01	

Table 5 utilising current equation (9.16) of prEN1995-1-1:

$$\eta = 1,52 - 0,55k_{imp}, \text{ when } 1,0 \leq k_{imp} \leq 1,5 \text{ else } \eta = 0,69$$

TABLE 6 – COMPARISON OF MEASURED VIBRATION VELOCITIES AND VIBRATION VELOCITIES CALCULATED TO prEN1995-1-1 EXCEPT USING A MODIFIED EQUATION (9.16).

Test no.	Longitudinal floor construction	Transverse floor construction	Support type at edge	Imposed load	0.7 kN receiver load?	PEAK VIBRATION VELOCITIES			RMS VIBRATION VELOCITIES		
						Measured unfiltered	Calculated	Calcul. Unfilt.	Measured unfiltered	Calculated	Calcul. Unfilt.
21	72 x 253 posijoists at 600	22 P5 particleboard	T-F	0	No	0.0164	0.0214	1.30	0.0027	0.0036	1.32
20	72 x 253 posijoists at 600	22 P5 particleboard	T-F	0.15	Yes	0.0176	0.0224	1.27	0.0037	0.0038	1.02
8	72 x 253 posijoists at 300	22 P5 particleboard	T-F	0	No	0.0139	0.0201	1.45	0.0026	0.0026	0.99
5	72 x 253 posijoists at 300	22 P5 particleboard	T-F	0.15	Yes	0.0095	0.0185	1.94	0.0019	0.0027	1.39
13	72 x 253 posijoists at 600	22 P5 particleboard	Masonry	0	No	0.0119	0.0238	2.00	0.0025	0.0038	1.52
12	72 x 253 posijoists at 600	22 P5 particleboard	Masonry	0.15	Yes	0.0216	0.0253	1.17	0.0036	0.0046	1.28
33	72 x 253 posijoists at 600	22 P5 particlebd (glued)	T-F	0	No	0.0172	0.0194	1.13	0.0025	0.0031	1.26
34	72 x 253 posijoists at 600	22 P5 particlebd (glued)	T-F	0.15	Yes	0.0175	0.0206	1.18	0.0036	0.0035	1.00
						Mean	1.43			Mean	1.22
						Min	1.13			Min	0.99

Table 6 utilising proposed modified equation (9.16) to prEN1995-1-1: $\eta = 1,52 - 0,55k_{imp}$, when $1,0 \leq k_{imp} \leq 2,2$ else $\eta = 0,31$

Discussion

The paper was presented by P Hamm

P Dietsch commented that this is an interesting case where standardization work of the working group has concluded while essential related research is still on-going.

S Breneman asked about the open office system with beams spanning 12 m with CLT and whether there would be a difference between beam supported floors or wall supported floors. P Hamm responded that beam supported floors have lower frequencies and more deflection under the 1 kN load. Also that their findings and observations are applicable to both cases.

I Abeysekera asked if the UK Vrms signal was taken over one time step or over the entire signal. P Hamm said over one time step but would need to confirm. I Abeysekera asked about the position of the walker and sensor. P Hamm said sensor was always positioned at centre while walker was positioned at the center for resonance measurements and walker walked around for transient vibration measurements. I Abeysekera questioned whether the test matched calculated mode shape when the walker walked around and discussed the influence of the walker's walking position relative to the geometry of the floor.

P Dietsch asked I Abeysekera as the main investigator of the formulas covered in this paper, if he compared his proposed model with test results and whether Arup has test data. I Abeysekera said that the model was based on mechanistic approach. They have some test results of long floors with CLT on glulam but not for shorter floors.

A Frangi questioned whether so many performance classes needed to be proposed especially when so many of them are deemed unacceptable. He commented that fewer classes maybe less economical but would simplify design and he asked who made the decisions on these classes. P Hamm said that the performance classes should be set by individual countries and based on the information from floors in Germany and UK, a large range of floor performance levels were needed.

Revision of testing standards to determine the seismic capacity of timber connections according to Eurocode 8

Christophe Sigrist, Bern University of Applied Sciences (Switzerland)

Daniele Casagrande, Institute of Bioeconomy, National Research Council of Italy (Italy)

Maurizio Piazza, University of Trento (Italy);

1. Introduction

The current paper presents the ongoing work within the Working Group 1 of CEN TC124 for the revision process of testing standards to determine the seismic capacity of timber connections according to Eurocode 8. A Technical Specification (TS 12512) is being prepared in order to clarify how the test methods reported in EN 12512 should be adopted to determine the seismic capacity of connections used in dissipative zones in timber structures. An innovative method for the determination of the seismic capacity of dissipative timber connections is presented. This method is based on the proposal presented in Casagrande et al. (2020) by analysing the results of an experimental campaign of different types of mechanical connections subjected to cyclic tests. Work is currently undertaken to link design standards and testing standards aiming for a consistent definition of basic parameters for the design of timber structures under earthquake impact.

2. Requirements and needs from Eurocode 8

2.1 The current version of Eurocode 8

The requirements for the seismic capacity of dissipative connections are reported at Clause 8.3.3 of EN 1998-1 (Eurocode 8 - Part 1) in terms of ductility ratio and reduction of resistance as function of the ductility class (i.e. either medium – DCM or high – DCH) which timber structures are designed for.

Clause 8.3.3 in fact reports that a *“dissipative zone shall be able to deform plastically for at least three fully reversed cycles at a static ductility ratio of 4 for ductility class medium (DCM) structures and at a static ductility ratio of 6 for ductility class high structures (DCH), without more than a 20% reduction of resistance”*.

The dissipative connections in timber structure need to deform plastically with a ductility ratio equal either to 4 or 6 for a medium and high ductility class, respectively, when subjected to cyclic load testing. It is noteworthy to mention that the demand in terms of ductility ratio is independent of the structural typology (e.g. *nailed wall panels with nailed diaphragms, hyperstatic portal frames with doweled and bolted joint*) and is the same for all types of connections (e.g. nailed, screwed, bolted connections).

Two different interpretations can be given for the “*reduction of resistance*”. The former is related to the reduction of resistance between the first and third cycle at a value of displacement corresponding to requested ductility ratio. This interpretation seems to be consistent with the “short” procedure reported in the European Standard for cyclic testing of connections EN 12512. The latter is referred to the reduction of resistance in the softening branch of the 1st Envelope Curve (EC) obtained from the cyclic test and corresponds to one of the three conditions adopted to determine the ultimate displacement of connections. No clear explanation and direct reference to Clause 8.3.3 of Eurocode 8, however, is reported in EN 12512.

Casagrande et al. (2020) argued that the “short procedure” in EN 12512 might have been included to reflect the provision at Clause 8.3.3 of Eurocode 8. For this reason, the “reduction of resistance” might be interpreted as being the reduction of strength between the 1st and 3rd cycle, see Figure 1. Germano et al. (2015) gave the same interpretation for the investigation on the seismic capacity of sheathing-to-framing connections. Nevertheless, it is noteworthy to mention that only the European Standard for cyclic testing of timber connections take into account the reduction of strength for repeated load cycles at the same values of displacement. Other international load protocols (e.g. CUREE protocol) define reduced subsequent displacements on each level of the loading sequence and, as a result, the reduction of strength between the 1st and 3rd cycle is not considered.

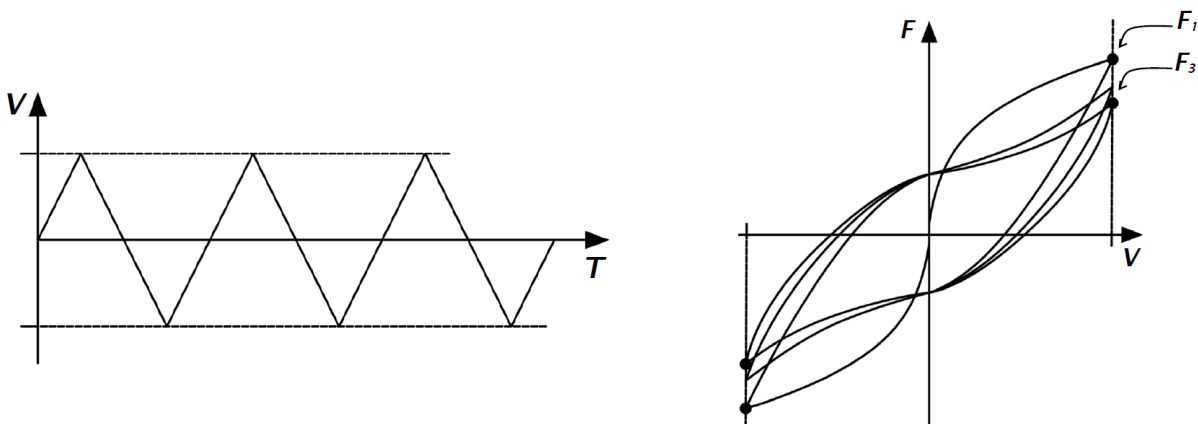


Figure 1. Short procedure in EN 12512 and definition of reduction of strength between 1st and 3rd cycle.

2.2 The revision process of Eurocode 8

A significant revision process of the “timber” chapter of Eurocode 8 is being conducted within the Working Group 3 of the CEN TC250/SC8 committee 'Design for Earthquake Actions' (Follesa et al., 2018). New definitions of the timber structural types, modifications of the behaviour q-factors, clear indications on the choice of dissipative zones and capacity design rules to avoid any local and global brittle failure are provided (Fragiacomo et al., 2019).

An important modification under discussion also regards the requirements for the seismic capacity of dissipative timber connections. In order to ensure an adequate amount

of energy dissipation and an almost constant level of load under repetition of medium-to-high amplitude plastic displacements, the low-cycle fatigue strength of dissipative connections needs to be determined by means of cyclic tests.

Differently from the current version of Eurocode 8, in the new version the requirements in terms of ductility ratio of dissipative zones are indicated for all structural types both in medium (i.e. DC2) and high (i.e. DC3) ductility classes, see Table 1. The required values of ductility ratio have been defined on the base of research results, i.e. Follesa (2015), Rossi et al. (2019), Jockwer and Jorissen (2018) for each structural type.

Table 1. Values of required ductility for dissipative connections in new Eurocode 8.

Current version of Eurocode 8				
Structural type	Dissipative sub-assembly/joint/2D-or 3D-nailing plate/connection	Type of ductility	μ	μ
			DC2	DC3
All	Not specified	Displacement/rotational	4	6
New Eurocode 8				
Structural type	Dissipative sub-assembly/joint/2D-or 3D-nailing plate/connection	Type of ductility	μ	μ
			DC2	DC3
a) Cross laminated timber structures	Hold-downs, tie-downs, foundation tie-downs, angle brackets, shear plate	Displacement	1,8	1,8
	Screwed wall panel-to-panel joints	Displacement	-	3,5
b) Light-frame structures	Connection (nail/screw/staple)	Displacement	3,5	5,5
c) Log structures	Shear wall	Displacement	1,4	-
d) Moment-resisting frames	Beam-column joint	Rotational	4,0	7,0
e) Braced frame structures with dowel-type connections	Braced Frame	Displacement	1,4	-

The methodology proposed by Casagrande et al. (2020) is adopted to define the seismic low-cycle fatigue strength of a dissipative timber connection. Ductility ratio, reduction of strength between the 1st and the 3rd cycle and the loss of strength related to the value of strength obtained from monotonic tests (i.e. nominal strength) are taken into account simultaneously.

Two new factors are introduced at this purpose. The strength impairment factor φ_{imp} is determined as the ratio of the reduction of strength $\Delta F = F_1 - F_3$ between the 1st and 3rd cycle at the same value of displacement v and the force at the first cycle F_1 , see Equation 1 and Figure 2. The factor k_{deg} is calculated as the ratio of the ultimate load F_u on the 1st envelope curve (EC) in a cycle test and the maximum load (i.e. nominal strength) F_N obtained from a previous monotonic test, see Equation 2.

$$\varphi_{imp}(v) = \frac{F_1(v) - F_3(v)}{F_1(v)} \quad (1)$$

$$k_{deg} = \frac{F_1(v_u)}{F_N} \quad (2)$$

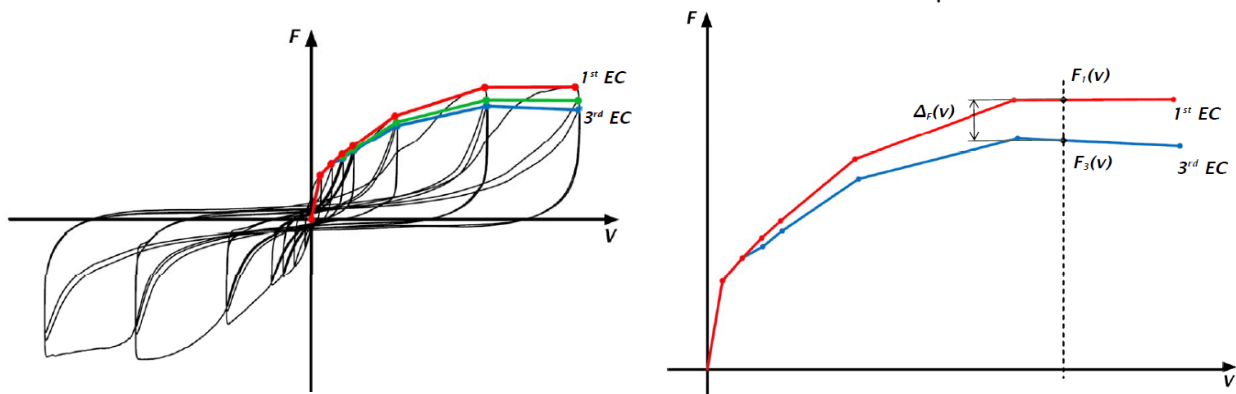


Figure 2. 1st and 3rd envelope curves (ECs) in cyclic tests a); reduction of strength between 1st and 3rd envelope curve (b).

A value of ϕ_{imp} not greater than 0.3 for a value of displacement v corresponding to the ductility ratio reported in Table 1 is required to limit the reduction of strength between the 1st and 3rd cycle and avoid any significant reduction of load under cyclic testing.

In order that the cyclic strength capacity of a dissipative connection is not significantly smaller than the nominal strength obtained from a monotonic test (the nominal strength is in fact adopted to determine the characteristic and design strength of the connection), a limit value not smaller than 0.8 is required for k_{deg} , see Figure 3. A similar approach is adopted in in ANSI/AISC 341-10 for the determination of low-cycle fatigue strength of steel beam-to-column joints.

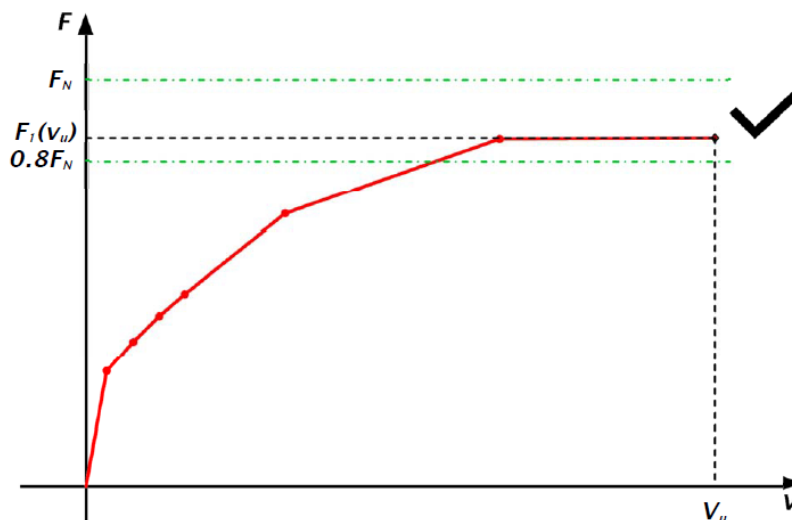


Figure 3. Ultimate load determined on the 1st envelope curve in cyclic tests and nominal strength obtained from monotonic test.

In the new Eurocode 8, the factor k_{deg} is also used to take into account the strength degradation in the calculation of the seismic design strength $F_{Rd,d}$ of dissipative zones for verifications of DC2 and DC3 design at significant damage limit state as reported in Equation 3.

$$F_{Rd,d} = k_{mod} \cdot k_{deg} \cdot \frac{F_{Rd,k}}{\gamma_M} \quad (3)$$

where $F_{Rd,k}$ is the characteristic value of the strength of the dissipative zones and k_{mod} is the modification factor for duration of load and service class according to Eurocode 5. The material partial factor for material properties γ_M can be related to accidental design situations when the strength degradation due to cyclic loading is appropriately accounted for in the evaluation of the strength of dissipative connections.

3. The TS 12512 as link between EN 12512 and Eurocode 8

In the context of the European Normative, the EN 12512 represents the Standard for the execution of cyclic testing. Nevertheless, the current version of EN 12512 does not provide any reference regarding how the results obtained from cyclic testing can be used in the seismic design of a timber structure according to Clause 8.3.3 of EN 1998-1. Detailed information and explanations are needed regarding the application of EN 12512 when the results from cyclic tests are adopted to define the seismic capacity of dissipative timber connections.

Two load procedures are provided in the current version of the EN 12512. However, it is not specified which procedure should be used relating to the scope of the test. A clear indication if either short or complete procedure should be adopted for the scope of Eurocode 8 is not reported.

It is noteworthy to mention that for some connections, the strength degradation is certainly influenced by the number of cycles performed. As a result, from a complete procedure higher values of reduction of resistance are expected than for the short procedure. This aspect seems to be very important since many connections could not achieve a ductility of 4 and 6 complying with a reduction of strength lower than 20% if a complete procedure was applied but they could with a short procedure.

Clear indications on how to calculate the “reduction of resistance” required by Eurocode 8 should be also provided. The EN12512 in fact does not specify if the reduction of resistance is to be intended as either the reduction of strength between the 1st and the 3rd cycle or the loss of strength along the softening branch on the 1st envelope curve. Moreover, the methods included in the current version of EN 12512 are not suitable for the determination of the seismic capacity according to the new Eurocode 8.

For these reasons, within the Working Group 1 of CEN TC124 a Technical Specification (i.e. TS 12512) is being prepared in order to clarify how the test methods reported in EN 12512 should be used to determine the seismic capacity of timber connections used in dissipative zones according to Eurocode 8.

Due to the fact that the revision process of Eurocode 8 is still in progress, two different steps for the elaboration of TS 12512 have been scheduled. In the first step, the TS

12512/1 will clarify how the test methods included the current version of EN 12512 need to be used to determine the seismic capacity of connections according to Clause 8.3.3 of the current Eurocode 8. In a second future step, the TS 12512/2 will provide a complete methodology for cyclic testing according to the new Eurocode 8.

3.1 The TS12512/1

The Technical Specification TS12512/1 is being created to describe the test methods for determining the ductility ratio and the reduction of resistance from experimental data of connections to be used in the seismic design of timber structures according to Clause 8.3.3 of EN 1998-1. The test method can be summarized in the following five steps.

- i) A quasi-static monotonic test is conducted according to EN 26891 up to either the failure of the test specimen or to 30 mm of applied displacement.
- ii) The yield displacement $v_{y,m}$ and the corresponding yield load $F_{y,m}$ are determined by using the method b) (also known as “tangent” method) of the current version of EN 12512.
- iii) The short procedure of EN 12512 is adopted to perform quasi-static cyclic test. The short loading procedure prescribes the execution of three fully reversed cycles at an amplitude equal to $v_{y,m} \cdot \mu$, where μ is the required ductility ratio from Eurocode 8. The value of μ can be either 4 or 6 depending on ductility class of the structure.
- iv) The reduction of resistance $R_F(v)$ between the 1st and the 3rd cycle is determined at a displacement amplitude v equal to $v_{y,m} \cdot \mu$ considering only the first half of the hysteresis loops (e.g. either compression or tension loop) as:

$$R_F(v_{y,m} \cdot \mu) = \frac{F_1(v_{y,m} \cdot \mu) - F_3(v_{y,m} \cdot \mu)}{F_1(v_{y,m} \cdot \mu)} \cdot 100\% \quad (4)$$

- v) The connection is regarded as dissipative for high ductility class if it does not exhibit any failure before completing the cyclic loading procedure and the reduction of strength $R_F(v_{y,m} \cdot 6)$ for a ductility level μ equal to 6 is smaller than or equal to 20%. The connection is regarded as dissipative for medium ductility class structure if it does not exhibit any failure before completing the cyclic loading procedure and the reduction of resistance $R_F(v_{y,m} \cdot 4)$ achieved for a ductility level μ equal to 4 is smaller than or equal to 20%.

3.2 The TS12512/2

The Technical Specification TS12512/2 will describe the test methods for determining the seismic capacity of dissipative connections according to the new Eurocode 8 in terms of ductility ratio, taking into account the reduction of strength between the 1st and the 3rd cycle as well as the loss of strength related to the value of strength obtained from monotonic tests. The methodology proposed by Casagrande et al. (2020) will be discussed and investigated on the base of experimental tests which will be carried out

in next future. A first proposal for the application of this test method can be summarized in the ten following steps:

- i) A quasi-static monotonic test is conducted according to EN 26891 up to either the failure of the test specimen or to 30 mm of applied displacement.
- ii) The nominal strength F_N is determined from the monotonic test as the maximum value of load. The yield displacement $v_{y,m}$ and the corresponding yield load $F_{y,m}$ are calculated by using the method *b)* of the current version of EN 12512.
- iii) A cyclic test is performed by using a displacement-controlled cyclic loading procedure which involves displacement cycles grouped in phases at incrementally increasing displacement levels. The values of displacement of all cycles are determined based on the yield displacement $v_{y,m}$ from the monotonic tests. Either the “complete” procedure of the current version of EN 12512 or a new procedure, see Table 2, will be assumed after that results from ongoing experimental tests will be examined with the aim to investigate the influence of number of cycles on the strength degradation of connections.

Table 2. Loading procedure for EN12512 and new proposal.

EN12512	N. of cycles	1	1	3	3	3	3	3	3	3	3
	Step [$v_{y,m}$]	0.25	0.50	0.75	1.00	2.00	4.00	6.00	(+2.00)
New proposal	N. of cycles	1	1	3	3	3	3	3	3	3	3
	Step [$v_{y,m}$]	0.25	0.50	0.75	1.00	2.00	3.00	4.00	5.00	6.00	(+1.00)

- iv) The 1st and 3rd envelope curves (ECs) are established from the first and third cycles, respectively, see Figure 1.
- v) The ultimate load $F_{u,c}$ of the cycle test is evaluated on the 1st EC as the load corresponding to the minimum value of displacement related to: the failure of the specimen (a), 80 % of the maximum load for displacement values lower than 30 mm (b) and 30 mm (c). The ultimate displacement $v_{u,c}$ is defined as the value of displacement on the 1st LSEC corresponding to $F_{u,c}$.
- vi) The yield displacement $v_{y,c}$ of the cycle test is evaluated on the 1st EC by using the method *b)* of the current version of EN 12512.
- vii) The strength impairment factor ϕ_{imp} is calculated for all values of displacements smaller than or equal to $v_{u,c}$. The displacement at the maximum reduction of resistance $v_{u,\phi30}$ is determined as the value of displacement corresponding to a strength impairment factor ϕ_{imp} equal to 0.30 (if exists), see Figure 4.
- viii) The ultimate displacement v_u that takes into account the reduction of strength is calculated as the minimum of $v_{u,c}$ and $v_{u,\phi30}$. The load $F_1(v_u)$ on the 1st EC corresponding to v_u is determined as well.
- ix) The factor k_{deg} is calculated according to Equation 2. If $k_{deg} < 0.8$, the value of ultimate displacement v_u can be reduced up to the value of displacement $k_{deg} = 0.8$. If

Eq. (2) is not satisfied for any other value of displacement, the connection should not be used for dissipative connections.

- x) The ductility ratio μ is calculated as the ratio of the ultimate slip v_u and yield slip $v_{y,c}$ and compared with required values reported in Table 2. The connection can hence be classified as dissipative either for medium (DC2) or high (DC3) ductility class of the timber structure.

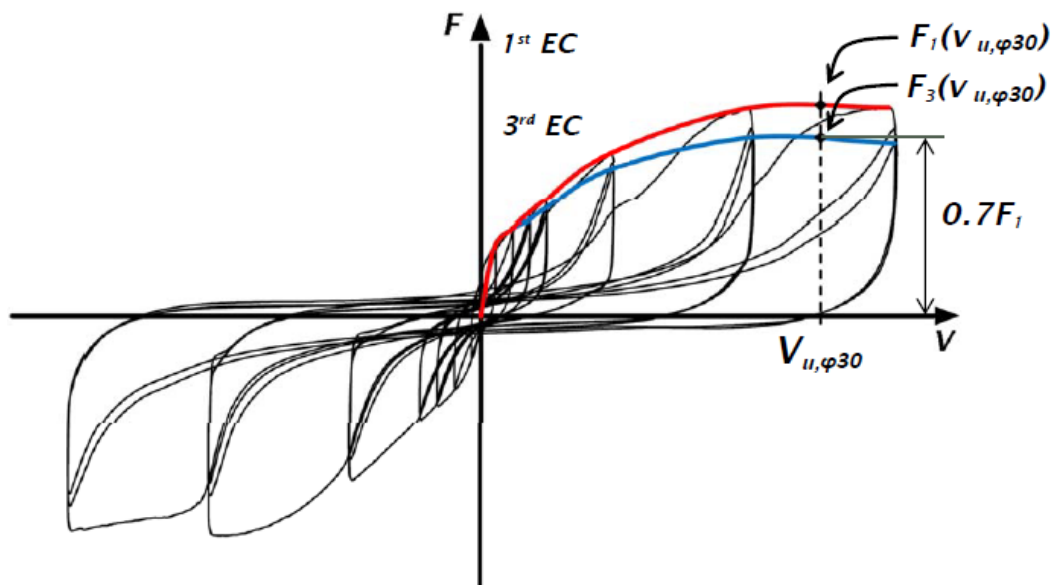


Figure 4. Determination of the displacement at the maximum reduction of resistance $v_{u,\varphi 30}$.

4. Experimental tests

4.1 Introduction

Ductility may be obtained on connector level, connection level or system level. For each situation testing standards are available. Several testing standards are currently under revision which gives the opportunity to “harmonise” them and to bring the targeted results in line with the needs of Eurocode 8.

The determination of low cycle ductility on connectors and the corresponding testing setups and testing protocols are given in (pr)EN 14592. Similarly, EN 409 also aims at determining low cycle ductility of single connectors. Both standards present difficulties regarding the application of loads or displacement on connectors.

The purpose of the experimental investigation carried out by Alves, Zare (2020) was set to evaluate and analyse the behaviour of connections with fully threaded $\varnothing 8$ mm RAPID self-drilling screws (Schmid Schrauben, Austria) with cylinder heads used on CLT and LVL members under cyclic loading. Two different configurations – a |||-type configuration with screws set perpendicular to the panel plane and a |-|-type configuration with screws set perpendicular to the edge of the inner member into the end grain – were used to determine the cyclic ductility following the ideas developed above. The goal was to perform cyclic tests on the screws that are submitted to a severe number

of cycles of load in tension and compression at set levels of displacement. The goal is to prove that the connection with ductility ratio of 4 or 6 can be regarded as dissipative for a medium and high ductility class of structure, respectively. The application of various testing routines aimed at comparing different procedures of cyclic tests. As usual the testing phase consisted of two parts: a monotonic test was performed first and in a second test setup the cyclic test. Some selected results are presented in the following section.

The monotonic compression test is required to provide the load-displacement curves for the connections and from there the yield load and displacement parameters to define the cyclic testing procedure are obtained. The yield point was estimated using several methods provided in the standards and related literature: the method as indicated in the current EN 12512, the “Equivalent Energy Elastic-Plastic” EEEP method, the SIA 265 method and the method proposed by Yasumura & Kawai (1998).

The analysis of the load-displacement curves from the monotonic tests yields very different, at time unexpected shapes. Two local maximum values as well as the presence of two different linear relationship between the applied load and the measured displacement have often been observed providing a wide range of interpretations. A thorough analysis of possible load-displacement behaviour has been carried out and categorised by Flatscher (2017).

4.2 Results from monotonic testing

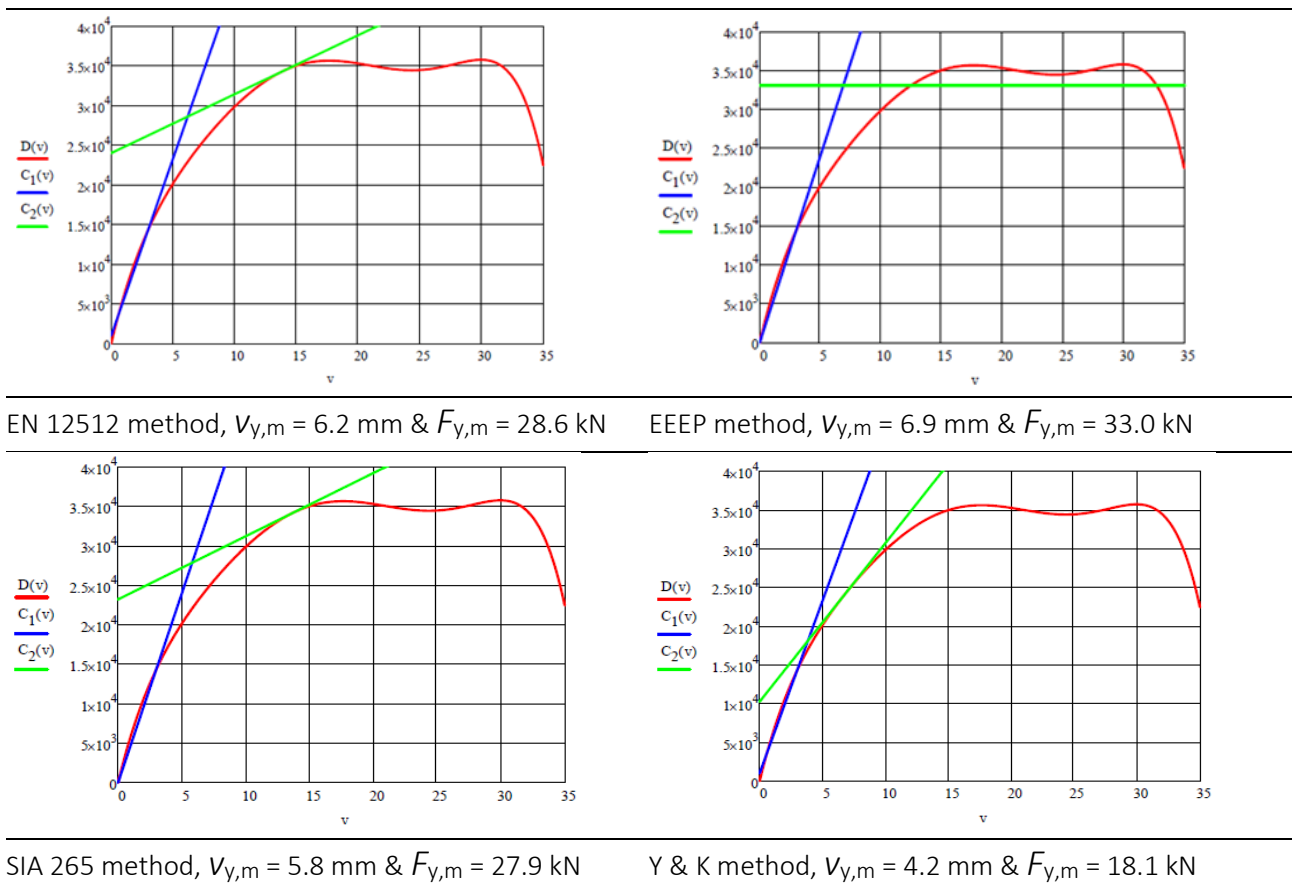
The load displacement curves were analysed using the four methods indicated above for the definition of $F_{y,m}$ and $v_{y,m}$. To obtain the slope of the elastic portion on the graph (or initial stiffness K_{ser}) a linear curve is fit to the curve from the origin of the graph and intersecting the point of the load-slip curve at 40% of the maximum (estimated) force achieved $F_{40\%}$ as it is the case for both the EEEP method and the SIA method. Concurrently, EN 12512 and the method by Yasumura & Kawai consider a linear curve considering two points on the load-slip graph: the first point being at 10% of the (estimated) maximum force $F_{10\%}$, and the second point at $F_{40\%}$. The slope of this secant is then defined to be the elastic portion (or the K_{ser}) of the connection. For every load displacement curve analysed, two values for K_{ser} were obtained, with the values from EEEP/SIA being slightly higher than those from EN 12512/ Yasumura & Kawai.

The second linear curve is determined applying three different approaches. The first approach, common to both the SIA and the EN 12512 method, is to place a tangent line with a slope equal to $1/6 K_{ser}$ on the load-slip curve. The x and y coordinates of the intersection between these two straight lines represent $F_{y,m}$ and $v_{y,m}$ respectively. These two values are defined to be the yield displacement and yield force. The EEEP method is based on a full linear-plastic model. A horizontal line is fit to the curve in order to simultaneously equalise the areas between the experimentally determined load-displacement curve, the linear elastic inclined line and the full plastic horizontal line respectively. The ordinate at which this horizontal line is placed corresponds to the value of $F_{y,m}$ and the x coordinate of the intersection between the sloped line and the

horizontal one yields $v_{y,m}$. The method proposed by Yasumura & Kawai positions another secant, including $F_{40\%}$ and $F_{90\%}$, and by placing it tangent to the load-slip curve. The intersection between the first and second lines then defines $F_{y,m}$ and $v_{y,m}$.

The approach by Yasumura & Kawai represents the most conservative approach yielding the lowest values for $F_{y,m}$ in all tests and for $v_{y,m}$ in most of the tests. Whereas the EEEP gives the highest values for $F_{y,m}$ and $v_{y,m}$ for most of the tests. Further examination also indicates that this method is more sensitive to the presence of multiple local maximums.

Table 2. Prinzipal for the determination of the $F_{y,m}$ and $v_{y,m}$ by different methods.



The evaluation of these results shows the difficulty to best distinguish between an elastic and a plastic range of the experimental load-displacement curve. For a maximum of 30 mm displacement, obtained for the maximum load clearly corresponding to $v_{u,m}$ in this case, the elastic displacements $v_{y,m}$ ranging from 5.8 mm to 6.9 mm are determined. This means that the connection considered could – after performing a cyclic testing program – fulfil the ductility requirement of 4 but never the ductility requirement of 6. The limitation of the ultimate displacement to 30 mm for monotonic tests is currently under discussion.

From these tests it can also be concluded that the method to determine the elastic displacement is of minor importance. If maximum displacements of a connection sub-

stantially smaller than 30 mm are obtained, any estimated elastic displacement determined by any method described above could be retained to determine $v_{y,m}$ and therefor define the cyclic test regime. As a matter of fact, a static ductility of more than 3 as for instance defined in SIA 265 in considering the proportion $v_{u,m} / v_{y,m}$ is promising. Knowing that connections with large numbers of connectors usually show high stiffness and little ultimate displacement it is of prime importance to define v_u in order not to overstress the connection after the first cycles. Therefor another approach was discussed, assuming a ductility of 6 and an elastic displacement of $30/6 = 5$ mm that can be used to set up the cyclic testing regime. If a cyclic ductility of 4 is targeted for a specific connection a good estimate for $v_{y,m}$ representing 25% of v_u from a monotonic test could be used.

4.3 Definition of cyclic tests

To proceed with cyclic testing the guidelines presented in the current EN 12512, as well as the proposal for the TS 12512 were considered. The main difference between the new proposal and the complete procedure of EN12512, see Table 2, is the inclusion of two additional sub-cycles with $3 v_{y,m}$ and $5 v_{y,m}$ in a first stage to load the connection in a more “gentle” way. One of the main interests in this campaign was to compare the results from both test routines, to compare them with the short procedure and to quantify their validity.

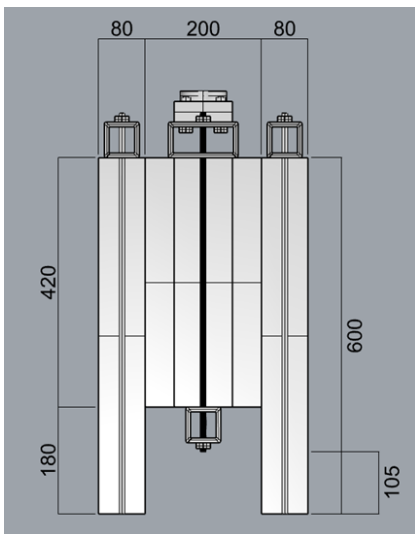


Figure 5. Test setup for $|-|$ type CLT/CLT/CLT connection for cyclic testing in compression and tension.

Thereafter, using a set displacement of $v_{y,m} = 5$ mm the cyclic tests were set up defining the cycles as follows: one cycle at $0.25 v_{y,m}$ and $0.5 v_{y,m}$ followed by 3 cycles at every level of displacement at $0.75 v_{y,m}$, $1.0 v_{y,m}$, $2.0 v_{y,m}$, $4.0 v_{y,m}$, $6.0 v_{y,m}$ based on the current standard and extended cycles applying one cycle at $0.25 v_{y,m}$ and $0.5 v_{y,m}$, followed by 3 cycles at every level of displacement at $0.75 v_{y,m}$, $1.0 v_{y,m}$, $2.0 v_{y,m}$, $3.0 v_{y,m}$, $4.0 v_{y,m}$, $5.0 v_{y,m}$, $6.0 v_{y,m}$ based on the draft version for the standard. Furthermore, two additional cyclic tests were carried out with only one phase were selected, setting either $4.0 v_{y,m}$ or $6.0 v_{y,m}$ corresponding to the short procedure according to EN 12512. For

each connection configuration at least one cyclic test was carried out for each of the four procedures, four configurations each undergoing four procedures, resulting in 16 cyclic tests. Initially the rate of slip was set to 0.02 mm/s, after running the first test and realizing the amount of time needed to complete a single test, the rate was increased to 0.2 mm/s, another point to be adapted in the future standard.

4.4 Results from cyclic testing

Selected results on connections with CLT only are presented below to show the principal behaviour of one type of screw under cyclic loading being representative for the configurations tested within the experimental investigation carried out at BFH / AHB.

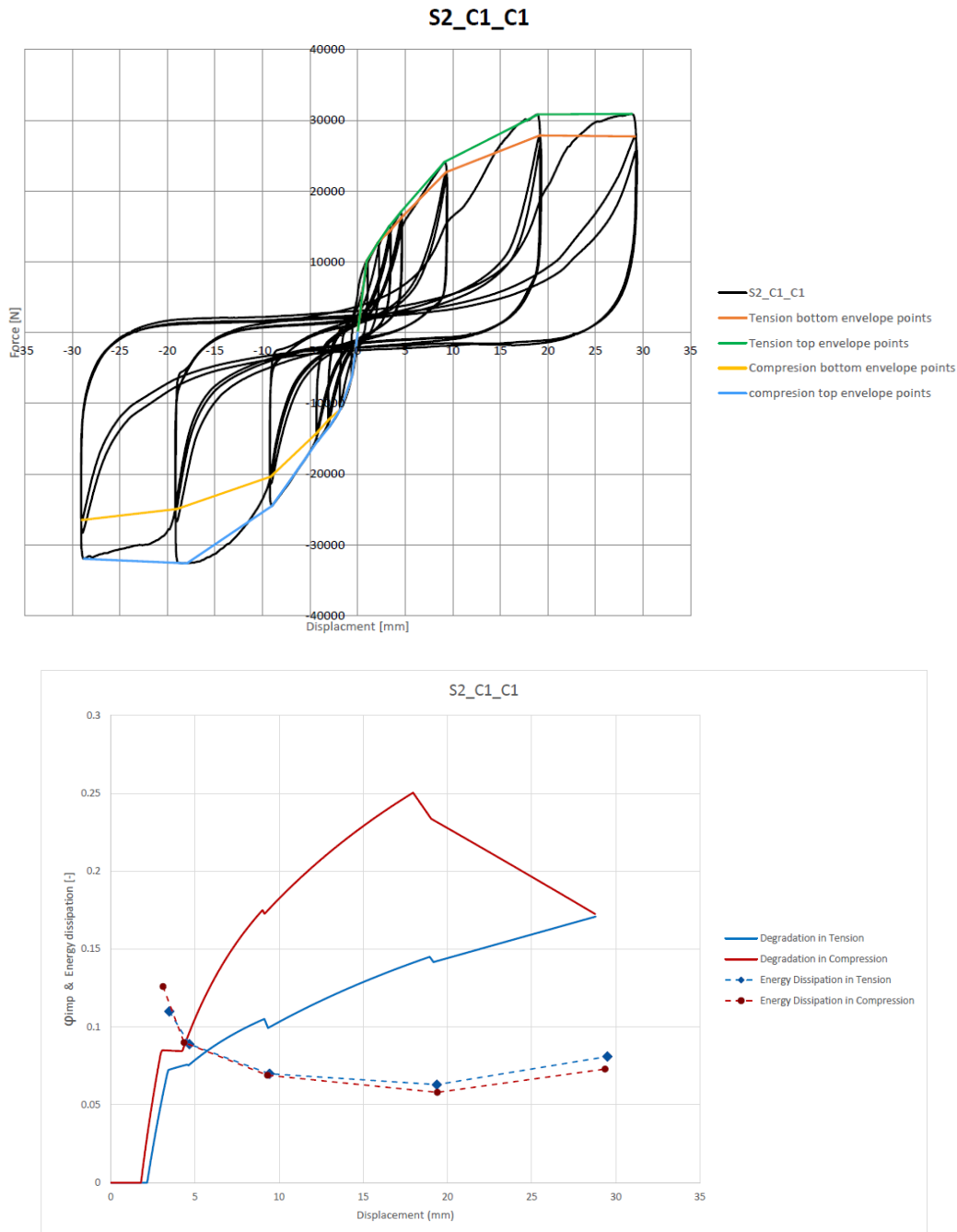


Figure 6. Plotting of the cyclic test S2C1C1 (|-|-type configuration) shows how the current version of the EN 12512 preserves the connection until the end of the test.

4.4.1 *Representative results from |–| -type configuration according to EN 12512*

In the case of test S2_C1_C1, a |–| -type configuration with CLT and screws set perpendicular to the edge of the inner CLT member is considered. The current test procedure defined in EN 12512 allows to accomplish the required 6.0 $v_{y,m}$ sub-cycles without significant changes in the values of force obtained. As Figure 6 above shows, the value of the force in compression and in tension for 6.0 $v_{y,m}$ is not significantly smaller when comparing to the obtained force at the first cycle applying 4.0 $v_{y,m}$. In all tests the nominal force F_N obtained from the monotonic test was reached in the 4.0 $v_{y,m}$ sub-cycle in at least one of the phases – compression or tension. In 75% of these tests F_N was reached in both compression and tension in the 4.0 $v_{y,m}$ sub-cycle. Compared to the monotonic test where $F_N = 38.9$ kN was measured a reduction of the connection strength is obtained and a factor of degradation of $k_{deg} \approx 0.8$ is calculated. The strength impairment factor ϕ_{imp} is calculated for all values of displacements and indicates that the reduction of strength along the cycles is obtained gradually. According to these results a cyclic ductility of 6 is obtained and the connection is considered to be dissipative belonging to the high ductility class DC 3.

4.4.2 *Representative results from ||| -type configuration, to the new proposal*

In the case of test S1_C1_C2, a ||| -type configuration (all members arranged in the same direction) with CLT and screws set perpendicular to the panel plane is considered. The inclusion of additional cycles at 3.0 $v_{y,m}$ and 5.0 $v_{y,m}$ for the full procedure (“new proposal”) greatly degrades the connection before completion of the test as shown in Figure 7. A sharp increase in the degradation of the connection after the 3.0 $v_{y,m}$ sub-cycle is noted. For the two final sub-cycles at 5.0 $v_{y,m}$ and 6.0 $v_{y,m}$ only a small percentage of the maximum load is recorded. According to these results, even that full 3 cycles at 4.0 $v_{y,m}$ are completed, a cyclic ductility of 4 is not obtained as $\phi_{imp} > 0.30$ and therefore the connection cannot be considered to be dissipative belonging to the medium ductility class DC 2.

The number of sub-cycles seems to considerably influence the degradation of the connection. Up to the 4.0 $v_{y,m}$ sub-cycle, a total of 14 phases has been completed – the same number of steps it takes to reach the end of the 3.0 $v_{y,m}$ phase in the draft version of the test which seems to present a maximum.

The strength impairment factor ϕ_{imp} is again calculated for all values of displacements and indicates that the reduction of strength is obtained suddenly. Compared to the monotonic test where the nominal force $F_N = 35.2$ kN was obtained (much lower than the force reached in the cyclic test with load $F_1(v=4v_y) > 40$ kN!) a sharp reduction of the connection strength is observed and a factor $k_{deg} \gg 0.8$ is calculated. As stated earlier, from a complete procedure higher values of reduction of resistance are expected than from the short procedure. This aspect was verified in performing the short procedure aiming at a cyclic ductility of 4 and 6 respectively.

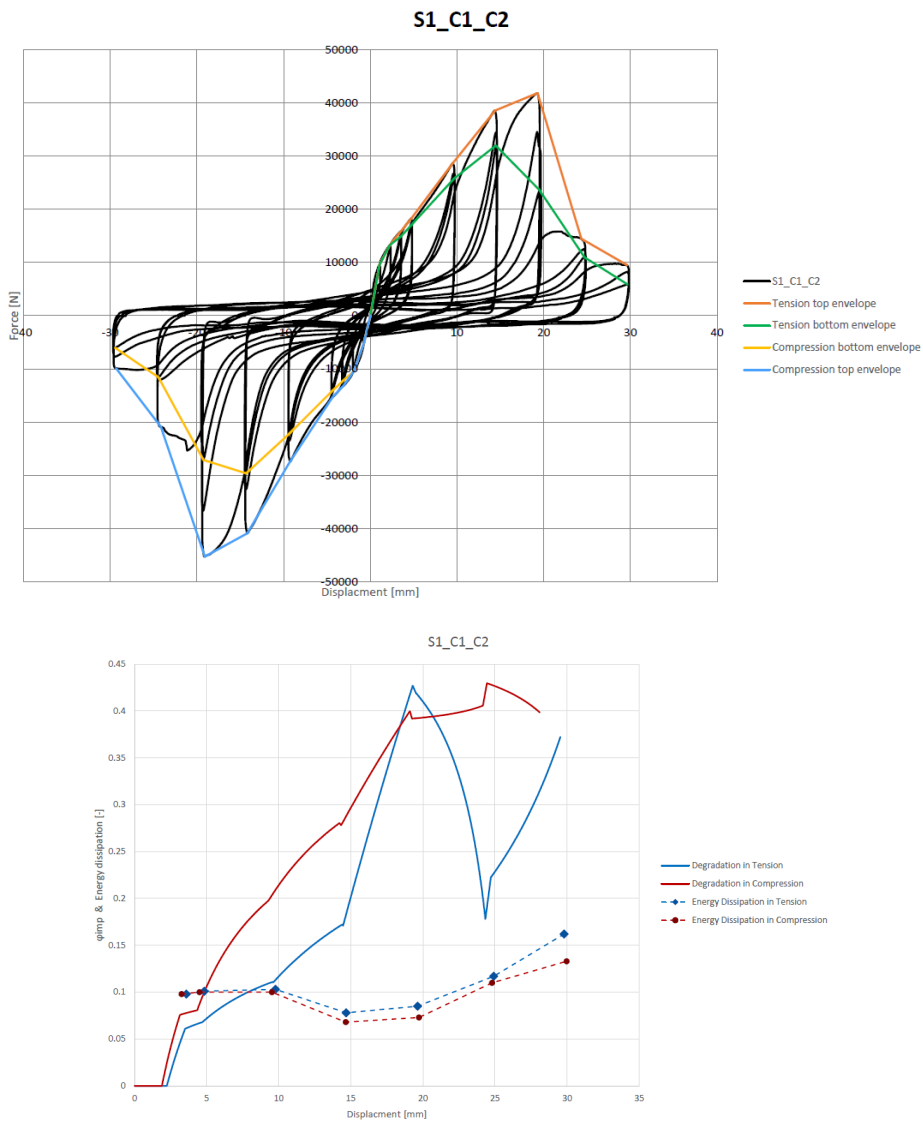
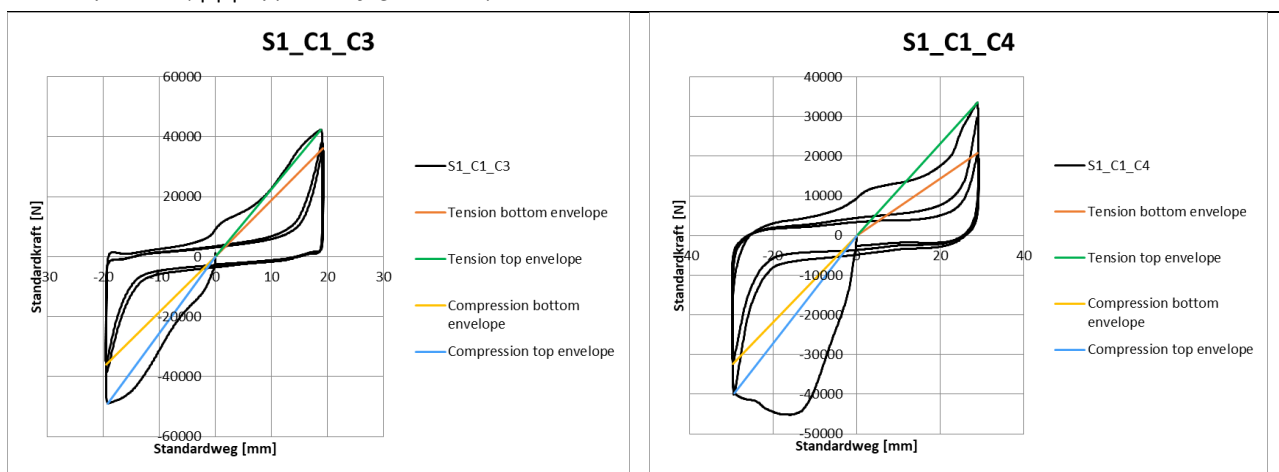


Figure 7. Plotting of the cyclic test S1C1C2 (||| -type configuration) shows how the addition of 3 V_y and 5 $v_{y,m}$ into the long procedure unnecessarily degrades the connection.

Table 3. Comparison of the short method at two levels of set displacements to aim at medium or high ductility class (||| -type configuration).



3 cycles at 4 $v_{y,m}$
 ϕ_{imp} in compression 27.4%
 ϕ_{imp} in tension 16.3%

3 cycles at 6 $v_{y,m}$
 ϕ_{imp} in compression 19.3%
 ϕ_{imp} in tension 37.2%

The results from the test series S1_C1 – using identical connections on CLT – was performed. Both setups lead to the same results, namely that the required number of cycles can be completed and that the connection can be classified as belonging to the medium ductility class DC 2. A good performance of the connection can be observed: applying set displacements of $4v_{y,m}$ only leads to a reduction of strength in the case of the last cycle of tension loading with $\phi_{imp} = 0.16$. The procedures investigated are consistent with the “short” procedure reported in the current standard EN 12512.

5. Conclusions

To best apply TS 12512 and the future EN 12512 simplifications and clear indications regarding what test at what stage should be carried out are needed. A “rough” estimation of the maximum deformability of the connection from monotonic tests and applying the tangent method or the EEEP method can be taken to determine $v_{y,m}$. Even simpler, the maximum displacement from the monotonic tests could be divided by 4 or 6 depending on the target ductility class. The maximum displacement of a connection to be considered – 30 mm today – must be discussed. The short procedure is suitable to evaluate the reduction of resistance and to assess the ductility class of the connection. A reduced number of cycles for the complete procedure seems adequate and could be $0.75 v_{y,m}$, $1.0 v_{y,m}$, $2.0 v_{y,m}$, $4.0 v_{y,m}$ for medium ductility and $0.75 v_{y,m}$, $1.0 v_{y,m}$, $3.0 v_{y,m}$, $6.0 v_{y,m}$ for high ductility connections in order not to prematurely destroy the connection at low cycles of testing.

Further investigations should be carried out in order to extend these findings to connections presenting higher numbers of connectors or to other type of connectors (nails, dowels, bolts) and diameters in order to better cover the wide array of variables influencing the results. A greater variety of tests on connection compositions may indicate certain patterns among classes of screws, number of connectors and so on.

6. References

- Alves T, Zare A, (2020) Screwed connections under cyclic loading - comparison of test methods, term paper, BFH / AHB August 2020
- American Society Standard Method (ASTM) E2126-11 (2018) - Standard Test Methods for Cyclic (Reversed) Load Test for Shear Resistance of Vertical Elements of the Lateral Force Resisting Systems for Buildings.
- ANSI/AISC 341-10 (2010) Seismic Provisions for Structural Steel Buildings, American institute of steel construction.
- Casagrande D, Bezzi S, D'Arenzo G et al. (2020) A methodology to determine the seismic low-cycle fatigue strength of timber connections in Construction and Building Materials Volume 231, 20 January 2020, Article number 117026.
- Eurocode 8 (2013) EN 1998-1:2004+A1:2013, Eurocode 8 – Design of structures for earthquake resistance part 1: General rules, seismic actions and rules for buildings. Brussels, Belgium: CEN, European Committee for Standardization

- EN 12512:2001/A1:2005, Timber structures – Test methods – cyclic testing of joints made with mechanical fasteners. Brussels, Belgium: CEN.
- EN 26891:1991, Timber structures – Joints made with mechanical fasteners – General principles for the determination of strength and displacement characteristics. Brussels, Belgium: CEN, European Committee for Standardization.
- Flatscher G, (2017) Evaluation and approximation of timber connection properties for displacement-based analysis of CLT wall systems, doctoral thesis, Graz University of Technology, April 2017
- Follesa M, (2015). Seismic design of timber structures - A proposal for the revision of Chapter 8 of Eurocode 8. Ph.D. Thesis. Università degli Studi di Cagliari, Italy, 2015.
- Follesa M, Fragiacomò M, Casagrande D, Tomasi R, Piazza M, Vassallo D, Canetti D, Rossi S (2018). The new provisions for the seismic design of timber buildings in Europe. *Engineering Structures*, Special issue “Seismic Wood Structures”, Vol. 168, 1 August 2018, pp. 736-747.
- Frangiaco M, Follesa M, Casagrande D, Piazza M (2019) The revision of the timber chapter of the Eurocode 8. 5th International Conference on Structural health Assessment of Timber Structures, SHATIS 2019, 25-27 September 2019, Guimaraes, Portugal.
- Germano F, Metelli G, Giuriani E (2015) Experimental results on the role of sheathing-to-frame and base connections of a European timber framed shear wall, *Constr. Build. Mater.* 80 315–328.
- Jockwer R, Jorissen A (2018). Load-displacement behaviour and stiffness of lateral connections with multiple dowel type fasteners. *Proceedings of Meeting 51 of the International Network on Timber Engineering Research (INTER)*, 13 - 16 August 2018, Tallinn, Estonia, Edited by R. Görlacher, paper No. 51-07–7.
- Rossi S, Giongo I, Casagrande D, Tomasi R. Piazza M (2019) Evaluation of the displacement ductility for the seismic design of light-frame wood buildings, *Bulletin of Earthquake Engineering*, 17(9), pp. 5313-5338.
- SIA 265 (2012) *Holzbau*, Schweizerischer Ingenieur- und Architektenverein, Zürich
- Yasumura M, Kawai N (1998) Estimating seismic performance of wood-framed structures, In *Proc., 5th World Conf. on Timber Engineering (WCTE)* Montreux, Switzerland, 2, 1998, pp. 564–571.

Discussion

The paper was presented by C Sigrist and D Casagrande

J Dolan commented that he is involved in a test program considering collapse. The results indicated the short period buildings showing higher level of collapse compared to general observed behaviour in real earthquakes. Modeling large displacement greater than 0.8 F_{max} as a post peak response would be needed for collapse considerations. He suggested that obtaining information for 0.4 F_{max} as a post peak response would be appropriate. C Sigrist responded that there is much information on monotonic tests and the approach to conduct fewer cyclic tests with push out may be appropriate as test methods not only for connections but for components and structures would also be needed. J Dolan added that system behaviour would take over after post peak behaviour and it would be important to model this for collapse.

G Hochreiner stated that inclusion of damping information would be important. C Sigrist responded that this is included via the cyclic tests.

U Kuhlmann said that the thesis of F Bruehl was just finalized dealing with ductility under static loading. Even though this is different from cyclic loading the information may be useful for consideration here and absolute deformation limits would be important. D Casagrande agreed that deformation limitation would need to be considered. A Ceccotti discussed why reduction of resistance was needed in the standard for consideration.

G Hochreiner agreed that maximum deformation limit would be needed. He also stated that minimum spacing distance for development of plastic behaviour of connections would be needed also. C Sigrist responded that rules for connection spacing requirements are available in standards.

F Lam commented that test protocol should reflect correct failure modes of structures under earthquake excitations. Under the CUREe project cyclic test protocols were developed by considering computer simulations of the behaviour of single degree of freedom systems under different earthquakes. Would this approach be considered here later. D Casagrande said that they are aware of the CUREe protocols and will consider them later. J Dolan commented that the CUREe protocol will be updated to consider large displacements.

P Quenneville asked will this protocol consider supplementary energy dissipative devices. C Sigrist stated that this area should be considered in different work and not here. P Quenneville commented that it is strange that different protocols would be needed for supplementary energy dissipative devices as these should be considered as part of the system. C Sigrist disagreed and D Casagrande said that new Eurocode 8 has plans for a new standard to address this area.

Quantifying Robustness in Tall Timber Buildings

Konstantinos Voulpiotis¹⁾, Jochen Köhler²⁾, Robert Jockwer³⁾, Andrea Frangi¹⁾

¹⁾ Chair of Timber Structures, Institute of Structural Engineering (IBK), Swiss Federal Institute of Technology (ETH) Zurich, Zurich, Switzerland

²⁾ Department of Structural Engineering, National Technical University of Norway (NTNU), Trondheim, Norway

³⁾ Division of Structural Engineering, Chalmers University of Technology, Gothenburg, Sweden

Keywords: Scale; Consequences; Disproportionate Collapse; Compartment; ALPA

1 Introduction

Tall buildings where timber has a significant structural role are becoming increasingly popular owing to the technological progress of timber products and the subsequent adaptation of building codes. However, the complex structural behaviour of timber causes a number of challenges for the engineers, such as difficulty to satisfy serviceability criteria (e.g. vibrations) and long-term behaviour (e.g. creep), and avoidance of brittle failure modes. One challenge that is notoriously difficult to satisfy, and is receiving increasing attention recently, is the design for the avoidance of disproportionate collapse in case of damage, in other words, the design for structural robustness.

The current state-of-the-art of structural robustness is detailed in the authors' previous publication (Voulpiotis, et al., 2019), with the relevant references. This present paper summarises the qualitative framework detailed in the previous publication and describes in detail a complete robustness quantification framework, along with an example case study building demonstrating how the framework is applied. Conclusions and building code-related recommendations are presented in the end.

2 Qualitative Framework (Summary)

The two key concepts for a qualitative approach to structural robustness are the consideration of the structure in different levels of the scale, and the design against both localised and systematic exposures (Voulpiotis, et al., 2019). Popular design methods for robustness, such as Compartmentalisation, Alternative Load Path Analysis (ALPA), and Key Elements shall not be used as “one size fits all” methods, but should rather

be combined in the appropriate building scales in order to design the structure for any type of exposure. A combination of robustness methods in different scales would have greatly increased the survival chances of famous collapses such as the Bad Reichenhall Arena, which is described in Winter & Kreuzinger (2008).

For a tall building (vertically stacked compartments), the resulting structure when following this method resembles modern skyscrapers: a combination of mega-columns and braces (key elements) forming strong-border compartments, containing frames which can internally arrest a collapse via alternative load paths (Figure 1).

When timber is involved in the loadbearing structure, the robustness framework per se remains the same, however the specific methods to achieve the alternative load paths and compartment borders may be very different. This is discussed in more detail in the quantification chapter. An interesting case study of a tall timber building which applies some of these qualitative methods is Treet in Bergen, Norway (Malo, et al., 2016).

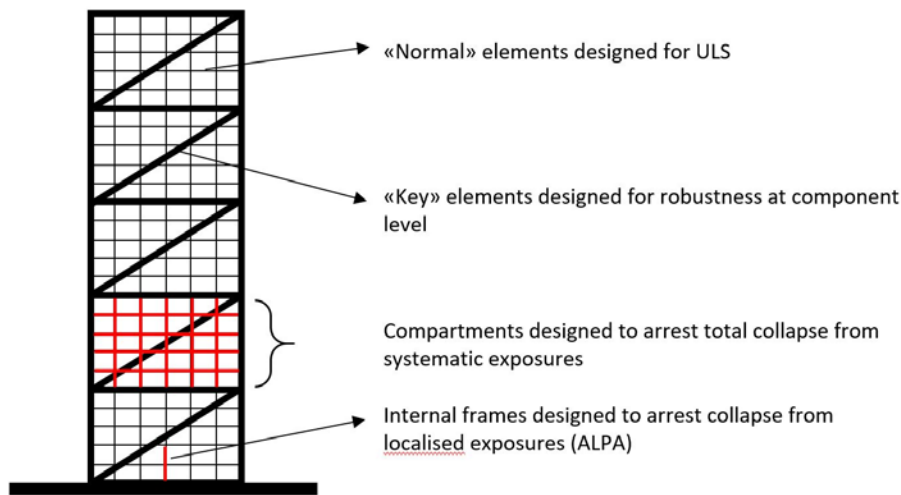


Figure 1: Qualitative example of a tall building designed for robustness in multiple levels of the scale

3 Quantitative Framework

3.1 Mathematical Definitions

The basic mathematical definition of robustness is described in detail in Starossek & Haberland (2010) by evaluating the probability of disproportionate collapse in three parts: exposure $P(E)$, vulnerability $P(D|E)$, and robustness $P(C|D)$. When these values are combined with the respective consequences (direct C_{Dir} , and indirect C_{Ind}), the expected consequences (i.e. risk) may be calculated (Baker, et al., 2007). These are shown in Equations 1 and 2 below. For a more comprehensive summary of the above, please refer to last year’s publication, Voulpiotis, et al. (2019).

$$\mathbb{E}[C] = \mathbb{E}[C_{Dir}] + \mathbb{E}[C_{Ind}] \tag{Eq.1}$$

Expected Consequences
Expected Direct Consequences
Expected Indirect Consequences

$$\mathbb{E}[C] = (P(E) \times P(D|E)) \times C_{Dir} + (P(E) \times P(D|E) \times P(C|D)) \times C_{Ind} \tag{Eq.2}$$

To quantify robustness, we will use the robustness index mentioned in last year's publication, described in detail in Baker, et al. (2007). Given an initial damage to a structure (direct consequences C_{Dir}), which may or may not cause further damage (indirect consequences C_{Ind}), the robustness index, I_{Rob} , is defined as the ratio of the expected direct consequences to the expected total consequences (Equation 3). That is, the robustness index evaluates the disproportionality of consequences relative to an initial damage scenario. The minimum value of zero means that all consequences are indirect (no robustness), while a maximum value of one means that all consequences are direct (maximum robustness).

$$I_{Rob} = \frac{\mathbb{E}[C_{Dir}]}{\mathbb{E}[C]} = \frac{\mathbb{E}[C_{Dir}]}{\mathbb{E}[C_{Dir}] + \mathbb{E}[C_{Ind}]} = \frac{C_{Dir}}{C_{Dir} + P(C|D) \times C_{Ind}} \quad \text{Eq.3}$$

It is important to realise that this index is relative only to a specific damage scenario, and the probability of that scenario occurring has cancelled out of the equation. The scenario probabilities will come back in the quantification later in the chapter.

Three elements are required for the calculation of the robustness index:

- A sufficiently accurate structural model. This may be anything from a simple analytical expression to a complex numerical model, depending on the case study. Since the analysis of interest is collapse of various different structures, a dynamic, nonlinear finite element model is preferred.
- A method to propagate uncertainties in that model to calculate $P(C|D)$ and, optionally, to calculate the sensitivity indices to determine which model inputs contribute the most (or the least) in the probability of failure. This may be a simple Monte Carlo Simulation, which works well with analytical expressions, or very fast numerical models. For a complex finite element model, metamodelling techniques such as polynomial chaos expansions and support vector classifications are necessary due to their computational efficiency.
- A method to estimate the consequences C_{Dir} and C_{Ind} from the results of the model run. To avoid an overly complex and potentially unreliable calculation, we propose a simplified approach where consequences are measured in terms of the floor area of the failed part of the building. Hence, $C_{Dir} = A_{Fail,Dir}$ and $C_{Ind} = A_{Fail,Ind}$. In addition, $A_{Fail,Ind}$ may be factored to take into account the increased cost per square meter of indirect consequences relative to the cost per square meter of direct consequences, since the former is more likely to include fatalities. This factor may be determined from base values of insurance companies, however it is beyond the scope of this paper. Regardless, the assumption becomes irrelevant when different concepts of the same structure are compared, as we show below.

These three elements constitute the three main steps in the calculation of the robustness index, given a structure and appropriate probabilistic input variables. It should not be forgotten, however, that these steps must be performed multiple

times, for different damage scenarios, in order to obtain an average robustness index. Only then can one talk about evaluating the robustness of a structure (i.e. reaction to the unforeseen). The sequence is depicted in Figure 2:

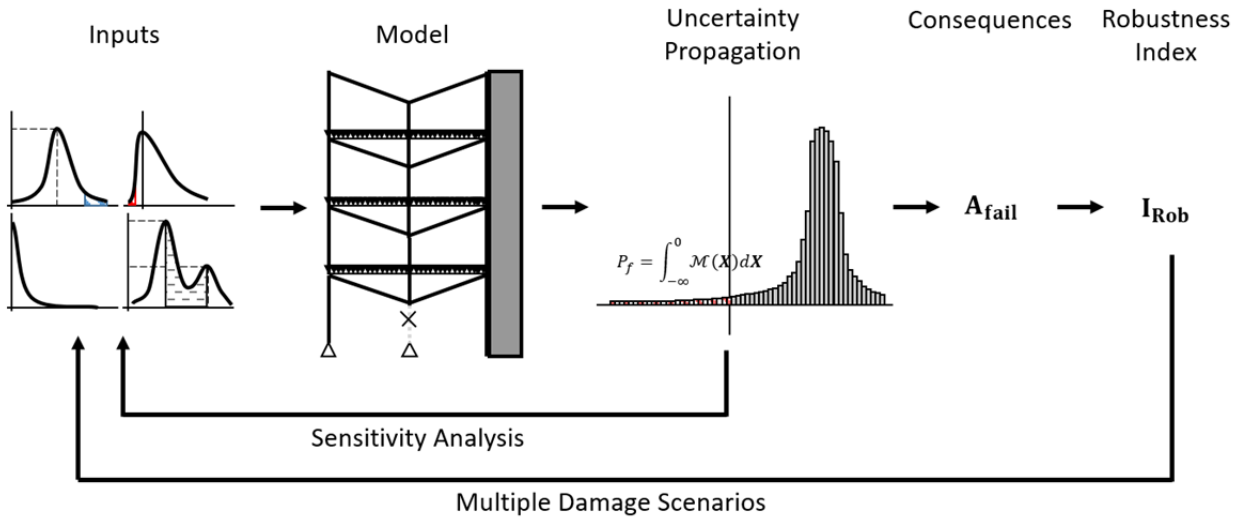


Figure 2: Algorithm to calculate the robustness index for a given structural concept

3.2 Complete Framework Proposal

Let us assume a building structure with a base conceptual design and the designer’s goal being to improve this building’s robustness. We can recommend any number of different modifications to the structure, such as the addition of columns, or diagonals, or the moment stiffening of connections. Each of the modified designs, as well as the initial base concept, shall be analysed according to Figure 2. The average robustness index shall be calculated from the robustness indices of each assumed damage scenario weighted by the probability that this scenario occurs, $P_s = P(E) \times P(D|E)$. Given k different concept designs/modifications, the average robustness index of the k^{th} design for n scenarios is given in Equation 4:

$$I_{Rob(k,av)} = \sum_{i=1}^n (W_i \times I_{Rob(k,i)}) \tag{Eq.4}$$

Where W_i is the weighting factor for the i^{th} scenario, given in Equation 5:

$$W_i = \frac{P_{Si}}{\sum_{i=1}^n P_{Si}} = \frac{(P(E) \times P(D|E))_i}{\sum_{i=1}^n (P(E) \times P(D|E))_i} \tag{Eq.5}$$

Comparing the average robustness indices for the different building concepts allows us to rate these concepts according to their quantified robustness and compared to the base concept. *This is exactly the basis of the proposed framework: the goal is not to analyse a large number of completely different structures which fit the remit of a building design and compare their robustness performance, but rather explore the effectiveness of design decisions for improving the robustness of an initial conceptual design, whose base geometry has been selected according to numerous other factors such as location, project size, architecture, local materials and expertise, et cetera.*

For a complete comparison, a measure of the cost of each option must be included in the calculation, for example the volume of timber material, V_k . We define the Normalised Geometry Rating (NGR) of a given concept k , in Equation 6:

$$NGR_k = \frac{I_{Rob(k,av)}}{I_{Rob(1,av)}} \times \frac{V_1}{V_k} \tag{Eq.6}$$

Obviously, an NGR below 1 means the proposed concept performs worse overall (that also includes options with better robustness but disproportionately higher cost). The entire process is summarised in Figure 3:

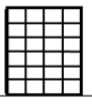
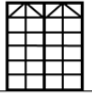
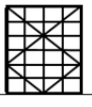
Robustness Optimisation	Scenario 1	Scenario 2	...	Scenario n	Average I_{Rob} (Separate for localised and systematic exposures)	Measure of base cost, e.g. material volume	Normalised Geometry Rating (NGR)
Base Concept 	$I_{Rob(1,1)}$	$I_{Rob(1,2)}$...	$I_{Rob(1,n)}$	$I_{Rob(1,av)}$	V_1	$\frac{I_{Rob(1,av)}}{I_{Rob(1,av)}} \times \frac{V_1}{V_1} = 1$
Concept 2 	$I_{Rob(2,1)}$	$I_{Rob(2,2)}$...	$I_{Rob(2,n)}$	$I_{Rob(2,av)}$	V_2	$\frac{I_{Rob(2,av)}}{I_{Rob(1,av)}} \times \frac{V_1}{V_2} = ?$
...
Concept k 	$I_{Rob(k,1)}$	$I_{Rob(k,2)}$...	$I_{Rob(k,n)}$	$I_{Rob(k,av)}$	V_k	$\frac{I_{Rob(k,av)}}{I_{Rob(1,av)}} \times \frac{V_1}{V_k} = ?$
	$I_{Rob,av(1)}$	$I_{Rob,av(2)}$...	$I_{Rob,av(n)}$			

Figure 3: Algorithm to calculate the normalised geometry ratings for a given structure

3.3 Connection with Scales and Qualitative Design

This quantification procedure can be used to evaluate the conceptual options determined from the qualitative framework of chapter 2. Let us categorise each improvement concept k (in terms of NGR_k) in its respective scale: stiffening the connections would be an improvement in the connection scale, adding diagonals would be an improvement in the compartment scale, and so on. The maximum NGR values for each scale may be compared in order to determine which scale affects the building's robustness most effectively. That is, the scale-based NGR is the tool to help the designer choose a robust, cost-effective building concept. In addition, sensitivity indices (first or higher orders) may be calculated given enough analyses. This could be used as an alternative to the maximum NGR values in order to shift the focus of the design to the appropriate scale. This is shown in Figure 4.


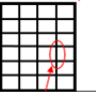
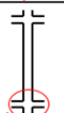
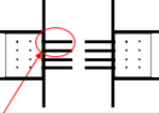
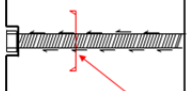
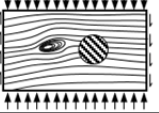
	Level	Design Method	Responsibility	Max(NGR)	Level Sensitivity
Whole building		Compartmentalisation	Structural Engineer (Conceptual Design)	NGR_{system} NGR_{local}	$S_{building}$
Compartments		Alternative Load Path Design	Structural Engineer (Conceptual Design)	NGR_{system} NGR_{local}	$S_{compartment}$
Components		Key Element Design	Structural Engineer (Conceptual Design)	NGR_{system} NGR_{local}	$S_{component}$
Connections		Robust Connection Design	Structural Engineer (Detailed Design)	NGR_{system} NGR_{local}	$S_{connection}$
Connectors		Key Connector Design	Supplier	NGR_{system} NGR_{local}	$S_{connector}$
Materials		Material Grading / Robust Manufacture	Supplier	NGR_{system} NGR_{local}	$S_{material}$

Figure 4: Complete scale-based robustness framework with quantification

3.4 Quantification Remarks

The *NGR* values are based on the relative changes between different designs and damage scenarios. The observations are thus not sensitive to possible lack of precision in the assumptions. Equation 6, however, is still a preliminary calculation which may not yet be optimally balancing the robustness index and building costs.

4 Case Study Tall Timber Building

A simplified tall timber building case study has been analysed based on the proposed framework, in order to demonstrate how the procedure works.

4.1 Structural Model

A simple 3x3 bay, 10-storey timber building was modelled in Dassault Systèmes' Finite Element software Abaqus®. The bay size is 5m and the storey height is 3m. Instead of using the interface, the structure was generated using a Python® script for speed and parametrisation, as well as to be able to interface with Matlab® for the uncertainty propagation. The building comprises 100x320mm beams and 200x200mm columns, as well as 200mm thick, 2-way spanning 5-ply Cross-Laminated Timber (CLT) panels for the core walls and 120mm thick, 2-way spanning 3-ply CLT panels for the floors. The timber material is Spruce (*Picea abies*) with stiffness properties taken from Sandhaas, et al. (2020). A linear elastic behaviour was assumed for the material; plasticity and failure were concentrated in the connections by defining connector behaviours in Abaqus®. The ground level walls are rigidly fixed to the

ground, and the ground level columns are pinned to the ground (translational fixity only). In addition to the members' selfweight, the floors are loaded with an additional 1kN/m^2 dead load to take into account floor finishes, and a 0.5kN/m^2 imposed load (from $w = 2.4\text{kN/m}^2$ and $\psi_2 = 0.2$, simulating the acting live load for a residential building in an accidental scenario). The members have been approximately sized to not reach failure stress (assuming C24 softwood and partial safety factors) under full loading conditions, without considering wind and snow loads: this calculation is not shown and only serves to have an approximately realistic member size for a building of this scale.

Three versions of the building were created: concept 1 (the base structure) has pinned beam-to-column and beam-to-wall connections. The ability to develop alternative load paths has been introduced in two further concepts of the same building: In concept 2, moment resistance was introduced in the beam-to-column and beam-to-wall connections. In concept 3, the connections remained all pinned and diagonal members were introduced in the corner bays of the top floor. Both improved concepts have substantially strengthened column-to-column vertical connections in order to be able to carry loads upwards in tension. Necessarily, the column dimensions were also increased by 50%. The structural differences are outlined in Figure 5. All concepts have pinned floor-to-beam and floor-to-wall connections, and rigid wall-to-wall connections.

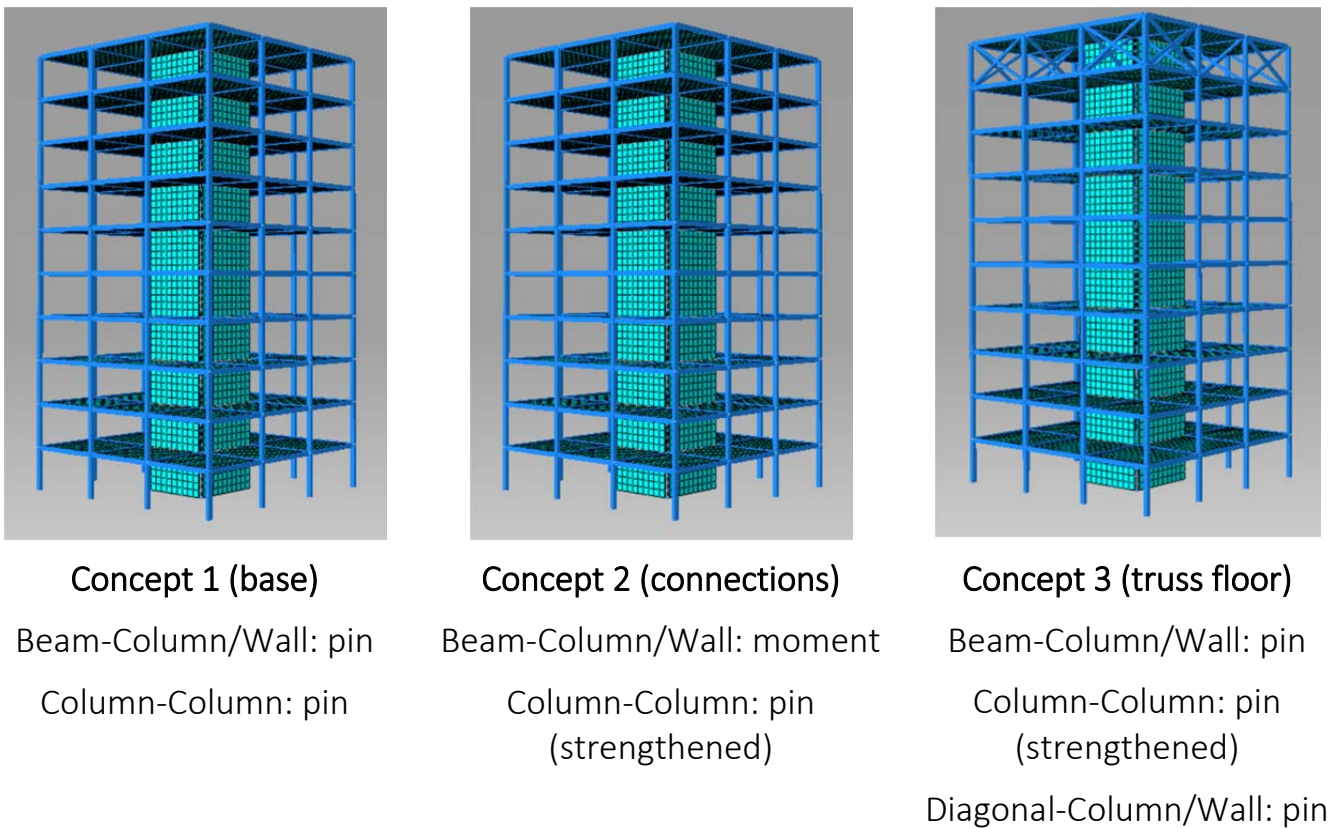


Figure 5: Comparison of the three building versions

All but the wall-to-wall connections were modelled as linear elastic with failures at the loads corresponding to the section strength of the respective degree of freedom

(uncoupled). This simplification makes the absolute results inaccurate, however the relative results of concept comparison remain valid.

The solver employed for the analysis is the Abaqus/Standard implicit dynamic solver with a quasi-static application, which is very powerful in following the (potential) collapse of the structure incrementally. The mass matrix of the structure is assembled using the density of the materials. The model is analysed in a time length of three seconds, with load ramping, in small, automatic time increments to follow the acceleration of parts upon connection failure.

4.2 Consequence Estimation

Two damaged versions of the building are analysed: a ground floor corner and edge column removal respectively. The output variables saved in each analysis were the vertical deflections at the centre nodes of each floor panel. A post-processor was written in Matlab® in order to determine whether collapse has occurred, and to distinguish between different collapse types.

Indirect failure has been simplified to a binary status of each building bay: by measuring the resulting deflection at the centre of each floor slab, a flag of zero (no collapse) or one (collapse) is given. We believe the coarseness of this approach is realistic: for massive elements such as glued laminated beams and columns and CLT floors, collapses of fractions of a bay are unlikely. The deflection limit for failure used here is 1m. This is also realistic since all normal deflections of a healthy structure are well below this value, while deflections of a collapsed floor are well above it.

The absolute deflections and failure flags are printed in a three-dimensional matrix corresponding to the bays of the building, in terms of their x-y-z position. Each unique 3D failure matrix of zeros and ones corresponds to a unique collapse scenario, which can be named or numbered accordingly and used as a unique collapse class identifier. In this case study we only studied one collapse class per damage scenario, therefore a final flag of one or zero was used to identify a general case of collapse or no collapse respectively. This assumption is valid when the strength or stiffness properties vary identically for all members (see uncertainty propagation section below). For models of higher uncertainty dimensionality, multiple types of collapse may occur for the same initial damage scenario.

Calculating the indirect failure area, $A_{Fail,Ind}$, is a straightforward process of multiplying the failure matrix of zeros and ones with the bay area (a matrix with bay areas may be used for non-symmetric buildings) and summing all the terms. The process is shown in Figure 6 (for a simple 2D case).

In the case of a column removal scenario, the direct failure area, $A_{Fail,Dir}$, is assumed to be the area at a radius of half a bay size from the failed column. For a corner column this corresponds to a quarter bay, while for an edge column this corresponds to a half bay. This assumption is independent of the structure type around the failed column (e.g. the floor type).

While systematic exposures are of great interest for holistic robustness, they have not yet been investigated in this case study.

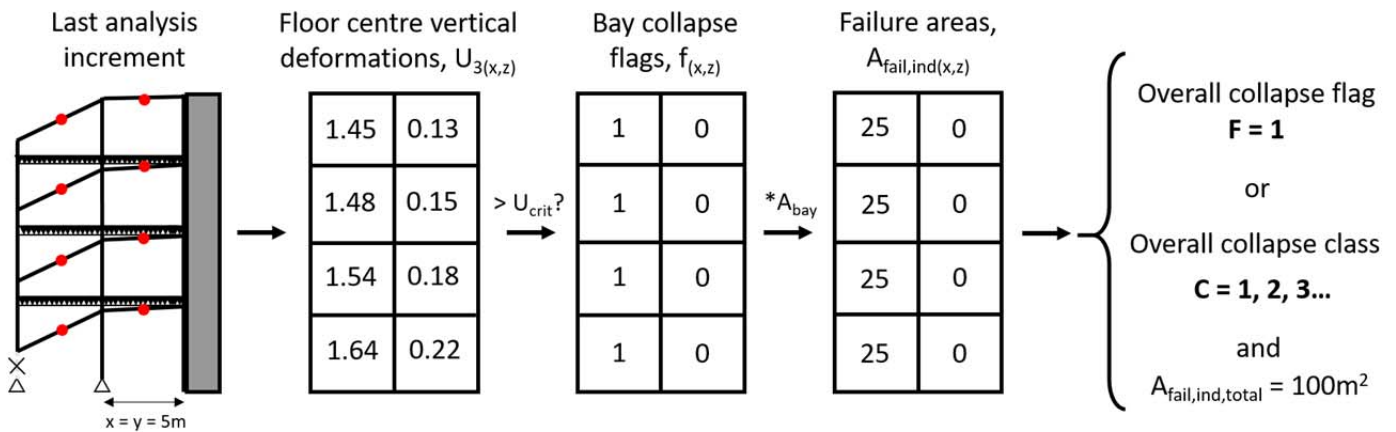


Figure 6: Failure area calculation procedure (2D example)

4.3 Uncertainty Propagation

All geometry variables are treated as constants (deterministic). For simplicity, the only inputs that we vary probabilistically are the timber stiffness and imposed live load, as shown below with their probabilistic properties.

Table 1: Model probabilistic variables

Variable	Distribution	Mean	CoV
Timber Stiffness (E)	Lognormal	11000 MPa	10%
Imposed UD Load (W)	Gumbel	0.5 kN/m ²	22%

We did not vary the actual connection strength explicitly to keep the model uncertainty dimensionality to a minimum. We are currently working on adaptive meta-modeling techniques, which will allow us to later introduce a much larger number of input variables. Connection strength is however already affected probabilistically from the material stiffness: the failure initiation is force-based and a structure that deflects more will, with the geometrical nonlinearities, put more load on the connections.

The Abaqus® Python script is run externally via Matlab® while editing the input file on every run to carry out the simulations for different realisations of the input variables. The uncertainty quantification software developed at ETH Zürich, UQLab®, is used to propagate the uncertainties (Marelli, et al., 2019). Two uncertainty propagation methods were applied here: a regression-based method for smooth model outputs, and a classification-based method for non-smooth model outputs.

The Least Angle Regression method for sparse polynomial chaos expansion (PCE) was the chosen smooth output method. Using very few model runs, a series of computationally inexpensive polynomial functions were built (one for each deformation output, that is one for each floor slab) to approximate the desired model output. A poly-

nomial degree of up to 10 was allowed, with the final degree being the one that minimises the leave-one-out error. No further technical details on the method itself are presented in this paper, the interested reader can refer to Blatman & Sudret (2011).

When model outputs are non-smooth, support vector classification (SVC) is an efficient machine learning method which uses a small training set of values (here, model runs) and is able to analytically predict the class (here, collapse flag) for any new given set of inputs. In this case study the collapse flags together with a nonlinear (Gaussian) kernel function were used to create the classification. Full details on the method are presented in Basudhar, et al., (2007).

Both methods are surrogating the Abaqus® model such that a large number of model evaluations can be carried out very fast. We are therefore able to calculate probabilities of failure by running Monte Carlo Simulations on the model surrogates with a very large input sample and simply counting the number of failures.

In the study of collapse, the results are continuous within disjointed regions of the output domain. Therefore a two-step process is possible, with a support vector classification used to first determine which class the random input vector leads to (collapse vs no collapse), and the polynomial chaos expansion used to subsequently estimate the actual deformations. A detailed example of the two-step method is presented in Maliki & Sudret (2019).

4.4 Tentative Results

The six models (three concepts in two damage scenarios each) were run 30 times each, for the same random input vector. Unfortunately, none of the simulations showed a combination of collapses and no collapses: each concept/damage pair either certainly collapsed (concept 1 – Figure 7), or certainly did not collapse (concepts 2 & 3). This prevented us from using the SVC method to calculate the probability of failure, therefore a collapse probability of one for concept 1 and zero for concepts 2 & 3 was used from the raw data. More simulations should be run with more probabilistic input parameters, a wider input sample, and with modified connections to get more diverse results. Nevertheless, the overall methodology is valid, and the post-processing of the data according to

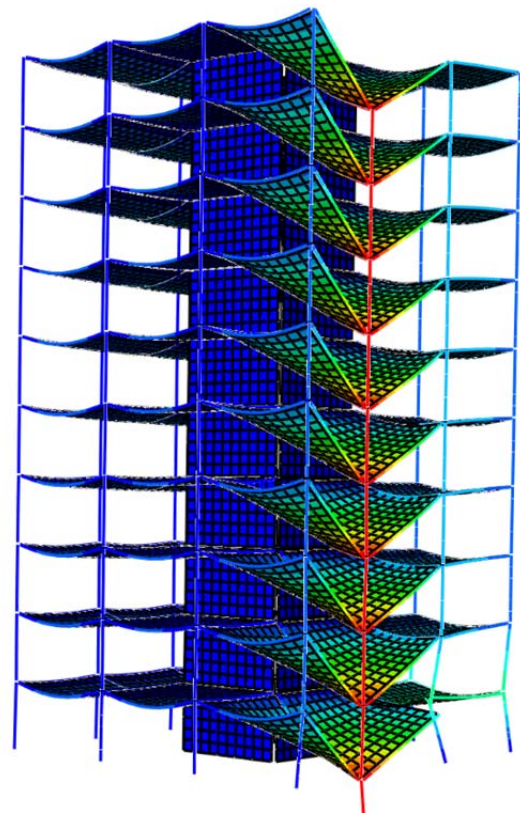


Figure 7: Collapse of the base geometry at damage scenario 2

Figure 3 and assuming equiprobable damage scenarios yielded the results summarised in Table 2 below:

Table 2: Robustness results for the case study

	Scenario 1	Scenario 2	$I_{Rob(av)}$	V_t	NGR
Concept 1	$I_{Rob} = 0.0168$	$I_{Rob} = 0.0138$	0.0153	406.4	1
Concept 2	$I_{Rob} = 1$	$I_{Rob} = 1$	1	424.4	62.6
Concept 3	$I_{Rob} = 1$	$I_{Rob} = 1$	1	431.9	61.6
W_S	0.5	0.5			
$A_{fail,Dir}$	6.25	12.5			

Clearly, both concepts 2 and 3 offer a substantial robustness improvement for the base geometry, with little added timber volume, V_t . It is not surprising that very little added material cost is involved in building truss diagonals in order to avoid the potentially problematic moment resisting connections in timber. However a comparison beyond the material volume is certainly required for a fair choice. Construction costs, architectural considerations, local expertise, and maintenance issues must all be involved in a more holistic “cost” parameter to be used in Equation 6.

4.5 Improvements

Although the model is defined in detail, some critical properties, such as connection behaviour, have been chosen with little analysis and as such the case study is only used to demonstrate the framework procedure and not to draw conclusions from the results. More importantly, substantial amount of scripting has been done to allow every detail of the building to be tuned by simply editing some variables in the code. Since the procedure is object-oriented, the model inputs, structure, uncertainty propagation, and post-processing can each be improved independently in order to make the results more accurate. Continuing from this example, the building connections shall be fully designed and modelled more accurately with nonlinear behaviour and appropriate failure values. A more detailed material model is also required, to include failure stresses and plasticity where appropriate. Finally, a longer total time interval and many more damage scenarios need to be studied, which is just a matter of computational budget. At the same time, we are making a call to all researchers who have working models to get in touch in order to populate the robustness framework with more complete sub-models (e.g. accurate CLT floor models, accurate connection models, et cetera).

5 Impact on Design Codes

The requirement for structural robustness in building codes has always been a sensitive topic, to a large extent because of its philosophical dimension (very much like the oftentimes abstract concept of quality). In this paper we have taken some important steps towards a more objective robustness framework, on a quantifiable risk basis. Despite the early stage of development, some tentative proposals for future building code developments can be already presented. These ideas may not be applied in the existing building codes directly, but should rather be a trigger for more discussion on how future codes should be addressing the topic of robustness.

The existing consequence/importance class categorisation for robustness requirements is well understood and accepted in the engineering community (Mpidi Bita, et al., 2019). Based on chapters 2 and 3 of this paper, the robustness framework presented may be implemented in three categories of increasing complexity and for buildings of increasing consequence/importance class:

1. Low Importance buildings: qualitative approach only. This may apply to most low to medium-rise simple buildings where a quantification of robustness is not necessary. The conceptual methods described in chapter 2, i.e. in Voulpiotis, et al. (2019), are enough to design a sufficiently robust building.
2. Medium Importance buildings: quasi-quantitative approach. This may apply to any important building whose structure is relatively common and where an explicit quantification of robustness is not necessary. We suggest the calculation of the NGRs for common structure types, such as truss-type tall timber buildings and hybrid concrete core and timber post & beam tall timber buildings. The engineers may then be able to refer to a table of values similar to Figure 4 and invest resources in improving the appropriate scales in their given building.
3. High Importance buildings: full quantitative approach. This may apply to any unique, high importance building, such as new types of tall timber buildings. The engineers should carry out a full explicit quantification of the risks according to this paper and make specific improvements to the structure. Building codes may impose a minimum average robustness index that the design must satisfy.

We recommend practicing engineers and researchers to give their feedback on the quantitative framework and to use their models as described in chapter 4 in order to start collectively producing results to improve the practical understanding of robustness and aid codification discussions.

6 Conclusion

We have summarised the previously discussed qualitative approach to designing buildings via a powerful conceptual design based on addressing robustness in multiple levels of the scale. The focus of this paper was to build on this framework and present a method of quantification in order to make calculated, cost effective design decisions for any building in order to increase its robustness.

Given a base building that requires improvement in terms of robustness, the quantification method operates on three pillars: a structural model of the building able to simulate collapse, an uncertainty propagation method able to calculate the reliability of the building during different damage scenarios, and a consequence estimation method able to calculate the impact of these different damage scenarios in the building. This sequence is repeated for different versions of the base building. The resulting Normalised Geometry Rating (NGR) is a numerical robustness improvement (or deterioration) measure of a modified structure against its original and can be used in combination with the qualitative scale approach to identify and work on the scale of the building that has the highest impact-to-cost ratio for robustness measures.

The application of the framework has been demonstrated with a simple case study of a tall timber building, with the focus on the complete procedure and not the results. The object-oriented approach allows us to improve the accuracy of the results continuously, by making the modelling techniques increasingly detailed. This is an opportunity for engineers and researchers to collaborate and help generate data for many different types of (tall) timber buildings. Such a collective effort would help identify the best robustness strategies and may shape the robustness requirements of future building codes.

7 Acknowledgements

The authors are thankful for the financial support of the Albert Lück Stiftung which makes this research possible. Special thanks also go to COST Action FP1402 for enabling the collaboration between ETH Zurich and the NTNU in Trondheim.

The authors would also like to thank and congratulate the organisers of the first online INTER meeting, which ran smoothly and did not inhibit the fruitful discussions and peer feedback. This feedback has once again been incorporated in the present paper and is very highly appreciated.

8 References

- Baker, J. W., Schubert, M. & Faber, M. H., 2007. On the Assessment of Robustness. *Structural Safety*, Issue 30, pp. 253-267.
- Basudhar, A., Missoum, S. & Sanchez, A. . H., 2007. Limit state function identification using Support Vector Machines for discontinuous responses and disjoint failure domains. *Probabilistic Engineering Mechanics*, 23(1), pp. 1-11.
- Blatman, G. & Sudret, B., 2011. Adaptive sparse polynomial chaos expansion based on least angle regression. *Journal of Computational Physics*, 230(6), p. 2345–2367.
- Maliki, M. & Sudret, B., 2019. *A two-stage surrogate modelling approach for the approximation of models with non-smooth outputs*. Hersonissos, Proceedings of the 3rd International Conference on Uncertainty Quantification in Computational Sciences and Engineering.
- Malo, K., Abrahamsen, R. & Bjertnæs, M., 2016. Some structural design issues of the 14-storey timber framed building "Treet" in Norway. *European Journal for Wood Production*, Issue 74, pp. 407-424.
- Marelli, S., Wicaksono, D. & Sudret, B., 2019. *The UQLab project: steps towards a global uncertainty quantification community*. Seoul, 13th International Conference on Applications of Statistics and Probability in Civil Engineering, ICASP13.
- Mpidi Bitá, H., Huber, J., Voulpiotis, K. & Tannert, T., 2019. Survey of contemporary practices for disproportionate collapse prevention. *Engineering Structures*, Volume 199.
- Sandhaas, C., Sarnaghi, A. K. & van de Kuilen, J.-W., 2020. Numerical modelling of timber and timber joints: computational aspects. *Wood Science and Technology*, Volume 54, pp. 31-61.
- Starossek, U. & Haberland, M., 2010. Disproportionate Collapse: Terminology and Procedures. *Journal of Performance of Constructed Facilities*, 24(6), pp. 519-528.
- Voulpiotis, K., Köhler, J., Jockwer, R. & Frangi, A., 2019. *Robustness in Tall Timber Buildings - An Improved Framework*. Tacoma, International Network for Research in Timber Engineering (INTER).
- Winter, S. & Kreuzinger, H., 2008. *The Bad Reichenhall ice arena collapse and the necessary consequences for wide span timber structures*. Miyazaki, Proceedings of the World Conference in Timber Engineering (WCTE) 2008.

Discussion

The paper was presented by K Voulpiotis

P Dietsch asked if the model can differentiate between single cause failures versus systematic failures. K Voulpiotis responded yes this can be done by reduction of strengths in a series of members.

P Dietsch stated that the CLT elements were assumed to act as 2-D plates. In practice mostly 1-D action is available in CLT. K Voulpiotis responded that the 1-D action is not too interesting for the robustness studies. This can be considered easily by changing the a few lines in the computer code. Floor to beam connections are very important.

E Serrano asked when you talked about robustness at different scale there seemed to be no coupling between these scales. If you change one scale how would it impact the analysis? K Voulpiotis responded that it is the combination of scale that make this work more interesting. This is not done yet but can be studied easily with more computer runs.

G Fink stated that in reality member and connection sizes are designed to be slightly over the target. How would you consider this in terms of robustness. K Voulpiotis stated that ultimate limit states were considered to consider the geometry. R Jockwer added that the study aimed to get nominalized rating for robustness and one could assume for over design of member ahead in the model and also consider the precise case for comparison.

U Kuhlmann asked about the direct and indirect consequence definition. K Voulpiotis explained as an example the direct consequence as the area supported by the failure of a column.

4 Peer review of papers for the INTER Proceedings

Experts involved:

The reviews are undertaken by long standing members of the INTER group which is a community of experts in the field of timber engineering.

Procedure of peer review

- Submission of manuscripts: all members of the INTER group attending the meeting receive the manuscripts of the papers at least four weeks before the meeting. Everyone is invited to read and review the manuscripts especially in their respective fields of competence and interest.
- Presentation of the paper during the meeting by the author
- Comments and recommendations of the experts, discussion of the paper
- Comments, discussion and recommendations of the experts are documented in the minutes of the meeting and are printed on the front page of each paper.
- Final acceptance of the paper for the proceedings with
 - no changes
 - minor changes
 - major changes
 - or reject
- Revised papers are to be sent to the editor of the proceedings and the chairman of the INTER group
- Editor and chairman check, whether the requested changes have been carried out.

5 Meetings and list of all CIB W18 and INTER Papers

CIB Meetings:

- 1 Princes Risborough, England; March 1973
- 2 Copenhagen, Denmark; October 1973
- 3 Delft, Netherlands; June 1974
- 4 Paris, France; February 1975
- 5 Karlsruhe, Federal Republic of Germany; October 1975
- 6 Aalborg, Denmark; June 1976
- 7 Stockholm, Sweden; February/March 1977
- 8 Brussels, Belgium; October 1977
- 9 Perth, Scotland; June 1978
- 10 Vancouver, Canada; August 1978
- 11 Vienna, Austria; March 1979
- 12 Bordeaux, France; October 1979
- 13 Otaniemi, Finland; June 1980
- 14 Warsaw, Poland; May 1981
- 15 Karlsruhe, Federal Republic of Germany; June 1982
- 16 Lillehammer, Norway; May/June 1983
- 17 Rapperswil, Switzerland; May 1984
- 18 Beit Oren, Israel; June 1985
- 19 Florence, Italy; September 1986
- 20 Dublin, Ireland; September 1987
- 21 Parksville, Canada; September 1988
- 22 Berlin, German Democratic Republic; September 1989
- 23 Lisbon, Portugal; September 1990
- 24 Oxford, United Kingdom; September 1991
- 25 Åhus, Sweden; August 1992
- 26 Athens, USA; August 1993
- 27 Sydney, Australia; July 1994
- 28 Copenhagen, Denmark; April 1995
- 29 Bordeaux, France; August 1996
- 30 Vancouver, Canada; August 1997
- 31 Savonlinna, Finland; August 1998
- 32 Graz, Austria; August 1999

- 33 Delft, The Netherlands; August 2000
- 34 Venice, Italy; August 2001
- 35 Kyoto, Japan; September 2002
- 36 Colorado, USA; August 2003
- 37 Edinburgh, Scotland; August 2004
- 38 Karlsruhe, Germany; August 2005
- 39 Florence, Italy; August 2006
- 40 Bled, Slovenia; August 2007
- 41 St. Andrews, Canada; August 2008
- 42 Dübendorf, Switzerland; August 2009
- 43 Nelson, New Zealand; August 2010
- 44 Alghero, Italy; August 2011
- 45 Växjö, Sweden; August 2012
- 46 Vancouver, Canada; August 2013

INTER Meetings:

- 47 Bath, United Kingdom; August 2014
- 48 Šibenik, Croatia; August 2015
- 49 Graz, Austria; August 2016
- 50 Kyoto, Japan; August 2017
- 51 Tallinn, Estonia; August 2018
- 52 Tacoma WA, USA; 2019
- 53 Online Meeting; 2020

The titles of the CIB W 18 and INTER papers (starting from 2014) are included in the complete list of CIB/INTER papers: <http://holz.vaka.kit.edu/392.php>

